NANO-MULTILAYERED SELF-ADAPTIVE HARD PVD COATINGS FOR DRY HIGH PERFORMANCE MACHINING

NANO-MULTILAYERED SELF-ADAPTIVE HARD PVD COATINGS FOR DRY HIGH PERFORMANCE MACHINING

By

LI NING, B. Sc., M. Sc. (Mechanical Engineering)

A Thesis
Submitted to the School of Graduate Studies
in Partial Fulfillment of the Requirements
for the Degree
Doctor of Philosophy

McMaster University
Hamilton, Ontario, Canada

DOCTOR OF PHILOSOPHY (2007)
(Mechanical Engineering)

McMaster University
Hamilton, Ontario, Canada

TITLE: Nano-multilayered Self-adaptive Hard PVD Coatings for Dry High Performance Machining

AUTHOR: Li Ning, B. Sc., M. Sc. (Mechanical Engineering)

SUPERVISORS: Dr. M. Elbestawi and Dr. S. C. Veldhuis
Department of Mechanical Engineering
McMaster University

MUNBER OF PAGES: xxiii, 218

Abstract

In this research, quaternary nitride nano-multilayered coatings of the form TiAlCrN/Me_xN were comprehensively characterized. Based on this research principles which can be applied for guiding coating design were developed using the concept of self-adaptability.

Comprehensive studies were performed on the following aspects: the tribological properties of the coatings at elevated temperatures, tool life, and cutting forces, tribo-oxide formation, wear mechanisms and wear progression, chip characteristics and the mechanisms of chip formation. The techniques applied for comprehensive characterization of the coatings were mainly Scanning Electron Microscope/Energy Dispersive Spectrometer (SEM/EDS) and X-ray Photoelectron Spectroscopy (XPS).

The concept of self-adaptability as applied in this research is defined as the ability of a system to provide an improved response to an external stimulus such as friction, temperature, stress and strain. Self-adaptability plays a role in the formation of tribo-oxides on the tool surface under the elevated temperatures associated with dry high performance machining and the tribo-oxides formed in this case work as either liquid or solid lubricants in the cutting zone depending on their respective melting points. The tribo-ceramics (Al-O, W-O, Nb-O and Cr-O) formed during cutting process, were found to be extremely beneficial for an improvement on tool performance. They provided a synergetic action which served to protect the cutting

tool by 1) lubricating the cutting zone to reduce friction, 2) insulating the substrate surface from oxidation as well as thermal attack, and 3) dissipate the energy during friction to reduce cutting edge and surface damage. However, due to high stress generating during high performance machining the liquid tribo-oxide lubricants did not provide any significant improvement in tool life. This was attributed to an inability to retain them in the cutting zone due to high contact pressures. Also these liquid phase formations on the surface were found to cause the spallation of the coating layers.

The adaptability of the coating also affects the chip formation process over the life of the tool. Among the parameters of the chips used to characterize wear behavior of a cutting tool, one of the key factors was the contact length between the chip and the tool rake face. The ability to maintain an optimal contact length was a major factor for achieving a long tool life. Too short of a contact length results in a short tool life because of excessively high stress concentration on the cutting edges. It was found that slight seizure was needed within the running-in stage to obtain a certain contact length and the ability to continuously provide excellent lubricity had a significant contribution to reducing further growth in seizure intensity.

Typically saw-tooth chips were generated except when a new sharp cutting edge with good lubricity was used. In this case continuous chips were observed. The cross-sections of saw-tooth chips revealed four deformation zones, i.e., white layer zone, friction zone, primary shear zone and a less deformed zone as a result of the combined effect of strain hardening, thermal softening, quenching phenomena and saw-tooth chip formation. The chip temperature estimation indicated that the cutting tool experienced a temperature of approximately 850 to 1100°C or above at a cutting speed of 220 m/min to 300 m/min. The study of chip formation further confirms that lubricity, ability to dissipate energy and thermal stability are the most important properties for coated tools to achieve a long tool life.

Among the adaptive coatings investigated in this research, the nano-multilayered TiAlCrN/NbN coating achieved excellent tool performance due to its enhanced self-adaptive properties under elevated temperatures. The tool life achieved with the TiAlCrN/NbN coated tool was increased by more than four times as compared to the best commercial available nano-crystalline coating TiAlCrN. The TiAlCrN/NbN coated tools are able to yield an acceptable tool life even when the cutting speed reached 400 m/min and hence makes a great contribution to productivity improvement.

A coated tool should be treated together as the coating controls the tool life while both the structure and the properties of the substrate material have a great impact on the performance of the cutting tool as well. A fine-grained substrate material possesses the combined properties of both high toughness and high hardness and had a significant contribution to tool performance especially for the severe cutting conditions under which the substrate was gradually exposed at the cutting edge as wear progressed.

Overall in the on-going effort to improve wear resistance of a hard coating it was found that between the two ways to improve tool performance, i.e. hardness improvement as represented by superhard nano-composite coatings such as a $TiAlN/Si_3N_4$ coating and adaptability improvement by adaptive nano-laminated $TiAlCrN/Me_xN$ coatings, the latter was more beneficial for tool life enhancement under the proposed cutting conditions.

Acknowledgements

First and foremost I would like to express my gratitude to my supervisors Dr. Elbestawi and Dr. Veldhuis for their continuous guidance, critical review of my work and support throughout the research.

I would like to express my special thanks and appreciation to Dr. Fox-Rabinovich and Dr. Dosbaeva for their detailed discussions, constructive suggestions and great help during the project work.

I want to take the chance to thank my committee members Dr. Provatas and Dr. Shankar for their supervisory insight into my work and annual guidance.

I would also like to express my appreciation to Dr. Koproch, Jim Mclaren and Warren Reynolds who helped me with sample preparation, SEM/EDX analysis and the preparation of the experimental tests. I also want to thank Jeff, Aml, Etienne and Stephane for their help.

This work was made possible by the incredible foresight of Kobe steel. Funding for this research came from the following organizations: Kobe Steel, McMaster University, NSERC and OGS. Their support is gratefully acknowledged.

With family's help, my dream can become true. I would like to thank my son, Weiyi, my daughter, Joyce, my mother and my parents-in law for their understanding, patient and support. My special thanks to Weiyi, for his great help on taking care of his little sister.

Finally, to my husband, without your help this could not have been possible.

Contents

List of Illustrations

List of Tables

Nomenclature

W_t	Total work
W_e	Elastic work
W_p	Plastic work
K_e	Elasticity index
K_e	Plasticity index
$P_{\max}$	Maximum load
$P_{loading}$	Loading force
$P_{unloading}$	Unloading force
h	Indentation depth
dh	Differential indentation depth
h_t	Maximum penetration depth
h_r	Residual depth
h_p	Effective penetration depth
E_r	Reduced elastic modulus
E_f	Elastic modulus of film
E_i	Elastic modulus of indenter

S	Contact stiffness
A	Projection of contact area between the indenter and the coating specimen
α	A constant
k	A constant
H	Hardness
F_T	Tangential force
F_N	Normal force
F_x	Cutting force component in X axis
F_y	Cutting force component in Y axis
F_z	Cutting force component in Z axis
F_r	Resultant cutting force
μ_{eff}	Effective friction coefficient
A_a	Apparent contact area
A_{true}	True contact area
C	Constant
μ	Coefficient of friction
τ_{true}	True shearing stress
σ_{true}	True normal stress
τ_f	Shearing stress of film
τ_{soft}	Shearing stress of soft material

$\tau_{sticking}$	Shearing stress of sticking zone
$\tau_{sliding}$	Shearing stress of sliding zone
E_0	Energy in a frictional body
E_t	Transformed energy
ΔU	Internal energy change of a frictional body
t_c	Chip thickness
a_e	Pick feed / step over distance
a_p	Depth of cut
D	Diameter of ball end mill
f_t	Feed per tooth
κ	Cutting edge angle
θ	Rotational angle
N	Spindle speed
n	Number of cutting flutes
V_c	Cutting velocity
$V_{c\max}$	Maximum cutting velocity
H_0	Hardness of initial grain size
d	Diameter of grain
K	Constant

Chapter One

Introduction

Dry machining, hard machining and high speed machining are modern manufacturing processes. Presently, an increasing number of manufacturers are using dry high speed machining of hardened materials over conventional processes to reduce costs and minimize their impact on the environment. High speed machining is preferred by industries, especially die/mold, automotive and aerospace industries, due to the advantages of high material removal rate, close to net shape surface quality, relatively low cutting force, high dissipation of heat by chip removal and greatly reduced polishing times for dies/molds. A typical example application for dry high speed hard machining is the manufacturing a die from a hardened block of tool steel.

As cutting speeds increase cutting temperatures also go higher especially with dry machining of hard materials. In these cases, the cutting tools lose their typically excellent room temperature properties which results in an extremely short tool life. In order to achieve an acceptable tool life, dry high speed hard machining requires cutting tool materials with high hot hardness, improved fracture toughness, excellent adhesion, friction reduction properties, good diffusion and oxidation resistance at these high temperatures. Coating technology, involving the deposition of hard thin films onto the tool, has the potential to provide the required high temperature properties for the cutting tools in these applications. Today, more than 80% of machining operations are conducted with coated tools. Among the types of coatings available on the market, titanium-based hard thin films are most commonly used. This is due to the fact that they tend to improve the wear resistance in many cutting applications by reducing friction, adhesive wear, diffusive wear and oxidation wear, overall protecting the tool from thermal attack and reducing the mechanical stresses on the substrate.

There are two commonly used deposition methods, i.e., Chemical Vapor Deposition (CVD) and Physical Vapor Deposition (PVD). Due to the type of residual stress formed during the coating deposition process, PVD coating is more suitable for intermittent cutting processes like ball nose end milling which is studied in this research.

Every coating has its limited maximum working temperature. Beyond this temperature the coating loses its protective properties. For example, the maximum working temperatures of TiN, TiAlN and TiAlCrN coatings are approximately 600°C, 800°C and 1000°C, respectively. However, under severe cutting conditions the cutting temperature could exceed 1100°C, and commercial available coatings are not able to give an acceptable tool life under such high temperatures. Therefore, coatings that are able to survive the high cutting temperatures experienced in the proposed application are critically needed.

1.1 Motivation

Identifying and refining a coating able to operate in a high cutting temperature environment and tuning the operating conditions to best utilize the desirable properties of a coating is the inspiration for this research. There are two possible ways to approach this challenge. One is to develop super hard coatings with high hot hardness so that the tool can still maintain sufficient strength, hardness and toughness under high temperature. However, high hardness is usually accompanied with brittleness, and high brittleness is a poor property for an interrupted process like milling making it susceptible to the impact forces generated as the cutter enters and exits the cut. The other approach is to develop coatings with excellent lubricity properties that lubricate the cutting zone and hence decrease the cutting temperature.

Generally, under aggressive cutting conditions the tool/chip contact in the sticking zone on the rake face of the tool reaches nearly 100% due to the high contact stresses generated during the cutting process. In this case cutting fluids can hardly penetrate into the tool/chip interface region. Thus to meet the lubricity needs in the tool/chip contact region the concept of “self-adaptivity” is applied to coating design. A self-adaptive coating in this case refers to a coating that naturally generates beneficial tribo-films (tribo-oxides) on the surface of the tool under the conditions experienced during machining. These films serve to reduce the coefficient of friction, overall improving the cutting conditions and hence prolonging the life of the tool.

The structure of the coating also plays a major role in determining the fracture toughness of a coating. It has been found that nano-multilayered or superlattice coatings provide better resistance to micro-chipping and crack propagation, as compared to monolayer coatings. This is accomplished by arresting the crack propagation within the layers of the coating. The multilayered coating also helps to transfer elements to the tool surface, which serves to replenish the tribo-film formation process in the tool/chip contact region. Therefore, nano-multilayered TiAlCrN based PVD coatings were selected for detailed study in this research.

1.2 Research Objectives

The major goal of this research is to find advanced coatings which greatly increase productivity and prolong tool life under the severe cutting conditions associated with dry high speed machining of hardened materials.

Another goal was to understand why a particular coating performed better than another. To this end detailed investigations into the phenomena taking place in the cutting zone were carried out including: friction in cutting zone, formation of tribo-oxides, tool life, as well as investigations into wear types and wear mechanisms, chip types and mechanisms of chip formation, cutting force, and cutting temperature.

The last goal was to look for ways to extend this benefit through refining the coatings and tuning the cutting conditions to get higher performance tooling and thus develop a framework that coating companies and end users can use to develop coatings and processes for other dry high performance milling applications.

1.3 Thesis Outline

A short description of each chapter in this thesis is given below.

Chapter 1. INTRODUCTION. This chapter first introduces the importance of this research topic, the motivation of the research, and the research objectives.

Chapter 2. LITERATURE REVIEW. This chapter provides a detailed overview on dry high speed machining, cutting phenomena associated with high speed machining, recent developments in hard coatings and characteristics of hard coatings.

Chapter 3. BASICS OF COATING DESIGN. This chapter first describes the requirements of the cutting zone, how a coating affects the cutting process and the requirements and functions of the three critical wear zones on a tool, and then discusses the possible ways to improve the functions of a hard PVD coating to meet the requirements. Methods include adding additional alloying elements, reducing grain size, changing coating structure, and designing lubricous coatings.

Chapter 4. CONCEPT OF SELF-ADAPTABILITY. This chapter introduces the concept of self-adaptability, describes the tribological phenomena taking place in the cutting zone, and discusses the self-adaptability that takes place in a coating and outlines how it affects tool service life.

Chapter 5. EXPERIMENTAL WORK. This chapter presents the experimental setup for the cutting tests, the coating deposition and related coating characterization techniques.

Chapter 6. RESULTS AND DISCUSSIONS. This chapter shows the results obtained from this research, especially from the study of TiAlCrN/BCN, TiAlCrN/WN and TiAlCrN/NbN, and discusses tool life, formation of tribo-oxides, cutting forces, cutting temperature, tool wear, wear mechanisms and chip formation.

Chapter 7. CONCLUSIONS AND FUTURE WORK

In this chapter, a summary of this research is given; the contributions and findings from the research are presented; and future research work is recommended as well.

Chapter Two

Literature Review

2.1 Introduction of Dry High Speed Machining (HSM)

The range of cutting speeds used for high speed machining varies with the workpiece materials being machined. Figure 2.1 shows the generally accepted cutting speeds for high-speed machining of various workpiece materials [Schulz and Moriwaki, 1992]. For example, a cutting speed of 500 m/min is considered high-speed machining for cutting alloy steel while this speed is considered conventional when cutting aluminum.

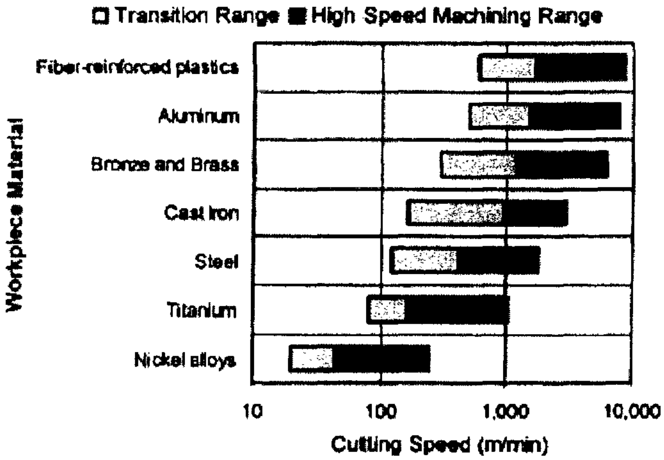

Figure 2.1 High-speed ranges in machining various materials [Schulz and Moriwaki, 1992]

The advantages of HSM are reported mainly with regard to the following aspects: high material removal rates, reduction in lead times, low cutting forces, ability to dissipate heat through chip removal which results in a decrease in workpiece distortion and an increase in part precision and surface finish [Fallböhmer, et al., 2000]. The major industries for HSM applications are the aircraft, automotive and the die/mold industries. For example, high-speed milling was applied to the machining of aluminum alloys for the manufacturing of complicated parts used in the aircraft industry. This technology has been successfully applied based on the significant improvements in machine tools, spindles and controllers [Tlusty, 1993]. With the development of cutting tool technologies, HSM has been used for machining alloy steels (usually hardness>30 HRC) for making dies/molds used in the production of automotive, electronic and plastic molding components [Dewes and Aspinwall, 1997]. In traditional die and mold manufacturing, dies/molds were made via the following route: first machined in their soft condition, then hardened followed by EDM (electrical discharge machining), grinding and/or hand polishing. In this way, a significant portion of the lead-time was spent hardening and polishing/manual finishing operations, as illustrated in Figure 2.2. The cost of machining and polishing was reported as taking approximately two thirds of the total manufacturing costs [Fallböhmer, et al., 1996]. In modern die/mold manufacturing, cavities can be directly produced from solid in the hardened tool steels by applying HSM processes. Using light depths-of-cut at high feed rates (high spindle speed but small feed per tooth) generates a machined surface very close to the designed geometry. Therefore, the polishing time in die/mold manufacturing process is greatly reduced and the lead time associated with hardening is avoided.

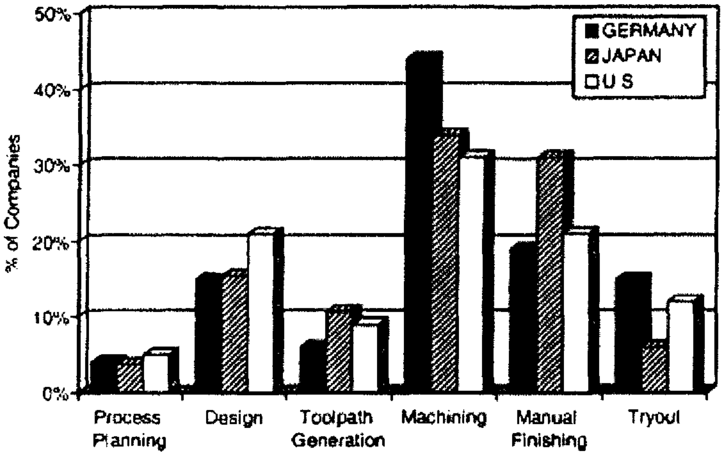

Figure 2.2 Lead-times in production of dies/molds [Fallböhmer, et al., 2000]

However, the common disadvantages from the applications of HSM are reported as follows: excessive tool wear, requiring special and expensive machine tools with advanced spindles and controllers, rigid fixturing, balanced tool holder, and lastly but most importantly the need for advanced cutting tool materials and coatings [Fallböhmer, et al., 2000].

Among the cutting tool materials such as HSS (high speed steel), carbide, ceramic, CBN (cubic boron nitride), PCBN, PCD (polycrystalline diamond) and diamond, carbide is the most common cutting tool material for machining castings and alloy steels. Carbide tools have a high degree of toughness but poor hardness as compared to CBN and diamond, as illustrated in Figure 2.3. Table 2.1 lists the properties of common cutting tool materials. In order to improve the hardness and surface conditions, more and more carbide tools are coated with hard coatings either by CVD (chemical vapor deposition) or PVD (physical vapor deposition), as shown in Figure 2.4.

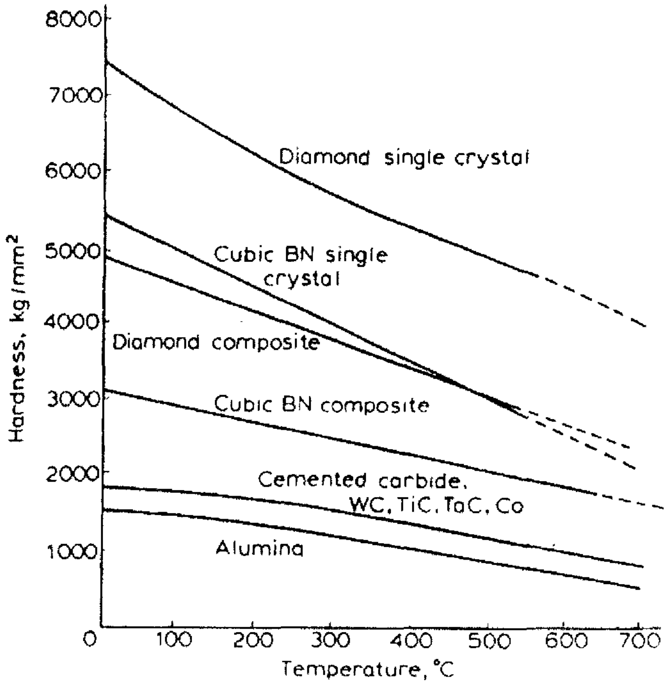

Figure 2.3 Hardness of cutting tool materials verses temperature

[Trent and Wright, 2000]

Table 2.1 Properties of advanced cutting tool materials [Fallböhmer, et al., 1996]

	Tool materials					Coatings		
	PCD	CBN	WC	SiN	AlO	TiN	TiCN	TiAlN
Micro hardness (HV)	6000	3500	1500 1800	1700	1600	2900	3000	3300
Coefficient of friction against steel in dry contact		0.24	0.6			0.4	0.4	0.3 0.5
Maximum working temperature (C)	600					600	400	815
Thermal conductivity (W/m K)	500	100	40-80	15 35	14 17			
Transverse rupture strength (MPa)	690 965	690	1700 2000	480 750	275 345			

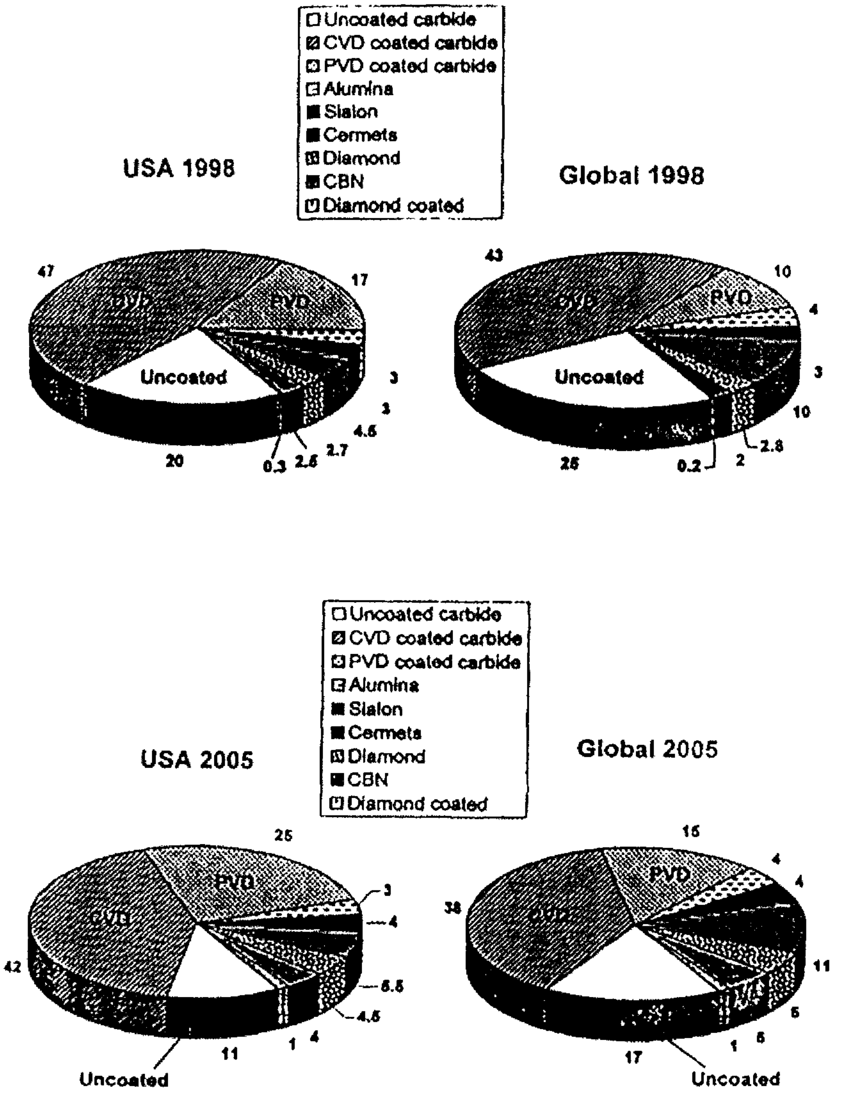

Sialon (Si-Al-O-N) - silicon nitride based material with aluminum and oxygen addition; Cermets (ceramic plus metallic components); CBN (cubic boron nitride)

Figure 2.4 A survey of U.S. and global markets on cutting tool materials

[Trent and Wright, 2000]

Generally, high speed machining involves high cutting temperature so the cutting tool must be chosen not only for its wear resistance, but also for its ability to retain this wear resistance at an elevated temperature.

Dry high speed machining of hardened steel has become attractive due to its economic and environmental benefits. For interrupted cutting such as milling, dry machining is beneficial for reducing thermal shock as well. It is well known that in metal cutting the contact stresses on the rake face of the tool near the cutting edge are very high and the degree of contact in the tool-chip interface reaches 100%. This means that the cutting fluids can hardly penetrate the cutting zone interface [Childs, 2006]. Therefore, the cutting tool is heated during cut and then cooled down rapidly out of cut if coolant is used and then heated up again on the next cycle. This may result in significant thermal cracking problems. However, self-lubricious coatings, which are found to generate oxidation tribo-films under these conditions, reduce friction and thus heat generation in the cutting zone. This makes them suitable candidates for dry high speed interrupted machining applications.

2.2 Tool Life, Tool Wear and Wear Mechanisms

2.2.1 Tool life and tool wear

There is no single universally accepted definition of tool life. The life needs to be specified with regard to the process aims. A common way of quantifying the end of a tool life is to put a limit on the average or maximum acceptable flank wear or the measured surface roughness. Figure 2.5 shows the general behavior of flank wear versus cutting time/cutting length. Tool life can be generally divided into three phases. During Phase I, there is an initial high rate of wear, where the sharp edge is worn rapidly and a finite wear land is established, followed by Phase II, where a steady increase in flank wear in proportion to cutting time/cutting length occurs. When the wear reaches a certain size and sufficient internal damage to the tool occurs the wear rate accelerates rapidly. This extremely high wear rate generally indicates that the tool is near the end of its functional life.

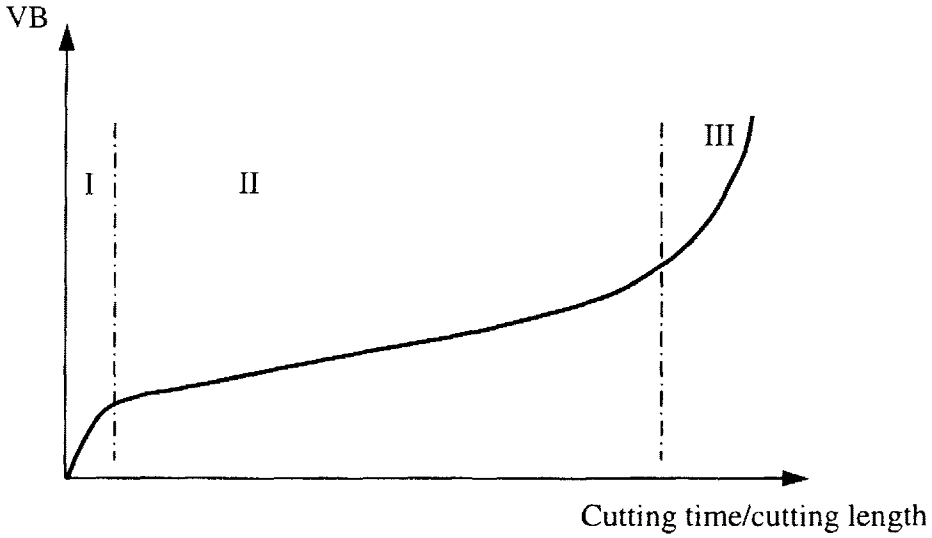

Figure 2.5 Development of flank wear vs. cutting time/cutting length

Tool wear is defined in ISO 8688-1 International Standard (1989) as: "Change in shape of the cutting part of a tool from its original shape, resulting from the progressive loss of tool material during cutting." The commonly recognized tool wear types are shown in Figure 2.6.

Flank wear (a) and notch (b, c)	Crater wear	Plastic deformation
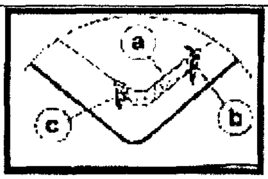	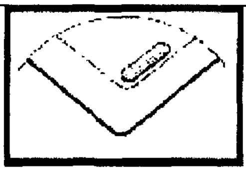	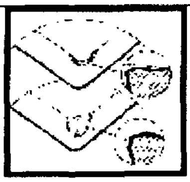
Built-up edge	Chipping	Flaking
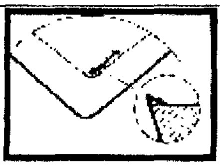	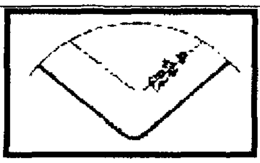	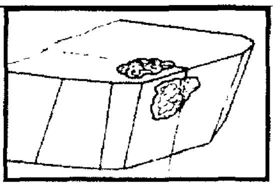
Edge chipping	Thermal cracking	Edge fracture or breakage
	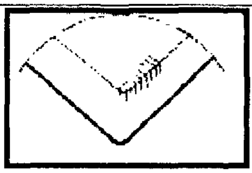	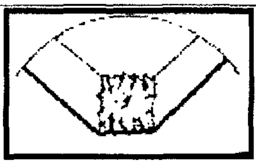

Figure 2.6 Types of tool wear [ISO8688-1]

These types of tool wear are explained as follows:

Flank wear is the most common type of wear. It generally exists in all machining applications and it can be observed on the flank face of the cutter and is caused mostly by tool abrasion and adhesion. Flank wear can affect the sharpness of the cutting edge and can also generate a wear land which affects the surface finish and dimensional accuracy of the workpiece.

Notch wear is also called depth of cut notch because its position is typically associated with the depth of cut. It is usually caused by the extra wear experienced due to oxides and hard layers on the surface of the workpiece as well as by chips hitting the edge causing it to chip in this region. Thus the mechanism of notch wear is a combination of abrasion, adhesion and oxidation.

Crater wear occurs on the rake face. There are two main reasons which cause crater wear. One is the chip flowing over the rake face of the tool and abrading the tool material. Another is the diffusion of elements from the tool due to high temperatures in the tool chip interface. Excessive crater wear usually results in catastrophic breakage of a tool.

Plastic deformation occurs when there are high temperatures and pressures on the cutting edge of the tool causing the edge to plastically deform.

Built-up edge occurs when portions of the chip adhere to the tool thus changing the cutting edge geometry. This will impact the cutting force and temperatures in the cutting zone. Once the built-up edge reaches a critical size it is removed and often takes a piece of the tool material with it. As the affinity of the tool material to the workpiece increases the tendency to form a built-up edge also increases.

Chipping of the cutting edge occurs when the cutting edge does not have enough strength to take the cutting loads. Due to the geometries experienced as the tool enters and exists cut tensile loads on the cutting edge can occur which result in chipping.

Flaking is defined as a loss of tool fragments in the form of flakes from the tool surfaces. It is mostly observed when coated tool inserts are used but may also occur with other tool materials.

Thermal cracking is mainly fatigue wear caused by a thermal cyclic load. Varying chip cross-sections, insufficient coolant and interrupted cuts are the operations where thermal cracks in tools are most likely to occur. Thermal cracking is usually perpendicular to the cutting edge.

Mechanical fatigue cracking takes place due to excessive shocks. It can occur when the loads on the tool are varying. These cracks are parallel to the edge.

Fracture is a result of catastrophic failure of the tool. It can happen due to faulty clamping of the insert, vibration in the system, excessive loads, or at the end of a period of intensive wear.

2.2.2 Wear mechanisms

During machining, high temperature, high contact pressure, high relative sliding velocities and the presence of cutting fluid in the tool-chip and tool-workpiece interfaces are major factors which affect tool wear. A wear mechanism is a result of a set of physical and chemical processes, which take place in the surface layers of a frictional and tribological system, as illustrated in Figure 2.7.

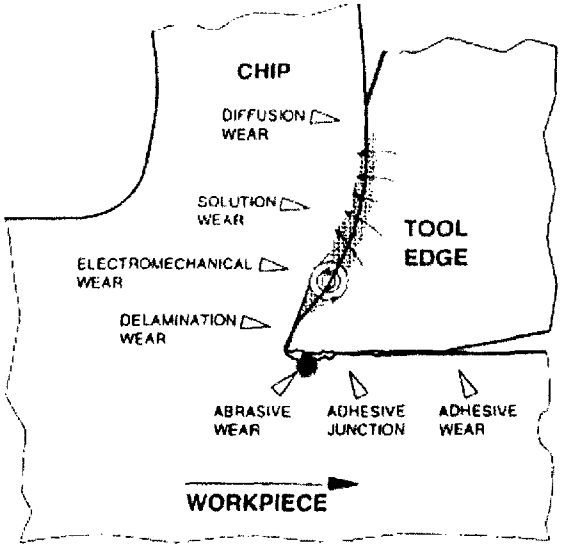

Figure 2.7 The different mechanisms of tool wear [Kopac, et al., 2001]

Tool wear can be attributed to the following wear mechanisms:

Abrasive wear is caused by a wear process in which a harder material scratches a softer material under normal pressure. This mechanism is significant for tool wear only when the workpiece material is very hard or contains hard particles. Hard particles presented in the chip wear the rake face while hard particles in the machined surface scratch the flank face. Flank wear and crater wear are the types of wear most frequently related with this mechanism. Using tool materials with high hardness, melting point and thermal conductivity can minimize the rate of abrasive wear.

Adhesive wear, also called attrition wear, occurs due to the intimate contact between the flank face of the tool and the freshly created surfaces on the workpiece and between the rake face of the tool and the underside of the chip. Several layers of workpiece material are compressed against the cutting edge at high temperature. After compression, the layers adhere to the cutting edge and usually become hard like the process of strength hardening. Some pieces of these layers may break off and take parts of the cutting edge away, i.e. notching or they may weld onto the tool edge and replace the real edge and cut the workpiece material, i.e., built-up edge. The welded layers and points are periodically sheared away and new welds are formed. Hence, built-up edge and notch wear are common types of wear associated with this mechanism. Adhesive wear usually occurs at relatively low cutting speeds associated with high pressure/high temperature on the cutting edge.

Diffusion is the process by which the atoms in the tool material have an affinity to the atoms in the workpiece material. The diffusion rate depends on the affinity of the materials, the temperatures in the cutting zone and the concentration gradient of the penetrating atoms. Chemical wear is mainly associated with crater wear and to a lesser extent flank wear and notch wear [Braghini and Coelho, 2001].

Oxidation wear is a type of chemical wear, which occurs when metals and oxygen are in contact. It can be accelerated at high temperature and/or high pressures. Notch wear is related to this mechanism.

Fatigue wear has two types, i.e., mechanical fatigue and thermal fatigue. The first is due to the alternating tensile and compression stresses on the cutting edge and the second is caused by the alternating cycles of heating and cooling. Unlike turning, milling is dynamic due to its intermittent nature that causes each tooth to undergo both mechanical and thermal loading and unloading. In every rotation of the cutter, each tooth has a stress cycle and a heating period followed by a cooling period. The cycling between heating and cooling produces thermal stresses that may exceed the yield stress of the tool material which can cause micro cracks. Chipping and catastrophic failure are the main types of wear related to this fatigue mechanism.

Generally, all forms of wear mechanisms simultaneously contribute to tool wear however there is usually one or two predominant wear mechanisms depending on the cutting conditions, the cutting stages, the material chemical composition, as well as mechanical properties and microstructure.

2.2.3 Factors affecting tool wear

Metal cutting is performed in a machining system (machine tool-spindle system-cutting tool-fixture-workpiece-cutting conditions). All the functional elements in this system more or less affect tool wear and tool life. Yen, et al. [2002] classified them into four groups shown in Figure 2.8.

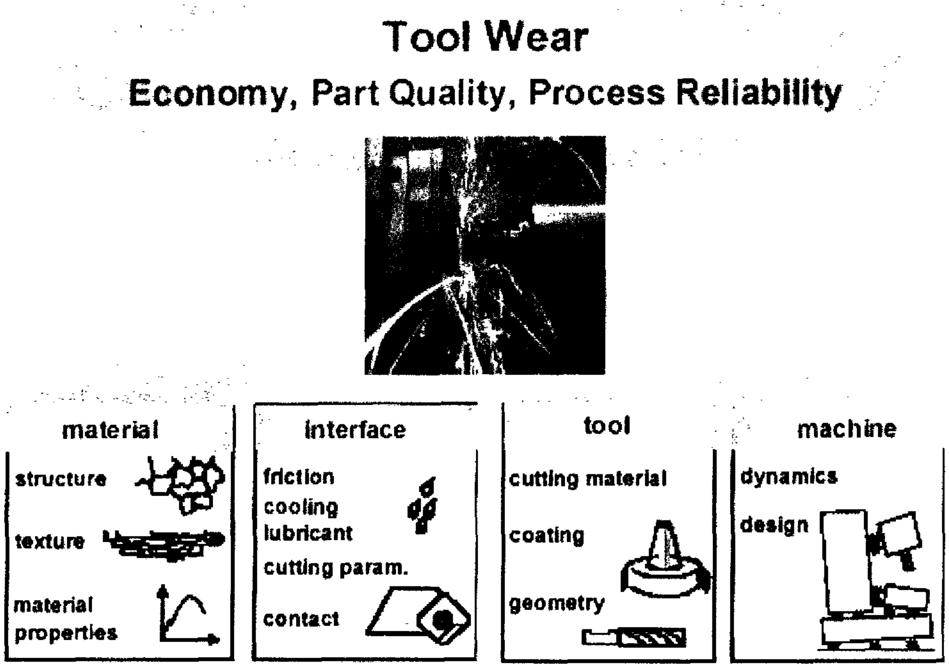

Figure 2.8 Tool wear factors in machining processes [Yen, et al. 2002]

Workpiece material group indicates that the physical properties of workpiece material such as mechanical and thermal properties, microstructure, and hardness; affect cutting forces, cutting temperatures and thus also affect tool wear.

Interface group between workpiece and cutting tool includes coolant and lubricant, tool-chip contact, cutting parameters (cutting speed, feed rate, axial depth of cut, radial width of cut). These parameters and conditions definitely affect tool wear.

Cutting tool group indicates that tool substrate materials (such as chemical composition, structure and grain size), tool coatings and tool geometry (rake angle, clearance angle, edge preparation, tool radius) are important factors for tool life.

Machine tool group indicates that the machine tool structure and all the other parts active in the cutting process such as spindle-tool holder system, and fixture for example play an important role in creating a successful cutting operation. Unstable cutting processes result in a fluctuating overload on the cutter and further lead to premature failure of the cutting edge by tool chipping and excessive tool wear.

2.3 Cutting Phenomena in High Speed Machining

The basic concept of HSM (high speed machining) involves machining at considerably higher cutting speeds and feed rates as compared with conventional practice. This was illustrated in Figure 2.1. Also because of the change in cutting conditions the cutting phenomena change as well.

2.3.1 Cutting temperature

Like traditional cutting, the heat generated during cutting in HSM is still from three zones, i.e., the primary shear zone radiating out from the tool tip into the workpiece/chip interface, the secondary shear zone at the tool/chip interface, and the contact interface between the clearance face and the machined surface. When the cutting speed is increased the ratio of heat flow with the chip increases as less time is available for heat to transfer into the workpiece. This subsequently reduces the total percentage of the heat flow into the workpiece and the cutting tool [Hirao, et al., 1998]. It has been reported that around 80~90% of the heat generated during HSM is transferred to the chip while 10~15% of the heat goes to the cutting tool and workpiece material [Matsumoto, et al., 1986; Dews, et al., 1999; Dimla D.E.S., 2000; El-Wardany, et al., 2000]. When low thermal conductivity coatings are used to protect the cutting tools, an even higher ratio of heat goes with the chip. Therefore given the complexity of measuring cutting temperature the chip temperature in HSM is a reasonable estimate of the cutting temperature.

The relationship between the cutting speed and cutting temperature has been intensively studied. When Salomon first reported what he termed HSM in 1931 he proposed that there was a peak cutting temperature at an intermediate cutting speed and there was a reduction in cutting temperature when cutting speed was increased from that point. However, most of the literature since this date has concluded that there is no corresponding reduction in cutting temperature at higher cutting speeds. Instead, cutting temperature increases as the cutting speed increases [Lezanski and Shaw, 1990; El-Wardany, et al, 1996; Chu and Wallbank, 1998; Abrao and Aspinwall, 1997; Liu, et al., 1997; Leshock and Shin; 1997; Wang et al., 1996]. However, it was found that the heat conducted into the workpiece reduced as the cutting speed increased because there was a shorter contact time for heat to penetrate into the workpiece. Also it was stated that the higher the hardness of the workpiece, the higher the temperature and the deeper the heat penetrated into workpiece [Matsumoto and Hsu, 1987]. McGee (1979) suggested that cutting temperature increased with cutting speed up to a maximum value which was equal to the melting point of the workpiece. When machining soft materials such as aluminum alloys, it can be said that there is no fixed limit to the cutting speed (without considering the limitation of machine tool) because the melting point of aluminum alloys (up to 660°C) is lower than the temperature at which cemented carbide and ceramic tool materials begin to lose their strength and wear rapidly [McGee, 1979]. However, in the cutting of iron, steel and other high melting point metals and alloys, the heat generated during cutting becomes a controlling factor when selecting cutting speed [Trent, 2000].

Therefore, the limit on cutting speed is actually determined by the properties of the cutting tools at the elevated temperatures experienced in the cutting zone.

In addition to cutting speed, how the other parameters affecting cutting temperature has been investigated as well. It was observed that cutting temperature increased as tool wear increased but feed per tooth did not significantly affect the cutting temperature [Dewes et al., 1999]. Ning et al. (2001) concluded that the cutting temperature increased with cutting speed and axial depth of cut when HSM ball end milling hardened AISI H13 steel. Abrao et al. (1996) concluded that the temperature increased with an increase in cutting speed, feed rate, depth of cut and tool wear when finish turning hardened AISI H13 steel. Abrao and Aspinwall (1997) found that cutting temperatures increased with feed rate, depth of cut and tool wear, respectively, when turning hardened AISI E52100 steel. They also concluded that the thermal conductivity of cutting tool material played a major role where a higher thermal conductivity of a cutting tool induced a lower tool/chip interface temperature. As a result, less heat would go to soften the chip, but the high heat level into the tool would weaken the tool material. Wang and Liu (1999) investigated the effect of tool flank wear on the heat transfer, thermal damage and cutting mechanics when hard turning AISI E52100 steel and asserted that the proportion of heat that went into the chip increased as flank wear increased accordingly, indicating that the heat generated at the tool/chip interface and tool/work interface was strongly dependent on the development of the flank wear. El-Wardany et al. (1996) concluded that the cutting edge temperature increased with feed and depth of cut when high speed turning the case hardened AISI 1552 steel. They also investigated the effect of tool geometry on cutting temperature. It was found that cutting edge temperature decreased with increasing tool nose radius since larger nose radius promotes heat conduction. However, by increasing the tool width chamfer the cutting edge temperature rose due to an increase in the tool/chip contact length. Therefore an optimal tool geometry exists to achieve a minimum cutting edge temperature. Also the cutting temperature measured for an interrupted cutting process such as milling is lower than for continuous cutting such as turning [Dimla, 2000; Stephenson and Ali, 1992; Chou and Evans, 1999]. The cutting temperature in intermittent cutting depends primarily on the duration of cutting time and non-cutting time per cut. Overall the temperature increases as the cutting time per cut increases [Stephenson and Ali, 1992].

In summary, the factors that affect cutting temperature include cutting speed, tool wear, workpiece material, depth of cut, feed, tool geometry, especially cutting edge geometry, thermal property of the tool material and type of cutting operation (continuous or interrupted).

Regarding the determination of temperatures at the tool/chip interface, cutting tool, workpiece and chip surface, the techniques used for measuring/estimating can be classified as follows:

- Embedded thermocouples and tool/chip thermocouples [Dewes, et al., 1999].
- Metallographic method, i.e., microhardness and microstructure analysis.
- Powders of constant melting point.
- Thermo-sensitive paints.
- Infrared method [Dewes, et al., 1999; Young and Chou, 1995].

- Chip color [Venkatesh et al., 1993; Ning, Y. et al., 2001].

In this research chip color is used for estimating the temperature in the cutting zone.

2.3.2 Tool wear mechanisms under high temperature

Cutting temperature is a major factor that affects tool wear mechanisms, tool life and surface integrity. Kopac et al. (2001) stated that low cutting temperatures produce pressure welding which result in built-up edge (BUE) formation, while high cutting temperatures trigger diffusion and oxidation processes. Diffusion processes between the chip and the top rake surface of the cutting edge result in crater wear and oxidation reactions with the environment which induce scaling of the cutting edge. Koshy et al. (2002) used PCBN tools machining hardened D2 (HRC 58) and found that chipping occurred when high speed milling. It was also found that adhesion and attrition were the governing wear mechanisms responsible for tool wear and that PCBN tools failed by fracture of the cutting edge. Wear mechanisms verses cutting temperature in continuous cutting and interrupted cutting have been intensively studied [Loffler, 1994; Kopac et al., 2001] and the commonly accepted conclusion shown in Figure 2.9 [Kopac et al., 2001]. In the lower cutting speed range, the dominant wear mechanisms are abrasion and adhesion while in the high cutting speed range, tool wear grows exponentially and is mostly attributed to the rapid increase of diffusion wear. In addition to diffusion wear, oxidation and also abrasion are the major wear mechanisms in the high cutting speed range.

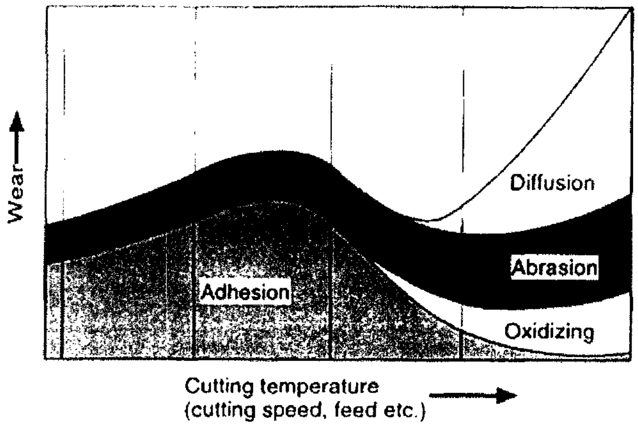

Figure 2.9 Wear mechanisms vs. cutting temperature [Kopac et al., 2001]

From a tribological point of view, tool surface protection against wear can be improved by:

- Increasing the wear resistance of the tool material surface.
- Influencing the frictional conditions in the contact zone.

Kopac et al. (2001) stated that in selecting appropriate surface protection to reduce surface wear, both the technical function of tribological systems together with variables (load, speed, temperature), and the wear mechanisms which are expected in the contact zone have to be taken into account.

Generally, if adhesion is the predominant wear mechanism, a surface protection layer on a tool should have a low inclination to cold weld and low shear strength. The most efficient ways to reduce adhesion are through sufficient lubrication and cooling, and thought the proper selection of tool-workpiece materials. Abrasive wear can be reduced by increasing the hardness of the cutting tool surface either by heat treatment or by applying very hard protective coatings. When several wear mechanisms are expected, multistage or combined surface protection should be planned [Fenske, et al., 1988].

2.3.3 Chip formation

The study of the chips generated during cutting goes back more than a century and still remains the focus of much attention. Although the goal of machining is to generate satisfactory machined surfaces the study of chip formation is very important because of the consumption of energy used in the formation and movement of the chip, and the main economic and practical problems concerned with metal removal rate, tool performance and the integrity of machined surface, can be understood by studying the behavior of the work material as it is formed into a chip and moves over the tool. Detailed knowledge of the chip formation process is also required for the understanding of the accuracy and condition of the machined surface of the desired component [Trent and Wright, 2001].

Chips can be classified into continuous, segmental (also called serrated or shear localized or saw-tooth), and discontinuous chips. Basically, the chips generated in hard machining are referred to as saw-tooth chips. Currently, there are two different theories associated with saw-tooth chip formation. One is called "crack theory" in which the chip formation starts with the initiation of a crack at the free surface of the workpiece and the crack further propagates towards the cutting edge of the tool. The crack soon ceases to grow at a point where severe plastic deformation of the material exists under higher level of compressive stresses. The chip segment caught up between the tool rake face and the crack is pushed out while the material in the plastic region just below the base of the crack is displaced along the tool rake face thus forming saw-toothed chips [Nakayama, et al, 1988; Shaw and Vyas, 1993, 1998; König et al., 1993; Elbestawi et al., 1996; Poulachon and Moisan, 1998; Vyas and Shaw, 1999]. Figure 2.10 shows the crack initiation caught during the cutting process by using a quick stop device. The different stages of saw-tooth chip formation were identified as well.

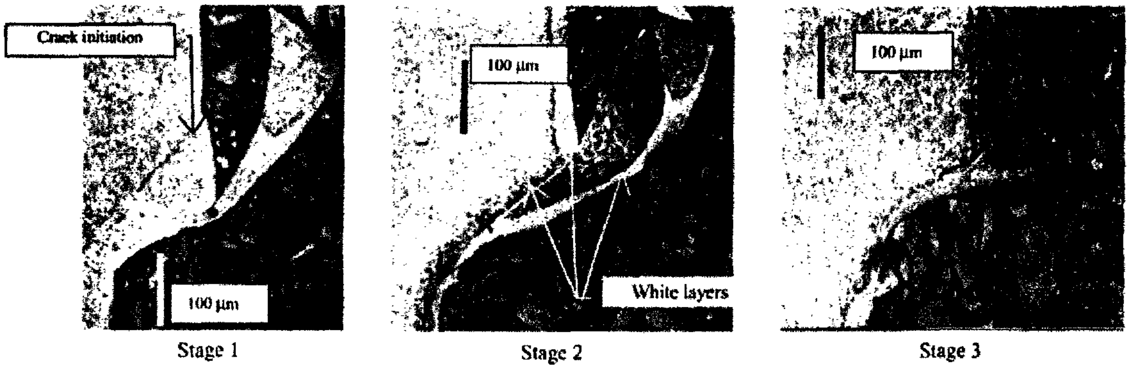

Figure 2.10 Crack initiation and saw-tooth chip formation obtained from quick stop testing [Poulachon and Moisan, 1998] (dry turning 100Cr6 steel HV760, whiskers reinforced ceramic, V=100 m/min, f=0.1 mm/rev, d=1 mm)

The other theory is called the "adiabatic shear theory" in which a thermoplastic instability occurs within the primary shear zone and the mechanism of deformation is the one in which the rate of thermal softening exceeds the rate of strain hardening and is often referred to as an adiabatic shear process (Figure 2.11) [Komanduri, et al., 1982; Davis, et al., 1996; Zhen-Bin and Komanduri, 1997; Palmai, 2005; Limido, et al., 2006].

It has been suggested that adiabatic shear may precede crack initiation and propagation within the uncracked region of the primary shear zone [Vyas and Shaw, 1999].

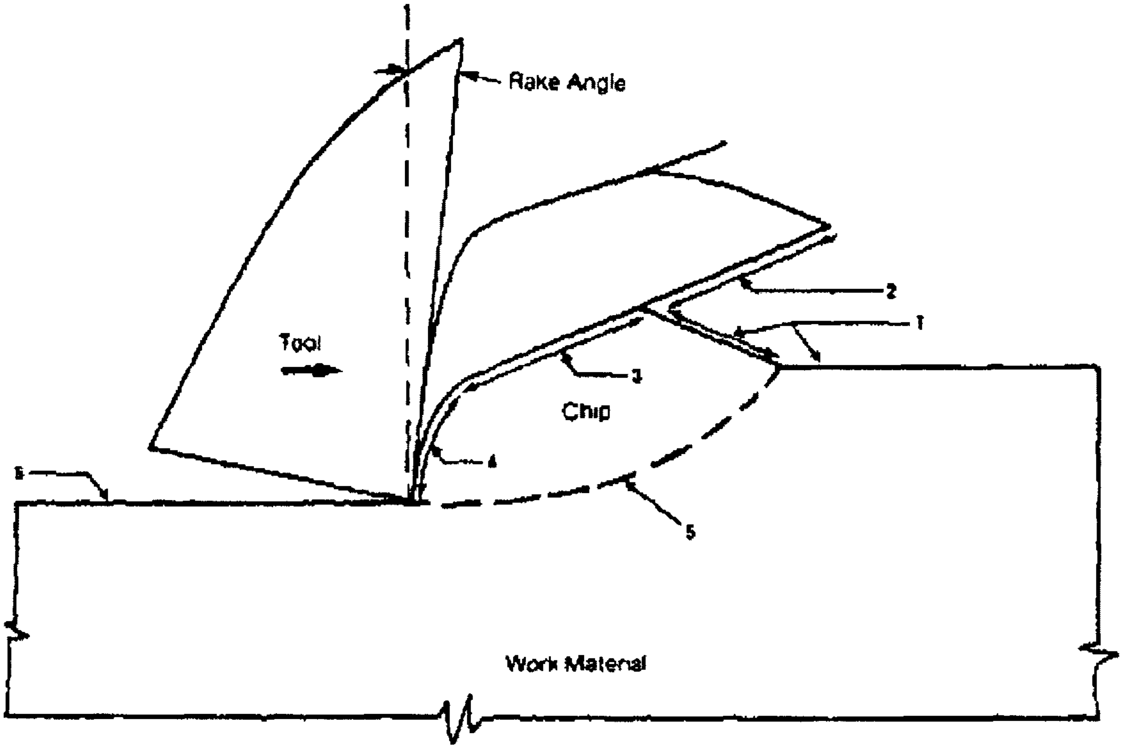

Figure 2.11 Schematic of the shear-localized chip formation process showing various stages in cycle of chip segmentation [Zhen-Bin and Komanduri, 1997]

The numbers in the Figure represents:

1. Undeformed surface
2. Part of the catastrophically shear failed surface separated from the following segment due to intense shear
3. Intense shear band formed due to catastrophic shear during the upsetting stage of the segment being formed
4. Intensely sheared surface of a segment in contact with the tool and its subsequent slide along the tool face
5. Intense localized deformation in the primary shear zone
6. Machined surface

Barry and Byrne [2002] studied the mechanisms of chip formation in machining hardened steels and they concluded that the primary instability within the primary shear zone during saw-tooth chip formation is the initiation of adiabatic shear at the tool tip and propagation partway to the free surface of the workpiece material while failure within the upper region of the primary shear zone near the free surface occurs through either "crack theory" or "adiabatic shear theory" depending on the cutting conditions. Under severe cutting conditions such as high workpiece material hardness and high cutting speed, failure was caused by ductile fracture; otherwise, failure occurs through large strain plastic deformation. Increasing workpiece material hardness, cutting speed, undeformed chip thickness and flank land as well as a more negative rake angle can result in saw-tooth chip formation [Barry and Byrne, 2002; Ekinovic, et al., 2004; Ng and Aspinwall, 2002; Wang and Liu; 1999; Jaspers and Dautzenberg, 2002; Konig, et al., 1984, 1990; Boeher, 1998; Kishawy and Elbestawi, 1997; Kishawy and Wilcox, 2003; PalDey and Deevi, 2003].

Konig, et al. (1984) explained the chip formation process in detail. Due to the negative tool rake angle used in their study high compressive stresses are created both on the cutting edge and in the material. Owing to the brittleness of the material, the high compressive stress initially leads not to material flow but to the formation of a crack. This crack releases the stored energy and acts as a sliding surface for the material segment, allowing the segment to be forced out between the parting surfaces. Meanwhile, plastic deformation and heating of the material occurred at the leading edge of the cutting tool.

Once the chip segment has slid away, renewed cutting pressure results in the formation of a fresh crack and chip segment.

How the cutting conditions affecting chip formation has been investigated intensively. Boehner, et al. investigated the effect of cutting speed, feed and tool wear on chip formation in hard ball end milling [Boehner, 1998; Boehner, et al., 1999]. Figure 2.12 shows different chips at different cutting speeds.

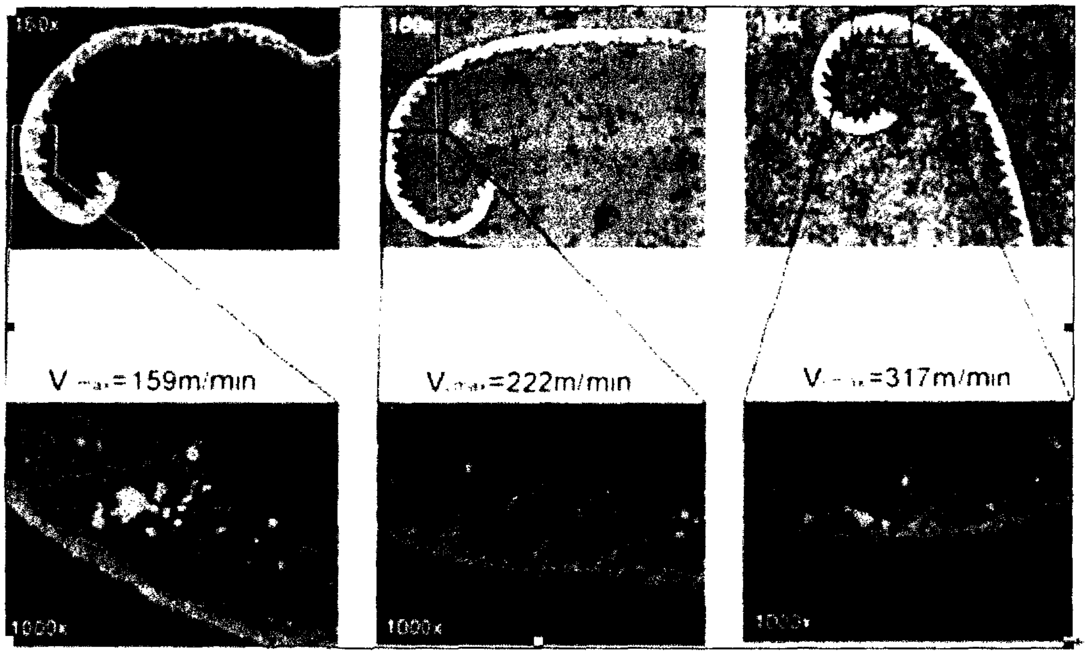

Figure 2.12 Chips at different cutting speed [Boehner, 1998]

From Figure 2.12 one can see that sharper chips are generated at higher cutting speeds while blunt chips are observed at lower speeds. The reason is that the lower cutting speed allows the heat generated by cutting to remain longer in the cutting zone as compared to the cases where higher speeds are used. Thus, the material has more time to soften and deform plastically. The crack is initiated due to the high pressure in front of the cutting edge advances towards the tool tip and is seized early in the plastic field material. A new chip forming cycle is started early and as a consequence the segmentation frequency increases. The higher the cutting speed is, the less time is left to soften the material. Once the crack initiates it advances in the direction of the tool tip and stops in the plastically deformed material zone. Consequently the chips at higher speed look sharper.

Chip curling at the tip of each chip is a typical phenomenon during the chip formation in high speed machining. Chip curling occurs because of an immense temperature increase in the first contact area between the chip and the tool. The temperature at the underside surface of the chip increases much faster than the free surface. As the temperature gradient of the chips increases, the resistance to curling decreases. It is normally expected that chip curling increases at elevated cutting speeds. However at higher speed, the plastic deformation zone is thinner and also the secondary shear zone decreases along the chip length, which leads to a decrease in the temperature gradient between the free surface and chip-tool-interface during the cut. Consequently, an increase in chip curling is not obviously observed as the cutting speed increases, as shown in Figure 2.12.

Chip curling is also strongly affected by the feed per tooth as well. Figure 2.13 shows different curled chips produced at different feeds per tooth.

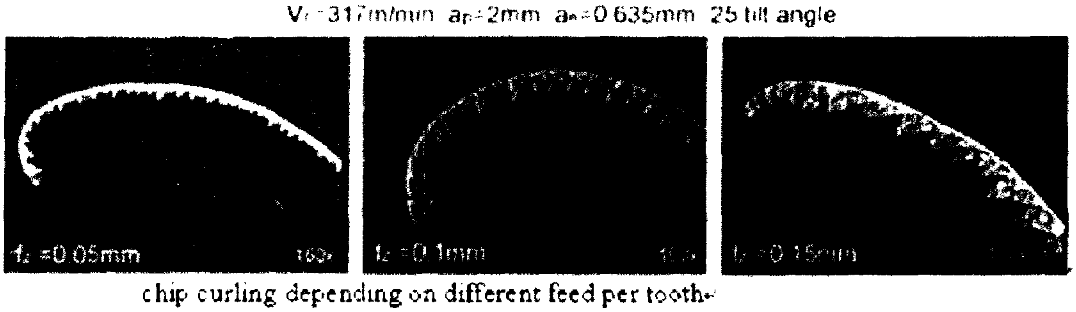

Figure 2.13 Chips produced at different feeds per tooth [Boehner, 1998]

There are two phenomena observed from Figure 2.13. One is that chip curling decreases as feed increases. Another is that chip segmentation frequency decreases as feed increases. The first phenomenon can be explained as: an increase of feed increases the deformed chip thickness. The thicker the chip is the higher its resistance to curling, even when a high temperature gradient between the chip-tool-interface and the free surface of the chip exists. At the highest feed per tooth (0.15mm) almost no chip curling can be observed, while at the lowest feed per tooth (0.05mm) the chip curls (Figure 2.13). The second phenomenon can be explained as follows: when feed increases, the deformed chip thickness is thicker and a higher pressure is imposed on the workpiece material; due to the higher pressure, the initiated crack propagates at a higher speed towards to tool tip to relieve the higher energy before it seizes in the softened material zone. Therefore, the segmentation separated from the workpiece by this crack is larger. Consequently, the segmentation frequency decreases (Figure 2.13).

Tool wear has a significant influence on chip formation. Figure 2.14 shows that chip curling decreases and the plastic deformation region gets thicker as the tool gets worn.

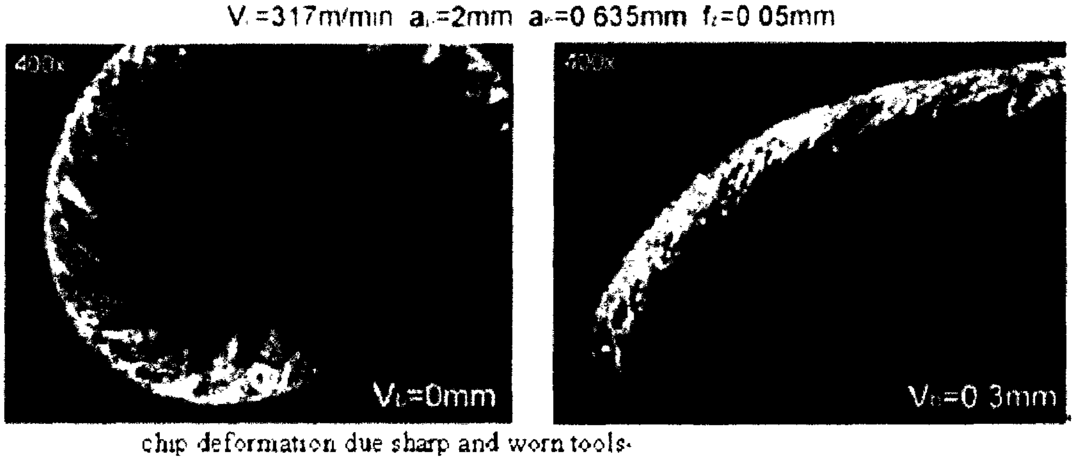

Figure 2.14 Chips generated by sharp and worn tools [Boehner, 1998]

This phenomenon can be explained in the following way: due to tool wear, more friction occurs causing extensive rubbing, and hence more heat is generated. This high cutting temperature in the cutting zone softens the workpiece material and hence, the plastic deformation occurs more easily. The larger plastic deformation zone stops the crack earlier and lowers the temperature gradient of the chip which then decreases the chip curling.

In summary, the frequency of chip segmentation, the degree of chip curling and the height of the saw-tooth depend on the cutting temperature, cutting pressure/cutting energy density, temperature gradient of the chip and the time that the chip is retained in the cutting zone. While all of these factors are related to the cutting conditions such as cutting speed, feed, depth of cut, tool wear, tool geometry, lubricity in the cutting zone and the presence of coolant.

2.3.4 Cutting forces

The comparison of wear mechanisms, surface integrity, chip formation and cutting force in hard machining has not been frequently or critically reported. However the influences of cutting parameters and flank wear on cutting forces has been studied in different machining operations. For instance, Elbestawi, et al. (1996) investigated the performance of whisker-reinforced ceramic tools in milling nickel-based superalloy and concluded that the average cutting force reduces with an increase in cutting speed as well as a lowering axial and radial depth of cut. Wang and Liu (1998, 1999) studied the effect of flank wear on the forces and temperatures in hard turning. Nakayama, et al. (1988) indicated that the cutting forces in the machining of hard materials are not necessarily high due to the following effects:

- Relatively small plastic deformation of the chip due to crack formation (see section 2.3.3).
- Relatively small area of tool-chip contact which reduces the friction force.
- After the cutting parameters that affect the cutting forces, rake angle and flank wear are the key factors in achieving successful hard machining.
- Larger negative rake angle on the tool increases the cutting force only a little while it results in a remarkable increasing in the thrust force.
- During the machining of hard materials, the high abrasiveness and high cutting temperature cause rapid tool wear and a worn flank surface with a blunt cutting edge raises the cutting forces, especially the thrust force, which further accelerates wear [Nakayama, et al., 1988].

2.4 Coating Deposition Technology

In recent years, hard thin coating films have been widely applied in cutting tools, molds and dies, and aerospace components due to their properties of high hot hardness, low thermal conductivity, low friction coefficient and good erosion resistance. These are important properties for machining due to the increased demands placed on modern machining processes such as high speed, dry environments, heavy cutting loads, and difficult-to-machine materials. Coating technology is one means of achieving good performance under these critical environments. Figure 2.15 summarizes the coating deposition processes typically used.

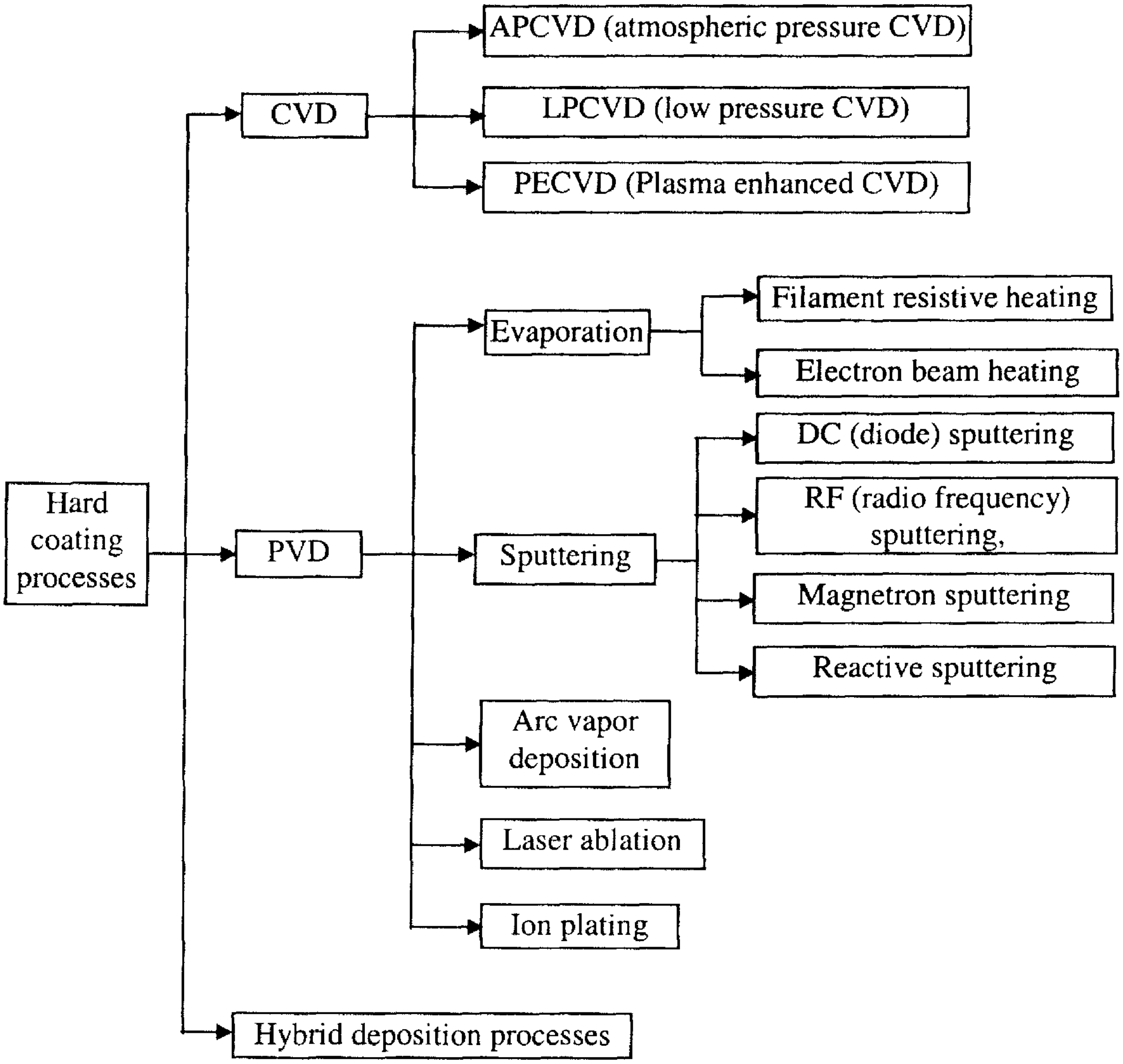

Figure 2.15 Deposition processes of thin hard coatings

2.4.1 Chemical Vapor Deposition (CVD)

Generally, CVD is the deposition of a solid on a heated surface from a chemical reaction in the vapor phase. This process takes place in a heated chamber at a temperature between 850 to 1000°C. This high temperature limits its application to thermally stable materials like cemented carbide. In this process the coating is formed through the chemical reactions of different gases as shown in Figure 2.16. The CVD process is well adapted to the deposition of multi-layered coatings because the process is relatively easy to regulate using various gases. The latest generation of CVD multi-layered coating for high-speed machining applications combine CVD and PVD methods. For instance, a multi-layered $TiC+TiCN+Al_2O_3$ coating additionally includes an outer TiN PVD layer. This layer protects the brittle Al_2O_3 layer against damage during the running-in stage of wear and improves the adaptability of the CVD multi-layered coating.

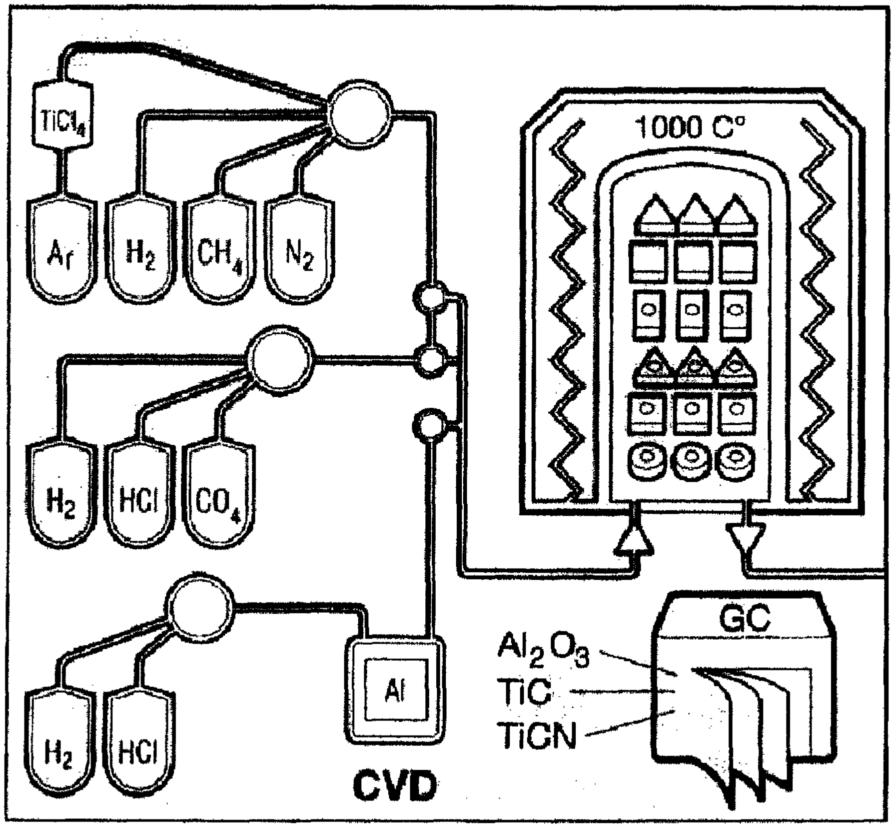

Figure 2.16 Scheme of chemical vapor deposition [Sandvik Coromant, 1994]

Compared with the PVD coating process, CVD coating does not need an ultra high vacuum and it has high throwing power for ease of filling deep recesses and other 3D structure. CVD coatings are generally thicker which is good for achieving a longer tool life however the process is not able to form a coating on a very sharp cutting edge and it is in general rougher than PVD coatings. In addition, CVD processes usually generate coatings with tensile residual stress at the surface. For the above reasons, CVD coatings are usually applied on tools that are used in continuous cutting operations.

In order to reduce the deposition temperature of CVD, a plasma-enhanced CVD (PECVD) (also called plasma activated CVD/PACVD) coating technique was developed. PECVD reactors operate under low pressure and do not depend completely on thermal energy to accelerate the reaction processes. They also transfer energy to the reactant gases by using a radio frequency induced glow discharge. This plasma enhanced application results in a significant reduction of deposition temperature down to 450 – 600°C. Now, different types of coatings such as monolayer, multilayer as well as nano-scale multilayer and nano-composite coatings [Stoiber, et al., 2000] can be deposited using this technique on a wide range of substrate materials.

2.4.2 Physical Vapor Deposition (PVD)

The development of PVD processes in the 1980's boosted the application of coatings for high speed and hot worked tool steel due to its relatively low deposition temperature (within 150~500°C). This is significant as it is below the tempering temperatures of these steels. Different from CVD processes physical vapor deposition (PVD) processes are performed in a vacuum and involve the condensation of neutral or ionized atoms of metals onto the substrate. Different PVD techniques are available for the deposition of hard coatings (see Figure 2.15).

Four basic elements are generally needed in a PVD process as listed below:

1. A vacuum chamber, evacuated with a pumping unit.
2. A vapor source (i.e., crucible, target).
3. A medium, usually argon based plasma.
4. A receiving area (i.e., parts / substrates) which are typically located opposite to the vapor source.

Figure 2.17 is a schematic layout of a PVD process based on magnetron sputtering. In this process the coating material is gradually removed from the metal target by bombardment with argon ions. At the same time a reactive gas is fed into the chamber. The gas contains the non-metallic component of the coating such as nitrogen or carbon. The ionized metal and gas particles are then accelerated against the substrates by an electric field. On impact they are deposited on the substrates as a thin coating. During the coating process the substrates are rotated to ensure uniform coating thickness everywhere.

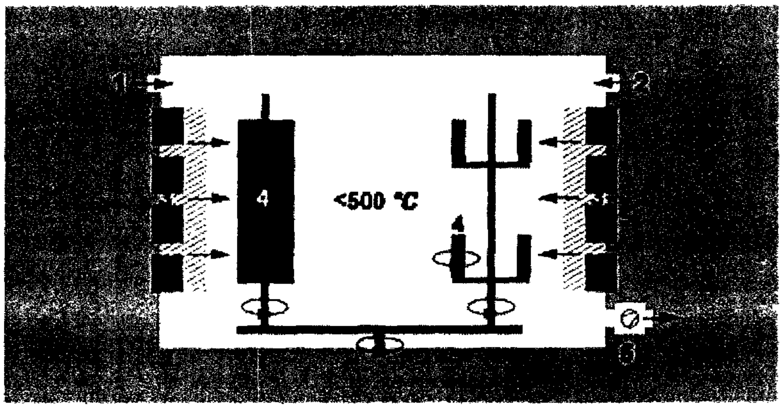

1-Argon, 2-Reactive gas, 3-Arc Sources (coating material and backing plate)
4-Components, 5-Vacuum pump

Figure 2.17 the schematic layout of PVD (magnetron sputtering) process [Balzers]

In order to increase target utilization and sputtering rates, an "unbalanced" magnetron process has been designed. In this case the magnetic flux from one pole is unequal to the other. Unbalanced magnetrons increase ion and electron bombardment of the growing film and the target utilization by as much as 30-40 wt%.

Figure 2.18 is a schematic diagram of a conventional direct cathodic arc source deposition. In this technique, the secondary electrons needed to sustain the glow discharge are emitted either by a thermal or a tunneling effect or by a combination of both phenomena. This results in very high electron current densities. Thus, arc plasmas are generally dense and contain a high percentage (60-80%) of metallic species which are ejected from the target and ionized. This confers a very high level of adhesion of the arc evaporated coatings, because of the possibility of metallic ion implantation in negatively polarized substrate(s). Moreover, the adequate polarization of parts with a complex shape (drills), leads to the synthesis of a homogeneous coating even in the shadowed sides of the part to be coated. Unfortunately, the evaporation of the target is generally associated with the ejection of melted particles (droplets) which leads to the formation of a large number of macroscopic defects during the growth of the coating. Thus, the arc evaporated coatings are relatively rough compared to magnetron sputtered films.

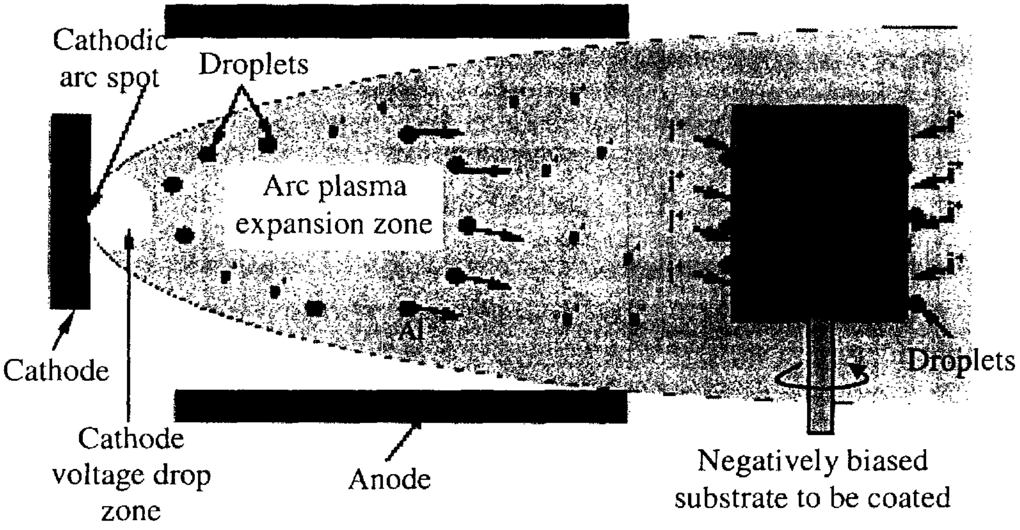

Figure 2.18 Scheme of the conventional direct cathodic arc deposition process [http://www.arcomac.com/technology.html]

For the deposition of TiAl-based coatings, the following techniques are the most widely used ones: cathodic arc vapor (plasma or arc ion plating) deposition [Han, et al., 1996; Wang, 1997; Suzuki, et al., 1998; Eizner, et al., 1996 Eizner; Ikeda and Sato, 1991]; magnetron sputtering (or sputter ion plating) [Kukla, 1997; Prengel, et al., 1997; Lugscheider, et al., 1999; Schäffer and Kleer, 2000]; and combined magnetron and arc processes [Donohue, et al., 1997; Smith, et al., 1997; Schönjahn, et al., 2000; Yamamoto, et al., 2005]. These PVD processes differ with respect to the type of evaporation of the metallic components and the plasma conditions employed during the deposition process. The transition of the metallic component to be deposited from a solid to a vapor phase (in which metal atoms are ionized in different ways) may be performed by the heating of an evaporation source (as in cathodic arc) or by sputtering of a target (as in magnetron sputtering). Cathodic arc and magnetron sputtering techniques allow for the evaporation of metals with different melting points such as Ti and Al from a Ti-Al alloy cathode/target. In the case of arc evaporation, a small limited cathodic area is evaporated with a very high energy arc that quickly moves over a spot on the metal surface to be evaporated. The plasma generated consists of highly ionized metal vapor [Lugscheider, et al., 1996]. In the case of sputtering, atoms are ejected mechanically from a target by the impact of ions or energetic neutral atoms, vacuum vaporization, ion implantation, etc. The most important and widely used methods for hard coatings are ion plating and magnetron sputtering. During deposition, the high-purity, solid coating material such as titanium, chromium and aluminium is either evaporated by heat or by bombardment with ion (sputtering). At the same time, a reactive gas (e.g. nitrogen or a gas containing carbon) is introduced; it forms a compound with the metal vapor and is deposited on the tools or components as a thin, highly adherent coating. In order to obtain a uniform coating thickness, the parts are rotated at uniform speed about several axes. The properties of the coating (such as hardness, structure, chemical and temperature resistance as well as adhesion) can be accurately controlled. PVD coatings are most widely used for a variety of cutting and stamping tool applications. This coating type has a few advantages when compared to CVD ones. In addition, PVD coatings do not embrittle the substrate material. This is very important for the majority of substrate materials of interest, including tool steels and other engineering materials. Lastly, the PVD process is extremely flexible as it is possible to synthesize a wide variety of coating compositions and multi-layer combinations, having unique structure characteristics and properties. Included in this are nano-structured materials, which are usually unattainable using other surface engineering techniques.

However, PVD processes have low operating pressures, usually between 0.1 and 1 Pa, which make PVD methods line-of-sight processes so that substrate rotation is necessary to obtain homogeneous and uniform coatings over relatively simple geometries.

In contrast to CVD process, PVD process generally induces desirable compressive residual stresses in the coating which is important for intermittent cutting processes like ball end milling. In addition, PVD processes can generate very thin coatings which are able to retain a very sharp cutting edge. Overall PVD processes are more flexible and have a wider range of applications than CVD coatings.

2.4.3 Hybrid vacuum deposition processes

Hybrid processes can involve the use of very different coatings or surface modification techniques, for example, PVD Arc processes combined with PVD magnetron sputtering [Donohue, et al., 1997; Smith, et al., 1997; Schönjahn, et al., 2000; Yamamoto, et al., 2005, Jeon, et al., 2004; Larsson, et al., 1996], PVD or CVD combined with CVD [Restello , et al., 2006]. Hybrid processes generate hybrid coatings and micro- or nano-laminated hybrid coatings offer opportunities to establish unique and controllable coating characteristics. A variety of interlayers have been used in hybrid coatings for various purposes [Celis et al., 1999]:

1. To enhance the adherence between coatings and substrates;
2. To prevent crack initiation and propagation;
3. To improve shock resistance;
4. To tailor the thermal expansion characteristics, which leads to good interfacial strength;
5. To prevent diffusion between substrates and coatings;
6. To enhance corrosion protection of coatings and substrates;
7. To enhance sliding wear resistance or lower sliding friction.

PalDey and Deevi (2002) reviewed coating deposition techniques and indicated that the most widely used techniques to deposit titanium-aluminum based coatings are:

- Cathodic arc vapor (plasma or arc ion plating) deposition process due to their Good adhesive strength.
- Magnetron sputtering (or sputter ion plating) due to its good surface roughness properties.
- Combined magnetron and arc processes which result in good adhesive strength and good surface roughness. For instance, the Arc Bond Sputter (ABS) PVD technique was developed by combining the features of a steered cathodic arc and an unbalanced magnetron process.

The advantages of cathodic arc ion plating:

- The cathodic arc process generates the highest quantity of ionized target atoms, 50~100%.
- High deposition energy resulting in a dense coating.
- High level of adhesion to the substrate due to the effect of ion bombardment or ion etching. During bombardment, high energy metal ions generated from the cathode bombard the substrate surface which is kept at a high negative bias of 500~2000V. In addition to cleaning and heating the substrate, energetic metal ions also knock off some metal atoms from the substrate or may penetrate the substrate lattice to atomic levels. This leads to defects and roughness on the substrate at an atom level and it is believed to be responsible for the improved adhesion of the coating.

The disadvantage of cathodic arc ion plating:

- The formation of macro particles (macro droplets) which are caused by the droplet formation during arc evaporation of a low melting point material and by the excess quantity of atoms that are produced by the very fast evaporation process which are not completely ionized before they arrive at the substrate surface.

Magnetron sputtered coatings have a columnar structure and a smooth coating surface without the presence of macro particles but the quantity of ionized target atoms is very low (1~5%).

Attempts have been made on reducing or eliminating the macro particles by employing filtered arc deposition (FAD) techniques [Fox-Rabinovich, et al., 2004] or magnetic filters [Yamamoto, et al., 2003]. Magnetic filters are the common way to reduce the formation of macro-particles, particularly when the target material contains a high amount of low melting point materials such as Al. According to the report [Yamamoto, et al., 2003], the number of emitted macro particles is greatly reduced by the implementation of the plasma enhanced arc-cathode (magnetic filters) and the surface roughness of the coating is also significantly improved from 0.16 to 0.08 μm (Ra).

Figure 2.19 is the schematic layout of a hybrid deposition process which combines the filtered arc deposition technique and the unbalanced magnetron sputtering process for the deposition of a multilayer nano-structured TiCrCN/TiCr+TiBC coatings [Gorokhovsky et al., 2006].

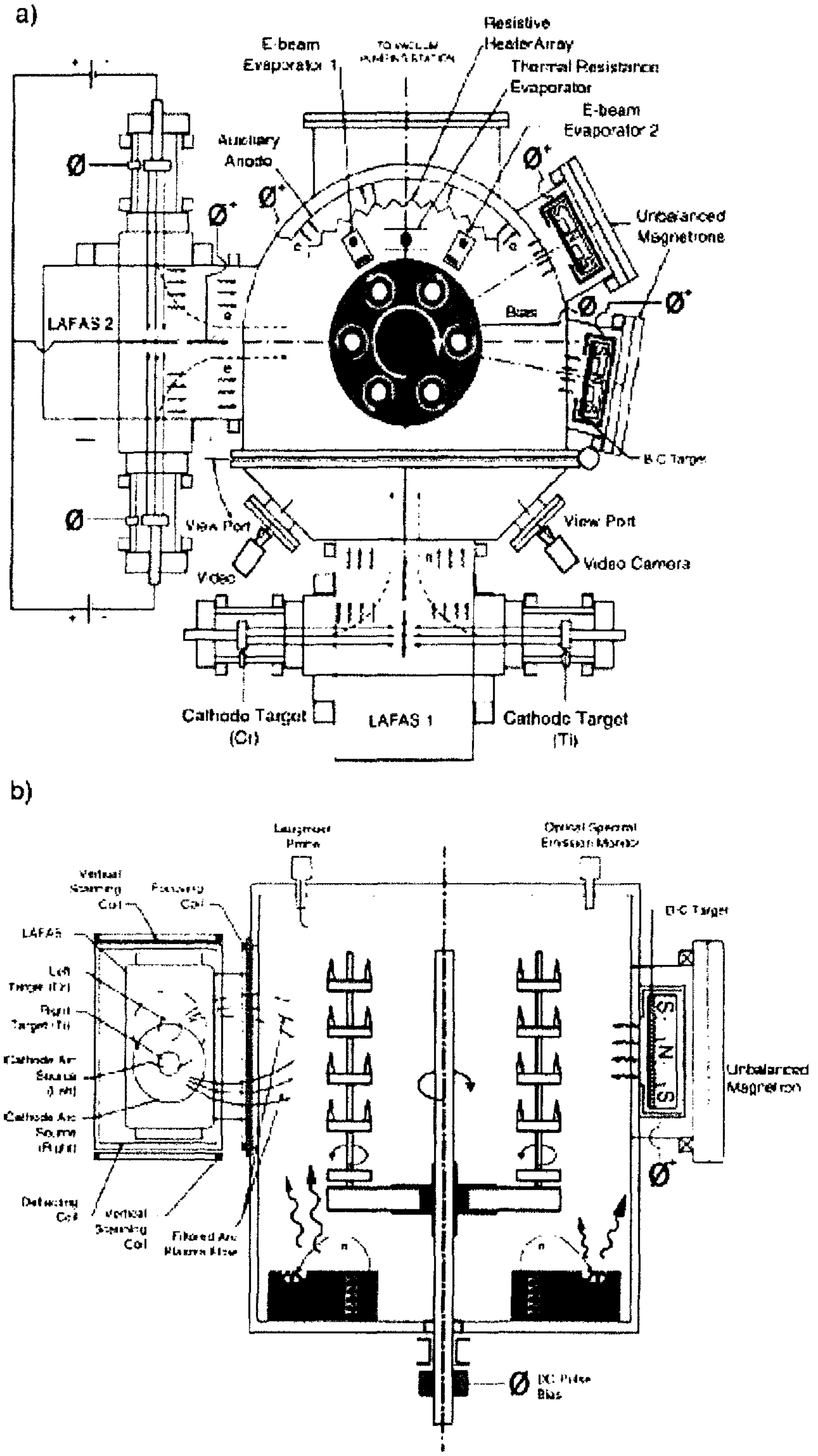

Figure 2.19 Schematic diagram of hybrid deposition (large area filtered arc deposition-unbalanced magnetron sputtering): a) top view, b) side view [Gorokhovsky et al., 2006]

2.5 Recent Developments in Hard Coatings

Engineering hard PVD coatings can be classified into five categories according to the coating structure. They are multi-component coatings, multiple-layer coatings, super-lattice coatings, dispersion coatings and nano-structured coatings [Jehn, 2000]. Based on the behavior of the coating in service, some recently developed coatings include self-lubricating coatings and smart coatings also referred to as self-organized coatings or self-adaptive coatings [Fox-Rabinovich, et al. 2006].

2.5.1 Multi-component coatings

Multi-component coatings include binary, ternary, quaternary and high component coatings.

The first successful binary hard coating materials were TiN and TiC. Their wear behaviors strongly depend on the applications such as working speed, workpiece materials and working temperatures. An improvement was found by alloying the binary components with metal and/or metalloid components.

Ternary coatings are carbonitrides of various compositions, e.g., Ti(C,N), and the addition of aluminum, e.g., (Ti,Al)N. The degree of improvement was very different when different working conditions were chosen. This especially holds true for (Ti, Al)N, for which the increase in tool life is much more pronounced under high cutting speeds when compared to TiN at standard conditions [Knotek, et al, 1987]. Also, the amount of the alloying element used strongly influences the wear behavior. Such investigations were extended to a large number of elements such as Cr, Nb, Zr, Hf, V, Mo, W, Al, Si. The base metal in most cases is titanium and to some extent also chromium [Jehn, 2000].

The study of quaternary and even more component coatings are focused on (Ti, Al)N based coatings with the additional elements such as V, Y, Si, Cr, W, Zr, Hf, Mo, B. It was found that a marked improvement in high temperature oxidation resistance with the use of a (Ti, Al, Y)N coating [Donohue, et al., 1997] and a (Ti, Al, Cr)N coating [Lewis, et al., 1999; Fox-Rabinovich et al.,2006]. Further, Y and Cr additions to (Ti, Al)N resulted in an even better oxidation resistance [Lewis, et al., 1999; Pflüger, et al., 1999]. A recent study by Fox-Rabinovich, et al. (2006) showed that small additions of Si and Y to (Ti, Al, Cr)N, of the form $Al_{55}Ti_{20}Cr_{20}Si_3Y_2N$, give excellent oxidation resistance. The coating improvements come from an increase in chemical stability, reduced adhesion to the workpiece materials and an increase in the oxidation resistance of the surface. On the other hand, the alloying additions result in a finer grained structure approaching an amorphous coating structure because of the altered diffusion parameters of the deposited atoms [Jehn, 2000]. In one situation, the lattice structure of the binary nitrides can contain high amounts of 'third' elements, like Al in (Ti, Al)N, without any change in the lattice structure. In contrast to this behavior, two- and multi- phase coatings can be found, like nc-TiN/α-Si_3N_4 in TiAlSiN coatings. In many cases ternary coatings show an amorphous structure as found in WSiN [Jehn, 2000].

The elements, molybdenum and tungsten are known as solid lubricants. They are added to modify the tribological properties of a hard coating. The coatings with 8% MoS_2 incorporated into the fcc structure of TiN are suitable for dry machining [Jehn, 2000].

2.5.2 Multiple-layer coatings

The idea of multi layered coatings is to assemble coatings with different functional layers to enhance adhesion, stop diffusion, arrest cracking, equalize stress, support load and provide outer layers selected for their friction and wear resistance.

A well known combination is a $TiC/Al_2O_3/TiN$ coating on a cemented carbide substrate. TiC has the close thermal expansion coefficient to cemented carbide and hence strong adhesion to the substrate is expected. Al_2O_3 has very low thermal conductivity (a temperature range of 20 ~ 1200 °C, the corresponding thermal conductivity is 25.8 ~ 5.43 $W/m/^{o}K$ [http://www.memsnet.org/material/]) so that it protects the substrate from heat attack during cutting. While TiN provides good wear resistance. For dry machining applications, B, W and MoS_2 are found to have good tribological properties. For example, an improvement of the tribological properties was found with TiN/TiB_2 coating. Lubricating layers of WC/C on top of TiN or TiAlN hard coatings, or MoS_2-based top layers on hard coatings like TiAlN, or MoS_2 layers on top of DLC coatings exhibit significant advantages when dry machining or using Minimum Quantity Lubricant (MQL) cutting [Jehn, 2000].

2.5.3 Superlattice coatings

Superlattice coatings are deposited based on the technology of layer sequence deposition. Such layer sequence structure can be easily deposited by PVD methods either by switching different sources on or off and by rotating the samples passed the different sources. The layer thicknesses possible with this technology are in the range of a few nm to approximately 100nm with a maximum hardness found to occur for coatings in the range of 5 – 20 nm. All coatings developed in this way aim to interrupt the perpendicular grain growth or improve the tribological properties of the coating. Because of the structure, superlattice coatings have the following common advantages:

- The numerous interfaces can result in an increase of hardness and strength because of grain size reduction.
- The crack propagation resistance of a superlattice coating increases due to the interfaces between layers.
- With a lubricant layer a superlattice coating can reduce cutting friction as compared to a coating with only a top lubricant layer.
- Generally, superlattice coatings result in an increase of tool life.

2.5.4 Dispersion/multiphase coatings

Dispersion coatings are characterized by the presence of a second phase in the form of small particles embedded in the coating matrix [Jehn, 2000]. In this case the deposited materials are very different in type or have very different lattice structures. Such coatings can be formed when depositing two different materials which do not form a completely mutual solid solution. For example, two- or three-phase coatings (TiN, TiB_2, BN) were observed in a Ti-B-N system depending on the process parameters and chemical composition [Rebholz et al., 1998]. It is not possible to predict a general tendency of the properties because of the different amounts and properties of the single phase as well as of the general influence of the process parameters [Jehn, 2000].

Multiphase composite coatings tend to be dense and fine grained because columnar grain growth is interrupted by the nucleation of another phase [PalDey and Deevi, 2003]. The benefits of dispersion coatings include the improvement of hardness, toughness and tribological properties depending on specific cases. For example, dispersed MoS_2 crystallites in a hard coating matrix can reduce the coefficient of friction and is suitable for dry cutting applications. The advantage of this structure is that the lubricant is dispersed and so there is a more continuous supply of the lubricating compound over the working life of the tool as compared to a simple MoS_2 top layer coating structure which disappears once it is worn away [Gilmore et al., 1998].

2.5.5 Nano-structured coatings

Nano-scaled coatings include multilayered coatings with individual layer thickness of a few nanometers, dispersion particles in the range of a few nanometers and structure modulations on the nanometer scale. Nano-composite coatings ($AlTiN/Si_3N_4$) exhibit extremely high hardness [Veprek, 1997]. The nano-scaled protective and functional tribological coatings (TiAlCrN/WN and TiAlCrN/NbN) show excellent tool performance under dry high speed cutting applications [Ning, et al., 2006, 2007].

2.5.6 Self-lubricating coatings

Self-lubricating coatings includes a lubricating compound in their structure that critically enhances the tribological characteristics of wear resistant coatings. Basically, there are two ways to achieve self-lubricating functions. One way is through the embedding of lubricious layers in the coating, for example, TiN-MoS_2 and TiAlN-MoS_2 [Lahres, et al., 1999]. This type of coating has the commercial name MoST and is a well known low friction coating. The MoST coatings are very efficient for cutting at low and moderate speeds as well as for stamping tools applications when intensive galling and seizure takes place. Further improvement can be gained by functionally grading the embedding lubricious layers. One example is to combine a relatively hard TiAlN phase with a softer MoS_2 phase with an increase in density of the latter phase toward the top of the surface [Savan, et al., 1999]. The limitation of these coating applications is the thermal stability of the lubricating layers. Another way is to design self-adaptive coatings which can form tribo-oxdes on the surface of a hard coating in response to the cutting conditions present. In this way tribo-films can play a key role as a solid lubricant during cutting.

2.5.7 Self-adaptive/self-organized/smart coatings

Self-adaptive, self-organizing and smart coatings have a similar concept, i.e., the coating systems are able to provide an optimum response to some external stimulus. They react to outside conditions, such as temperature, stress, strain or the environment, in a selective way. A common example is coated glass which changes its properties under high levels of light.

In metal cutting, the new generation of ‘smart’ wear resistant coatings is the multi-layered coatings that have a number of layers that meet the requirements of current stage of the wear processes [Fox-Rabinovich and Totten, 2007]. The service life of smart coatings can be divided into three stages, i.e., running-in stage, self-organizing stage and catastrophic stage, corresponding to the three phases of tool life. Running-in means that the cutting tool completes the first stage of tool wear at a very short period of cutting time and then starts the second stage of tool wear.

The service performance of multi-layered 'smart' coatings greatly depends on the state of the running-in stage because not every mode of the running-in phase can result in the tribological compatibility of the cutting tool/workpiece system [Kostetsky,1993; Bershadskiy, 1992]. Damaging modes during the running-in stage are also possible, especially during cutting. Thus the goal of friction control is to prevent serious surface damage at the running-in stage and transform the tribo-system from its initial state into a self-organizing mode.

In summary, the multi-layered 'smart' coatings for metal cutting should have the following properties:

- The coating should be able to form an anti-frictional layer as soon as the running-in stage is completed.
- The coating should be able to form protective and stable compounds to protect the tool from mechanical, chemical and thermal attack during cutting.
- The coating should be able to shorten the running-in stage and enter a self-organizing mode, start the stable stage of wear with a very low surface damage, maintain the self-organizing stable stage and hence prolong the tool life.

2.6 Characteristics of Hard Coatings

Coating properties include mechanical, chemical and thermal properties at room temperature and the elevated temperatures associated with dry high speed machining. Hardness, adhesion strength, chemical inertness, fracture toughness, thermal barrier and low friction are the basic requirements for hard coatings in this application.

Numerous technologies are involved in determining the properties of a coating. For example: destructive (indentation, scratch and impact tests) and non-destructive (laser ultrasonic, electron, neutron and X-ray sources) methods are used to determine the properties of coatings. FEA has been also used to determine the elastic-plastic properties of coatings [Bouzakis, et. al, 2001, 2003]. With Laser ultrasonic methods, the thickness of a coating and its elastic parameters can be obtained simultaneously [Schneider, et al., 1992]. Indentation testing and scratch testing can be combined to determine the hardness, elastic modulus, coating and interfacial fracture toughness and residual stress [Bouzakis, et al., 2001; Dyrda and Sayer, 1999; Xie and Hawthone, 2002; Harry, et al., 1999; Ivkovic, 2002] while impact testing can be used to determine the fatigue strength of the coating [Beake et al., 2004; Bouzakis, et al., 2002]. Furnaces and precise weight scales are commonly used for testing both short-term and a long-term oxidation resistance [Fox-Rabinovich, et al., 2005]. X-ray diffraction techniques have been used for measuring the residual stress through X-ray penetration depth and for analyzing the texture (orientation) of coatings [Takago, et al., 2002].

2.6.1 Microhardness

Nano-indentation hardness testing is used to characterize the micro-hardness, elastic modulus and to some extent fracture toughness of a coating. The operating principle is as follows: an indenter tip, normal to the sample surface, is driven into the sample by applying an increasing load up to a predefined value. The load is then decreased until partial or complete relaxation of the material occurs. The resultant load-depth curve is then used to calculate the mechanical properties such as hardness and elastic modulus. The load should not be more than 50 grams. The optimum load is 20 to 50 grams, which has to be guaranteed low enough so that the indenter does not penetrate through the coating. Beake and Smith (2004) indicated that there is no "safe depth range" at which the elastic response of a coated system to indentation is free of substrate influence, but the choice of a very low indentation depth should minimize the substrate contribution and provide a reasonable estimate of the elastic modulus of the coating. In their nano-indentation tests, the contact depth was 2-6% of the total coating thickness.

The output from the nano-indentation test is the load-penetration depth curve shown in Figure 2.19. Based on this curve the hardness and the reduced elastic modulus of a coating can be evaluated. As shown in Figure 2.20, ABC is the loading phase and CDE is the unloading phase; point C has the maximum load $P_{\max}$ and maximum penetration depth h_t. After unloading, the residual depth is h_r due to the spring-back of the deformed material. The area ABCF represents the total work (W_t) done by the external force and the area EDCF is the elastic work (W_e) by the spring-back of the deformed materials. Thus the plastic portion of the work (W_p, the area ABCDE) can be obtained by the difference of W_t and W_e.

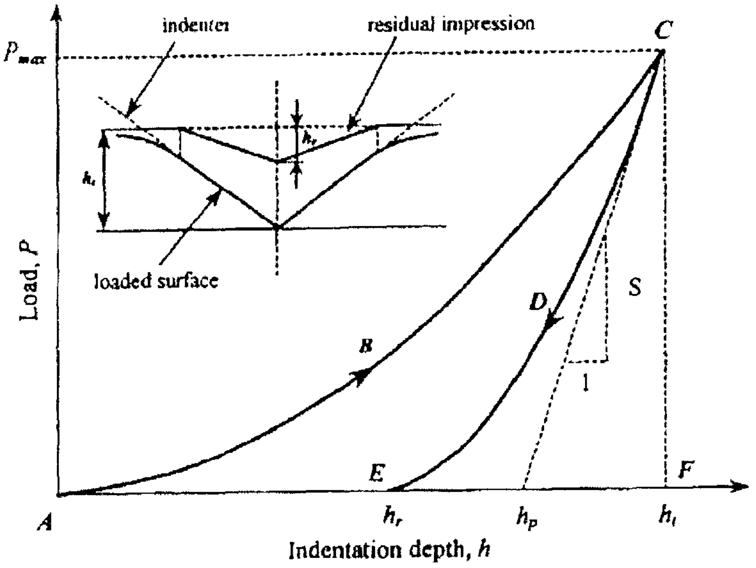

Figure 2.20 Load-indentation curve [Bruno, et al., 2003]

$$W_t = \int_0^{h_t} P_{loading}(h)\, dh$$

$$W_e = \int_0^{h_t} P_{unloading}(h)\, dh$$

$$W_p = W_t - W_e$$

The slope of the load-penetration depth curve at the maximum indentation depth is given by the following formulas [Bruno, et al., 2003]:

$$S = \left. \frac{dP_{loading}}{dh} \right|_{h=h_t} = \alpha \cdot E_r \sqrt{A}$$

Therefore, the reduced elastic modulus E_r is given by:

$$E_r = \frac{S}{\alpha \cdot \sqrt{A}}$$

here S represents the stiffness of the contact between the indenter and the coating specimen; A is the projection of the contact area; E_r is the reduced elastic modulus; α is a constant and equal to 1.167 for a Berkovich indenter.

The reduced elastic modulus E_r is also expressed as:

$$\frac{1}{E_r} = \frac{1-\upsilon_i^2}{E_i} + \frac{1-\upsilon_f^2}{E_f}$$

where E and υ are the elastic modulus and Poisson ratio and the suffix i and f represent the indenter and the film, respectively.

The relation between the penetration depth and the projection of the contact area for a perfect pyramidal or conical tip is:

$$A = kh_p^2$$

where h_p is the effective penetration depth defined in Figure 4.6 and k is a constant equal to 24.5 for Berkovich and Vickers indenters.

The hardness is defined as the maximum applied load divided by the projection of the contact area:

$$H = \frac{P_{\max}}{A}$$

Hardness is the most basic mechanical property to determine the wear resistance of a surface. In tooling applications, a variety of wear modes are involved such as abrasion, adhesion, attrition, diffusion, oxidation, plastic deformation and fracture. Hardness directly affects abrasive wear, which is the wear mode existing at all the stages of tool life. However, high hardness is usually associated with high brittleness, which generally results in poor fracture toughness. Therefore, coatings with a combination of high hardness and good toughness should be designed for tooling applications.

The ratio of W_p / W_t and h_r / h_t describes the elastic-plastic behavior of the material during a nano-indentation test.

The elasticity index K_e is considered as an elastic recovery parameter or a parameter of energy accumulation and is given by:

$$K_e = \frac{W_e}{W_t}$$

The plasticity index K_p is a parameter of energy dissipation during plastic deformation and is estimated by:

$$K_p = \frac{W_p}{W_t} = 1 - K_e$$

The relationship between the plastic index and the H / E_r ratio holds as follows [Beake, et al., 2007]:

$$\frac{W_p}{W_t} \approx 1 - 5\left(\frac{H}{E_r}\right)$$

W_p / W_t and H / E_r are the parameters that are found to have a positive relationship with fracture toughness of a coating. In general, coatings with higher W_p / W_t or lower H / E_r exhibit better fracture toughness.

The microhardness of a coating is greatly related to the resistance of abrasive wear. Hard coatings contribute to increased abrasive wear resistance as long as they maintain a higher hardness than the substrate at the machining temperature [Prengel, et al., 1998]. The abrasive wear is caused by hard particles/abrasives in the workpiece, e.g. cementite (microhardness 1200HV), chromiumcarbide (1700 HV) or alumina (2000HV), rubbing against the tool. To reduce abrasive wear the difference of hardness between the tool and the abrasives has to be as larger as possible.

When the cutting temperature is low, the microhardness at room temperature can be used as a coating selection criterion. However, when the cutting temperature is high, the coating selection has to consider hot hardness.

Chemical composition, coating structure such as multilayer, multi-phase coatings, grain size and even coating thickness are also factors that can be used to control the effective microhardness [Yao and Su, 1997].

2.6.2 Coating Adhesion

Coating adhesion to the substrate is one of the essential properties of a successful coating. If the adhesion strength is not high enough, the coating will be peeled away during cutting.

Scratch testing is a well-established qualitative method to assess the adhesion of the coating to the substrate. As shown in Figure 2.21, a spherical indenter is drawn across the coating surface under an increasing applied normal load. Coating adhesion is assessed from the critical load, Lc, at which delamination or other types of coating failure occurs. This is shown in Figure 2.22. Although acoustic emissions can be used to detect coating failure, the assessment is usually made by microscopic examination of the track after the scratch has been made.

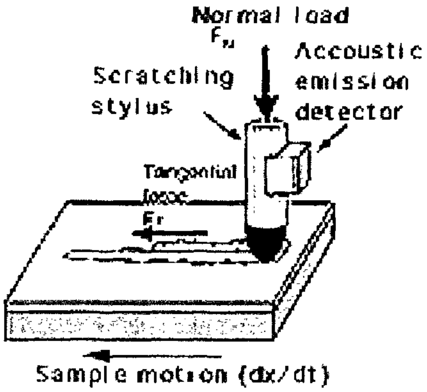

Figure 2.21 Scratch test

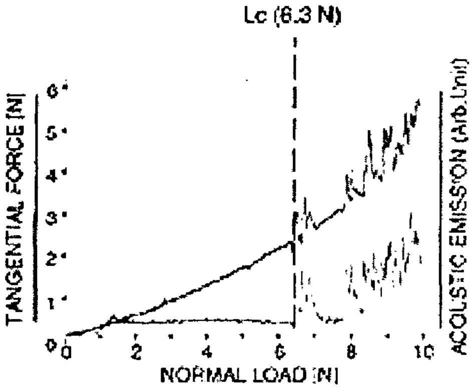

Figure 2.22 Experimental results

(http://www.csm-instruments.com/frames/csemsom.html)

From the scratch test the frictional force F_T can be measured and then the effective friction coefficient can be estimated using $\mu_{eff} = F_N / F_T$. If the curve of tangential force versus normal force does not obviously show the critical load as in Figure 2.23 a), the curve of effective friction coefficient versus the normal load may be used to find the critical load as in Figure 2.23 b) [Dyrda and Sayer, 1999]

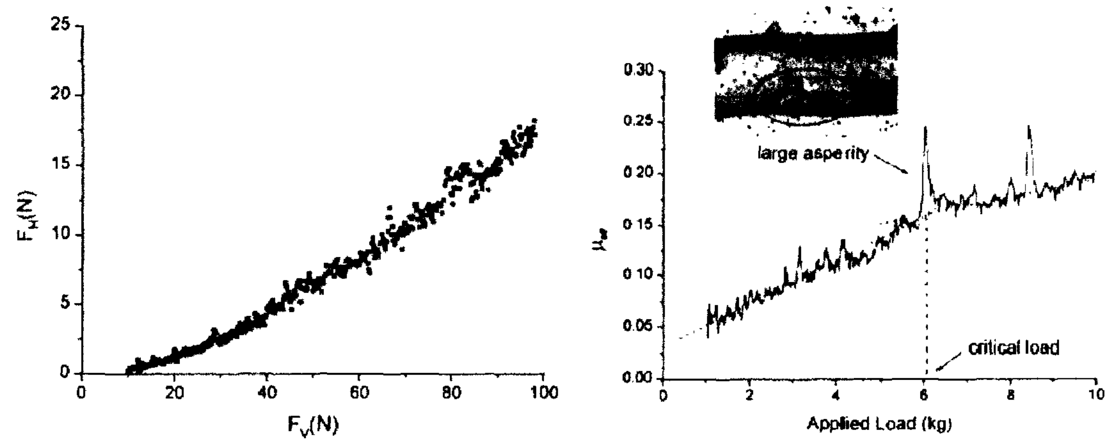

a) Friction load vs. normal load b) Vertical load vs. friction coefficient

Figure 2.23 The assessment of coating adhesion strength [Dyrda and Sayer, 1999]

If the scratch tests can be performed under elevated temperatures the adhesion strength at elevated temperatures can be determined too.

Coating adhesion can be increased by choosing the right underlayer in a multilayered coating. Material thermal expansion is one of the important properties affecting coating adhesion. For example, choosing TiC or TiCN as an interlayer for a WC substrate can achieve higher adhesion strength since their thermal expansion coefficients are closer to the one of WC as compared to TiN and Al_2O_3, shown in Table 2.2. It was reported that SiC thin films present a minimal thermal expansion coefficient mismatch when compared to WC-Co (5.3×10^{-6} K^{-1} *vs.* 5.4×10^{-6} K^{-1}) [Costa and Camargo, 2002]. Unfortunately, SiC has a very high dissolution rate in iron, therefore, it is not suitable for cutting steels because it dissolves in chips during machining [Fox-Rabinovich and Totten, 2007].

Table 2.2 Thermal expansion coefficients [Tsuchiya, 2004; Costa and Camargo, 2002]

Materials	Thermal expansion coefficient (K^{-1})
SiC	5.3×10^{-6}
WC	5.4×10^{-6}
TiC	7.4×10^{-6}
TiCN	8.4×10^{-6}
TiN	9.4×10^{-6}
Al_2O_3	8.2×10^{-6}

There are some other approaches to achieve better adhesion such as energetic bombardment, surface etching, surface treating, etc. [Tonshoff, et al. 1998, 2001 and 2002; Prengel et al., 1998] . Energetic bombardment on the substrate can create lattice defects that enhance rapid diffusion of a coating species at the interface and hence promote the bonding of diamond to a cemented substrate.

2.6.3 Fracture toughness

An impact fatigue test is used for accessing the fracture toughness of coatings. Figure 2.24 is a schematic of a NanoTest system from Micromaterials [Beake, et al., 2004]. This apparatus consists of a pendulum mounted on an essentially frictionless pivot such that a fixed or variable force can be applied to a test probe and the displacement of the probe can be measured by means of a capacitive transducer. A solenoid connected to a timed relay was used to produce the repetitive probe impacts on the surface. A cube-corner diamond indenter test probe was accelerated from a distance of 11 μm from the surface to produce each impact at applied loads of 15 mN. The experiments were computer controlled so that repetitive impact occurred (at the same position). The frequency was one impact every four seconds, while the test time was 600 seconds. Every test was repeated five times at different locations on each sample. Repetitive impacts were performed at the same position on the sample. A sharp probe was used to induce fracture quickly. The depth of failure was monitored vs. time. A longer time to fracture of the coating under analysis is related to a tougher more durable coating.

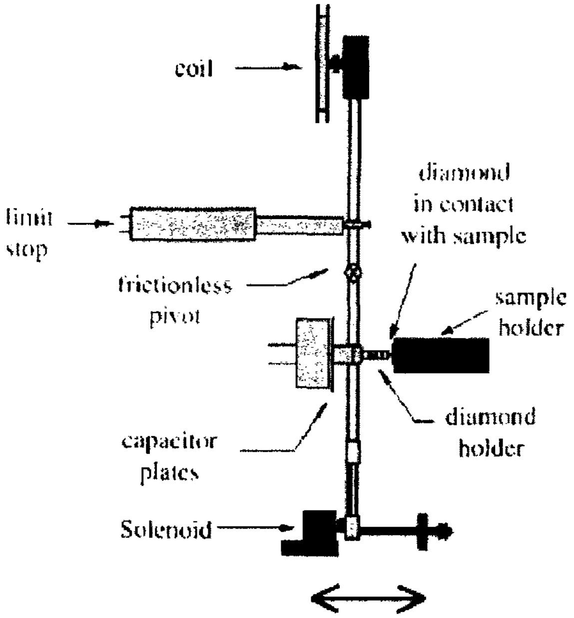

Figure 2.24 Schematic illustration of the NanoTest system for impact testing [Beake, et al., 2004]

Figure 2.25 shows how the results from impact tests look. From the curves (number of impacts verses depth), one can capture the advent of fracture in the coating.

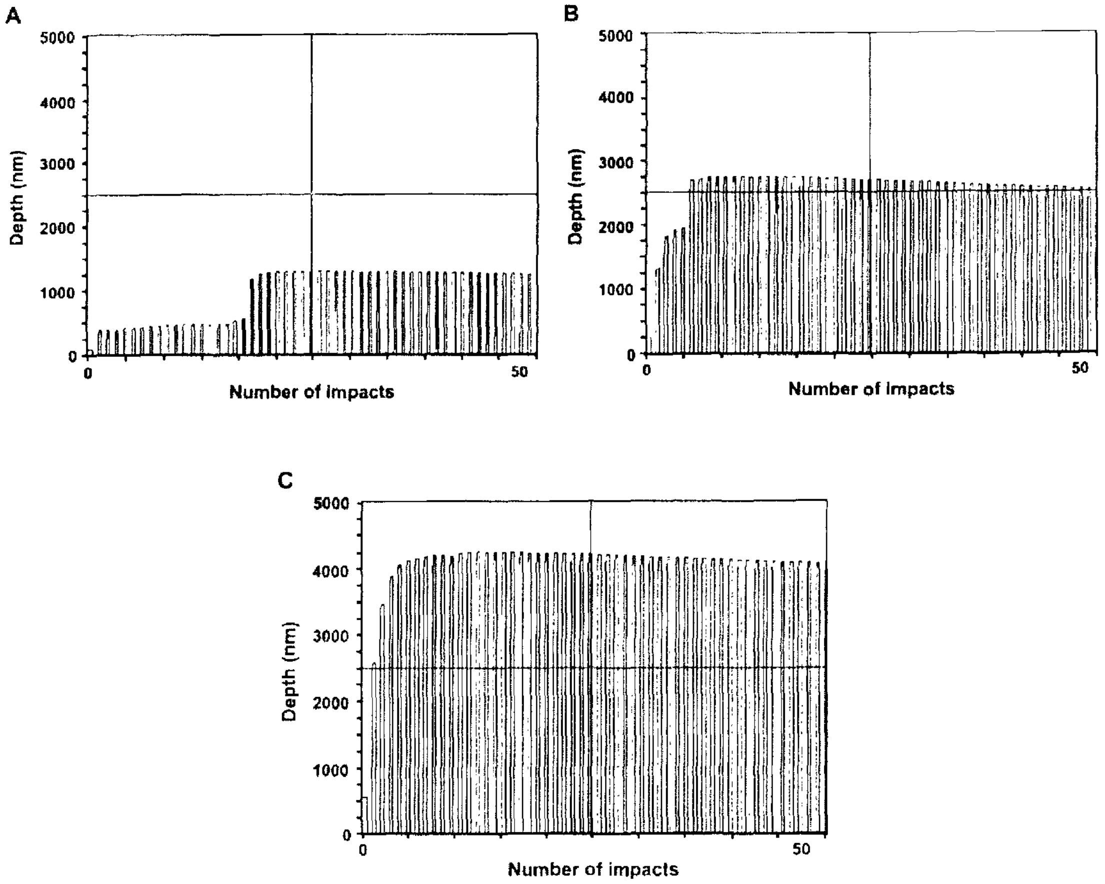

Figure 2.25 Illustrative impact results on the a-C:H coating samples

A) 1 mN; B) 5 mN; C) 15 mN. The number of impacts required for fracture is 18, 5 and 2, respectively [Beake and Smith, 2004].

2.6.4 Coefficient of Friction

A high coefficient of friction causes increased heat, leading to a shorter coating life or coating failure. However, a lower coefficient of friction can greatly increase tool life because a slick surface lets the chips slide off the rake face of the tool and a smooth surface can also reduce rubbing and ploughing in the tool nose area and on flank face, hence generating less heat.

Basically, there are two types of tribometers. One is linear tribometer, the other is rotational tribometer. A widely used experimental setup to measure friction coefficients and wear rates is the pin-on-disk test.

Figure 2.26 shows a linear tribometer. The linear tribometer reproduces the reciprocating motion. The instrument produces a friction coefficient for both the forward and backward movements of the stroke. In addition, the linear tribometer can be equipped with a heating element for testing a wide variety of temperatures.

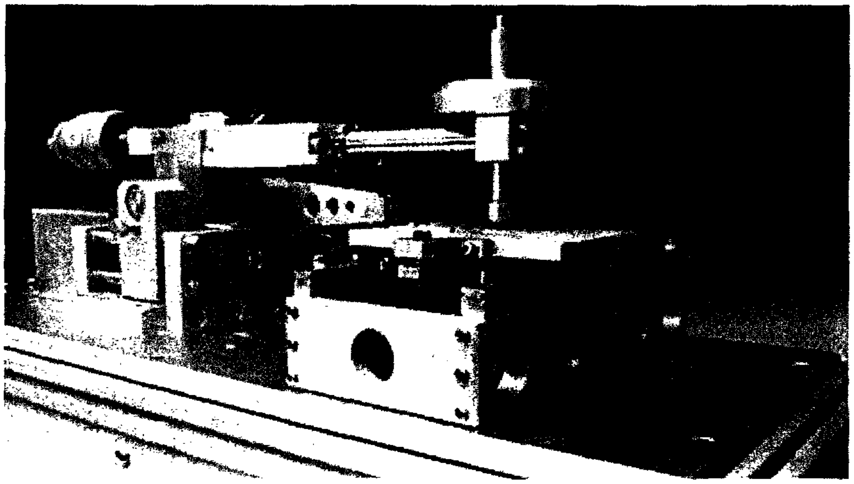

Figure 2.26 Linear tribometer (Linear speeds can go up to 100Hz with displacement as long as 105mm) [http://www.nanovea.com/tribometer.html]

Figure 2.27 shows a pin-on-disk tribometer. Pin-on-disk tribometer operates on the following principal:

- A flat, pin or sphere is loaded onto the test sample with a precisely known weight.
- The highly stiff elastic arm insures a nearly fixed contact point and thus a stable position in the friction track.
- The friction coefficient is determined during the test by measuring the deflection of the elastic arm of by direct measurement of the change in torque.
- Wear coefficients for the pin and disk material are calculated from the volume of material lost during the test.

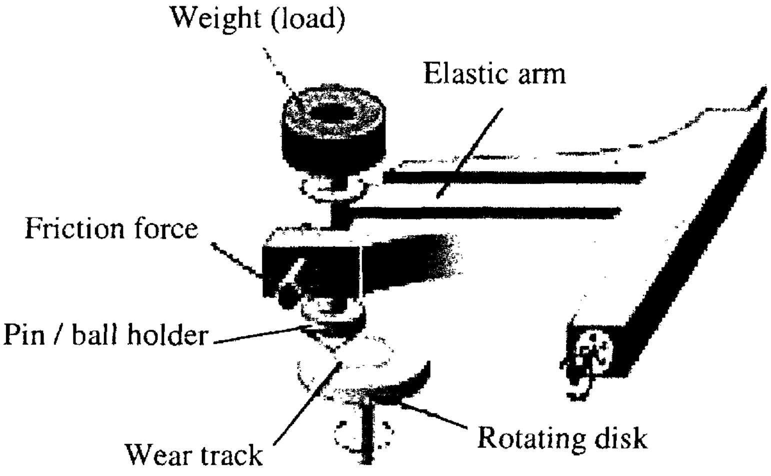

Figure 2.27 pin-on-disk tribometer [http://www.csm-instruments.com/]

This method can be used to determine the friction and wear behavior of almost every solid state material combination, with varying time, contact pressure, velocity, temperature, humidity, lubricants, etc. With a removable heating element enabling the rotating disk to reach temperatures up to 800° C (1000° C optional), the tribometer can be used for the analysis of friction and wear properties of materials at elevated temperatures (Figure 2.28a). Figure 2.28b shows another high temperature tribometer made by CSM Instruments.

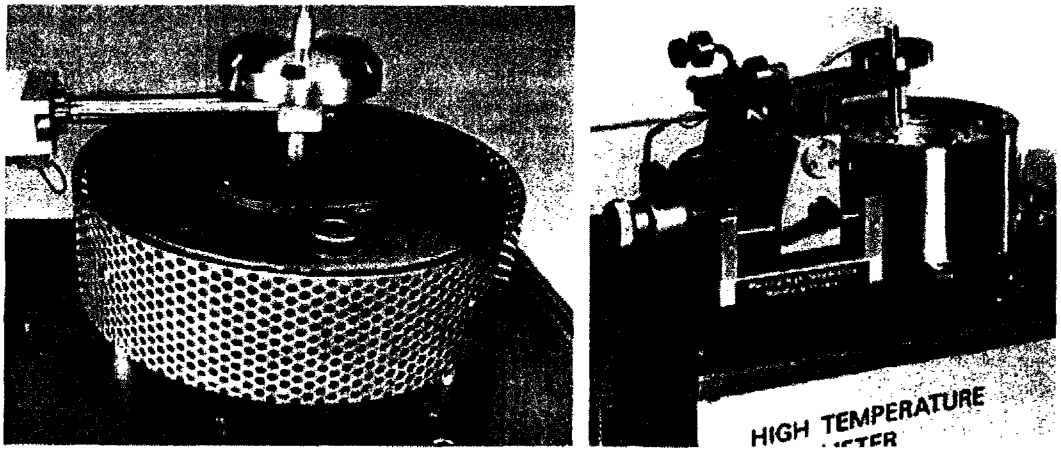

a) [http://www.nanovea.com/]

b) [http://www.csm-instruments.com]

Figure 2.28 High temperature pin-on-disk tribometers

Chapter Three

Basics of Coating Development

Machining is a cutting process in which the cutting tool interacts with the workpiece material and generates the machined surfaces and chips, as shown in Figure 3.1. Figure 3.1 also clearly shows that the interaction between the workpiece material and the cutting tool comes from three zones, i.e., primary shear zone, the secondary shear zone and frictional rubbing zone. In primary shear zone workpiece material is plastically deformed at a very high strain rate and a large amount of heat is generated. In secondary shear zone the freshly generated chips flow away through the rake face of cutting tool and more heat is generated and further plastic deformation takes place. In frictional rubbing zone, the rubbing and friction between the tool flank face and the machined surface cause more heat and plastic deformation. Together these zones are generally called the cutting zone or contact zone. During the interrupted cutting process such as milling, the cutting tool experiences both mechanical and thermal attacks, which is even worse than continuous cutting such as turning. Under severe cutting conditions, cutting tools experience intensive thermal attack and protecting the tools from thermal attack becomes more important with high speed machining as compared to conventional cutting processes. The heat that comes from these three zones diffuses into the substrate, the workpiece, and the chip body. Although the quantification of the contribution from the individual heat sources to the cutting temperature is unclear, it is obvious that a coating can definitely influence the level of heat created by the three heat sources and the proportion of the heat transmitting to the substrate. Figure 3.2 shows the role of coatings in the cutting process. In order fulfill all of these expectations coatings must be designed to protect the tool from thermal and mechanical attack under application conditions. This chapter shows the approaches used to design a coating for the proposed applications by choosing elements, controlling grain size, designing layered structures and employing the functionality of tribological compatibility.

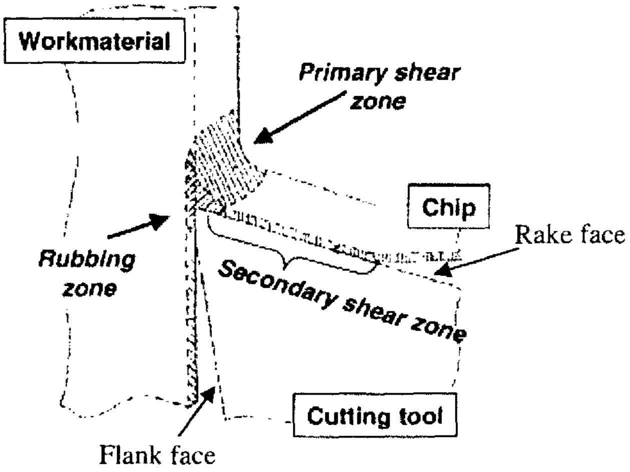

Figure 3.1 Three cutting zones [Rech, 2006]

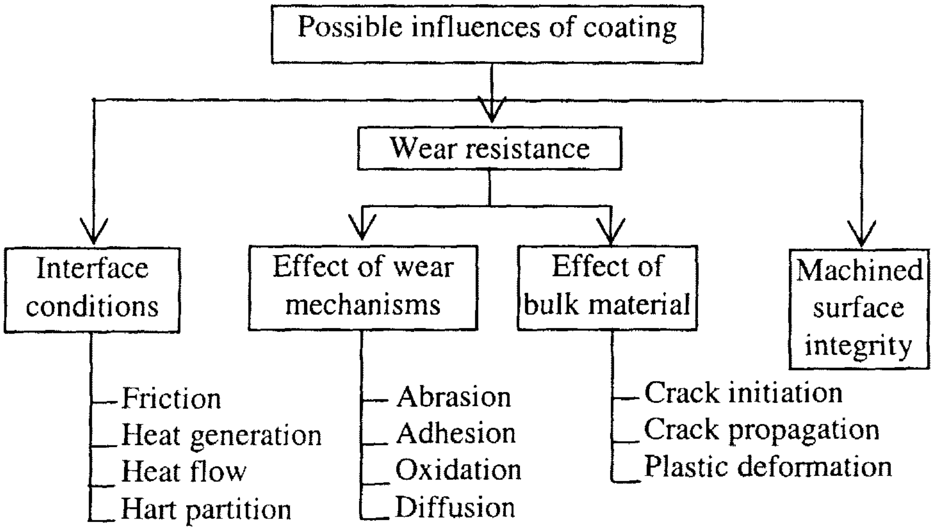

Figure 3.2 The factors the coatings affect during cutting process [Grzesik and Nieslony, 2003]

3.1 Requirements of Three Coating Zones

The protection of materials by hard coatings is one of the most important means of improving component performance, especially in the cutting tool industry. Designing a proper coating for a specific application is not easy because the requirements for the composite substrate/coating are often complex and many compromises must be accepted in order to meet the requirements. There are also three zones at the interface between the coating and the substrate, as shown in Figure 3.3. Each one has different requirements. The first zone is the interface between the substrate and the bottom layer of the coating where adherence, interaction/reaction of the substrate with the layer, and strains by thermal expansion misfit are critical points. The second one is the layer material within the coating where composition and microstructure determine properties such as hardness, strength, internal stress, fracture toughness, thermal stability, and thermal conductivity. The third one is the top surface of the coating where the interaction tendency of the layer material with the workpiece and the environment has to be considered.

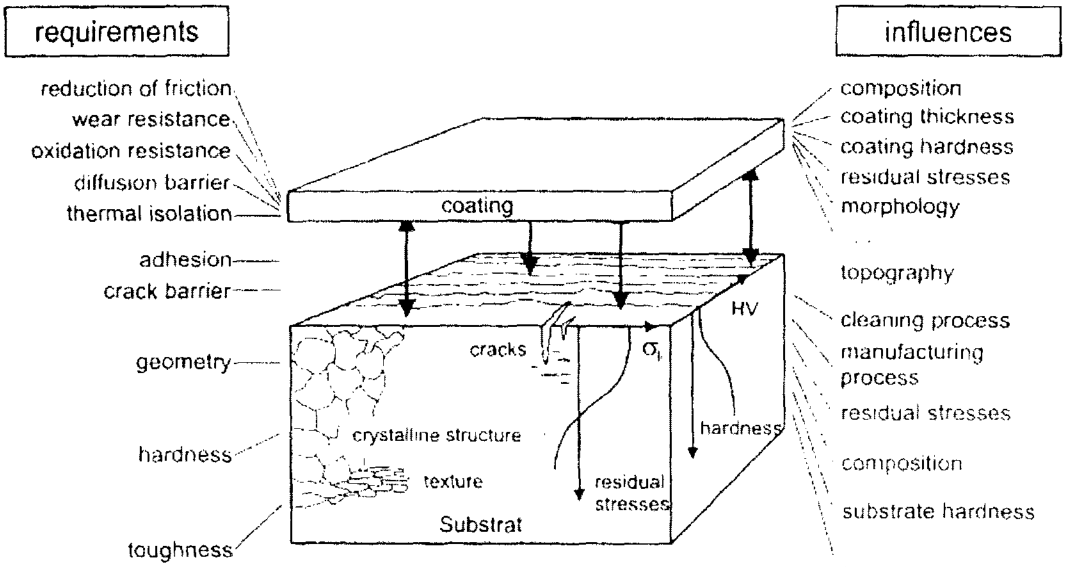

Figure 3.3 Requirements and influences on properties of the layer-substrate compound [Tönshoff, et al., 2002]

Although the coating is only 3~5 μm thick, it is expected to possess good adhesion to the substrate, a low friction coefficient, high hardness and toughness, good oxidation resistance, high hot hardness, good chemical and thermal stability as well as good crack propagation resistance for intermittent cutting tool applications. Therefore, it is very important to properly design and tailor coatings for specific applications.

3.2 Material Selection for Hard PVD Coatings

Selecting the right materials for a specific application is an important issue. The common elements for hard PVD coatings include the transition elements (Ti, V, Cr, Zr, Nb, Mo, Hf, Ta and W) because transition metals tend to have high tensile strength, density, melting and boiling points, and other elements such as Y, Al, Si, B, C, N and O, as described in Chapter 2.5. According to their chemical bonding character, hard materials for coatings can be divided into three groups, i.e., metallic hard materials (borides, carbides and nitrides of the transition metals), covalent hard materials (borides, carbides and nitrides of Al, Si, and B, as well as diamond), and ionic (ceramic) hard materials (oxides of Al, Zr, Ti and Be) [Holleck, 1986]. Figure 3.4 shows some of the underlying details.

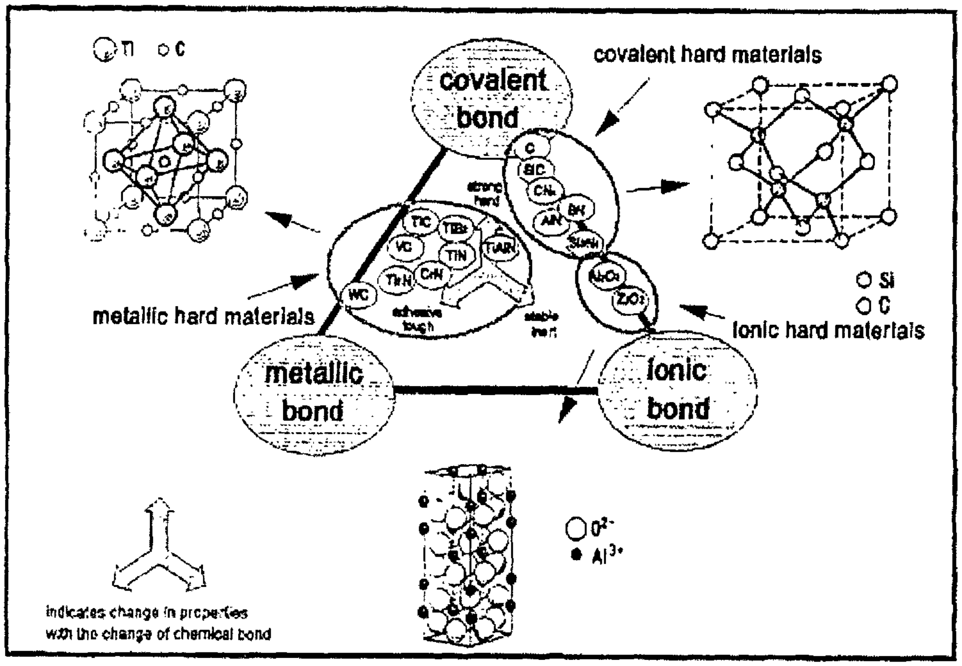

Figure 3.4 Different groups of hard materials with characteristic crystal structures [Holleck and Schier, 1995]

The typical properties of hard materials including metallic, covalent and ionic bonding are listed in Appendix A. Each group shows advantages and disadvantages with respect to specific applications. For example:

- Ionic (ceramic) hard materials are suitable for deposition on the top surface of a tool due to their high thermal stability and low interaction tendency [Holleck, 1986].
- Covalent bonded layer materials like AlN, BN, SiC and B_3C are difficult to realize as single layer coatings due to the lack of adherence or the high dissolution rate to metallic substrates like SiC. As a consequence covalent hard materials can be bonded into multilayer composites as wear resistant materials, improving high temperature properties [Holleck and Schier, 1995].
- The metallic hard materials seems to be the most common, suitable and versatile coating substances [Holleck, 1986].
- Optimum wear resistance can be achieved by multiphase or multilayer coatings [Holleck, 1986].

Numerous previous studies and applications have shown that (Ti, Al)N based coatings, which belong to metallic hard materials and have f.c.c lattice structure, have excellent performance under dry high performance machining due to the following major aspects:

- High hot hardness, as compared to TiC, TiN and TiCN, retains wear resistance under elevated temperatures.

- The formation of Al_2O_3, which belongs to ionic hard material with high thermal stability and low interaction tendency, protects the substrate.

Therefore, (Ti, Al)N based coatings are selected as the category for this study.

3.3 Effect of Coating Structures

Coating structures generally include monolayer, multilayer, multiphase, superlattice and nano-multilayer, etc. The idea of multilayer coating design comes from brittle ceramic bulk materials that use a fine grained multiphase structure with high amounts of interfaces which often provides an increase in toughness and crack propagation resistance [Holleck et al., 1995]. In addition to hardness, hard coatings are required to possess toughness because cracks, fractures or lack of adhesion due to high stresses can lead to early coating failure. The generation of interfaces in the coating by the formation of nanocrystalline or multilayer films should help to overcome these problems.

Multilayered coatings provide the following advantages:

- The deposition of alternative layers of different compounds can stop the grain growth. Therefore, the hardness of the coating increases due to grain size reduction and texture adjustment from columnar grained structure to a nanocrystalline structure.
- The numerous interfaces in multilayer coatings are the sites of energy dissipation and crack deflection leading to a drastic increase in toughness. Figure 3.5 shows the toughening mechanism.

- Individual columnar grains in a conventional PVD deposited coating deform plastically under mechanical loads resulting in large scale delamination of the coating as well as crack propagation in the perpendicular direction. In contrast, very fine scale delamination occurs at the surface of a multilayer coating with no evidence of plastic deformation and perpendicular crack propagation [PalDey and Devvi, 2003].

Therefore, multilayered coatings exhibit greater resistance to microchipping and material pullout during milling operation as compared to monolayer coatings.

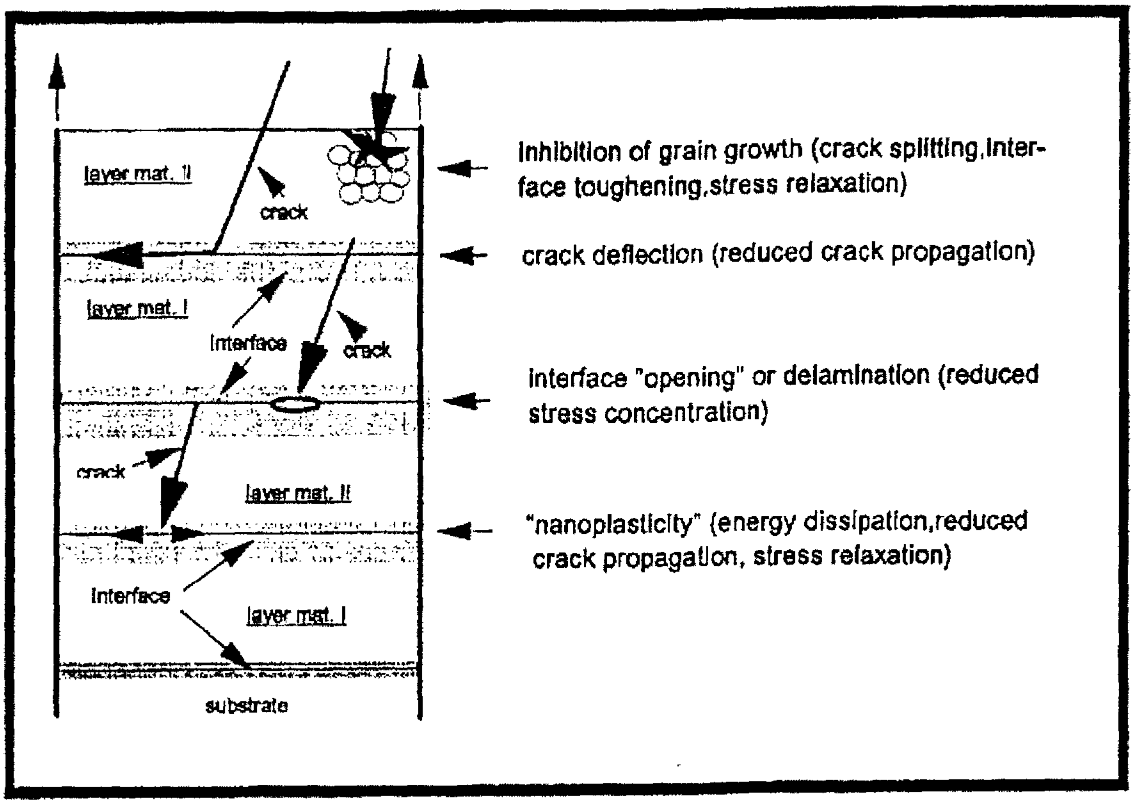

Figure 3.5 Toughness mechanisms in ceramic multilayer materials

[Holleck and Schier, 1995]

3.4 Effect of Grain Size

As shown in Figure 3.6, when the materials have grain sizes larger than 100 nm (0.1 μm), they are called conventional grain size materials. When the grain sizes are less than 100 nm, they are called nano-materials. With a decrease in grain size, the multiplication and mobility of the dislocations are hindered so the hardness of materials increases according to the Hall-Petch relationship: $H(d) = H_0 + Kd^{(-1/2)}$ [Zhang, et al., 2003], here d is the diameter of grain. However, when the grain size is further reduced below approximately 10nm the hardness of the coating is decreased due to grain boundary sliding. Material softening caused by grain boundary sliding is mainly attributed to a large amount of defects in the grain boundaries, which allow for the fast diffusion of atoms and vacancies under stress. Therefore a further increase in hardness requires the hindering of the grain boundary sliding activity.

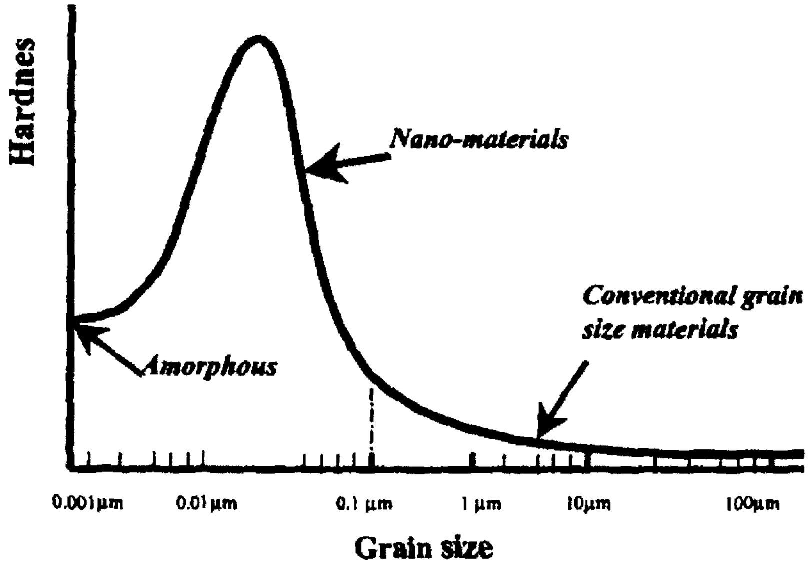

Figure 3.6 Hardness of a material as a function of the grain size [Zhang, et al., 2003]

3.5 Effect of Additional Alloying Elements

3.5.1 Chromium and yttrium

Adding Cr and Y to TiAlN based coating can further improve oxidation and corrosion resistance [Smith, et al., 1998]. Addition of 3% Cr and 2% Y drastically improved the oxidation behavior of TiAlN based coatings. The addition of Y led to extensive grain refinement and a more equiaxed structure due to the continuous nucleation process. The onset temperature of rapid oxidation was delayed from 870°C for $Ti_{0.46}Al_{0.54}N$ to 950°C for $Ti_{0.42}Al_{0.53}Cr_{0.03}Y_{0.02}N$. It was found that $Ti_{0.44}Al_{0.53}Cr_{0.03}N$ and $Ti_{0.42}Al_{0.53}Cr_{0.03}Y_{0.02}N$ had significant differences in their oxidation behavior. Without the presence of the element Y, rapid oxidation was initiated at 920°C and diffusion of substrate elements through the coating occurred at 950°C. In contrast, with additional Y, the coating oxidized only at the free surface of the coating. Because of the Y-O compound at the grain boundaries, the outward diffusion of substrate species and inward diffusion of oxygen atoms were significantly inhibited [PalDey and Deevi, 2003]. By the comparison study of TiAlN and TiAlCrN coatings, it was found that the addition of Cr to a TiAlN coating improved the tribological adaptability due to the formation of an additional lubricating oxide layer (Cr-O) [Fox-Rabinovich, et al., 2005].

3.5.2 Zirconium and vanadium

Addition of Zr and Al or V and Al to f.c.c. TiN causes further stabilization. The three metallic components possess different atomic radii and different electron configurations and may lead to a behavior observed in solid solution hardened materials [PalDey and Deevi, 2003].

The addition of Zr has a stabilizing effect on the f.c.c. TiN monocell. Furthermore, Zr forms stable oxides. The very thin zirconium oxide layer on top of the coating in the crater area can thus reduce diffusion wear. The hardness of TiZrN can reach the range of 33±2.6 GPa depending on the deposition process and chemical content. Therefore, TiZrN coatings exhibited better wear resistance as evidenced by low crater depth and low flank wear as compared with TiC, TiN and TiAlN coatings [Sproul, et al., 1993; Knotek, et al., 1986; Knotek, et al., 1996].

The addition of V contributes to coating stabilization. Previous study showed that the thermal stability of ternary TiVN coating was high, as no significant changes in the lattice parameter were detected even after annealing at 1000°C. TiVN coating has shown hardness in the range of 30.4-35.3 GPa (3100-3600 HV) and a good adhesive strength of 60-100 N at a V content of 52%. However, the coating with a 29% V content showed the best wear performance [Knotek, et al., 1990]. Conversely excessive vanadium content lowers the ductility of the coating so an optimum content of V addition is important for achieving good wear resistance.

A recent trend was to combine the advantages of TiAlN, TiZrN and TiVN coatings and hence quaternary coatings such as TiAlZrN and TiAlVN were developed. In this case it was found that increasing V decreased the hardness of the coating [Knotek, et al., 1987]. In summary, the addition of Zr or V to TiAlN based coatings can reduce both flank wear and crater wear.

3.5.3 Silicon

The addition of Si to Ti-Al based coatings increases the hardness, the oxidation resistance and thermal stability of the coatings. A comparison study between TiAlSiN coating and TiBN coating at high cutting speed was performed by Holubář, et al and it was found that $Ti_{0.50}Al_{0.45}Si_{0.05}$ coating exhibited a high thermal stability and the grain size of the coating remained stable up to a temperature of $1000^{o}C$. And the hardness of the coating increased after annealing at $900^{o}C$. The results showed that nanocomposite TiAlSiN outperformed TiBN coating at higher cutting speeds. This was attributed to the chemical inert nature of the coating at higher cutting temperature due to the higher content of Al and Si, and thereby, decreases the chemical wear typically experienced at higher cutting speeds [Holubář, et al., 1999].

3.5.4 Boron

Additional Boron leads to improved abrasive wear behavior of Ti-Al based coatings. Moreover, if h-BN is formed in hard TiB2 and TiN structure, it lowers the friction resistance of the coating due to its self-lubricating effect. On the other hand, the formation of cubic BN drastically increases the hardness of the coating. The addition of B in the TiAlN lattice improves the lubricated cutting performance by two orders of magnitude. The addition of both B and C in TiN lattice lowers the friction coefficient of the coating. A coating with a moderate hardness and a low elastic modulus can act as an excellent intermediate layer between a soft substrate and an ultra hard coating with a high elastic modulus [PalDey and Deevi, 2003].

3.5.5 Hafnium

Hf based carbides and nitrides possess higher melting temperatures as well as higher thermostability making them suitable for resistance to flank wear and crater wear as compared to Ti based carbides and nitrides. The melting temperatures of HfC, HfN, TiC and TiN are 3890, 3330, 3160 and 2950°C, respectively [Lugcheider, et al., 1999]. It was found that coatings with Hf and C possessed a lower thermal diffusivity as compared to a plain TiN coating. Therefore, these coatings can protect heat sensitive substrates under milling processes. Figure 3.7 shows the wear behavior of different hard components.

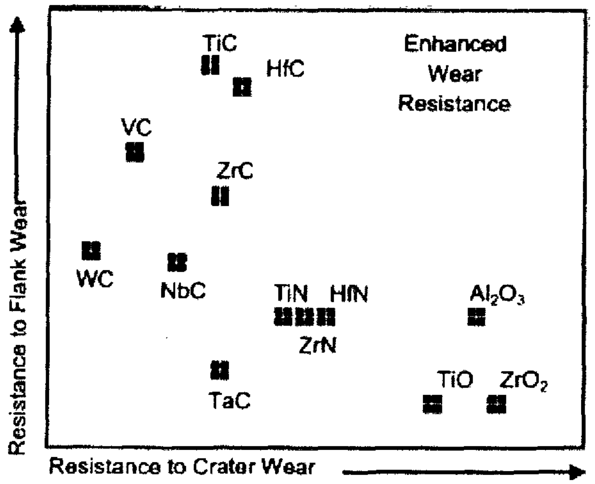

Figure 3.7 Wear behavior of different hard components [Lugcheider, et al., 1999]

3.6 Properties of Titanium Based Hard Coatings

The goal of this research is to develop novel coatings for increasing productivity and tool life. The means to increase productivity is using higher cutting speed. High speed generally results in high cutting temperature and high cutting temperature results in short tool life. In order to achieve the desired research goal, designing the coatings to improve the present properties of (Ti, Al)N based coatings, especially the properties at elevated temperatures, is necessary.

3.6.1 Hardness and hot hardness

Hardness influences abrasive wear resistance. Higher hardness generally results in lower abrasive wear. In metal cutting, the cutting temperature is generally in the range of 300-1000°C. In the applications of dry high speed machining, the cutting tools may experience temperatures higher than 1100°C. Therefore, retention of hardness at elevated temperature is very important. Figure 3.8 shows the hot hardness of five different coatings. TiC is the hardest at room temperature while at 1000°C (Ti, Al)N becomes the hardest. The retention of higher hardness of (Ti, Al)N coating may partially be attributed to the solid solution effect of Al in the TiN lattice [PalDey and Deevi, 2003]. When the temperature reaches 1000°C, (Ti, Al)N coating can maintain only half of its room temperature hardness.

Higher hardness at room temperature is also associated with a higher amount of residual stress in the coating and an optimal coating requires a lower compressive stress with a high microhardness value since the coating adheres well to the substrate at a low value of compressive stress [PalDey and Deevi, 2003]. For example, the microhardness of TiN film could be as high as 37 GPa with a compressive stress of 10 GPa [Martin, et al., 1999]. Although compressive residual stresses are desirable to some degree for retarding crack propagation and improving the fracture toughness of the coating, too high of a compressive stress can cause poor adhesion of the coating to the substrate. However, the (Ti, Al)N coating exhibited a lower internal stress in the range of 4.5-5.2 GPa even at as high a microhardness as 32.4 GPa. Therefore, (Ti, Al)N coating is preferred for wear resistant applications over a TiN coating.

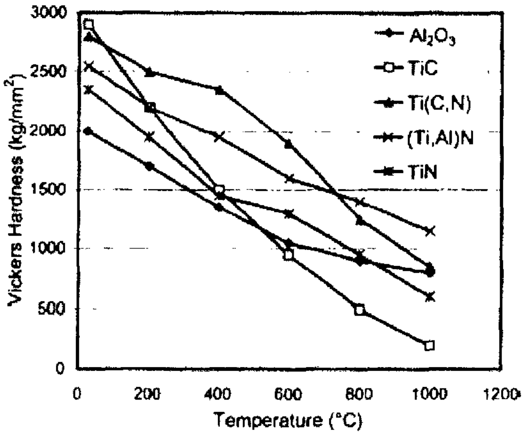

Figure 3.8 Temperature dependence of microhardness of five common coatings [PalDey and Deevi, 2003].

3.6.2 Oxidation resistance

Oxidation resistance is one of the key properties for tool coatings. If a cutting tool loses its oxidation resistance at elevated temperatures, it will fail quickly. However, a certain amount of oxides formed in the cutting zone may benefit tool performance.

Previous study showed that TiC, TiN, TiCN, TiAlN lose their oxidation resistance at approximately 400, 600, 600, 800-900°C respectively (Figures 3.9-3.10). TiAlN films containing 60-70% Al exhibited oxidation resistance in air up to 950°C [Zhou, et al., 1999]. TiAlN/VN coating started the coating surface oxidation at ≥ 550°C and the entire coating volume was oxidized at 672°C and then the coating spalled [Zhou, et al., 2004]. AlCrN is able to retain its oxidation resistance even at high temperature of 1100°C (Figure 3.10). From Figure 3.10 one can conclude that Cr has the function of improving oxidation resistance. The oxidation resistance of TiAlCr-based alloys at high temperature was studied by Fox-Rabinovich, et al. (2006) and they found that the synergistic doping by a small amount (0.1-0.5 at.%) of active metals such as Hf, Y or Si resulted in a significant improvement in the oxidation stability of the coating (Table 3.1).

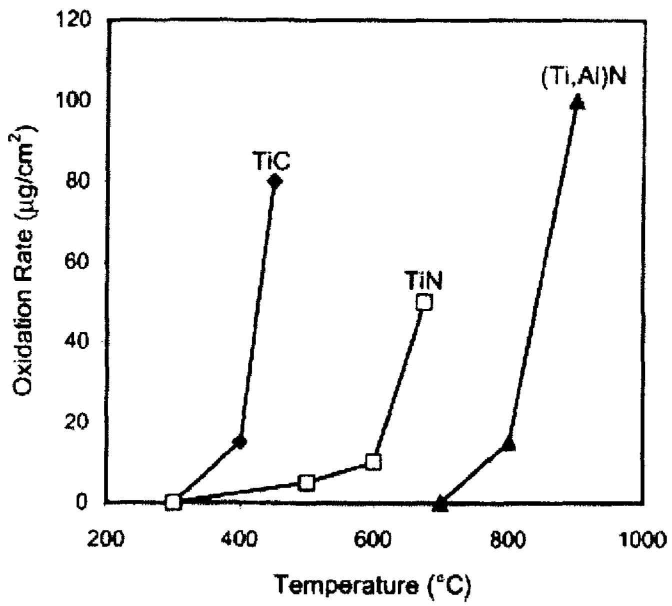

Figure 3.9 Oxidation rate of hard coatings [Knotek, et al. 1988]

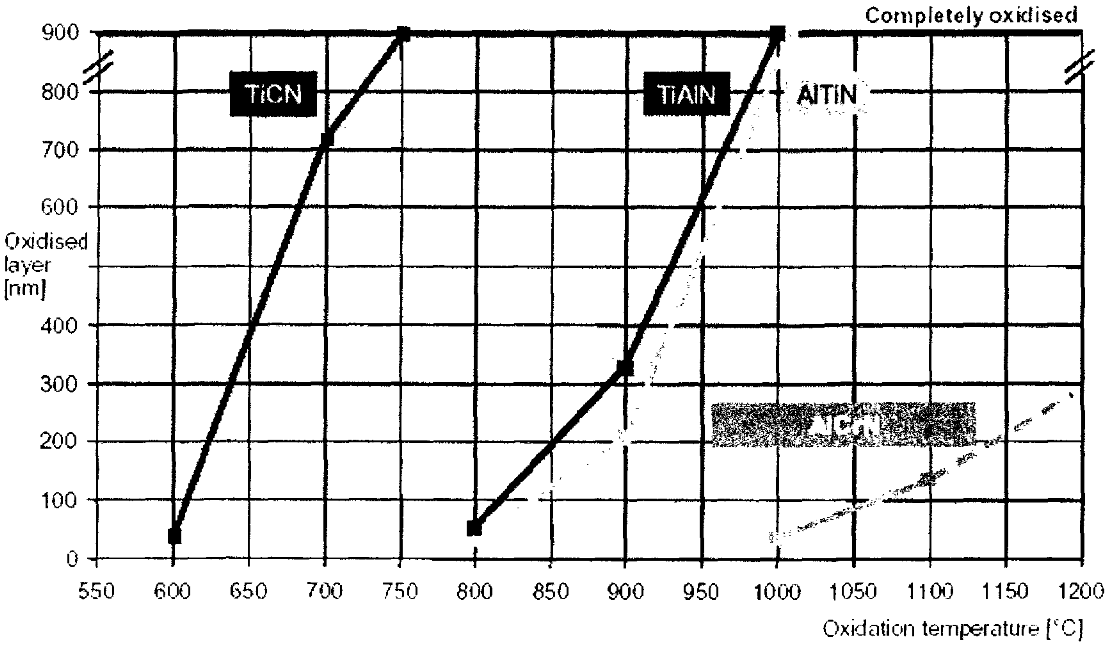

Figure 3.10 Oxidation resistance of PVD coatings [Kalss, Balzers Ltd.]

Table 3.1 Chemical compositions and weight gain after isothermal oxidation tests of the ternary TiAlCr-based alloys doped by Hf, Y, Si and Zr [Fox-Rabinovich, et al., 2006]

Nominal alloy composition	Measured alloy composition (at.%)	Weight gain, mg/cm^2	
		900 °C, 400 h	1100 °C, 100 hrs
$Ti_{0.25}Al_{0.60}Cr_{0.15}$	Ti-60.3Al-15.2Cr	0.175	1.25
$Ti_{0.24}Al_{0.60}Cr_{0.15}Si_{0.01}$	Ti-60.3Al-15.2Cr-0.9Si	0.25	1.73
$Ti_{0.245}Al_{0.60}Cr_{0.15}Si_{0.005}$	Ti-60.3Al-15.2Cr-0.55Si	0.168	0.77
$Ti_{0.25}Al_{0.55}Cr_{0.20}$	Ti-55.1Al-19.9Cr	0.165	0.78
$Ti_{0.248}Al_{0.55}Cr_{0.20}Zr_{0.002}$	Ti-55.1Al-19.9Cr-0.2 Zr	0.16	0.58
$Ti_{0.248}Al_{0.55}Cr_{0.20}Hf_{0.002}$	Ti-55.1Al-19.9Cr-0.2 Hf	0.13	0.41
$Ti_{0.248}Al_{0.55}Cr_{0.20}Y_{0.002}$	Ti-55.1Al-19.9Cr-0.2 Y	0.149	0.66
$Ti_{0.247}Al_{0.55}Cr_{0.20}Hf_{0.002}Y_{0.001}$	Ti-55.1Al-19.9Cr-0.2 Hf-0.1Y	0.09	0.45
$Ti_{0.243}Al_{0.55}Cr_{0.20}Hf_{0.002}Si_{0.005}$	Ti-55.1Al-19.9Cr-0.2 Hf-0.5Si	0.1	0.42
$Ti_{0.242}Al_{0.55}Cr_{0.20}Hf_{0.002}Si_{0.005}Y_{0.001}$	Ti-55.1Al-19.9Cr-0.2Hf-0.5Si-0.1Y	0.046	0.4

3.7 Lubricious Coatings

3.7.1 Introduction

Lubricants include vapor, liquid and solid lubricants. When liquid or vapor-phase lubricants are used, most often oxidation and /or chemical breakdown occur and thus render these lubricants useless at high temperatures [Erdemir, 2000]. Solid lubricants are more practical for use at high temperatures. However, it has been found that the conventional solid lubricants such as M_oS_2, graphite, hexagonal boron nitride (h-BN), become ineffective mainly because of chemical and/or structural degradation at elevated temperatures. In contrary to the finite lifetime of solid lubricants, oxide-based self-lubricious layers formed by the oxidation of metallic surfaces or alloys show exceptional advantages.

3.7.2 Oxide formation

The sliding contact interface of two solid bodies is subject to continuous physical, chemical and topographical changes. When sliding occurs in open air and at high temperatures or high velocities, most sliding interfaces including metals and non-oxide ceramics become oxidized. Thin oxide films formed on the sliding surfaces may, in turn, dominate the friction and wear behavior of these interfaces. If the sliding bodies differ chemically, two or more oxides may form on the sliding surface and dominate friction and wear [Erdemir, 2000].

Oxides formed at elevated temperatures in the cutting zone can be beneficial to the service life of a tool. Oxides with low friction coefficients can reduce the cutting load and generate lower cutting force, less heat, lower wear rate and hence provide longer tool life. Oxides with low thermal conductivity can prevent heat from conducting into the substrate and hence the substrate is able to provide sufficient strength under severe cutting conditions. Oxides with metallic plasticity features also have the ability to dissipate energy. However, the rapid formation of oxides, which is called oxidation wear, destroys the tools. Therefore, there are two critical temperatures related to oxidation. One is the starting point at which a small amount of oxides is formed. The other is usually called the on-set oxidation temperature at which the oxides are rapidly formed. The preferred working temperature for self-adaptive coatings should be controlled within these critical temperatures.

The oxidation behavior study of different coatings was used to find the proper working temperature range. For example, the oxidation behavior of nanoscale TiAlN/VN multilayer coatings were studied by [Zhou, et al., 2004]. It was found that surface oxidation occurred at >=550°C at the coating surface. At 672°C, the entire coating volume was oxidized and the coating spalled. V_2O_5 was found to form at >=600°C by XRD. V2O5, rutile-TiO_2 and $AlVO_4$ were identified at 600°C, with possible Al2TiO5 and VO2 phases. These observations indicate that TiAlN/VN coating is not suitable for the application of high cutting temperatures.

Chapter Four

Self-Adaptability under Friction

4.1 Friction in Metal Cutting

Frictional processes in metal cutting are complex. The mechanisms of friction include adhesion, the mechanical interactions of surface asperities, plowing of one surface by asperities on the other, deformation and /or fracture of surface layers such as oxides, and interference and local plastic deformation caused by third bodies, primarily agglomerated wear particles, trapped between the moving surfaces. Dry frictional processes can be divided into three stages (Figure 4.1). In the first stage, plastic deformation within the frictional bodies takes place independently due to mechanical interaction and it may lead to a damage of surface oxides at working temperatures (Figure 4.1a). The second stage is the initial stage of seizure (Figure 4.1b). Both conjoint deformation and independent deformation take place. The centers of seizure nucleate and plastic deformation develops during the interaction of the two metals' crystals. In the third stage, plastic deformation of conjoined crystals takes place at all sites (Figure 4.1c).

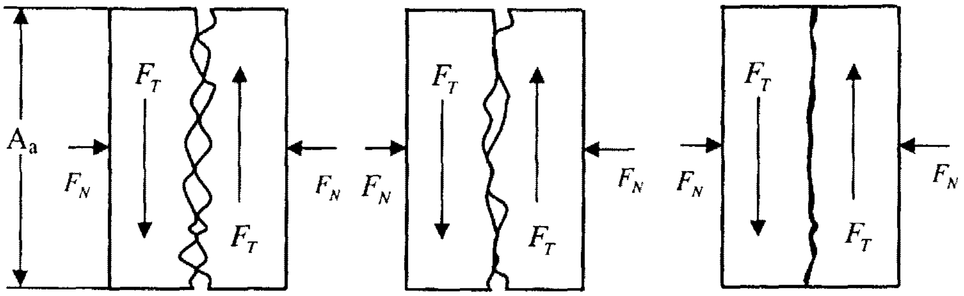

a) Stage one ($A_{true} << A_a$) b) Stage two ($A_{true} < A_a$) c) Stage three ($A_{true} \approx A_a$)

Figure 4.1 A schematic representation of dry friction in metal cutting

(A_a is the apparent area of contact, A_{true} is the true contact area)

The true area of contact between two rough surfaces is proportional to the normal force pressing them together:

$$A_{true} = C \cdot F_N \tag{4.1}$$

where F_N is normal force and C is a coefficient which is related to the hardness of the material and the roughness of the surface.

4.1.1 Sliding on films

For sliding friction (phase one), Coulomb's law is applied:

$$F_T = \mu \cdot F_N \text{ or } \tau_{true} = \mu \cdot \sigma_{true} \tag{4.2}$$

where F_T is the frictional/tangential force, F_N is the normal load and μ is the coefficient of friction.

When the asperity tips are covered with a thin layer of oxides, absorbed water or grease, the friction behavior dramatically changes. The film usually has a low mechanical strength and so it starts to deform and allows the two asperities to slide past each other when the tangential force per unit area acting on the film reaches the shear strength of the film τ_f. Therefore, the tangential friction force due to shearing the film on the surface of all the contacting asperities is expressed as:

$$F_T = \tau_f A_{true} \tag{4.3}$$

Combining equation 4.3 with equation 4.1 gives

$$\begin{aligned} &F_T = \tau_f C F_N \\ &\Rightarrow \mu = \tau_f C \end{aligned} \tag{4.4}$$

This simple equation explains why the friction force is so sensitive to surface films.

4.1.2 Shearing of welded asperities

An increase in the normal load on the contacting surfaces produces an increase in the true contact area. Relative motion between the surfaces produces shearing of welded asperities (adhesion) and some subsurface plastic flow (Figure 4.1b). Therefore, the frictional force F is given by the equation:

$$F_T = \tau_{soft} A_{true} \tag{4.5}$$

where τ_{soft} is the shear strength of the asperities of the softer material, but the frictional force is not linearly related to the normal force N. The shear strength for the softer material (τ_{soft}) is thermally dependent. Therefore, during the cutting process, the frictional force may go down or up depending on the combined effect of both material softening, work hardening and the real contact area.

4.1.3 Seizure

Seizure has been defined as solid phase weld between the primary atomic bonds of the direct contact surfaces. The essential feature of seizure is that atomic contact is established at the interface and the relative motion occurs within the softer material. When seizure takes place the true contact area equals the apparent contact area (Figure 4.1c). Thus the frictional force is given by:

$$F_T = \tau_{soft} A_a \tag{4.6}$$

In the cases of metal cutting, seizure may occur both at the tool-chip interface and between the flank face and the machined surface.

The previous research showed the existence of both sliding and sticking (seizure) conditions at the tool-chip interface as shown in Figure 4.2.

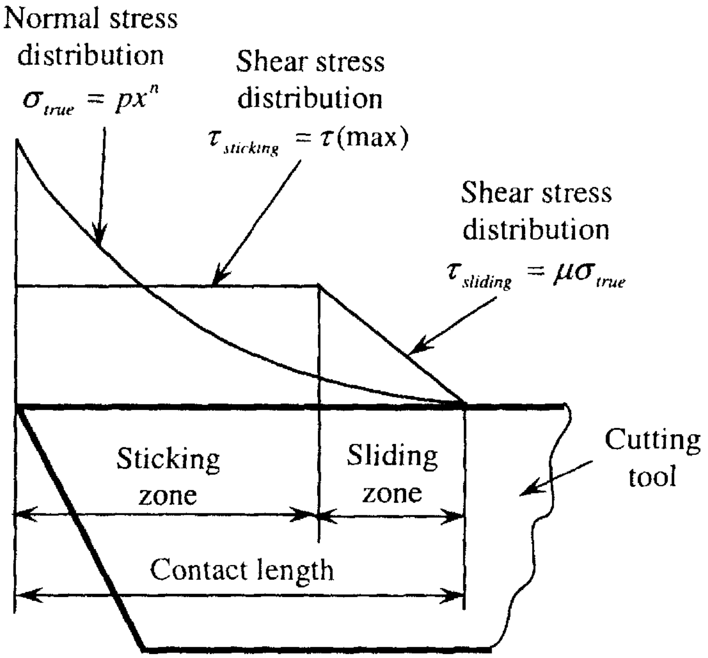

Figure 4.2 Sticking and sliding zones

The tribological condition of the tool–chip interface is basically controlled by the growth of the junction between the chip and tool surface, which gives rise to adhesion and friction. Adhesion is defined as a measure of the yield strength of a junction, i.e. the stress required to squeeze the asperities and bring them to a plastic state. Friction is a measure of the shear strength of the junction, i.e. the stress required to shear the asperities causing relative motion at the interface [Gekonde and Subramanian, 2002].

If the interface is lubricated well, the amount of metallic adhesion is so small that it is unable to withstand the released elastic stress when the load is removed. In this case, change over from elastic to plastic contact does not occur. Thus the friction is determined by the shear strength of the lubricant film itself and consequently, the conditions at the interface are essentially sliding. But this is not the case for a metal cutting process. In metal cutting, abrasive wear exists in the whole process. There is always plastic contact in the tool-chip interface. The friction force is determined by the shear strength of the lubricant film and the metallic junction. Abrasive wear dominates when the conditions at the tool–chip interface are essentially sliding. The occurrence of weak adhesion between the tool and the workpiece causes adhesive wear by the mechanical removal of tool material or built-up edge on the cutting edge when the adhesive junctions are broken as the chip flows over the tool.

Previous researchers indicated that when the junction growth proceeds until the whole geometric area is in contact gross seizure occurs at the interfaces. When seizure occurs, intense shear localization occurs, leading to thermoplastic shear deformation of a thin layer of the chip material adjacent to the tool–chip interface. The resulting high temperature at the tool–chip interface causes dissolution wear of the tool into the chip material. Dissolution wear is characterized by rapid crater formation at the rake face of a carbide tool and this diffusion wear mechanism can lead to a high wear rate of the tool. Eventually, the weakening of the cutting edge leads to catastrophic failure of the tool by intensive plastic deformation, fracture or edge chipping.

4.1.4 Lubrication at interface

Lubricants reduce friction between surfaces that are in relative motion. At any given rate, the force holding the parts together controls the intimacy of contact and thus has a direct influence on frictional force. When normal forces are quite low, the viscosity of an intervening layer of fluid can be the major factor in regulating friction. However, in metal cutting the average normal stress on the chip tool contact zone is extremely high, being in the range 200-800 MPa for steel (Trent, 2000) and the lubricants can hardly gain access to the seizure zone. Thus limited amounts of lubricants can get into the sliding zone. Under high speed machining lubricants may also lose their function due to decomposition at high temperatures.

Since the lubrication in the cutting zone is so critical for a successful cutting process, the cutting tools with lubricious coatings on or with coatings that have the ability to generate lubricious film during cutting processes would be able to achieve better performance.

4.2 Concept of Self-Adaptability

Self-adaptability can be defined as the ability of a system to provide an optimum response to some external stimulus such as friction, temperature, stress, strain, occurring in the environment.

Friction is an irreversible thermodynamic process in which energy dissipation takes place. The characteristics of the friction process changes with time. Therefore, the irreversible thermodynamics and the theory of self-organization are based on the second law of thermodynamics. The major concept in the second law of thermodynamics is entropy. Entropy is a measurement of the degree of organization in a system. When a system reaches its equilibrium state, the energy in the system is uniformly distributed and its entropy is maximal. When a system has a significant deviation from equilibrium, steady structures can be formed in the system. These structures formed under strongly non-equilibrium conditions are called dissipative structures and the process of the dissipative structure formation is called self-organization. A dissipative structure is different from an equilibrium structure. Equilibrium structures are formed and exist during reversible transformations while dissipative structures are generated and exist due to an exchange of energy, matter and entropy with the environment under strongly non-equilibrium conditions.

Tribological compatibility is related to the concept of self-adaptation / self-organization of tribo-systems. Under friction, the balance of energy received by a frictional body can be expressed as:

$$E_o = \Delta U + E_t$$

where E_o is the energy in a frictional body; ΔU represents the change of the internal energy of a frictional body; and E_t is the energy transformed from a contact zone into a frictional body.

To prevent energy transforming into a frictional body, a major part of the energy generated during friction has to dissipate. Surface tribo-films (the dissipative structure) serve as an intermediate body for energy dissipation. The formation of tribo-films is a tribo-system response to an external impact, i.e., friction and is aimed at reducing the external impact by decreasing the wear rate. Surface tribo-films perform protective functions, limiting the interactions (occurring during friction) into the depth of frictional bodies and reduce the intensity of such interactions. If the tribo-system cannot form stable tribo-films, it tries to stop friction by means of strong seizure and jamming. In this way the frictional system turns into a very severe condition and rapidly leads to tool failure.

4.3 Tribo-system and Stages of Tool Life

In the cases of metal cutting, the goal that a tribo-system works for is to achieve a low wear rate which implies a long tool life and high surface finish of a machined surface. The service life of a tribo-system can be divided into three stages, which is similar to the three stages of a cutting tool service life. The first stage is called the running-in stage; the second stage is called the post-running-in period; the third one can be called the catastrophic stage.

The running-in process can be divided into two phases. The first one is the frictional body interaction at the macro-level. During this period the actual contact area is increased as a result of plastic deformation and wear. The second one is the interaction of frictional bodies at the micro-level. Once the running-in stage is completed, surface equilibrium begins as a result of structural adaptability during friction.

The wear rate in the running-in stage depends on the intensity of the wear process and plastic deformation. The contact interactions between the frictional surfaces may create points of galling, build-up and tearing-off zones before the formation of initial seizure during the running-in stage. The degree of hardening and the depth of plastic deformation determine the intensity of surface damage. If plastic deformation takes place within the thin surface layers, the tribo-pair will operate without the further formation of seizure zones. This process can be enhanced by the deposition of special soft metal, solid lubricant coatings or by the application of self-lubricating alloys and composite materials [Fox-Rabinovich and Totten, 2006].

Plastic deformation of the surface layers is of great importance during the running-in process. Thermo-mechanical effects enhance the plastic deformation on the friction surfaces. Surface plastic deformation is accompanied by an intensive wear process during the running-in stage. The actual contact areas increase and the optimum surface roughness forms under the given conditions, which is independent of the initial surface roughness. The rate of the running-in process and its completeness are controlled by the characteristics of the materials of a tribo-system and their tendency to be compatible. Macro- and micro-damages from the running-in stage significantly influence the service life in the post running-in stage. It is very important for the running-in stage to provide a stable operation condition for the post running-in period without surface damage.

During the post running-in stage, the serviceability of a tribo-system is controlled by the wear resistance of the tool materials, their fatigue life, and their ability to resist against overloading and infringements of the lubricating layer without deep and irreparable surface damage. Prolonged and stable operation of a tribo-system can be achieved if the failure of tribo-systems is controlled by stable, steady wear.

Catastrophic stage may result from intensive seizure, oxidation and/or edge damage. The seizure process during friction is not static. During the relative sliding of surfaces, contact points are continuously regenerated and compression and shear strains develop as well. The development of the seizure process is accompanied by metal transfer onto the counterface.

Chapter 5

Experimental Work

5.1 Cutting Tool Geometries and Substrate Materials

The cutting tools for this study are tungsten carbide solid ball-nose end mills (10 mm, 2 flutes) from Mitsubishi. Two types of substrate materials are selected for the tools. They are C-2MB and C-2SB as shown in Figure 5.1. The C-2MB type has the maximum depth of cut which is 20 mm while the maximum cutting depth for C-2SB is 12 mm. Because of its shorter flutes, C-2SB type is stronger than C-2MB. In addition to this the overhang length of C-2SB can be shorter when it is clamped as compared to the C-2MB tool. The neck length of both mills is 30 mm. Generally, the center of a ball nose end mill tip is a dead spot (cutting velocity is zero), so it tends to rub and wear quickly, causing a poor surface finish. However, these tools called Miracle Nova are ground to provide a minimum of web thickness at the tip, the rate of wear can be reduced and chip evacuation can improve as well.

The chemical compositions of the substrate are listed in table 5.1. Figures 5.2 and 5.3 show the microstructures of the substrates. The hardness measurements show that C-

2MB mills, which have coarser grains, have lower hardness (HV 1650-1700) as compared to C-2SB tools (HV1950-2000) with finer grains.

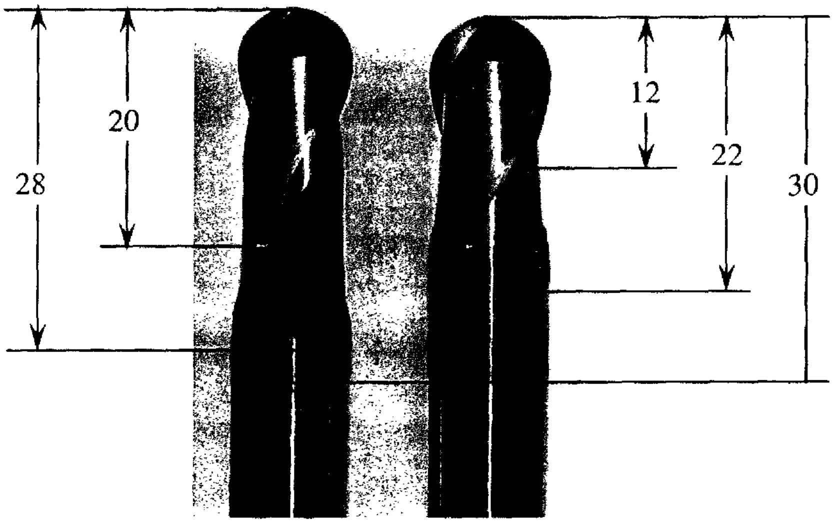

a) C-2MB b) C-2SB

Figure 5.1 Mitsubishi ball end mills (C-2MB and C-2SB)

Table 5.1 Chemical components of uncoated ball end mills

Components	WC	Co	TaC
Weight%	89.5	10	0.5

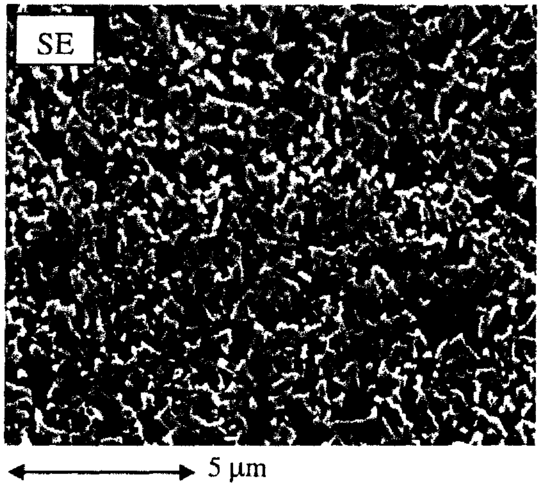

Figure 5.2 Microstructure of C-2MB ball end mill with hardness HV 1650-1700

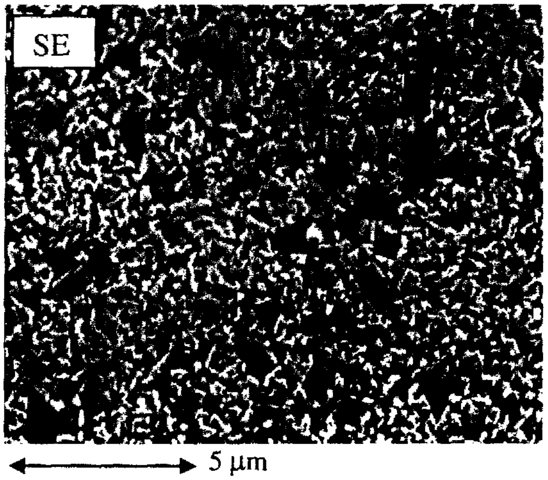

Figure 5.3 Microstructure of C-2SB ball end mill with hardness HV1950-2000

5.2 Experimental Setup for Cutting Tests

Figure 5.4 shows the experimental setup. The experiments were carried out on a 3-axis vertical milling center (Matsuura FX-5). A tool dynamometer (9255B, Kistler) was mounted on the table of the machine tool to measure the cutting force signals during machining. The signals were amplified through a charge amplifier (5010, Kistler) and recorded on a data recorder. The analogue signals were converted using a data translation analog-to-digital acquisition card and stored in a computer. Labview was used for the processing of the cutting force signals. 10 mm cemented tungsten carbide solid ball-nose end mills (C-2MB or C-2SB) (Figure 5.1) (Table 5.1 lists the chemical components) from Mitsubishi were used as substrate. Figure 5.5 shows the tool overhang length and flute length while Figure 5.6 shows the ball end mill used in a down milling operation and the undeformed chip geometry. The mills were coated by Kobe Steel Ltd., Japan. All the coatings were tested by machining hardened H13 die steel (Table 5.2 lists the chemical composition). The melting point of H13 is 1427°C. During the cutting process, tool wear was measured using an optical toolmakers microscope (Mitutoyo model TM) and chips were collected at different cutting lengths. The worn mills and collected chips were analyzed using Scanning Electron Microscopy (SEM) and Energy Dispersive Spectrometry (EDS). Multiple indicators were used for assessing coating performance including: force, wear, chip formation, surface finish and SEM/EDS analysis. If there was any inconsistency in the results the tests would have been repeated.

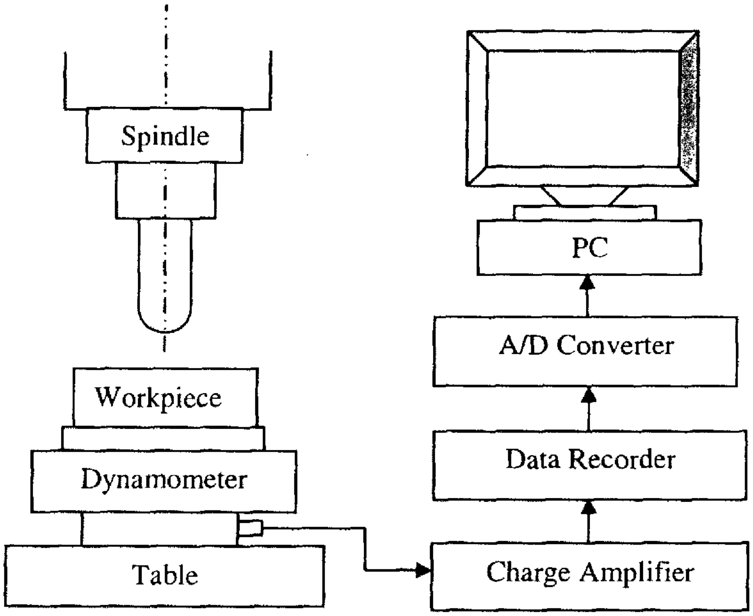

Figure 5.4 Experimental setup for cutting tests

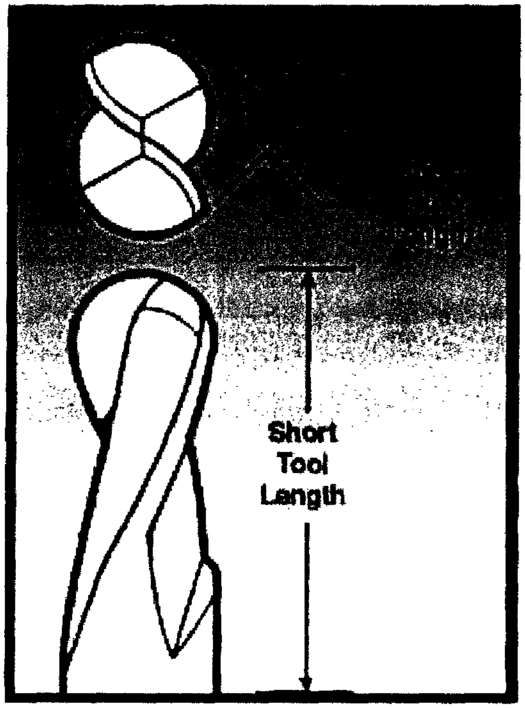

Figure 5.5 Solid ball end mill
(http://www.mmsonline.com)

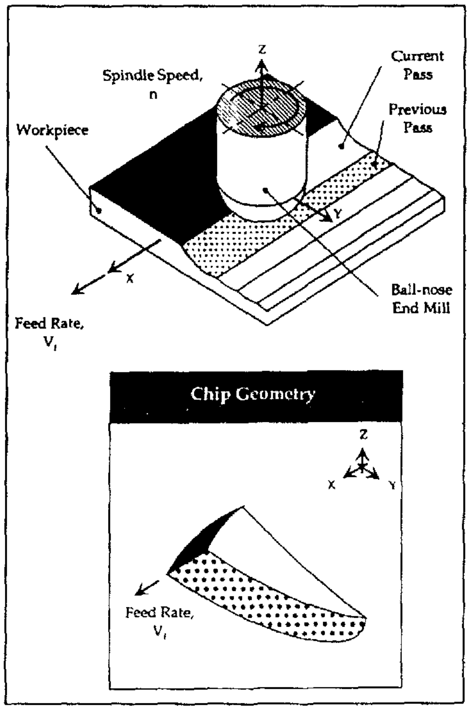

Figure 5.6 Ball end milling operation and chip geometry
[Rodriguez, 1997]

Two parameters need to be emphasized here. One is tool runout and the other is tool overhang length. Since high spindle speeds increase the severity of vibration at the tool tip highly rigid cutting tools are preferred to protect tool life and ensure a high surface quality. For end mills, this means:

- Use the shortest tool (clamped in the tool holder as close as possible to the end of the flutes).

- Choose a tool with shorter flutes (Figure 5.1) which assure a larger and more rigid central core.

For finishing, the feed per tooth and radial depth of cut (also called pick feed or step over) are generally very small, therefore, the tool runout has to be controlled at a very small range to assure identical cutting for both cutting edges. Otherwise, one edge has a very light cut or even without cutting while the other edge tolerates a heavy cut. This would result in intensive wear for the heavy cutting edge and lighter wear for the light cutting edge.

For the testing of developed and commercially available coated ball end mills, the tool runout was controlled to less than 6 μm and the tool overhang length is controlled as short as possible (2 ~ 4 mm above the end of the flutes).

Table 5.2 AISI H13 chemical composition

AISI H13	C	Cr	Mo	Si	Mn	Fe
Weight%	0.32-0.45	4.75-5.5	1.1-1.75	0.8-1.2	0.2-0.5	rest

5.3 Determination of Testing Conditions

The cutting parameters recommended by Mitsubishi for the finishing of hardened AISI H13, by using a coated 10 mm diameter solid ball end mill (Miracle Nova) coated with AlTiN coating, are as follows [http://www.mitsubishicarbide.com]:

- Axial depth of cut $\leq$ 0.06R, for this case, 0.3 mm, where R is the radius of the tool.
- Radial depth of cut $\leq$ 0.1R, for this case, 0.5 mm
- Spindle speed = 8,000 – 12,000 rpm
- Feed rate = 3000 mm/min, therefore, Feed per tooth $\leq$ 0.125 mm

It is suggested that if the depth of cut increases the spindle speed should be reduced. In final finishing, the radial depth of cut can be equal to the chip load per tooth. As is often the case with hard milling operations, both roughing and finishing are performed dry using air blast to assist in chip evacuation. The goal is to take light, quick cuts so that all the heat generated during the cut comes out with the chip to avoid distorting the workpiece.

However, the recommended cutting parameters are not suitable for the purpose of our study because of the following two aspects:

1. With this small axial depth of cut, the generated chip will be just like tiny dust. However, chips need to be collected for the study of coatings because the generated chips carry important information about the cutting process.
2. With the recommended cutting parameters, the coated tools will have very long tool life and the cutting tests will be very time-consuming.

As we know, cutting parameters directly affect material removal rate, chip formation, cutting forces, cutting temperature, tool life and surface integrity. Studying how the cutting parameters affecting the cutting performance is beneficial to selecting cutting parameters meanwhile maintaining high material removal rate. Moreover, we can determine the cutting parameters, which can result in the proper shape of chips for the study of coating development and investigation. The tests were performed using a new sharp ball end mill and a pre-worn one with 0.10 mm flank wear. The tools were coated with TiAlCrN coating. The cutting parameters are listed in Table 5.3.

Table 5.3 Cutting parameters

Test	Cutting speed (m/min)/(Spindle speed (rpm))	Feed per tooth (mm)	Axial depth of cut (mm)	Radial depth of cut (mm)
1	251.2 (8000)	0.06	5	0.6
2	314 (10000)	0.06	5	0.6
3	376.8 (12000)	0.06	5	0.6
4	314 (10000)	0.04	5	0.6
5	314 (10000)	0.08	5	0.6
6	314 (10000)	0.1	5	0.6
7	314 (10000)	0.06	3	0.6
8	314 (10000)	0.06	4	0.6
9	314 (10000)	0.06	5	0.2
10	314 (10000)	0.06	5	0.4
11	314 (10000)	0.06	5	0.8

Comparing the cutting parameters to the recommended ones by Mitsubishi, the axial depth of cut is greatly increased but the spindle speed is not reduced. It is obvious the cutting conditions in table 5.3 are for very extreme cutting conditions.

Figure 5.7 and Figure 5.8 show how the cutting parameters affect the cutting forces when the coated tool is sharp and slightly worn. Based on the results under the given cutting conditions, the following observations can be made:

- The cutting force in the Y-axis is dominant and is the most sensitive force component to the change of cutting parameters as compared to the other two force components.
- Increasing cutting speed to a certain level may result in the cutting force decreasing (Figures 5.7a and 5.8a).
- Changing feed per tooth and radial depth of cut do not have a significant influence on the X-axis and Z-axis force components (Figures 5.7b, 5.7d, 5.8b and 5.8d).
- Increasing the axial depth of cut can result in a significant increase in the resultant cutting force (Figures 5.7c and 5.8c).

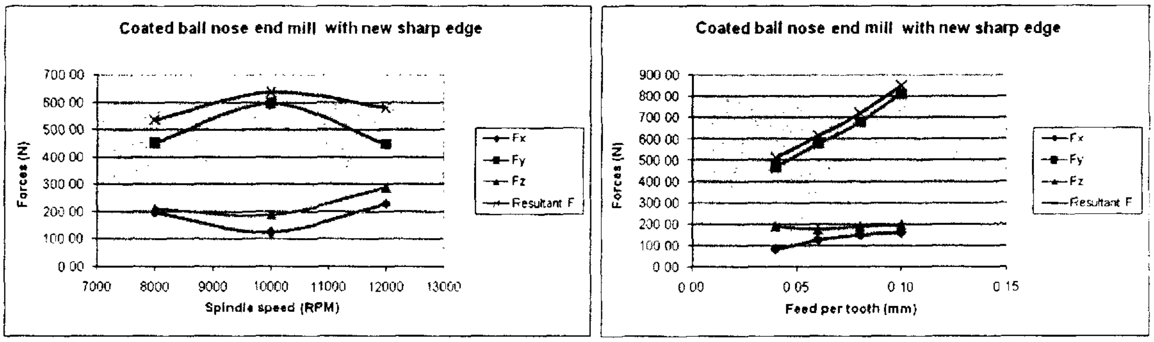

a) Cutting forces vs. spindle speed b) Cutting forces vs. feed per tooth

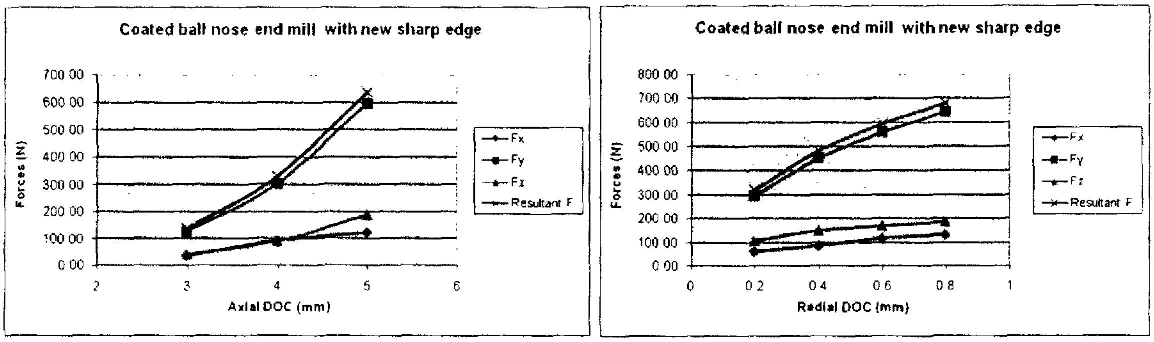

c) Cutting forces vs. axial depth of cut d) Cutting forces vs. radial depth of cut

Figure 5.7 Cutting forces vs. cutting parameters (new sharp tool)

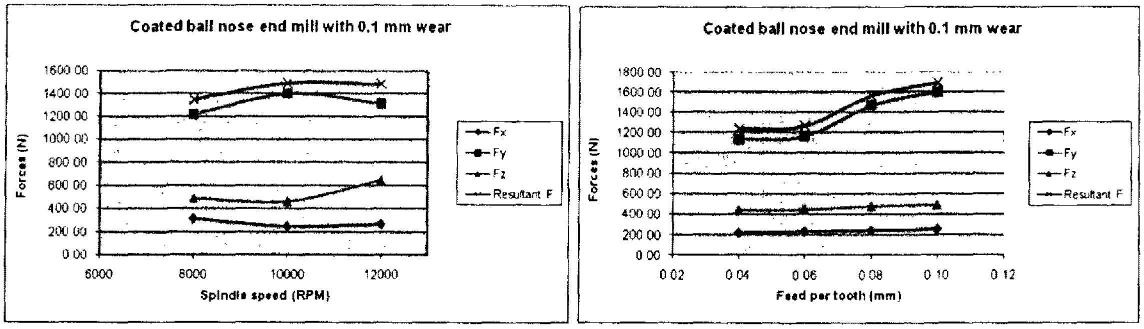

a) Cutting forces vs. spindle speed b) Cutting forces vs. feed per tooth

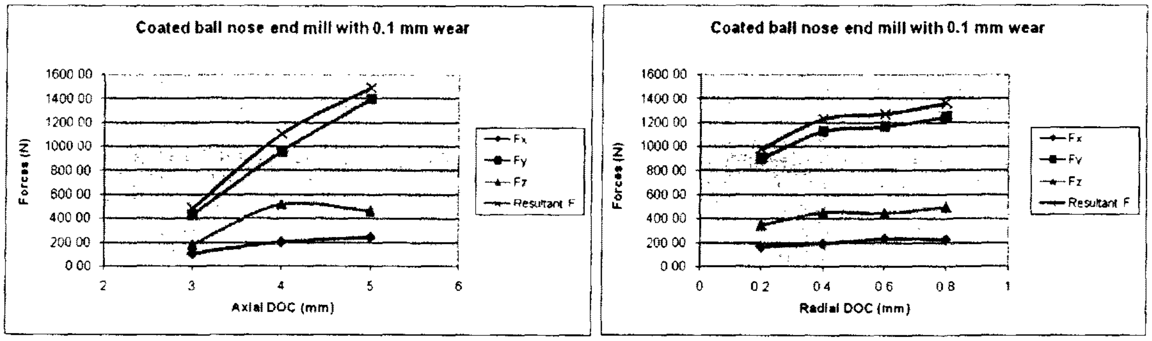

c) Cutting forces vs. axial depth of cut d) Cutting forces vs. radial depth of cut

Figure 5.8 Cutting forces vs. cutting parameters (worn tool, VB=0.10 mm)

The effect of cutting parameters on the new and worn tools is compared and the results are shown in Figure 5.9. Changing the cutting speed (Figure 5.9a) and the feed per tooth (Figure 5.9b) has almost the same degree of effect on the new and the worn tools. However, increasing the axial DOC (Figure 5.9c) and radial DOC (Figure 5.9d) has more effect on the worn tool than the new tool, especially the axial depth of cut.

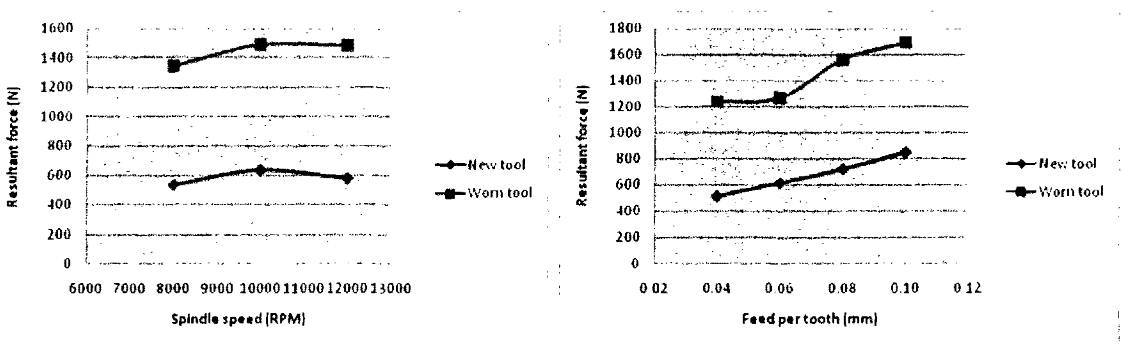

a) Resultant forces vs. spindle speed b) Resultant forces vs. feed per tooth

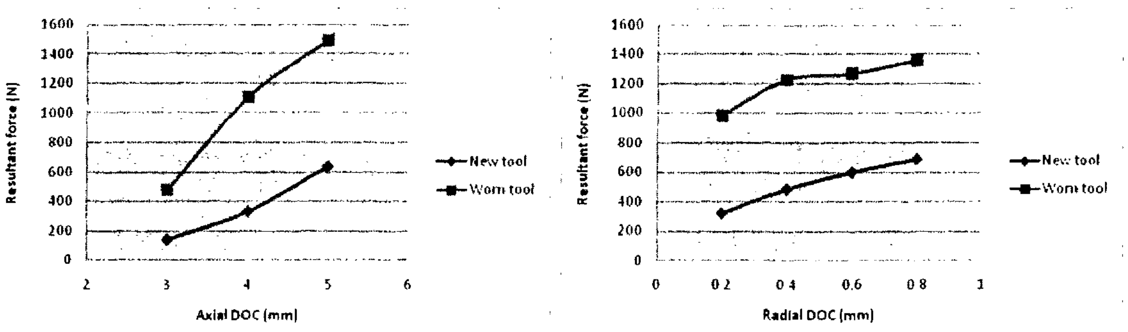

c) Resultant forces vs. axial depth of cut d) Resultant forces vs. radial depth of cut

Figure 5.9 Comparison of the effect of cutting parameters on new and worn tools

From the geometries of the chips (Figure 5.10), we can see that the axial DOC, radial DOC and feed per tooth control the deformed geometry of the chips.

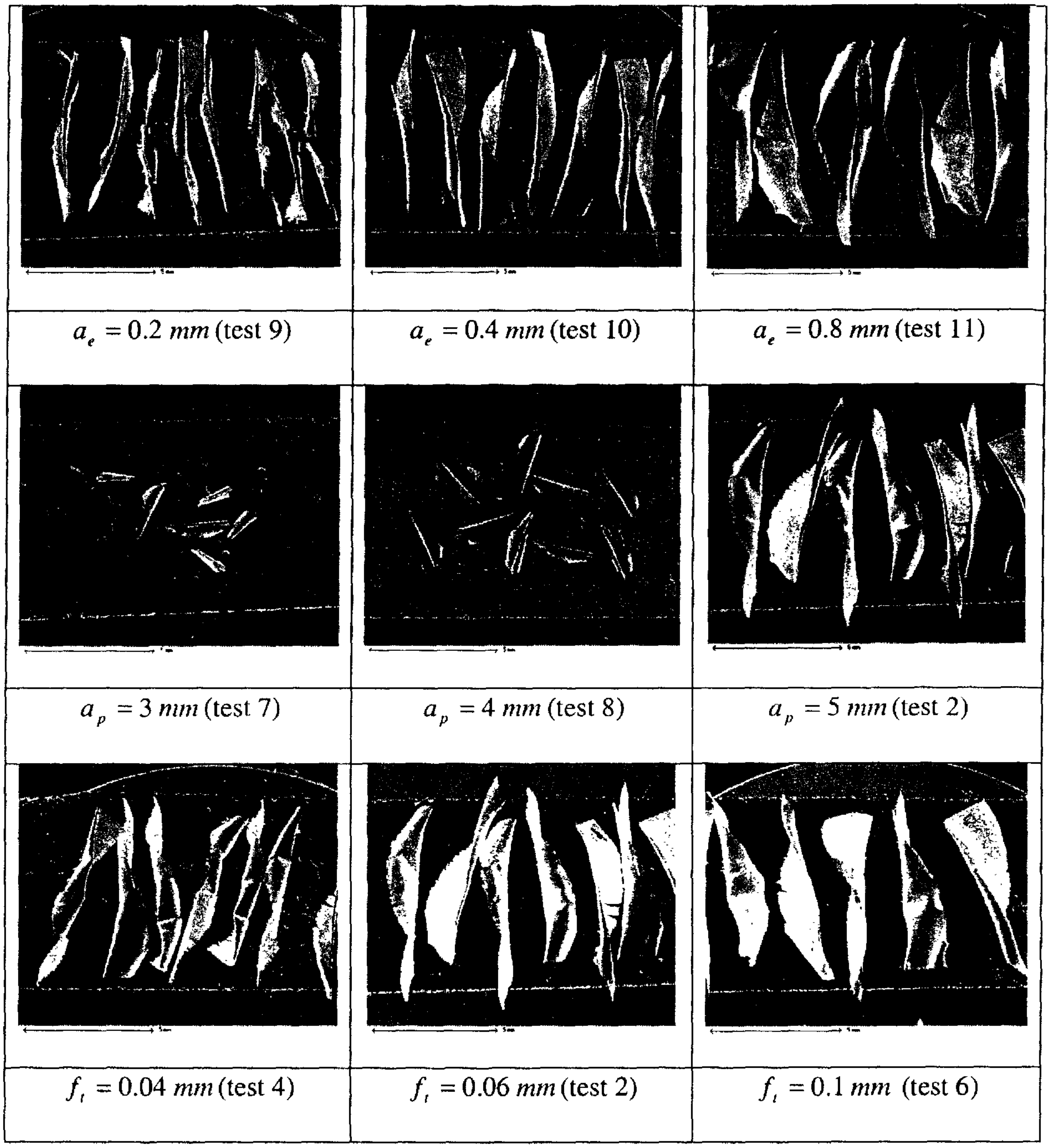

$a_e = 0.2\ mm$ (test 9)
$a_e = 0.4\ mm$ (test 10)
$a_e = 0.8\ mm$ (test 11)

$a_p = 3\ mm$ (test 7)
$a_p = 4\ mm$ (test 8)
$a_p = 5\ mm$ (test 2)

$f_t = 0.04\ mm$ (test 4)
$f_t = 0.06\ mm$ (test 2)
$f_t = 0.1\ mm$ (test 6)

Figure 5.10 Deformed chip shape vs. cutting parameters (new tool)

The undeformed chip thickness is mainly determined by feed per tooth, cutting edge angle and rational angle. It is expressed as:

$$t_c = f_t \cdot \sin\kappa \cdot \sin\theta$$

where κ represents the cutting edge angle and θ is the rotational angle. When the axial depth of cut is equal to the radius of the cutting tool, κ is in the range of 0 to 90°. The range of the rotational angle θ depends on the cutting edge engaging range with the workpiece. When both the axial and radial DOC equal the radius of the tool, the maximum undeformed chip thickness is equal to the feed per tooth.

The radial DOC and feed per tooth determine the cusp height of the machined surface. Increasing these two parameters result in an increase in surface roughness. For the purpose of increasing productivity and maintaining minimum increase of the cutting force, the first parameter that can be considered is cutting velocity, followed by feed per tooth and radial depth of cut.

By observing the color of the chips, it is found that when the tool is sharp increasing the cutting speed slightly changes the color of the chips. However, from the color of the chips generated by the worn tool, it is clear that increasing the cutting speed results in a large increase in cutting temperature. Therefore, tool wear plays a major role in determining cutting temperature.

By observing the shape of the chips, it is found that cutting velocity does not significantly influence the shape of the chips while changing the values of axial depth of cut, radial depth of cut and feed per tooth obviously changes the shapes of the chips (Figure 5.10). Based on the chip shapes from the preliminary tests, one can see that the following parameters are suitable for the investigation of chip formation, chip color, chip shape and chip undersurface.

- Axial depth of cut = 5.0 mm;
- Radial depth of cut = 0.4 - 0.8 mm;
- Feed per tooth = 0.06 - 0.1 mm

The cutting conditions used for the coating testing are summarized in Table 5.4.

Table 5.4 Cutting conditions

Solid ball end mill (substrate)	Tungsten carbide, C-2MB from Mitsubishi
Diameter (D)	10 mm
Number of cutting edges (n)	Two flutes
Workpiece material	Hardened H13 die/mold steel at HRC 48~50, HRC 55~57
Maximum cutting speed ($V_{c\max}$)	220m/min (7000RPM), 300m/min, 400m/min, 500m/min
Axial depth of cut (a_p)	5 mm
Feed per tooth (f_t)	0.06 mm/tooth
Stepover distance (a_e)	0.6 mm
Runout	< 6 μm
Overhang length (mm)	Around 31 mm
Type of milling operation	Down milling
Lubricant	Dry cut with 100psi compressive air blast

5.4 Deposition of Nano-multilayered PVD Coatings

As described in chapter 2, cathodic arc evaporation is a widely used coating process with a high deposition rate and a high degree of ionization of evaporated species. But the target materials need to have electro-conductivity and materials with a too high or too low of a melting point or poor mechanical strength cannot be used. However with the sputtering process which has a very low ionization ratio, various materials, which are hard to use in the arc process, are able to be deposited. In order to improve the ionization rate, the Unbalanced Magnetron Sputtering (UBM) and High Power Impulse Magnetron Sputtering (HIPIMS) technologies have been introduced. These technologies allow for more complex coatings both in terms of composition and structure. These coatings are currently under development to improve tool performance and new coating techniques have also emerged to deposit complex and high quality coatings. Combining arc and magnetron processes in a hybrid coater is a way to achieve this goal.

Nano-scale multilayered coatings in this research were deposited by Kobe Steel Ltd. using a new hybrid coating process that combines cathodic arc and unbalanced magnetron sputtering [Yamamoto, et al., 2005]. A plasma-enhanced arc source [Yamamoto, et al. 2003] and a UBM source were installed in a chamber. $Ti_{25}Al_{65}Cr_{10}$ manufactured by a powder metallurgical process was used as a target for the arc cathode while tungsten, boron carbon, niobium, etc. depending on the type of coatings, was used for a sputtering target. Tungsten carbide ball-nose end mills were heated up to about $500^\circ C$ and cleaned through an Ar ion etching process. Ar-N_2 mixture gas was fed to the chamber at a pressure of 2.7 Pa with a N_2 partial pressure of 1.3 Pa. The arc source was operated at 100 Amps for a 100 mm diameter target. The sputter source was operated simultaneously with the arc source and the input power to the sputter source was varied from 0 to 2.5 KW (for a 160 mm diameter target). The substrates were mounted on a rotating sample holder and passed in front of the arc and the sputter source alternatively during the deposition. The basic rotation speed of the substrate holder was 5 rpm and it was tuned up to 7 rpm and 10 rpm for investigating the effect of outer layer thickness on coating performance. The substrate bias was fixed to 30 V for all depositions. Figure 5.11 shows the cross-sectional Transmission Electron Microscopy (TEM) image highlighting the nano-scale multilayered nature of the coating. Because of the difference in the deposition rate of each evaporation source, the layers deposited by arc are thicker than the ones by the UBM. For instance, in TiAlCrN/WN coating (Figure 5.11), the period of layer cycle is approximately 17 nm. The WN layers are the darker layers due to the heavier atomic mass of tungsten.

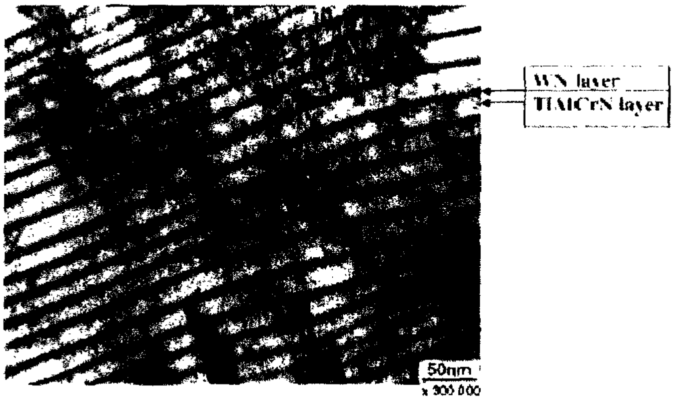

Figure 5.11 Cross-sectional TEM image of nano-multilayered TiAlCrN/WN coating. Parameters of deposition: arc source – 100A; Bias voltage – 30 V; Input DC power to the UBM source – 1.0 KW. Coating contains 10 at.% of W.

5.5 Friction Coefficient Measurement

Surface lubricity tests were performed on a specially designed apparatus as shown in Figure 5.12. To characterize a coating, ideally, a laboratory test should aim to simulate the contact conditions as closely as possible. This apparatus was designed to mimic an intensive adhesive interaction at the tool-chip interface. The coefficient of friction between the coating material and the workpiece material versus temperature was determined with the aid of this specially designed apparatus.

A rotating sample of the coated substrate (#2 – rotational pin with the diameter of 5 mm and the length of 30 mm) was placed between two polished specimens (#1 – disks of diameter 25 mm and thickness 5 mm) made of hardened die steel H 13 (hardness HRC 55-57). To simulate tool friction conditions, the specimens were heated by resistive heating to temperature ranging from 20 to 1000°C. A standard force of 2400 N was applied to generate plastic strain in the contact zone. With this setup the moment of plastic strain initiation could be observed on the surface of the polished samples. The torque was measured. The corresponding rotating pin made a spherical imprint. After measuring the size of the imprint, the shearing force can be determined and subsequently normal stress and shearing stress are obtained. The coefficient of friction was determined as the ratio of the shearing stress induced by adhesive bonds between the tool and the workpiece and the normal contact stress developed on the contact surface at different measuring temperatures. No less than three tests were performed for each kind of coating. The scatter of the friction parameter measurements was found to be around 5%.

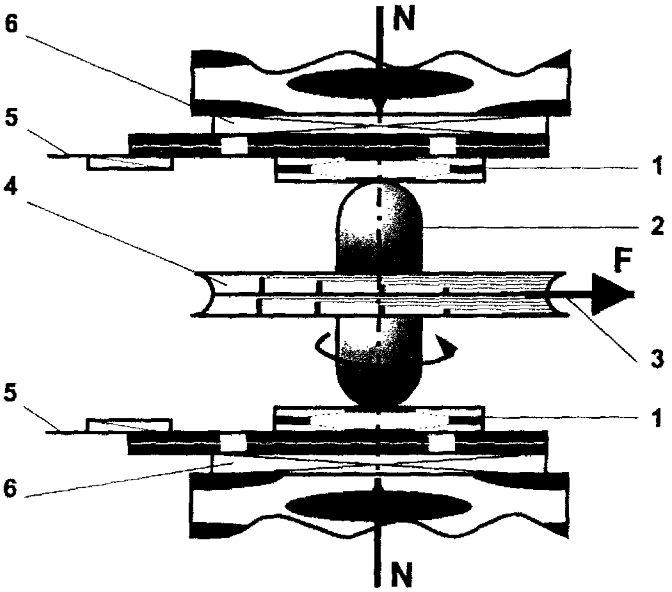

Figure 5.12 A schematic diagram of friction test apparatus [Fox-Rabinovich and Totten, 2007]

1 - specimen made of workpiece material; 2 – specimen made of tooling material; 3 – driving rope; 4 – driving disk ; 5 – electrical contact wires; 6 – isolating system.

5.6 Techniques for Coating Investigation

Various techniques were used to characterize the properties of the coatings and to investigate the performance of the tool. They are listed as follows:

- Hardness: Vickers hardness, micro-indenter, load 50 mN, Fischerscope 1000.
- Surface topography: Scanning Electron Microscopy (SEM), Philips 515 Scanning Electron Microscope with EDS and URSA version 1.3 software was used for SEM/EDS images (www.mektech.ca).
- Chemical composition: Energy Dispersive Spectrometer (EDS), Philips 515.

- Microstructure: Transmission Electron Microscope (TEM) used to study total thickness of the coating, layer thickness, multilayer period (JEOL 2010F Scanning Transmission Electron Microscope with EDS).
- Oxidation stability: a furnace (model No.: TL-20 from The Pottery Supply House) was used for interrupted oxidation test.
- Micrograph of surface morphology (grain size, grain boundary, texture, and fracture), element detection, wear mechanisms, chip shape, etc.: Scanning Electron Microscope/Energy Dispersive Spectrometer (SEM/EDS) are mainly used.
- Detection of oxides: X-ray Photoelectron Spectroscopy (XPS), VG ESCALAB MK2 spectrometer, is used to detect the oxides formed during the wear process.
- Crystal structure and chemical composition: X-ray diffraction (XRD) is a versatile, non-destructive technique that reveals detailed information about the chemical composition and crystallographic structure.
- Friction coefficient: a specially designed apparatus is used to mimic an intensive adhesive interaction at the workpiece/coated cutting tool interface (Figure 5.12).
- Chip cross-section samples are prepared for analysis of microstructure, microhardness, chip type and chip formation mechanisms. Preparation of chip cross-section samples has following steps: mounting the chips by using the clay and epoxy resin, then polishing and etching the samples. The samples are kept in a sealed jar to avoid oxidation.

Chapter 6

Results and Discussions

The coatings developed and tested in this research are for application in dry hard high performance machining. The research goal is to achieve high productivity, high quality and long tool life. In order to reach the goal, nano-multilayered self-adaptive PVD coatings were developed. These coatings were selected due to their advantages associated with their nano-structure and self-adaptibility properties as discussed in Chapter 3 and Chapter 4. TiAlCrN is considered as the base layer while the transient elements such as W, Ta, Cr, Nb and some other element such as B are considered for the thinner lubricious layer. The alternating TiAlCrN base layers and lubricous layers are deposited by alternating Unbalanced Magnetron Sputtering (UBM) and High Power Impulse Magnetron Sputtering (HIPIMS) to form a 3 micron overall thickness nano-multilayered coating. During this study, the content ratio of the chemical elements in the thicker TiAlCrN base layer is optimized; the phenomena of the developed nano-multilayered coatings under elevated temperatures are revealed; tool life, tool wear, wear mechanisms, chip formations, cutting forces and cutting temperatures are discussed in this chapter. The coatings developed in this research are compared with some commercially available nano-structured coatings as well.

6.1 Optimization of the TiAlCrN Base Layer

The purpose of tuning the TiAlCrN composition is to obtain an optimal composition specifically suited for dry high speed machining applications. In fact, four aspects need to be considered:

- The lattice structure of the coatings should stay with fcc structure of TiN;
- High aluminum content to form protective Al-O which serves a protective function for the tool;
- Certain amount of Cr to form Cr-O which is lubricious;
- Ti-O (rutile) should be avoided since rutile is not protective and it can oxidize very fast.

The varying chemical compositions and the corresponding crystal structures are listed in Table 6.1. It was found that the crystal structure of the first three coatings (Table 6.1) still stays with fcc structure of TiN. In order to keep the TiN fcc structure, 20% of Cr is needed when the content of Al is 70%. This is the well-known coating composition $Ti_{10}Al_{70}Cr_{20}N$. The composition, $Ti_{20}Al_{70}Cr_{10}N$, was not taken into account because its crystal structure turned to a hexagonal cubic structure which is known to not provide the desired mechanical properties.

It was found that too much Cr results in the formation of excessive amount of Cr-O tribo-films, which are not as protective as Al-O tribo-films. However, Cr-O oxides are lubricious. Therefore, a small amount of Cr-O films and a larger amount of protective Al-O films are preferred.

The testing results (Figure 6.1) showed that the composition, $Ti_{25}Al_{65}Cr_{10}N$, gave the best tool performance and hence was selected as the base layer for nano-multilayered coatings. Figure 6.2 shows the SEM images of the cutting edge, the flank face and the notch area when the tools reached the end of tool life. For the remained of this thesis, $Ti_{25}Al_{65}Cr_{10}N$ will be simplified as TiAlCrN.

Table 6.1 Chemical composition of the base layer

No.	Coatings (chemical composition)	Crystal structure
1	$Ti_{10}Al_{65}Cr_{25}N$	FCC
2	$Ti_{10}Al_{70}Cr_{20}N$	FCC
3	$Ti_{25}Al_{65}Cr_{10}N$	FCC
4	$Ti_{20}Al_{70}Cr_{10}N$	HCP

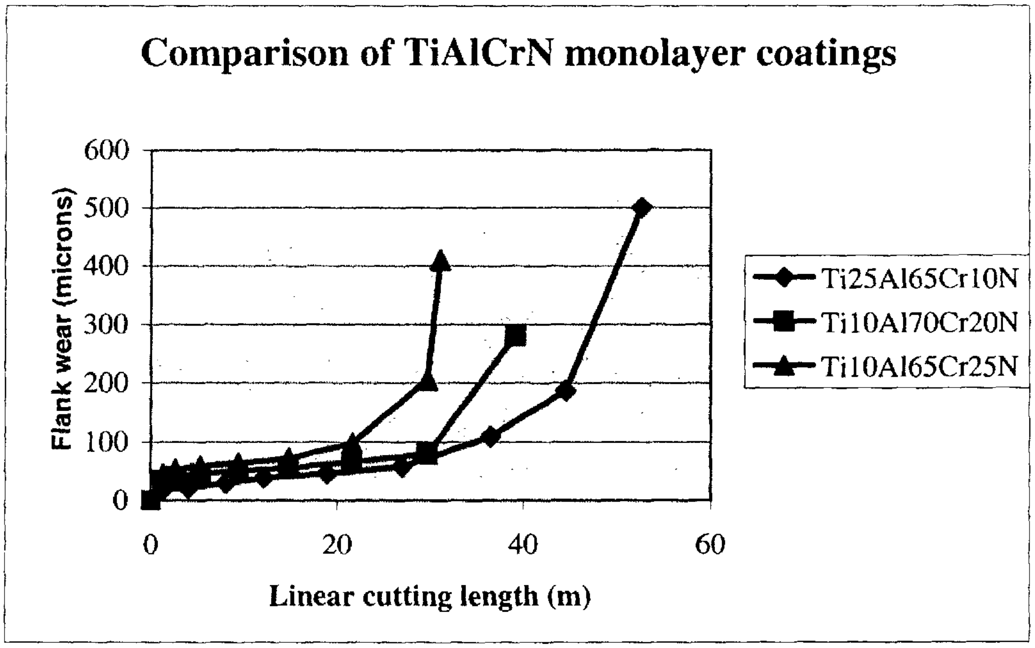

Figure 6.1 Tool life of TiAlCrN monolayer coatings (V_c = 300 m/min,)

Ti25Al65Cr10N (cutting length 52.7 m)

Ti10Al70Cr20N (cutting length 39.2 m)

Ti10Al65Cr25N (cutting length 31.1 m)

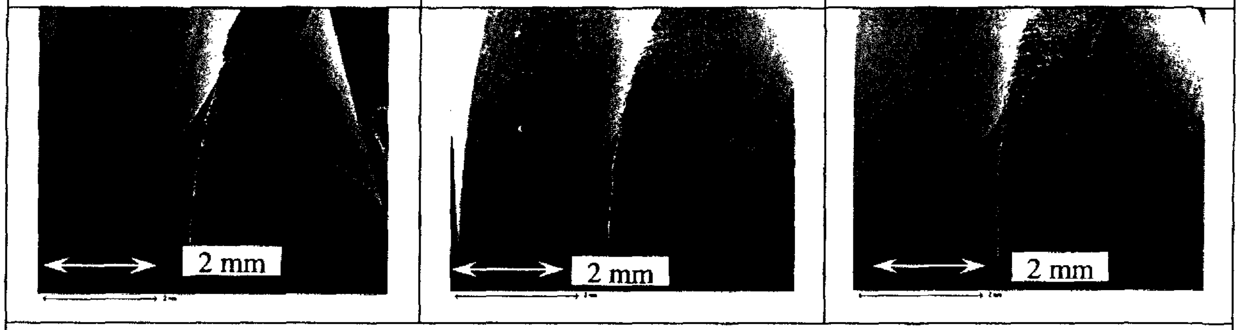

a) SEM images of the cutting edge

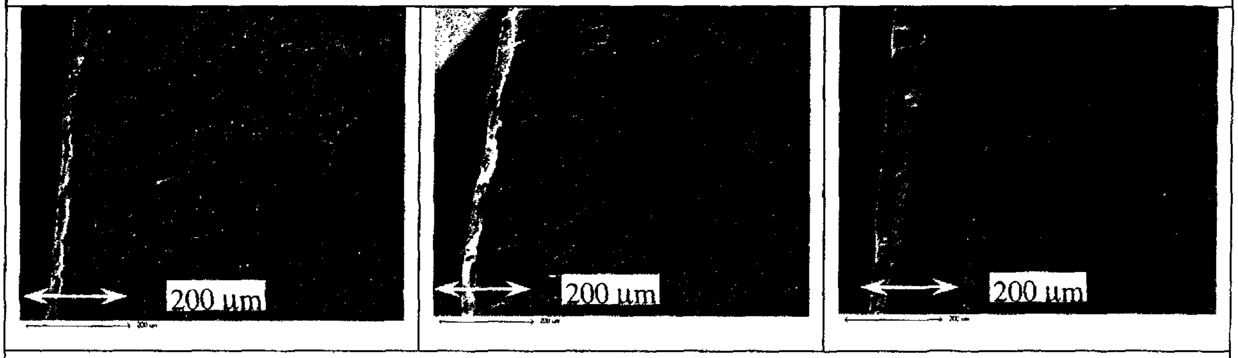

b) SEM images of flank face

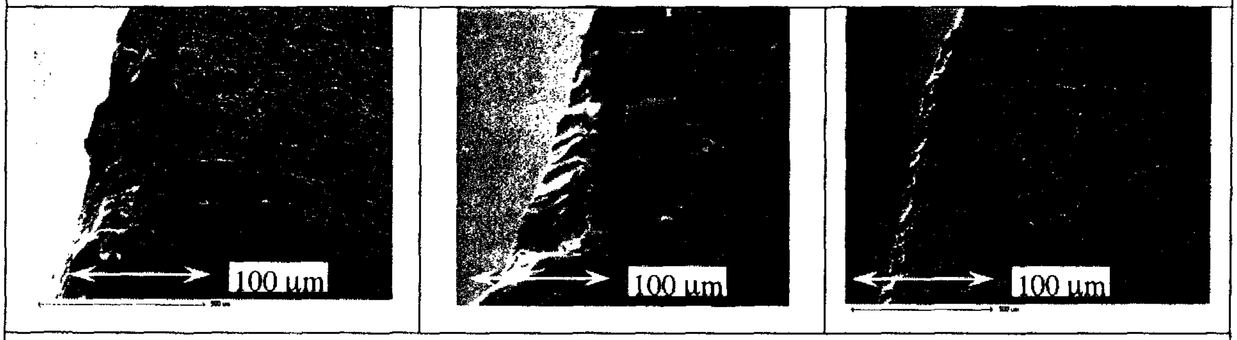

c) SEM images of notch area

Figure 6.2 SEM images of three base coatings at the end of tool life (C-2MB)

6.2 Nano-multilayered TiAlCrN/BCN Coatings

BCN was chosen as the lubricious layer due to its good tribological properties. The deposition process and parameters are described in chapter 5. Three coatings were deposited at different rotational speeds of the substrate holder. They were 1.5 RPM, 5 RPM and 10 RPM so that the layer cyclic period changed. Cutting tests were performed at the cutting speed of 220 m/min. The other cutting parameters are listed in Table 5.4. After the cutting length of 30 meters, it was shown that TiAlCrN/BCN (10 RPM) had the lowest flank wear among the three TiAlCrN/BCN coatings but its performance was not better than the monolayer coating TiAlCrN (Figure 6.3). Moreover, coating spallation was observed on three TiAlCrN/BCN coated worn tools (Figure 6.4). However, the smooth undersides of the chips were observed possibly due to the formation of low friction lubricous boron oxides. It was found that the melting point of boron oxide is lower than the cutting temperature estimated by the color of the generated chips so that boron oxides could not stay as a solid lubricant during the cutting process and will be squeezed out due to the high contact pressures. Also the liquid lubricant would eventually run out due to the limited supply of boron near the surface of the coating.

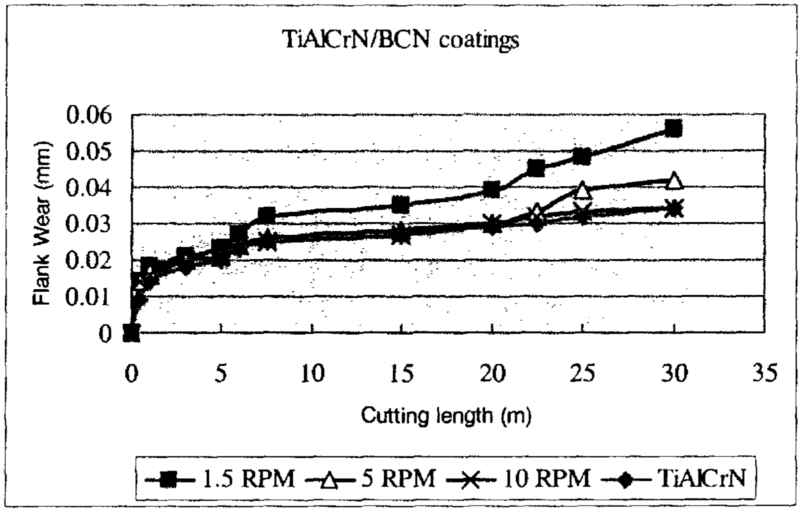

Figure 6.3 Tool wear curves of TiAlCrN/BCN coatings

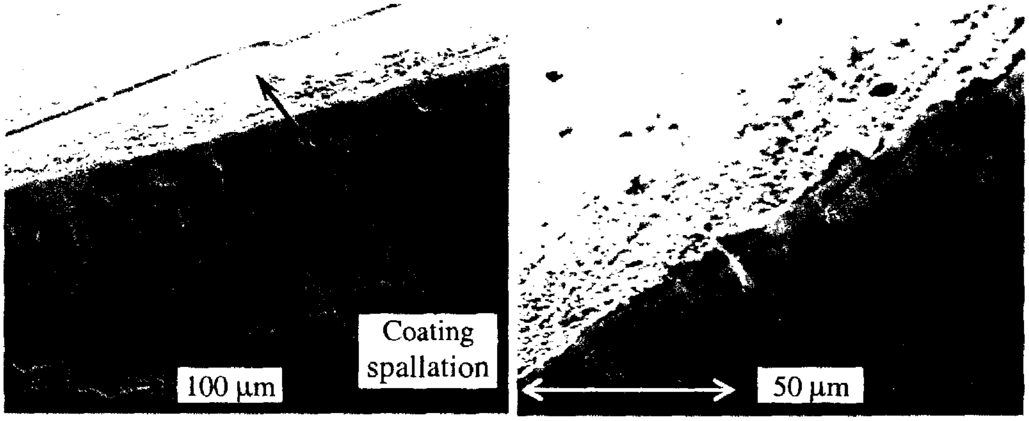

a) Rake face (1.5 RPM) b) Rake face (5 RPM)

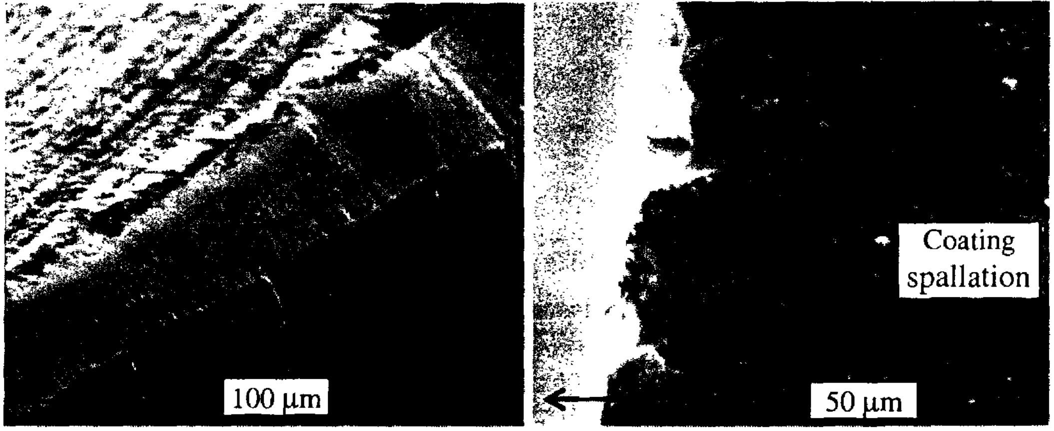

c) Rake face (10 RPM) d) Flank face (10 RPM)

Figure 6.4 SEM images of the worn tools at cutting length of 30 m

6.3 Nano-multilayered TiAlCrN/WN Coatings

Based on the results and observations of the TiAlCrN/BCN coated tools, it was predicted that solid lubricants should be beneficial for a cutting tool to achieve good performance under the conditions of dry hard high speed machining. Therefore, WN was selected as the second candidate of the lubricious layer because of the low coefficient of friction and the higher melting point of W-O. Three TiAlCrN/WN coatings were deposited by altering the power of the sputtering source from 0.5 kW, 1.0 kW to 1.5 kW so that the thickness of the lubricious layer increased as the source power increased. After the cutting length of 30 meters, it was not possible to identify the difference of these three coatings due to their similar performance and the flank faces were only worn around 18 microns but it was obvious that they all performed better than the TiAlCrN monolayer coating and as expected much better than the TiAlCrN/BCN coatings. In order to identify the difference, the cutting test was continued to 250 meters and then it was clearly shown that the one deposited using the 1.0 kW sputtering source had the lowest tool wear. The compositions and properties of the TiAlCrN monolayer coating and TiAlCrN/WN nano-multilayered coatings are listed in Table 6.2. Figure 6.5 shows the flank wear of the TiAlCrN and TiAlCrN/WN (1.0 kW) coatings vs. cutting length at the cutting velocity of 220 m/min. From this figure one can see that the tool coated with TiAlCrN/WN (1.0 kW) coating only has half of the wear as compared to the one with the TiAlCrN coating.

Table 6.2 Composition and properties of TiAlCrN and TiAlCrN/WN coatings

Input power to the sputtering source (kW)	Coating composition, at.% (EDX data)				Properties of the coatings			
	Al	Ti	Cr	W	Micro hardness (HV0.05) (GPa)	Elastic Modulus (GPa)	Weight gain, mg/cm^2 after 1-hour oxidation in air at 900°C	Flank wear after 250 m cutting (μm)
0	60.29	28.69	11.02	0	34.4	577	0.046	76
0.5	56.59	27.71	10.58	5.11	34.14	547	0.109	69
1.0	53.68	27.57	9.22	9.53	33.94	512	0.078	40
1.5	47.68	23.98	9.24	19.09	29.97	452	0.092	47

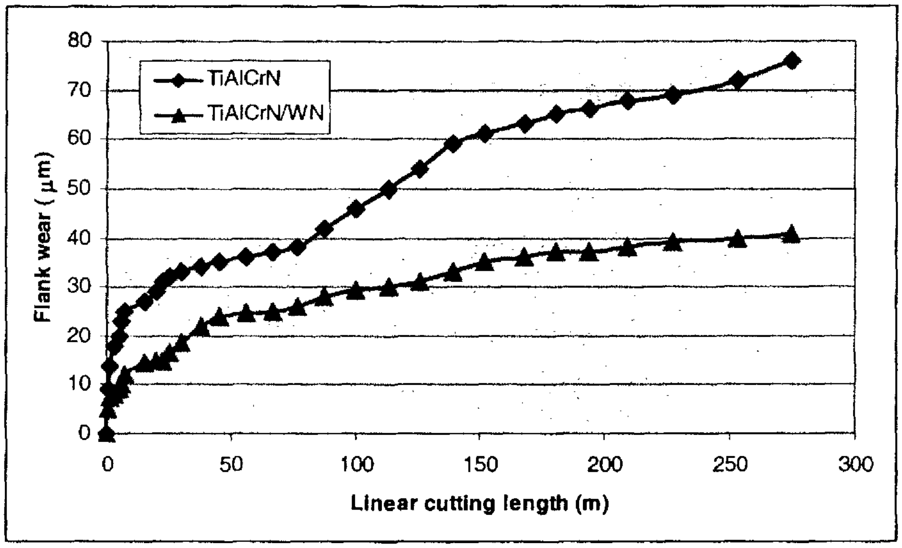

Figure 6.5 Tool wear of TiAlCrN and TiAlCrN/WN coatings vs. cutting length

The reason for the better performance of TiAlCrN/WN coating is related to the phenomenon of seizure which was described in Chapter 4. Seizure is a typical process in cutting operations. This is explained in Trent and Wright [2000]. In general the phenomenon of seizure controls the cutting tool wear behaviour and leads to an extremely short tool life. However, with nano-scale multi-layered TiCrAlN/WN coating there is very low seizure intensity on the flank and rake surfaces of a worn end mill (Figures 6.6, 6.7 and 6.17). SEM elemental mapping shows that it could be probably explained by the formation of protective alumina tribo-films on both the flank (Figure 6.6) and rake surfaces of the tool (Figure 6.7). The W-O tribo-films usually form on the rake surface (Figure 6.7) of the end mills with a TiAlCrN/WN coating. It is most likely that the non-protective rutile films or Al-Ti-O films are also present on the surface.

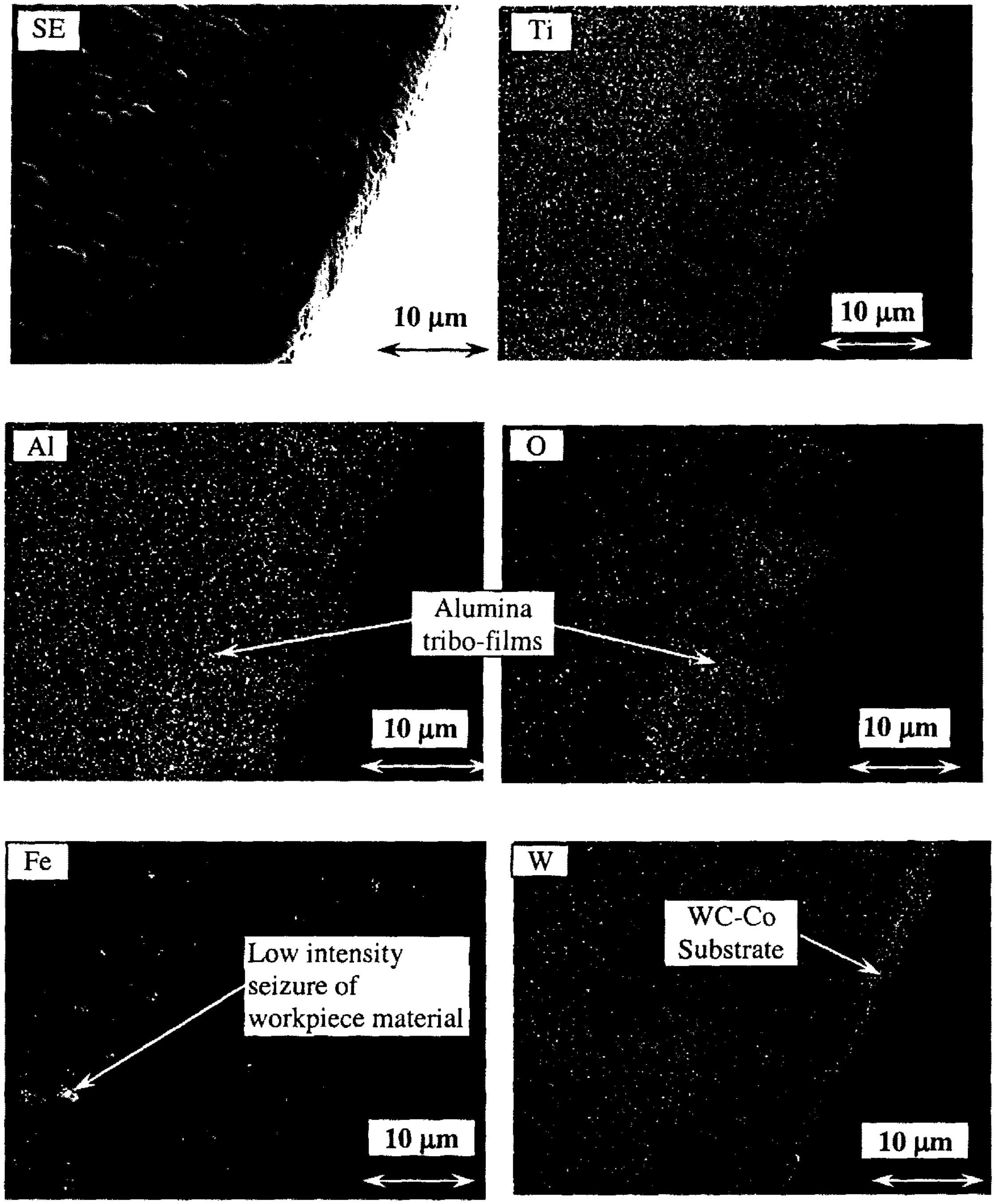

Figure 6.6 SEM image and EDX elemental maps of the worn flank surface of ball end mill with TiAlCrN/WN PVD coating

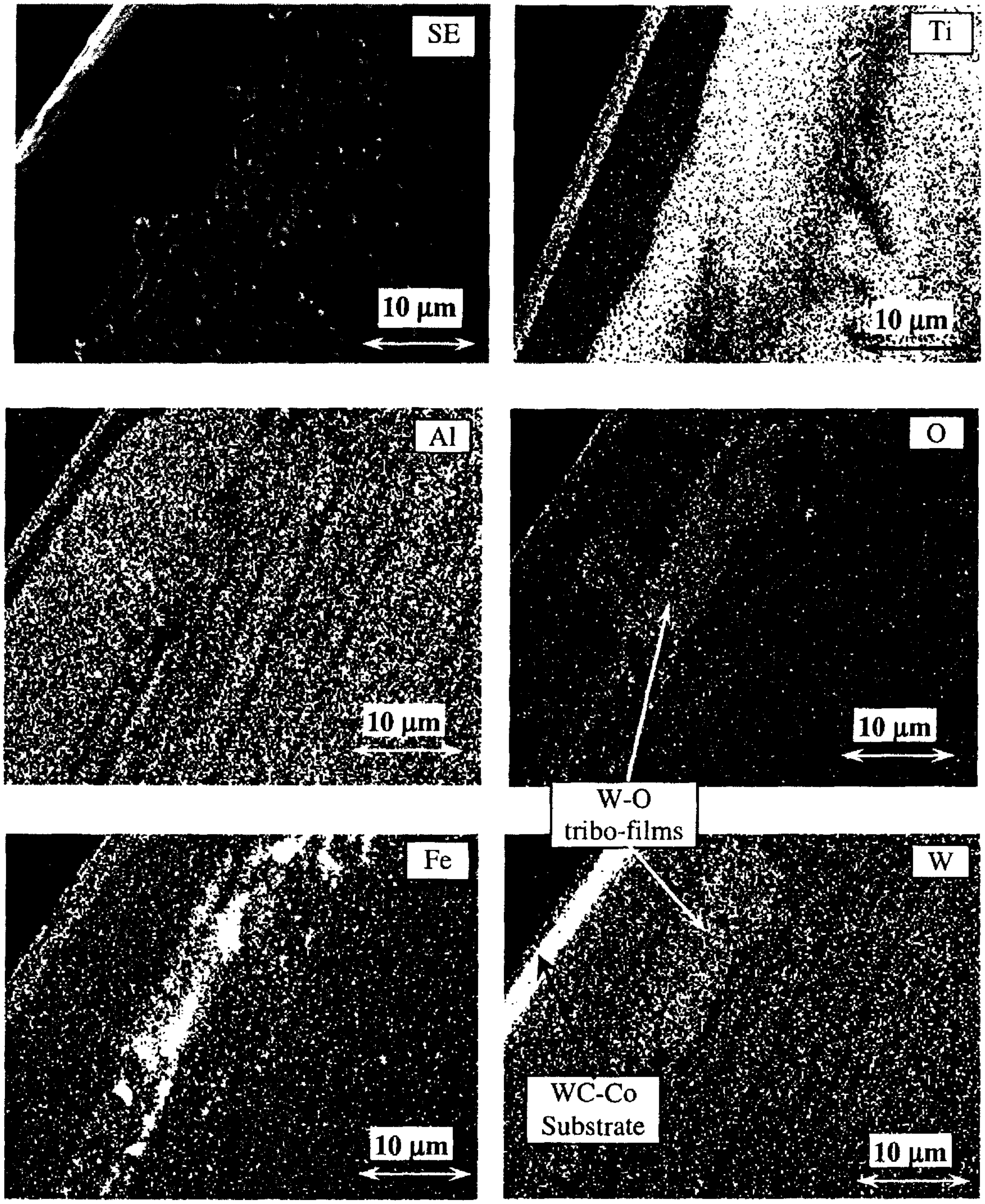

Figure 6.7 SEM image and EDX elemental maps of the worn rake surface of ball end mill with TiAlCrN/WN PVD coating

Figure 6.8 shows the intensive photoelectron lines on the electron spectrum for Ti, Al and W. After the curve fitting of the main components, it is possible to identify the nature of the tribo-films formed on the worn end mill surface. Calculations performed on the presented data show that around 60% of Ti, 50% of Al and 60% of W has been transformed into the tribo-oxide layers during cutting within the surface layer of the TiAlCrN/WN coating. The ability of the tungsten nitride nano-layer to form tribo-oxide seems to be superior to other metallic components of the coating (Figure 6.8). In contrast to the wear behaviour of a $Ti_{10}Al_{70}Cr_{20}N$ coating studied earlier [Fox-Rabinovich, et al., 2005], chromium tribo-oxides were not found on the worn surface of the TiAlCrN/WN coated tools (Figure 6.8).

The known aluminium oxides are gamma-alumina, theta-alumina and alpha-alumina. Gamma- and theta-alumina are two metastable phases of aluminum oxide existing at temperature approximately below 700°C while alpha-alumina is a stable phase, formed/converted from the metastable phases at higher temperature. Al_2O_3, has high melting point of 2054°C. It is insoluble in water and very slightly soluble in strong acids and alkalies. Gamma alumina is composed of minute colorless cubic crystals with specific gravity about 3.6. Alpha alumina is composed of colorless hexagonal crystals with specific gravity about 4.0. And sapphire belongs to alpha-alumina. During the cutting process with cutting temperature above 800°C to 1100°C, the stable alpha-alumina was formed on the tool rake and flank surfaces.

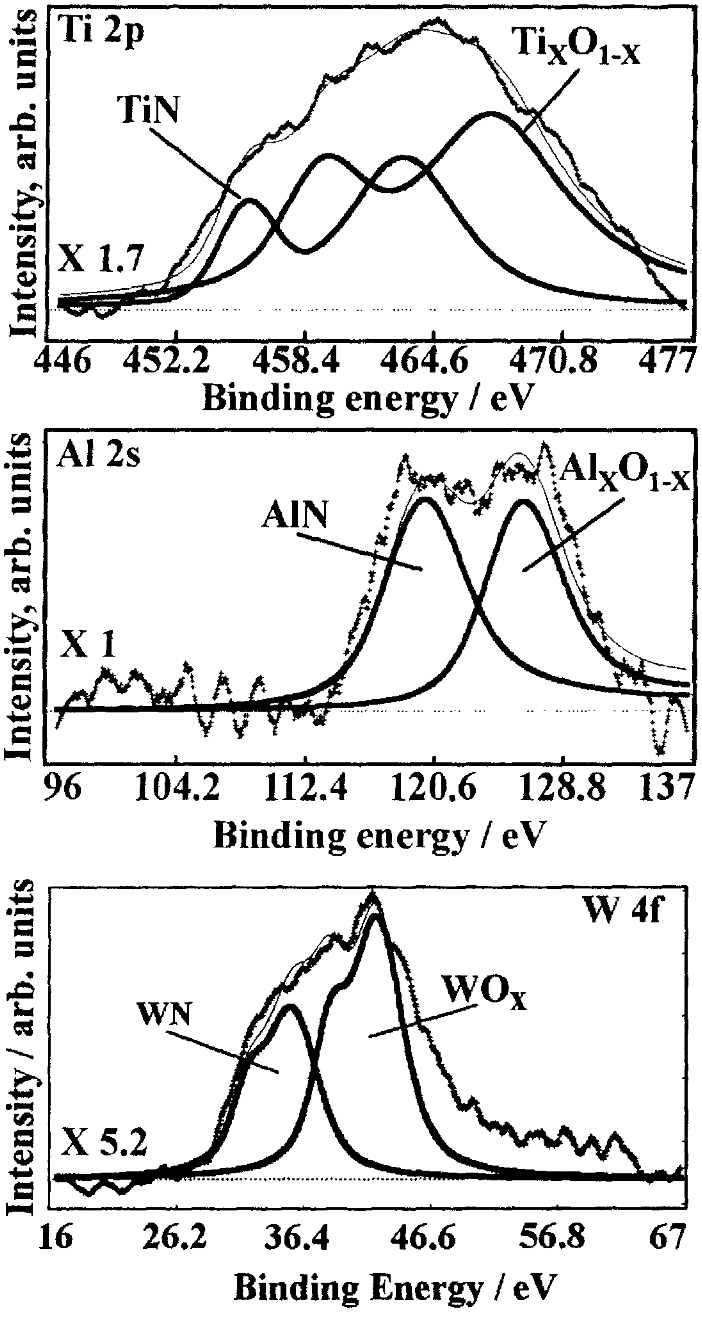

Figure 6.8 X-ray photoelectron spectra of Ti, Al and W for the worn surface of ball end mill with nano-multilayered TiAlCrN/WN coating

Significant structure transformation of the initial nano-multilayered structure of the TiAlCrN/WN coating has taking place during cutting (Figure 6.9). The microstructure of the worn cutting tool surface with the TiAlCrN/WN coating within an island-like seizure of the workpiece material was studied using TEM. Electron diffraction spots had been identified in the electron diffraction patterns of three zones. Zone A in Figure 6.9 presents a near-perfect (110) Fe (bcc) structure of the workpiece material (tool steel H13); Zone B shows a cubic WN structure; Zone C indicates the presence of a nano-crystalline structure of a TiAlCrN layer remote from the surface. Figure 6.9 shows that the initial nano-mulitilayered structure was destroyed within a thin superficial layer of the coating due to heavy loads and high temperatures generating at the tool/workpiece interface under severe conditions of dry high performance machining.

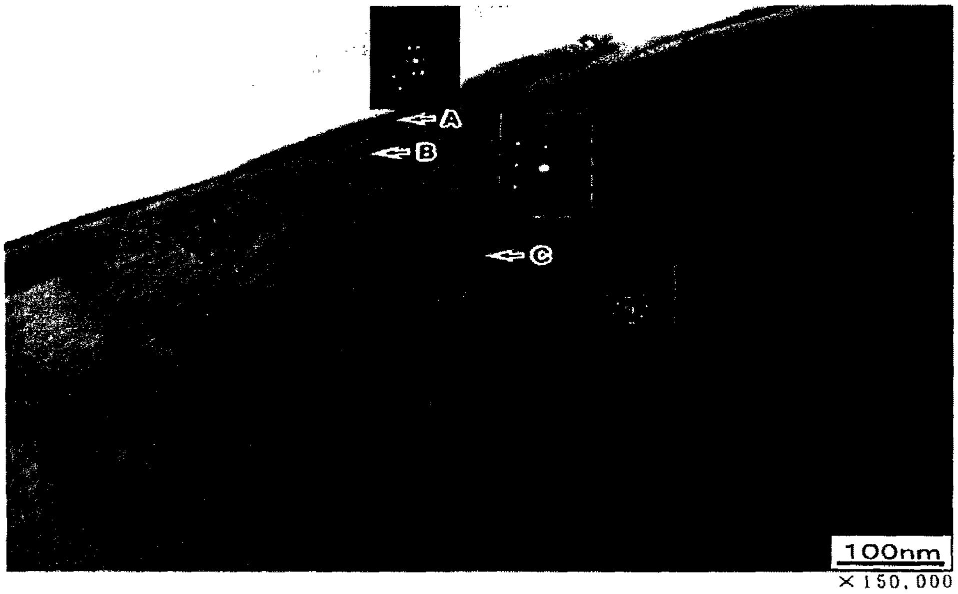

Figure 6.9 TEM images of the worn surface of ball end mill with TiAlCrN/WN coating with diffraction patterns A- (110)Fe (bcc); B-cubic WN; C-nano-crystalline structure of TiAlCrN (fcc)

6.4 Comparison of Nano-structured Coatings

For the purpose of comparison, five different PVD coatings, including three well-known commercially available coatings: nano-composite $AlTiN/Si_3N_4$, nano-crystalline $Al_{67}Ti_{33}N$ and mono-layered $Ti_{10}Al_{70}Cr_{20}N$, and two experimental nano-multilayered coatings: $Ti_{25}Al_{65}Cr_{10}N/BCN$ and $Ti_{25}Al_{65}Cr_{10}N/WN$, were tested. The properties of these coatings are listed in Table 6.3.

Table 6.3 The properties of commercial and experimental coatings

[Fox-Rabinovich &Totten, chapter 9, 10, 2006]

Coating	Structure	Micro hardness (HV0.05) (GPa)
$Al_{67}Ti_{33}N$	Nano-crystalline grain size 10-25 nm	30
$AlTiN/Si_3N_4$	Nano-composites, grain size 5-10nm	45
$Ti_{10}Al_{70}Cr_{20}N$	Nano-crystalline grain size 10-25 nm	34.5
$Ti_{25}Al_{65}Cr_{10}N/WN$	Nano-multilayer, 17nm/period	34
$Ti_{25}Al_{65}Cr_{10}N/BCN$	Nano-multilayer, 17nm/period	34

Figure 6.10 shows the coefficients of friction for the investigated coatings under the temperature range from 20 to 1000°C. The results show that the TiAlCrN/WN coating can maintain a very low coefficient of friction (0.06-0.08) over a wide range of temperature from 150 to 1000°C; the TiAlCrN coating also exhibits a relatively low coefficient of friction in a range of 0.086-0.01 over the same temperatures; the TiAlCrN/BCN coating has a low coefficient of friction (0.1) within the range of 150 to 450°C; the coefficient of friction of the AlTiN coating gradually increases from 0.13 to

0.25 as the temperature rises; and the AlTiN/Si_3N_4 coating starts with a high coefficient of friction 0.34 and then the coefficient of friction decreases as the temperature rises, at 600°C, the coating reaches its lowest coefficient of friction 0.14 and then increases up to 0.35 as the temperature rises up to 1000°C.

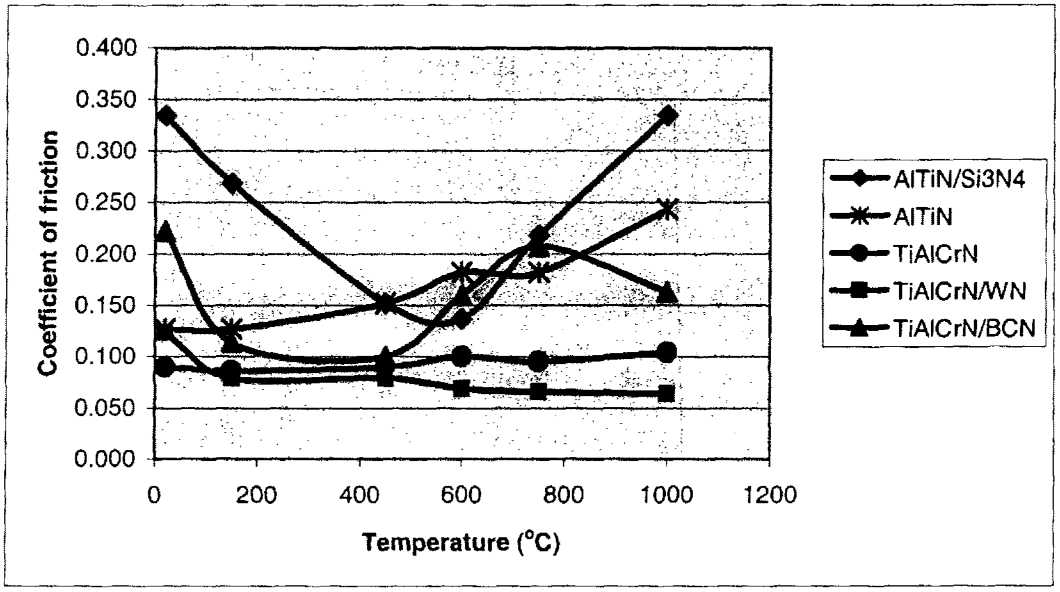

Figure 6.10 Friction coefficients of nano-structured coatings

Figure 6.11 shows the flank wear of the five coated ball nose end mills. Over a cutting length of 30 meters the nano-composite TiAlN/Si_3N_4 coating had the maximum tool wear followed by the nano-crystalline AlTiN coating, nano-multilayered TiAlCrN/BCN coating and mono-layered TiAlCrN coating, while the nano-multilayered TiAlCrN/WN coating had the lowest tool wear, which was approximately half that observed for the other coatings. The maximum resultant cutting forces were calculated from the measured forces and are shown in Figure 6.12. Similar to the trend of flank wear shown in Figure 6.11, the tool with the TiAlN/Si_3N_4 coating generated the highest cutting force while the one with the TiAlCrN/WN coating had the lowest cutting force.

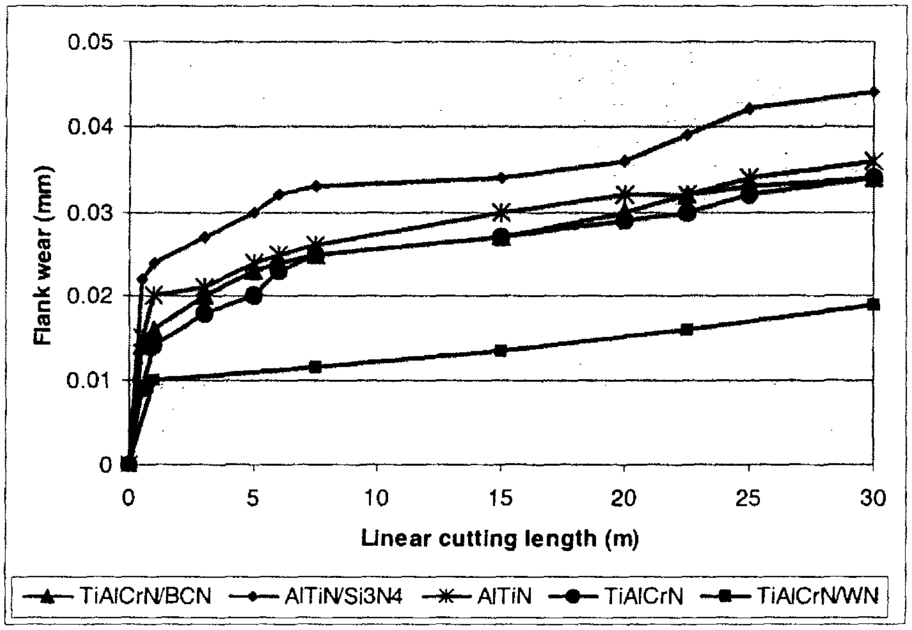

Figure 6.11 Tool wear curves of nano-structured coatings

(Dry machining AISI H13 using solid ball end mill of 10 mm with the coatings shown in the Figure at the cutting parameters: cutting velocity 220 m/min, axial depth of cut 5 mm, radial depth of cut 0.6 mm and feed per tooth 0.06 mm)

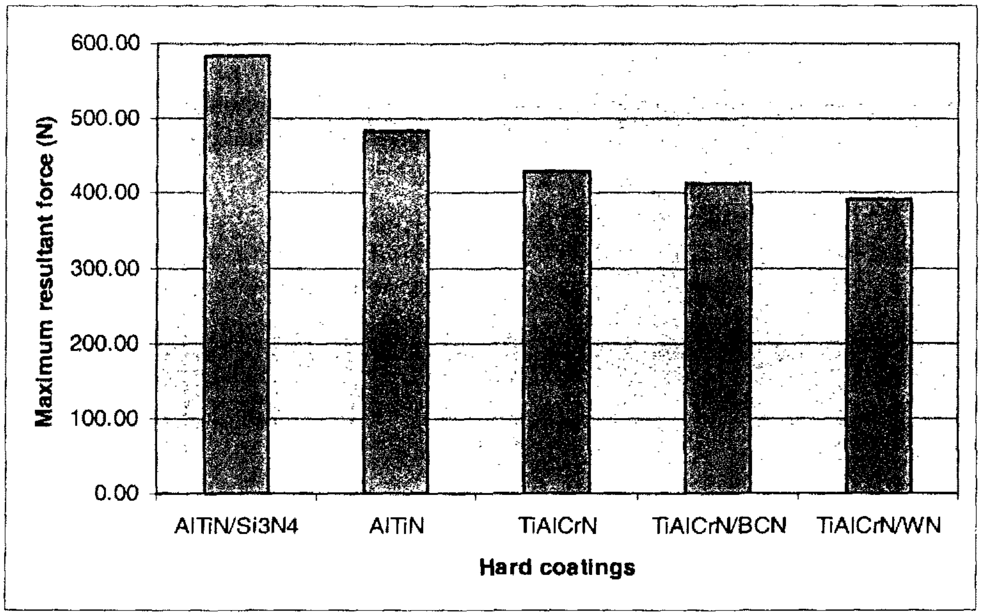

Figure 6.12 Maximum resultant forces of nano-structured coatings

Chips were collected during machining at various cutting lengths and Figure 6.13 shows the typical shapes of the collected chips at cutting lengths of 1 meter and 30 meters. Chips from the new, unworn coated tools have very similar shapes. Figure 6.13e shows the curliest chips generated by the TiAlCrN/WN coated sharp mill. After the tools cut 30 meters an obvious difference in chip shape was observed. The chips corresponding to the nano-composite AlTiN/Si_3N_4 coating (Figure 6.13a) and the nano-crystalline AlTiN coating (Figure 6.13b) were almost flat, with little curl, while the chips corresponding to the TiAlCrN/BCN coating (Figure 6.13d) and the TiAlCrN/WN coating (Figure 6.13f) showed significantly more curl. The chips from the TiAlCrN coating (Figure 6.13c) were in between in term of the degree of curl. Among these samples the chips from TiAlCrN/WN coating exhibited the highest degree of curl.

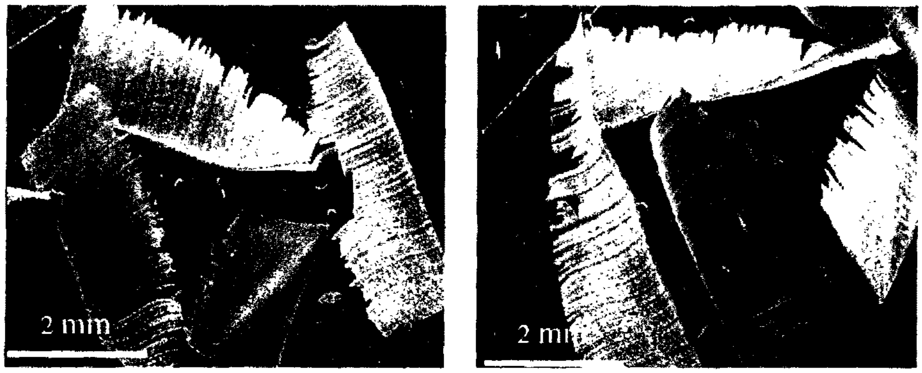

(a) AlTiN/Si_3N_4 (30 m) (b) AlTiN (30 m)

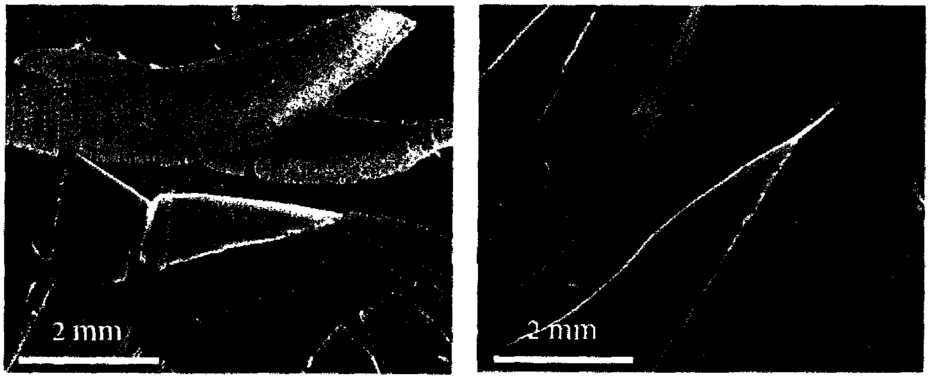

(c) TiAlCrN (30 m) (d) TiAlCrN/BCN (30 m)

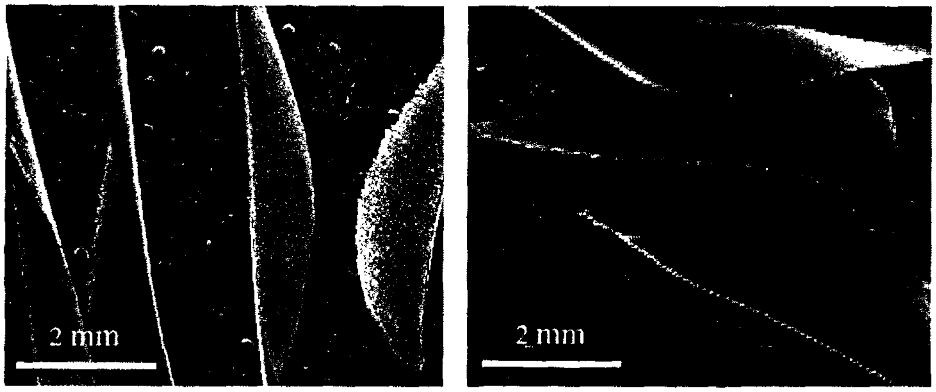

(e) TiAlCrN/WN (1 m) (f) TiAlCrN/WN (30 m)

Figure 6.13 SEM images of chip shape

Presently there is no reliable way to measure the cutting temperature precisely during a ball nose end milling process. Thus the cutting temperatures were estimated based on the relation (cutting temperature vs. chip color) presented by Venkatesh, et al. (1993) and Ning, et al. (2001) (Table 6.4). The relation between the color of the chips and the estimated temperatures for this study is shown in Table 6.5. It was observed that the chip color generated by the new coated tools were all a similar shade of light brown. After cutting 30 meters, the chips from the TiAlCrN/BCN and the TiAlCrN/WN coated tools changed to a golden brown shade while the ones from the AlTiN/Si_3N_4 and AlTiN coated tools became purple and brittle. From Table 6.5, we can see that after cutting 30 meters the cutting temperature increased only a little for the TiAlCrN/WN and TiAlCrN/BCN coatings while it increases by approximately 100°C for the AlTiN/Si_3N_4 and AlTiN coatings.

In order to identify the effect of the compressed air blast on the color of the chips, trial tests on the TiAlCrN coated tool with and without an air blast of 0.69 MPa (100 psi) were performed (Table 6.6). It was found that the color of the chips without the air blast was brown and purple while the one with the compressed air blast was light brown. The difference induced by the compressed air was approximately 80-100°C based on this color comparison approach.

Table 6.4 Chip temperature vs. chip color

Chip temperature vs. chip color [Venkatesh et al., 1993]		Chip temperature vs. chip color [Ning, et al., 2001]	
Chip temperature (°C)	Chip color	Chip color	Chip temperature (°C)
829	Light brown	Light brown	800-840
881	Golden brown	Brown	820-880
900	Dark brown+blue	Blue+brown	860-920
937	Light blue	Blue+purple	920-960
981	Dark blue	Dark blue	960-1000
		Dark blue+green	>1000

Table 6.5 Chip color vs. chip temperature

Coating	Cutting length (m)	Cutting condition	Chip color	Chip temperature (°C)
All coatings	1	0.69 MPa air blast	Light brown	800-840
TiAlCrN	30	0.69 MPa air blast	Dark brown	880-900
AlTiN/Si$_3$N$_4$	30	0.69 MPa air blast	Purple	920-960
AlTiN	30	0.69 MPa air blast	Purple	920-960
TiAlCrN/BN	30	0.69 MPa air blast	Golden brown	840-880
TiAlCrN/WN	30	0.69 MPa air blast	Golden brown	840-880

Table 6.6 Chip color vs. chip temperature with/without air blow

Coating	Cutting length (m)	Cutting condition	Chip color	Chip temperature (°C)
TiAlCrN	1	Without air blow	Brown+purple	900-920
TiAlCrN	1	0.69 MPa air blast	Light brown	800-840

The results from the SEM and the EDX analysis of the surfaces of the worn ball nose end mills are shown in Figures 6.14 to 6.17. Significantly different wear behaviors can be observed for different coatings. For example, a zone of intensive seizure was observed on the surface of a cutting tool with the nano-composite AlTiN/Si$_3$N$_4$ coating (Figure 6.14). Severe spallation of the coating layer on the tool with the TiAlCrN/BCN coating (Figure 6.15) was also seen. The cutting tool with the TiAlCrN coating (Figure

6.16) had a much higher rate of workpiece material pick-up than the tool with the TiAlCrN/WN coating (Figure 6.17) but was less intensive when compared to the nano-composite AlTiN/Si_3N_4 coating. Among all the tools the worn surface of the TiAlCrN/WN coated cutting edge had the lowest seizure intensity.

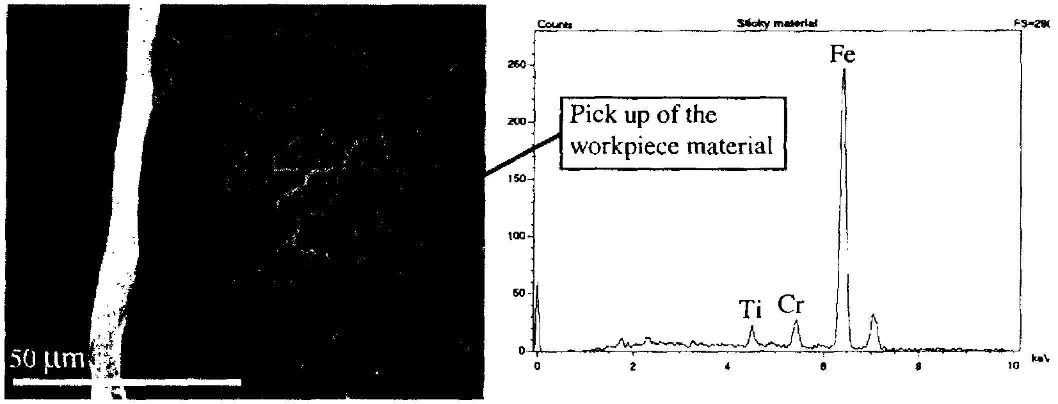

Figure 6.14 SEM image and EDX spectrum of flank face of ball end mill with AlTiN/Si_3N_4 coating

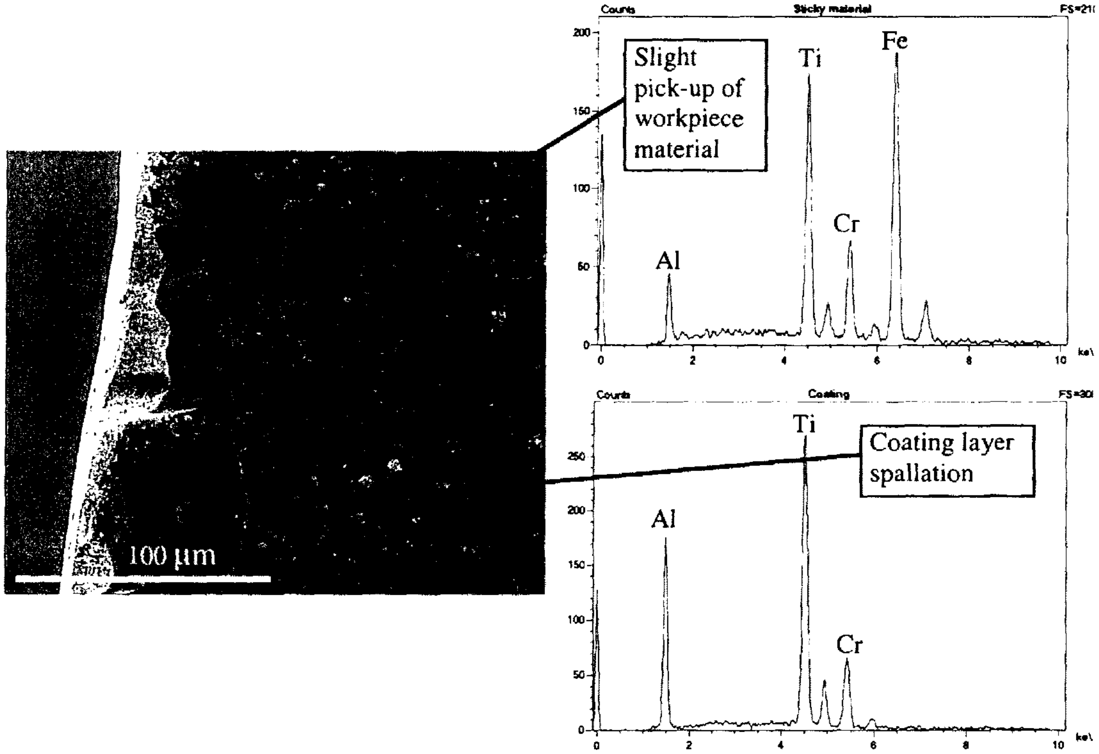

Figure 6.15 SEM image and EDX spectrum of flank face of ball end mill with TiAlCrN/BCN coating

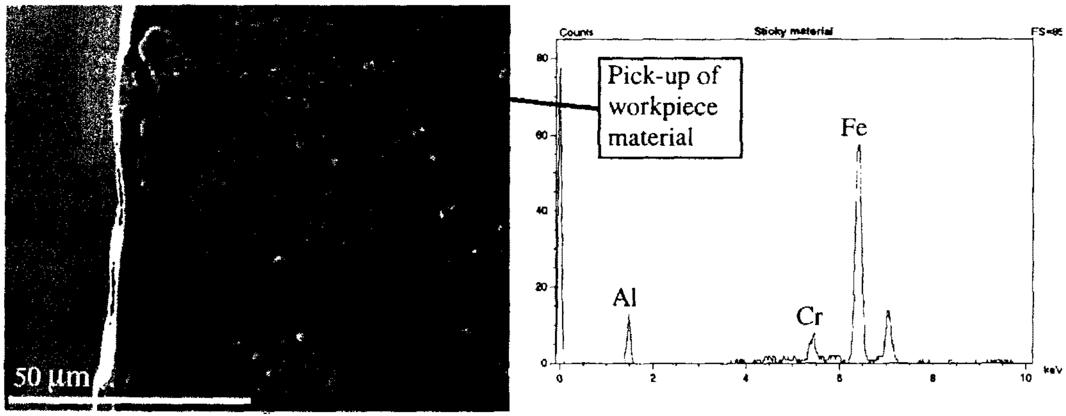

Figure 6.16 SEM image and EDX spectrum of flank face of ball end mill with TiAlCrN coating

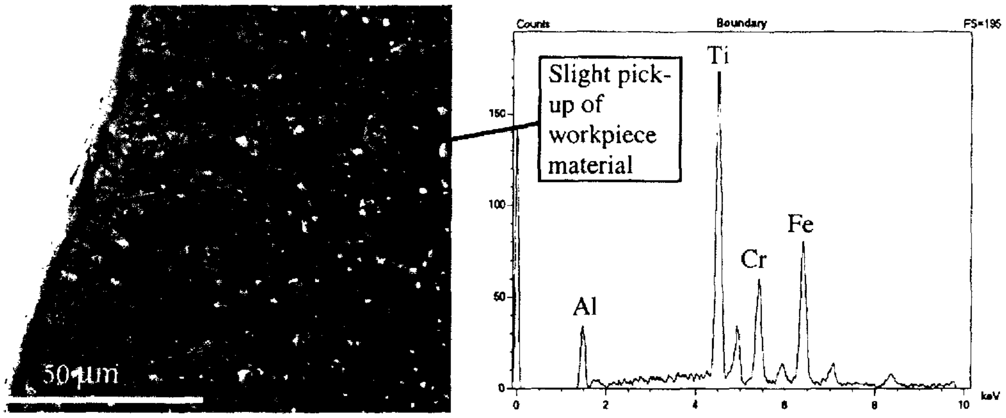

Figure 6.17 SEM image and EDX spectrum of flank face of ball end mill with TiAlCrN/WN coating

The results presented above highlight the importance of the lubrication properties of the coating and show the role that lubricity plays in dry high speed machining.

During the cutting operation chips are generated by a shearing action as a part of creating the final desired machined surfaces. In ball end milling the cutting velocity at the tool tip is zero and increases along the cutting edge to the depth of cut. The chip flow velocity increases from the tool tip to the depth of cut. Curly chips are typical of this cutting operation. Also there is friction at the tool-chip interface due to the pressure and the motion of the chip along the rake face. If the friction is high, the tool contact side of the chip can undergo further plastic deformation in the secondary shear zone after the plastic deformation on the shear plane of the primary shear zone. Since the chip flow faces large resistance due to high friction, chips become less curled and thicker with a corresponding increase in contact length. This friction has a significant influence on the cutting forces, temperature rise and the shape of the chip.

It is well known that alumina has excellent heat and oxidation resistance and a much lower thermal conductivity than the layer of nitride coating, cemented carbide tool substrate and the workpiece material such as AISI H13 [Fox-Rabinovich and Totten, 2006]. Therefore, it insulates the tool surface from the heat generated during chip formation and redirects the heat flow towards the chip. Alumina is also very hard and dense and its oxidation stability can be maintained up to 1200°C [Fox-Rabinovich and Totten, 2006]. Thus the thin film of alumina serves to protect the substrate material against abrasive wear, oxidation wear and crater wear [Fox-Rabinovich and Totten, 2006]. That is why all of the coatings studied in this paper are based on TiAlN-based coatings rich in aluminum.

The results show that the nano-multilayered TiAlCrN/BCN coating performed worse than the TiAlCrN/WN coating under dry high speed machining conditions. Boron oxide tribo-films are supposed to be formed under these conditions as a result of tribo-oxidation and it is known that boron oxides are good lubricants [Erdemir, 2000]. However, the melting point of boron oxide is low, typically 450°C [Erdemir, 2000]. Once the boron oxide forms at the tool surface it transforms to a liquid phase under the high cutting temperatures (see table 6.5) and then it is squeezed out of the cutting zone by the heavy forces acting on the frictional surface. It is also known that the onset oxidation temperature of boron oxides is about 800°C [Fox-Rabinovich and Totten, 2006] and the coated tool most probably loses its oxidation stability above this temperature. Figure 6.15 shows the phenomenon that one coating layer is peeled off revealing the next layer. Based on this mechanism these cutting edges are not protected to the same degree and thus lose their strength and fail much faster than with the other nano-multilayerd coatings.

The main reasons for the poorer performance of the nano-composite AlTiN/Si_3N_4 coating and nano-crystalline AlTiN coating in this study as compared to the nano-multilayered TiAlCrN/WN coating are their higher coefficient of friction values and the resulting poorer lubricity in the cutting zone (Figure 6.10). High friction in these cases results in intensive seizure in the tool-chip interface as the chips flow over the tool (Figure 6.14). Therefore, in addition to their hardness and oxidation resistance, the friction characteristics of the hard coatings should be optimized.

However, tool life and wear behavior could be improved if the self-lubricating properties of the coatings at elevated temperatures can be enhanced. A good example here is the TiAlCrN/WN nano-multilayered coating.

It is found that the nano-multilayered TiAlCrN/WN coating is able to generate tungsten oxides due to the tribo-oxidation process (Figure 6.8). During the running in stage, a certain amount of local sticking of workpiece material to the coated tool surface enhances the formation of the W oxide tribo-films (Figure 6.7). This sticking of workpiece material to the tool surface leads to intensive heat generation [Trent and Wright, 2000; Ning, et al., 2001] and rapidly transforms tungsten from the WN nano-layer closest to the top friction surface and forms the oxide tribo-film (Figure 6.8). Tungsten oxide has a high melting temperature around 1500°C and it has low shear strength [Erdemir, 2000] so it is present at the cutting tool/workpiece interface as a solid high temperature lubricant. In addition, tungsten oxide is able to retain a relatively high hardness of around 15-22 GPa at elevated temperatures [Endemir, 2000].

The formation of the tungsten tribo-oxides during the running-in stage prepares an excellent working environment in the cutting zone for the post-running-in stage. Therefore, both intensity of seizure and the coefficient of friction values drop (Figures 6.17, 6.10), decreasing the cutting forces (Figure 6.12) and heat generation at the tool/workpiece interface (Table 6.5), which ultimately results in the overall wear intensity reduction (Figure 6.5). In synergy with the other tribo-oxides (in this case alumina) that are forming during the friction of TiAlCrN nano-layers (Figure 6.8), this formation of a lubricious tungsten oxide leads to a significant tool life increase. By combining this data with tool life data found in Figure 6.5 one can conclude that the lubricious/protective tribo-oxide films predominantly isolate the workpiece from the cutting tool surface. Surface damaging wear mechanisms such as seizure become close to the external wear with critically lower wear intensity. That is why dry machining of the hardened H13 steel becomes quite efficient if the nano-multilayered TiAlCrN/WN coating is applied onto the cutting tool surface.

The nano-multilayered structure of the coatings plays a significant role in the improvement of wear behaviour. It is possible that the nano-scale multilayered structure critically enhances two beneficial phenomena: 1) mass transfer at the start of the running-in stage that results in quick generation of tribo-oxides with the suitable composition and microstructure; 2) selective oxidation within the island-like seizure zones with the further formation of tribo-oxides that critically reduce the intensity of this surface damaging process, resulting in tool life improvement.

Thus the self-adaptive, synergistically alloyed, nano-multilayered coatings are promising materials for severe tribo-applications associated with high temperature and stress. Metallurgical design of coatings used for severe applications should be based on the understanding of the synergistic action during friction of alloying elements that are present in nano-multilayered coatings. The direction of research that deals with the complexity of friction, including in-depth understanding of the self–organization process and the improvement of hard coatings based on this phenomenon, should be considered as a significant trend for future development of wear resistant coatings.

The study of chip cross-section was performed. The results, shown in Figure 6.18, demonstrate that the microstructure of the chips strongly depends on the type of coating applied. The chips generated by the ball end mill with $Al_{0.65}Ti_{0.35}N$ nano-crystalline coating has a very wide hardening zone (Figure 6.18a), which corresponds to the estimated temperature presented in Table 6.5. The chips formed by the tool with $Al_{0.65}Ti_{0.35}N/Si_3N_4$ nano-composite coating have a narrower hardening zone as compared to the one on the chips by $Al_{0.65}Ti_{0.35}N$ coated too. Further observations show that no intensive flow zone but micro-cracks exist on the chips, which indicates that the chips are quite brittle due to high cutting temperature (Figure 6.18b). In contrast, the chips generated by the self-adaptive TiAlCrN/WN coating has a very narrow hardening zone and a flow zone with intensive plastic deformation (Figure 6.18c), which indicates lower friction and lower cutting temperature as compared to the other two categories of coatings above.

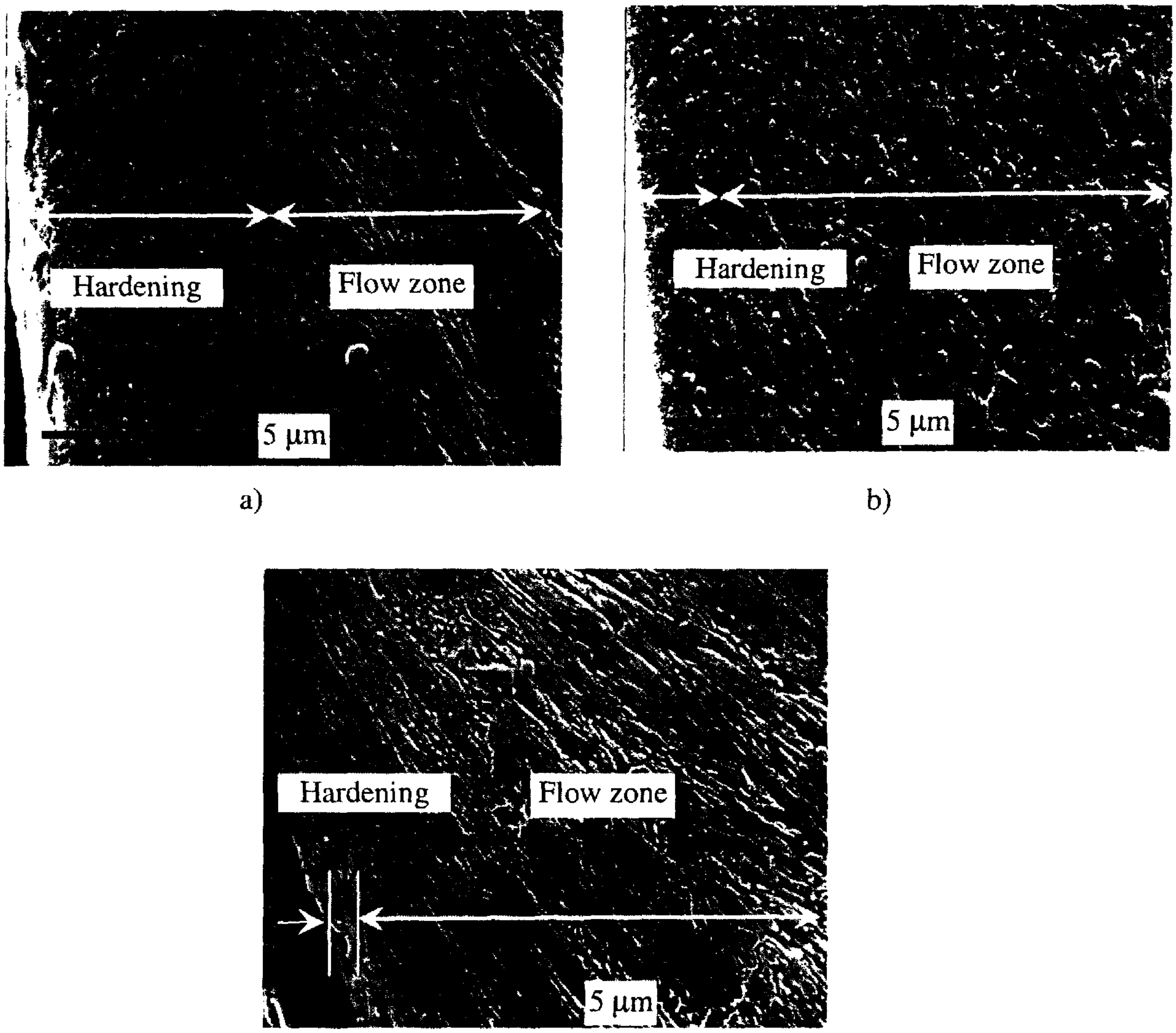

a)

b)

c)

Figure 6.18 SEM images of chip cross-sections. a) chips generated by $Al_{0.65}Ti_{0.35}N$ coated tool; b) chips by the $Al_{0.65}Ti_{0.35}N/Si_3N_4$ tool; c) the chips generated by the self-adaptive TiAlCrN/WN coating.

The microhardness measurements were also performed on the chip cross-section versus the distance from the chip undersurface (Figure 6.19). The results show that intensive hardening of the workpiece material occurs when nano-composite $Al_{0.65}Ti_{0.35}N/Si_3N_4$ coating or nano-crystalline $Al_{0.65}Ti_{0.35}N$ coating is applied. In contrast, an effect of chip softening takes place when self-adaptive TiAlCrN/WN coating is applied. The phase composition was analyzed by performing Roentgen analysis. The results show that a mixture of retained austenite and martensite formed on the undersurface of the chips generated by the tool with $Al_{0.65}Ti_{0.35}N$ coating. There is a minor amount of the retained austenite on the chips formed by the $Al_{0.65}Ti_{0.35}N/Si_3N_4$ coated tool while no austenite was found on the chip surface from the self-adaptive TiAlCrN/WN coating (Table 6.7). These results further confirm the self-adaptability of TiAlCrN/WN and its functions on the reduction of friction and cutting temperature.

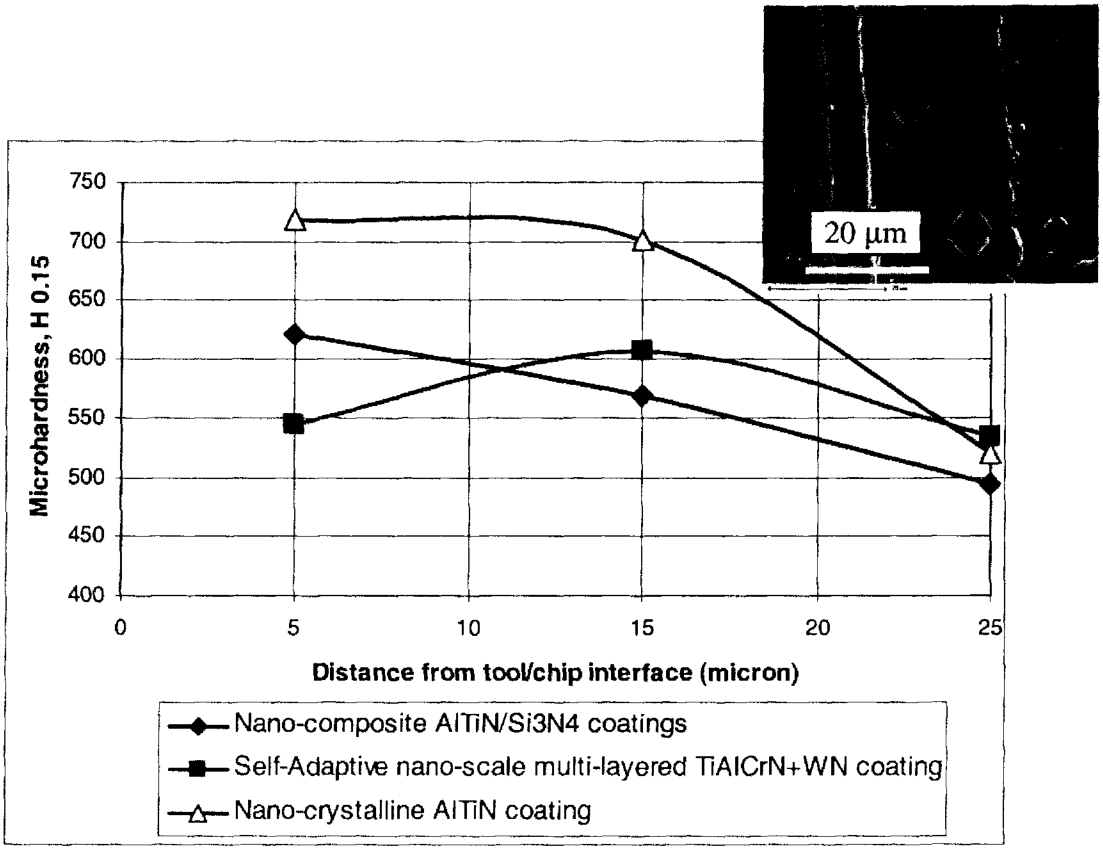

Figure 6.19 Microhardness of the chips vs. the distance from tool/chip interface

Table 6.7 Phase composition on the chips undersurface (X-ray Diffraction (XRD) data).

Coating	Phase composition of the chips undersurface
Nano-crystalline AlTiN	$\alpha+\gamma$ (some amount)
Nano-composite AlTiN/Si3N4	$\alpha+\gamma$ (traces)
Self-adaptive TiAlCrN/WN	α only

6.5 Nano-multilayered TiAlCrN/Me$_x$N Coatings

The results from the investigation of TiAlCrN/BCN and TiAlCrN/WN coatings give the following conclusions:

1. The formation of tribo-oxides working as solid lubricants (W-O) during cutting greatly improve the performance of the cutting tool.
2. The formation of the liquid lubricating films (B-O) is not beneficial under the aggressive cutting conditions used in this study.
3. Under the dry hard high performance machining at the cutting speed of 220 m/min, the cutting temperature can go approximately from 850^{o}C to beyond 1000^{o}C. If the cutting speed is increased the cutting temperature will go even higher.
4. The power to the sputtering source and the rotational speed of the sample holder are recommended to be set to 1 kW and 5 rpm, respectively.

These guidelines are used for further coating development. For the applications of higher cutting speeds, more transition metal nitrides of V and VI periods, excluding Vanadium and Molybdenum, were considered as candidates for investigation. Table 6.8 lists the melting points of the transitional metal oxides and other related oxides from high to low. In order to obtain solid lubricants during friction, Vanadium and Molybdenum should be excluded because they belong to the liquid lubricants under the proposed cutting conditions. Therefore, only the transitional elements such as Ta, Cr, W and Nb were considered in nano-multilayered TiAlCrN/Me$_x$N coatings.

Table 6.8 Oxides and their melting points

Oxides	Melting point (°C)	Boiling point (°C)
Cr-O	2435	~4000
Al-O	2054	~3000
Ta-O	1872	
Ti-O	1870	2972
Nb-O	1520	
W-O	1500	1730
Mo-O	795	1155
V-O	690	1750
B-O	450	1860

The substrate type C-2SB was selected for coating performance investigation at the cutting speed of 300 m/min and above because tool breakage occurred for the substrate type C-2MB before the tools reached the tool wear criteria (Figure C.1). The coated tools were tested at higher cutting speed of 300 m/min. Very impressive results were obtained. Figure 6.20 shows how their flank wear changes with respect to the cutting length at the cutting speed of 300 m/min. In this study the nano-multilayered coatings outperformed the monolayer TiAlCrN coating. TiAlCrN/WN coating still showed good performance at this higher cutting speed. However, the TiAlCrN/NbN coating had the best performance among them.

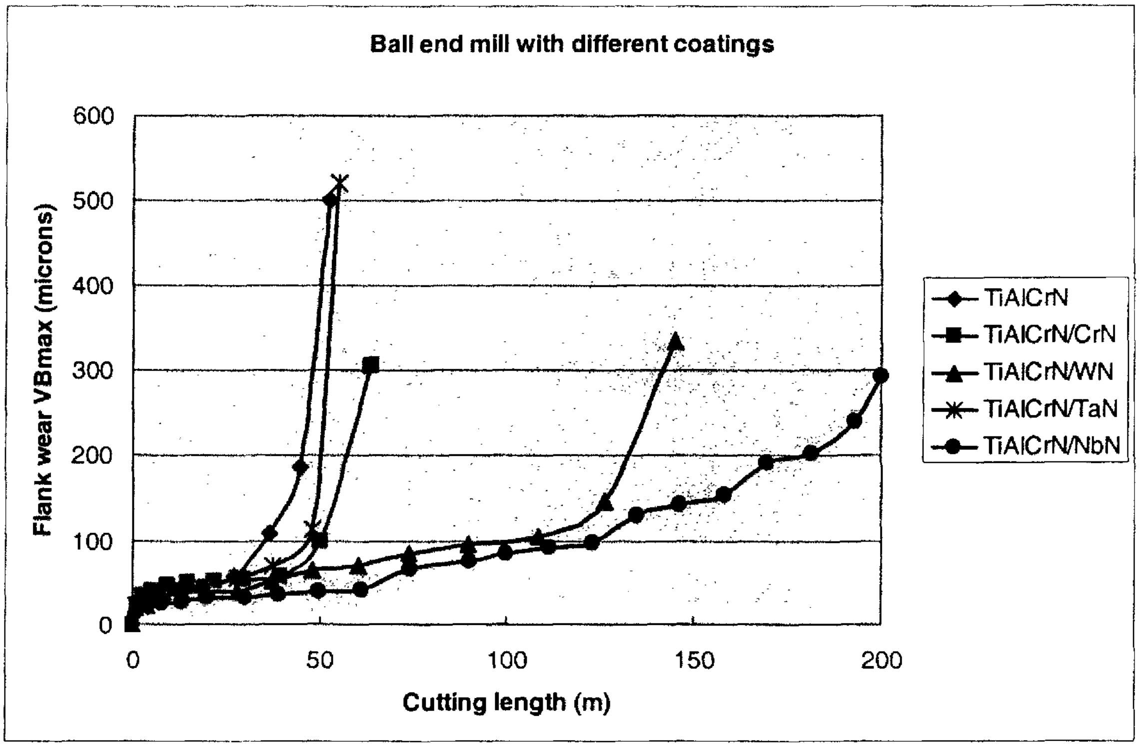

Figure 6.20 Tool wear curves of ball end mills coated with TiAlCrN based coatings (cutting speed of 300 m/min)

6.6 The Effect of Contact Length on Tool Performance

It is found that the cutting tool performance depends on not only wear resistance, the condition of lubricity, hot hardness, and toughness but also on the contact length between the chip and the tool rake face. As described earlier, if the chip-tool contact area becomes too large, high frictional force will be generated during cutting and hence high cutting temperature as well, subsequently, seizure phenomenon becomes more intensive which eventually results in tool failure. On the contrary, if the chip-tool contact length is too small, the cutting pressure and cutting temperature are concentrated in a very small region at the cutting edge. Under this condition, the cutting edge undergoes severe attack from both force and temperature with the cutting tool failing rapidly. In general the shorter the chip-tool contact length, the curlier the chips. Figure 6.21 shows that the tool with the $Ti_{25}Al_{65}Cr_{10}N$ coating generated extremely curly chips (needle-like chips) at the very beginning of cutting. From the undersurface of the chips (Figure 6.21), it is observed that the surfaces are quite rough, which indicates that the coefficient of friction is not low.

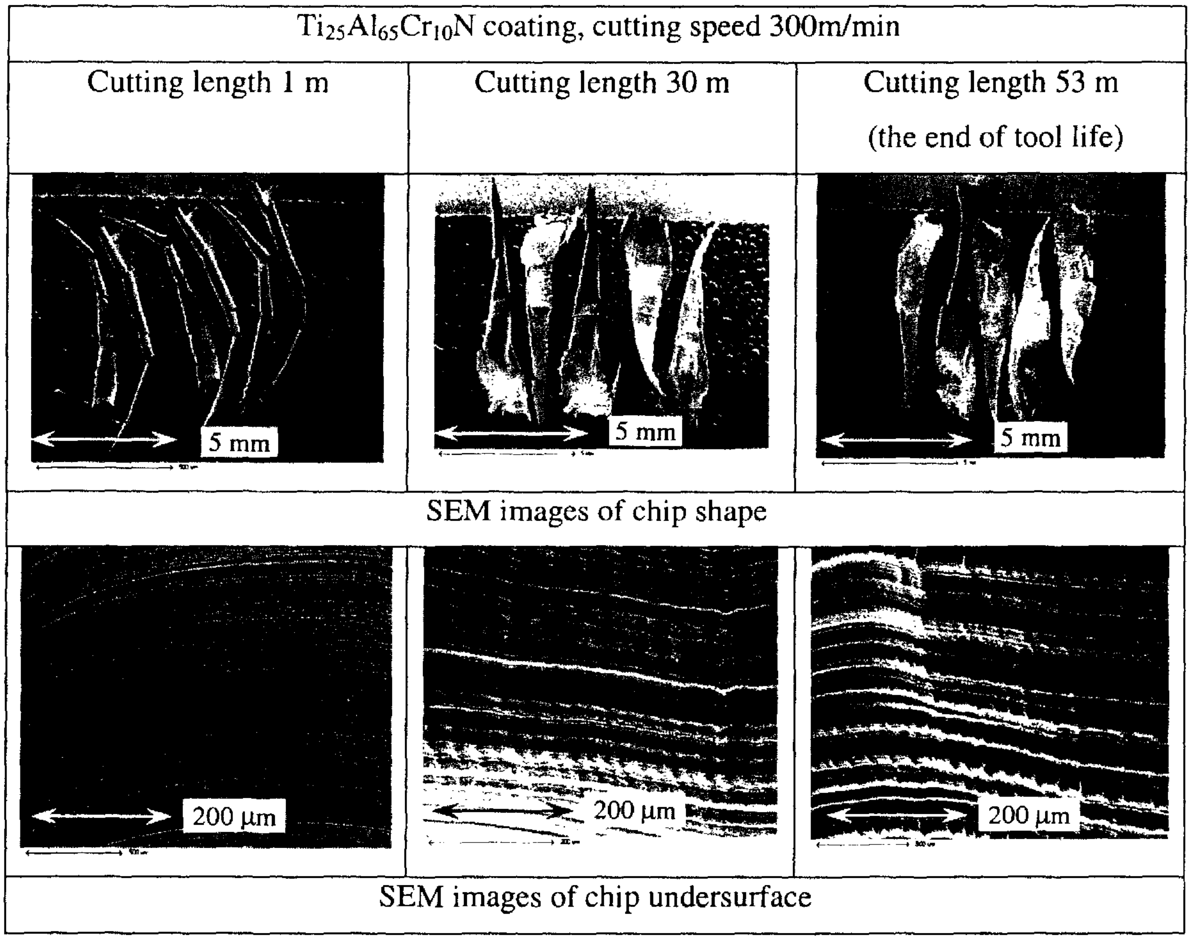

Figure 6.21 SEM images of chip shapes and undersurfaces ($Ti_{25}Al_{65}Cr_{10}N$)

Regarding the TiAlCrN/TaN coating, the changes in chip shapes versus cutting lengths are very interesting (Figure 6.22). At the very beginning, the chip shape is quite similar to the ones generated by the TiAlCrN/WN coated tool machined with a cutting velocity of 220 m/min. The contact length corresponding to this type of chip shape seems optimal. However, as the cutting length increases, the chips become curlier. At the cutting length of 30 m, the shape of the chips changes to needle-like chips which is just similar to the ones generated by $Ti_{25}Al_{65}Cr_{10}N$ at the very beginning of the cutting process. Because of the short contact length, the cutting edges undergo high pressure and temperature. Therefore, the tool quickly reaches the wear criteria of 0.3mm. From SEM images of the undersurface of the chips, it can be inferred that the tribological property of the TiAlCrN/TaN coating against H13 tool steel is superior to the one for $Ti_{25}Al_{65}Cr_{10}N$ at an elevated temperature.

TiAlCrN/TaN coating, cutting speed 300m/min		
Cutting length 1 m	Cutting length 30 m	Cutting length 55 m (the end of tool life)
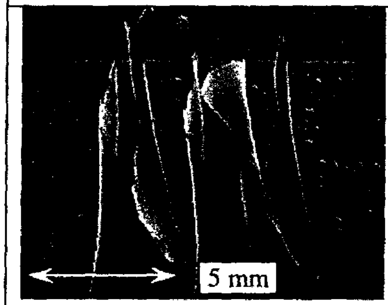	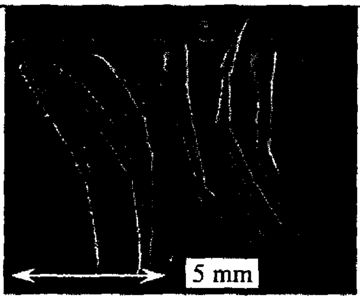	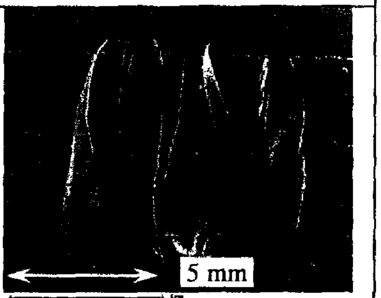
SEM images of chip shape		
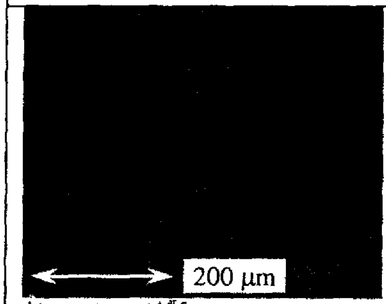	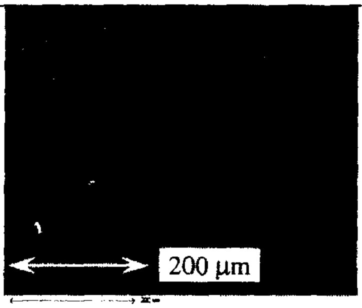	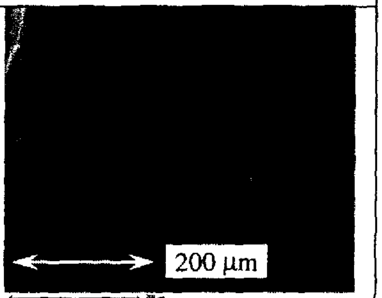
SEM images of chip undersurface		

Figure 6.22 SEM images of chip shapes and undersurfaces (TiAlCrN/TaN)

For TiAlCrN/CrN coating (Figure 6.23), the undersurfaces of the chips start with a slightly rough surface. As the cutting length increases the shape of the chips become less curly and the undersurfaces become coarser, which indicates the high temperature lubricity properties are not good.

TiAlCrN/CrN coating, cutting speed 300m/min		
Cutting length 1 m	Cutting length 30 m	Cutting length 63 m (the end of tool life)

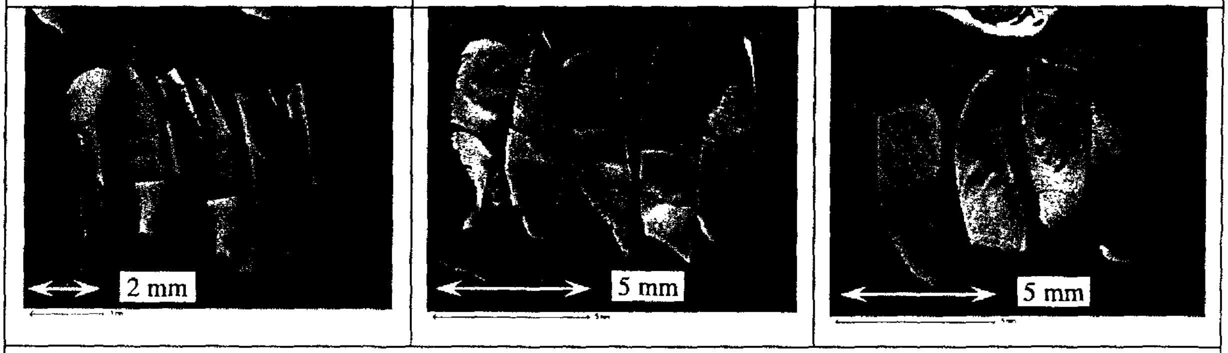

SEM images of chip shape

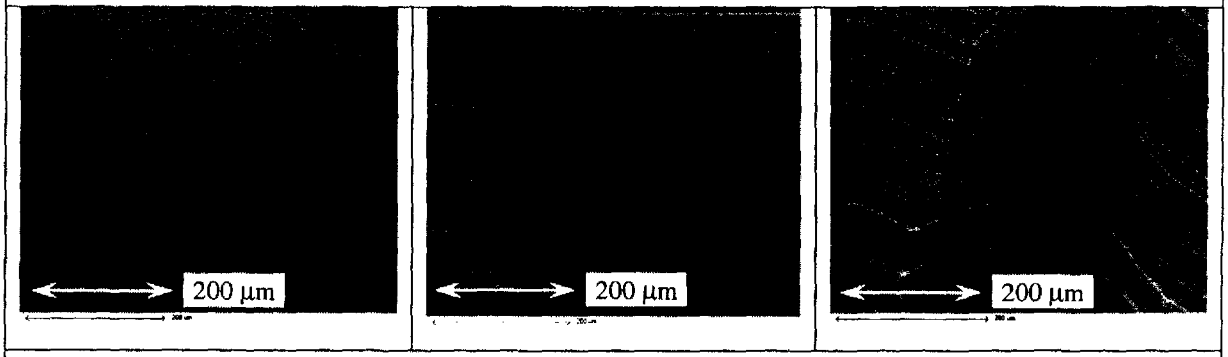

SEM images of chip undersurface

Figure 6.23 SEM images of chip shapes and undersurfaces (TiAlCrN/CrN)

TiAlCrN/WN coating (Figure 6.24) also starts with a similar undersurface to the one of TiAlCrN/CrN. However, as the cutting length increases to 30 m, the undersurface is more smooth than the one generated at the very beginning and the shape of the chips is still curly but much less curl than the one from a new tool. When the tool reached its tool wear criteria, one can still see quite smooth chip surfaces, which indicate that this coating has very good high temperature tribological properties.

<table>
<tr><td colspan="3">TiAlCrN/WN coating, cutting speed 300m/min</td></tr>
<tr><td>Cutting length 1 m</td><td>Cutting length 30 m</td><td>Cutting length 145 m
(the end of tool life)</td></tr>
<tr><td>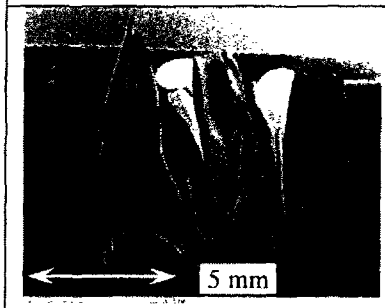 </td><td>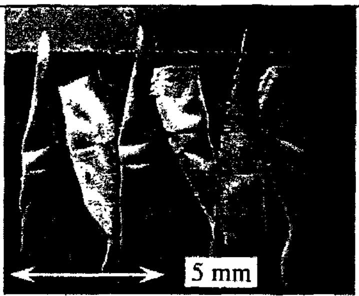 </td><td>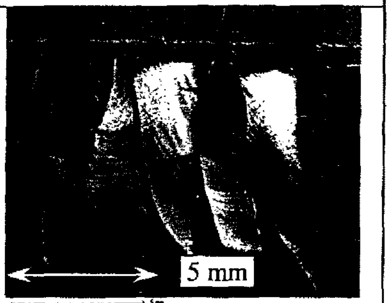 </td></tr>
<tr><td colspan="3">SEM images of chip shape</td></tr>
<tr><td>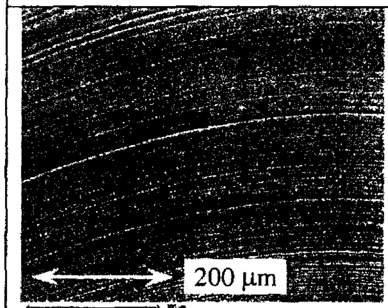 </td><td>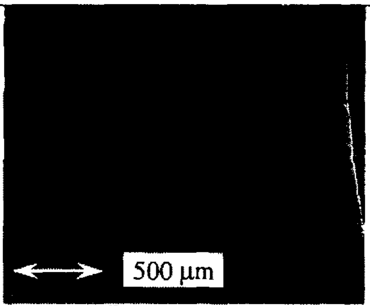 </td><td>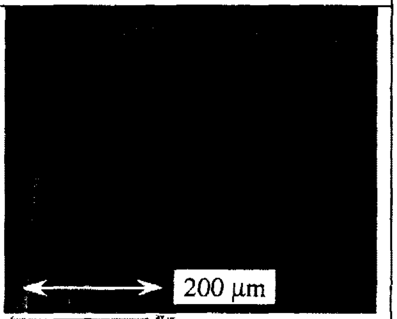 </td></tr>
<tr><td colspan="3">SEM images of chip undersurface</td></tr>
</table>

Figure 6.24 SEM images of chip shapes and undersurfaces (TiAlCrN/WN)

Figure 6.25 shows the chips generated by the best candidate, TiAlCrN/NbN coating. For this case it starts with a very rough undersurface of the chips and the degree of curly is quite optimal. When the tool cuts 30 meters, the undersurfaces of the chips become smooth, which is quite similar to the chips generated by the TiAlCrN/WN coating, however, the shape of the chips is a bit curlier than the ones from the TiAlCrN/WN coating. Due to its ability to maintain the optimal cutting condition under severe cutting condition, the TiAlCrN/NbN coated tool yields the longest tool life.

TiAlCrN/NbN coating, cutting speed 300m/min		
Cutting length 1 m	Cutting length 30 m	Cutting length 180 m (the end of tool life)
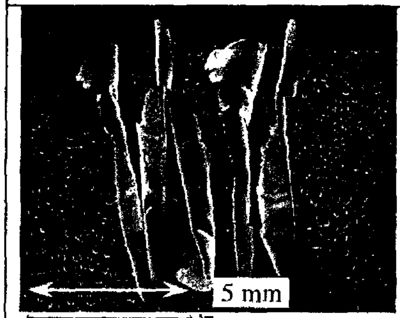	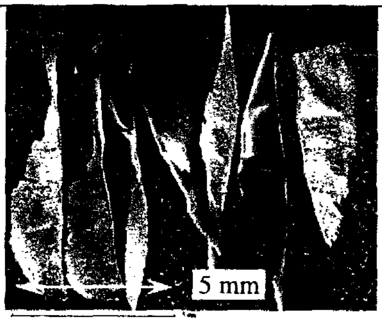	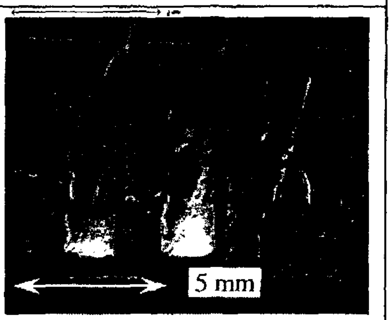
SEM images of chip shape		
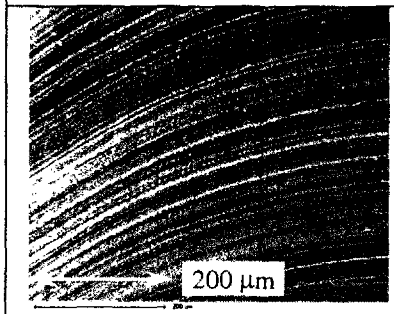	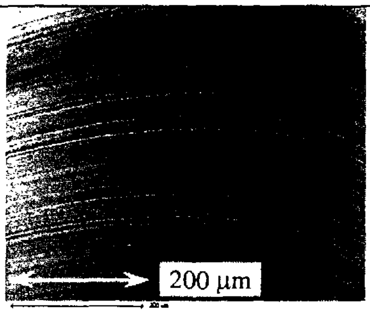	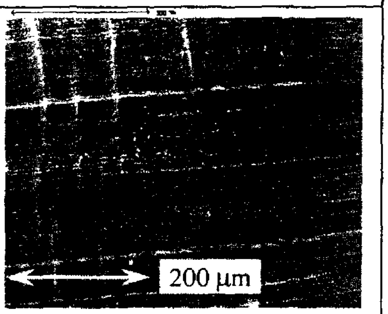
SEM images of chip undersurface		

Figure 6.25 SEM images of chip shapes and undersurfaces (TiAlCrN/NbN)

From observations made on the chips, the following statements can be made:

- Tool-chip contact length cannot be too short or too long. A short contact length causes the cutting pressure and temperature to be concentrated on the cutting edge, therefore, the cutting edges are prone to premature damage and hence have a short life. On the contrary, a long contact length results in high friction and hence high cutting forces and high cutting temperature which also have negative effects on the performance of the tool.
- There is an optimal contact length, the ability to maintain this condition under severe cutting condition is one of the key factors for a tool to achieve the longest tool life.
- The degree of curling and the smoothness of the undersurface of the chips are associated with conditions of favourable lubricity in the cutting zone.

6.7 Nano-multilayered TiAlCrN/NbN Coatings

Since the TiAlCrN/NbN coating exhibited the best performance among the coatings studied, it was chosen for further study. As usual, optimizing the content of Nb was performed.

Like the deposition of TiAlCrN/WN coatings, TiAlCrN/NbN coatings were deposited on the ball end mills (type C-2SB) by varying the power (0.5 kW, 1.0 kW and 2.5 kW) to the sputtering source. The thickness of the lubricious layer NbN increases as the power increases from 0.5 kW to 2.5 kW. Table 6.9 lists the composition and properties of the coatings corresponding to the different powers of the sputter source. The data in Table 6.9 shows that the sputtering power does not have significant influence on the microhardness of the three Nb coatings; however, it affects the elastic modulus and oxidation resistance of the coatings. The introduction of NbN layers on the TiAlCrN base layers results in an increase in coating plasticity and a slight decrease in oxidation resistance. It was found that the TiAlCrN/NbN coating, deposited using the sputtering power of 1.0 kW and having approximately 4 at.% of Nb, has better oxidation resistance than the other two coatings with about 2 at.% of Nb and 10 at. % of Nb. Without the addition of NbN, the microhardness of the coating is approximately 35 GPa, while with the addition of NbN, the microhardness of the three coatings does not vary significantly with the input of DC power but stays around 31 GPa. However, a slight decrease in elastic modulus is observed as the content of Nb increases. The oxidation resistance of the coating has a significant impact on the wear resistance of the cutting tools under high performance dry machining conditions. Due to the affinity of Nb with oxygen, the short-term oxidation resistance of nano-multilayered TiAlCrN/NbN coatings is lower compared to a mono-layered TiAlCrN coating.

Table 6.9 Composition and properties of the coatings corresponding to the power of the sputtering source

The parameter of the coating deposition: input of power on the sputter source, kW	Composition of the coating, at % (EDX data)				Properties of the coatings		
	Al	Ti	C	Nb	Microhardness, GPa	Young Modulus, GPa	Weight gain, mg/cm^2 after short-term (1 h) oxidation in air at 900 °C
0	60.29	28.69	11.02	0	34.4	577	0.046
0.5	63.79	24.24	10.22	1.75	31.60	560.67	0.068
1.0	62.58	24.12	9.49	3.81	31.67	539.00	0.055
2.5	57.95	23.63	9.14	9.28	31.61	501.49	0.088

Figure 6.26 shows the coefficient of friction (COF) of TiAlCrN/NbN coatings from room temperature up to 1000°C. At high temperatures of 1000°C, the COF of TiAlCrN/NbN coatings strongly depends on the amount of Nb in the overall layer of the coating, which is related to the thickness of the NbN nano-layers. The optimal amount of Nb in the coating is around 4 at. % in this nano-multilayered coating for the smallest coefficient of friction can be achieved in the temperature range of 900 - 1000°C. This temperature range and slightly above is the cutting temperature range for the cutting tests investigated. The COF values are high for this coating at the temperatures below 800°C but TiAlCrN/NbN (4%) becomes slightly lower compared to TiAlCrN coating (Figure 6.26) at temperatures around 1000°C.

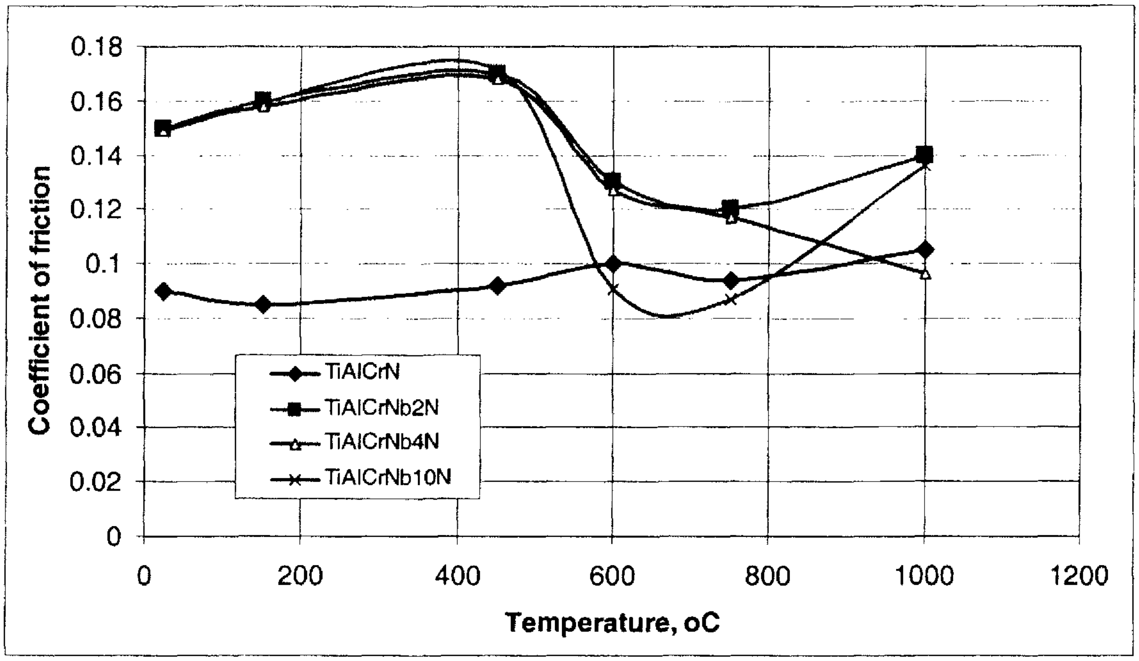

Figure 6.26 Coefficient of friction of TiAlCrN/NbN coatings vs. temperature

Figure 6.27 shows the tool life of these three coatings. It is found that the tool life of the TiAlCrN/NbN coatings with varying Nb content corresponds to the COF values at elevated temperatures. TiAlCrN/NbN (10% / 2.5 kW) coating has the worst performance while TiAlCrN/NbN (4% / 1.0 kW) and TiAlCrN/NbN (2% / 0.5 kW) coatings have very similar tool life. The longest tool life is achieved by a nano-multi-layered TiAlCrN/NbN coating with overall Nb content of 4 at. %.

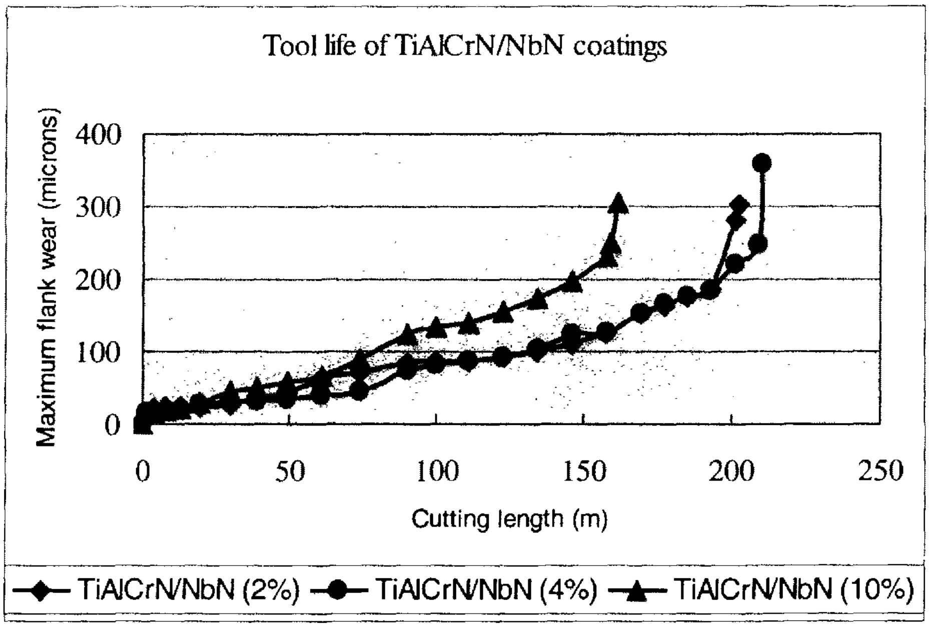

Figure 6.27 Tool life with different TiAlCrN/NbN coatings deposited on C-2SB (cutting speed: 300 m/min)

In order to compare how well the coatings protect the cutting tools, all three TiAlCrN/NbN coated tools were taken out for SEM study at the cutting length of 100 m. Figure 6.28 shows the SEM images of the cutting edge, flank face, notch area and rake face. Comparing these three coatings, one can see that the value of the maximum flank wear has no big difference at a cutting length of 100 m (Figure 6.27). However, the SEM images reveal a bigger difference (Figure 6.28). For instance, obvious cutting edge micro-chipping can be observed on the cutting edge of the TiAlCrN/NbN (10%) coated tool. Comparing TiAlCrN/NbN (2%) and TiAlCrN/NbN (4%), very similar wear pattern can be observed in the notch area (Figure 6.28c); however, the average flank wear of the TiAlCrN/NbN (4%) coated tool is narrower than the one of the TiAlCrN/NbN (2%) coated tool (Figure 6.28b). Therefore, TiAlCrN/NbN (4% / 1.0 kW) coating was selected for further wear progression study.

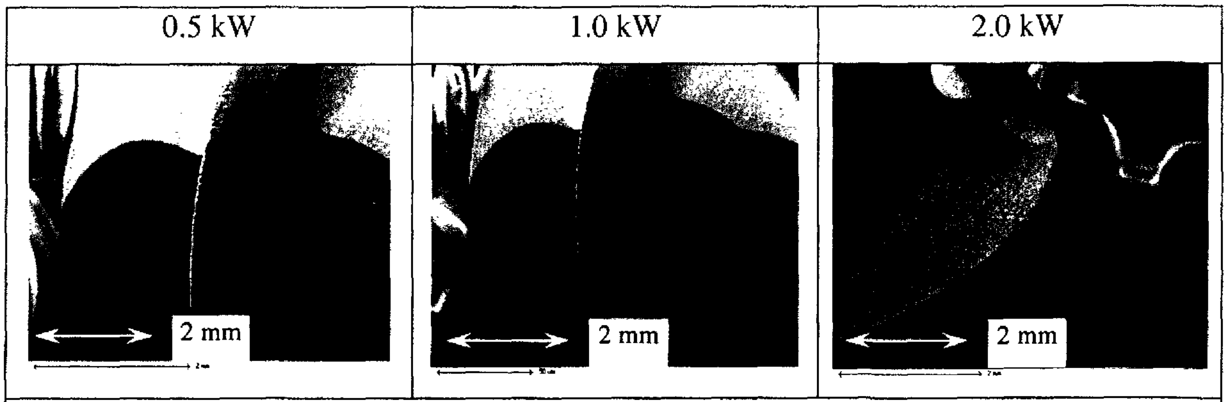

a) SEM images of the cutting edge (TiAlCrN/NbN)

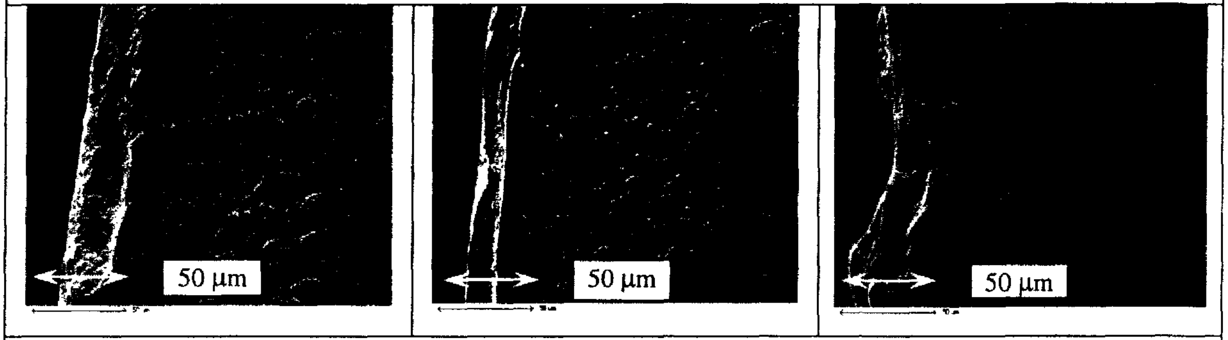

b) SEM images of flank face

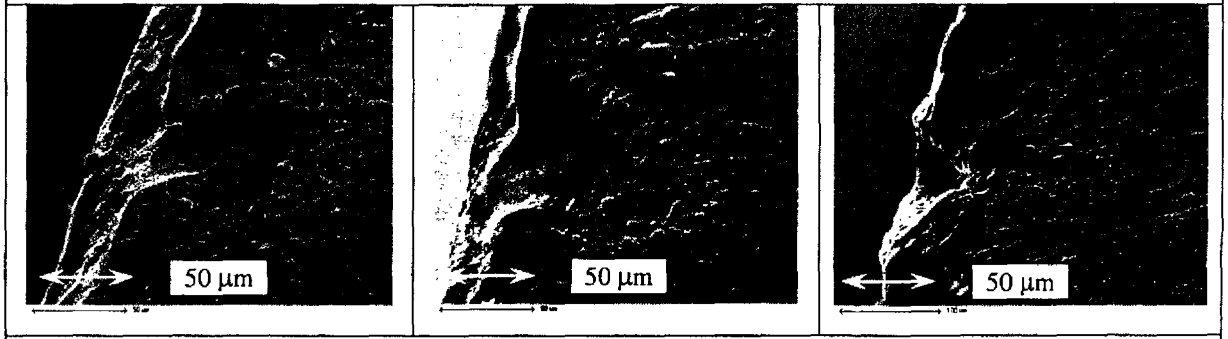

c) SEM images of notch area

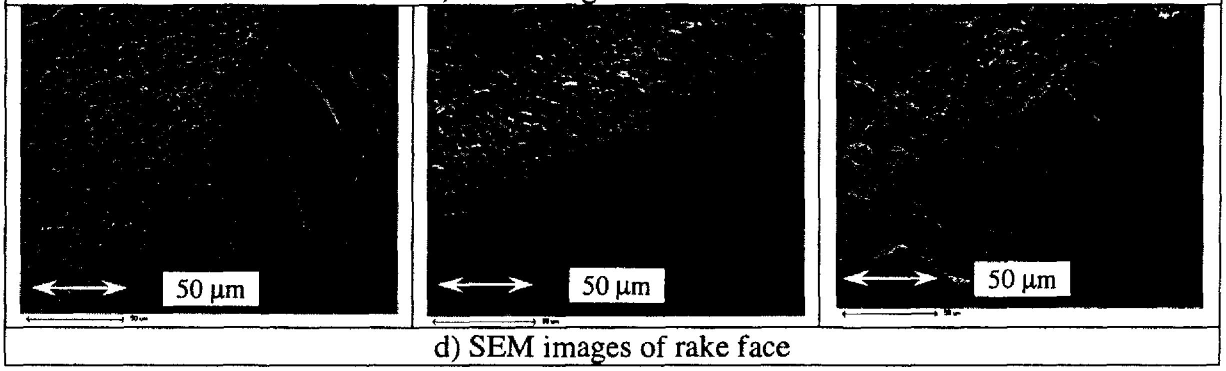

d) SEM images of rake face

Figure 6.28 Comparison of three TiAlCrN/NbN coatings at the cutting length of 100 m

6.8 Wear Progression Study of TiAlCrN/NbN Coating

Since the novel nano-multilayered TiAlCrN/NbN (4 at. % / 1.0 kW) was the best coating, it was used to perform comprehensive investigation of the wear behavior, reveal the progression of the wear process and chip formation, and present suggestions for extending the performance of the machining process. The coating was deposited on the same ultra-fine grained cemented carbide ball nose end mill (C-2SB, 10 mm diameter). The tool was tested by dry machining of hardened steel AISI H13 (HRC 55-57) at the higher cutting speed of 300 m/min. In order to track the tool wear progression SEM and EDX studies were intermittently performed. During the cutting process, the chips were collected, and the flank wear and the corresponding force components were measured. Based on the measured force components, the maximum average forces were computed and a matrix with tool wear and corresponding force components at different cutting lengths was formed. Figure 6.29 demonstrates the changes of the maximum cutting forces during the tool life for the TiAlCrN/NbN coated tool. The two force components Fy (the direction of radial depth of cut) and Fz (the direction of axial depth of cut) increase at very low rates until the cutting length reaches 165 m and show a very similar trend to the corresponding wear curve for this tool (Figure 6.27). While in the feed direction, the cutting force component Fx shows a slight drop in the middle range of tool service life. This is not uncommon as a machining process is very complex and there are many factors which affect cutting forces in addition to tool wear such as cutting zone temperature which can vary with wear substantially. Furthermore, factors interact with each other and dominate at different stages during cutting. For example the drop in Fx might be due to the improvement of lubricity in the cutting zone because of the formation of the protective oxides. When the increase of cutting force component due to tool wear is less than the decrease of force by the improvement of lubricity, the force component drops. Table 6.10 lists the correlation of wear to the cutting forces and the percentage of force increment. One can see that the Fy (direction of radial depth of cut) and the Fz (direction of axial depth of cut) are highly correlated to flank wear. Therefore, Fy and Fz are recommended for monitoring the cutting tool.

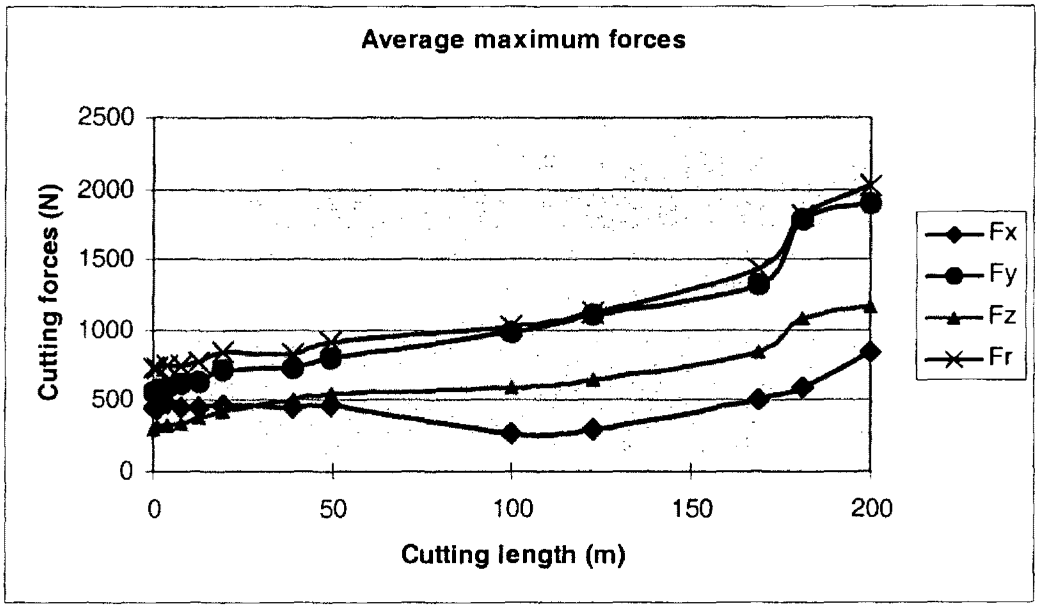

Figure 6.29 Cutting forces vs. cutting length (TiAlCrN/NbN (4%))

Table 6.10 Correlation of wear with cutting forces and the percentage of force increase

	Vbmax (μm)	Fx(max) (N)	Fy(max) (N)	Fz(max) (N)	Fr(max) (N)
Cutting length 0.2 m	10	456.18	568.81	292.72	728.81
Cutting length 200 m	292	845.21	1889.49	1169.43	2022.03
Percentage of force increment	-	85%	232%	299%	-
Correlation to wear	-	0.64	0.94	0.95	-

6.8.1 Tool wear and wear mechanisms

The tool wear progression on the rake and flank faces of the ball end mill from the new to the worn tool is exhibited in Figure 6.30. Figure 6.30a shows how the new tool surfaces look. In this case a droplet phase of different size could be observed on the surfaces (Figure 6.30a). Based on the study of the worn surfaces of the cutting tools by means of EDX analysis, five wear zones were identified. They are: worn coating region, exposed substrate material, crater wear zone, seizure zone and build-up area, as shown in Figures 6.28b-e.

It was found that very small areas of substrate were exposed at the very cutting edge after a short cutting distance of 3.9 m (Figure 6.30b). As the cutting length increased the coating was wearing out and the substrate material was exposed more intensively. Therefore, the exposed substrate zone was getting wider which lead to intensive tool/chip interaction and temperature growth (Table 6.11). This process had a gradual character. TiAlCrN/NbN coating showed excellent protective ability up to the length of cut around 150 m. Up to this length of cut no evidence of intensive interaction at the tool/chip interface was found and the wear rate was relatively low (Figures 6.28a-c and 6.25). When the exposed area of the substrate material at the cutting edge became wider, the cutting temperature became higher due to the interaction between the non-protected cutting edge and the chip during friction (Table 6.11). As the temperature increased above 1000°C the coating lost its protective ability and intensive seizure could be observed on both the flank and rake faces (Figure 6.30d-e). As the exposed substrate area became wider, two zones in this area were formed: 1) worn substrate zone which was formed as a result of rubbing and sliding by chips (Figure 6.30d); 2) crater zone, which was caused by diffusion as the chips moved through the rake face under high temperatures (Figure 6.30d). At the same time seizure zones were formed on the rake and flank faces of the tool as a result of the workpiece material adhering to the tool surfaces during chip formation (Figures 6.28d and 6.28e). At the initial stages of wear one could barely see a seizure zone (Figure 6.30b) because the tool/chip contact length was quite short (chips were curly, Figure 6.34a). Once the tool became dull, the cutting temperature and cutting forces became higher, the contact length grew (chips became less curly (Figures 6.31b-f) and consequently, the seizure zones in both the flank and rake faces became wider (Figures 6.28d and 6.28e). The built-up zones were composed of workpiece material, substrate material and coating elements, and they were located in the flank/worn coating band interface and rake/worn coating band interface. The built-up zone formed due to workpiece material rubbing along the cutting edge, carrying some substrate and coating materials which then stuck to the cutting zone during chip formation (Figures 6.28b-c).

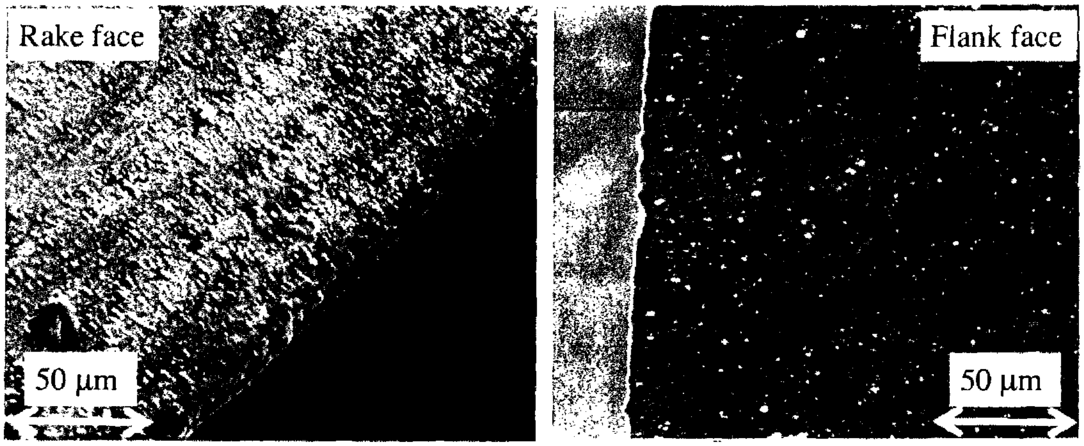

a) TiAlCrN/NbN new cutting edge

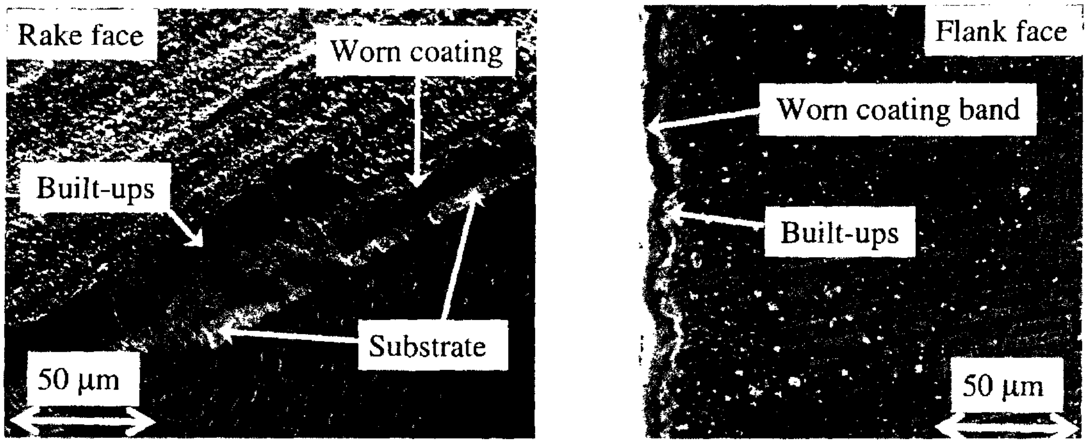

b) TiAlCrN/NbN 3.9 m cutting length

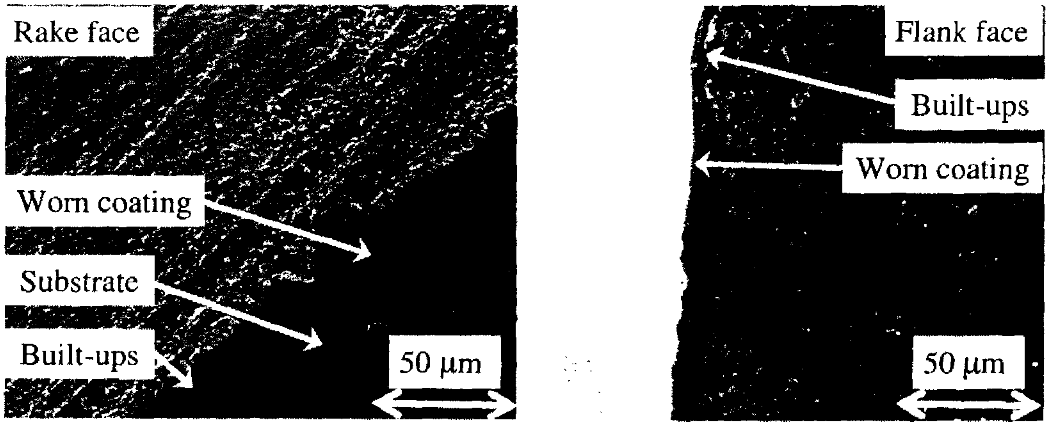

c) TiAlCrN/NbN 100 m cutting length

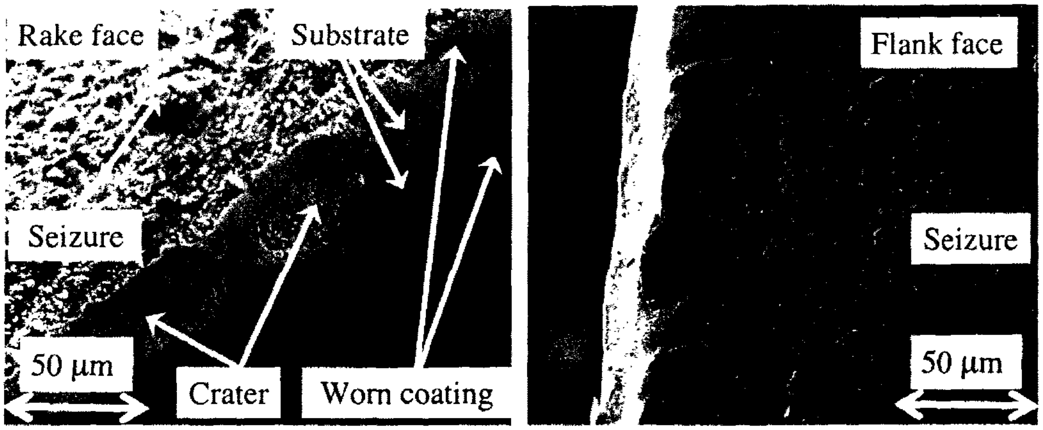

d) TiAlCrN/NbN 150 m cutting length

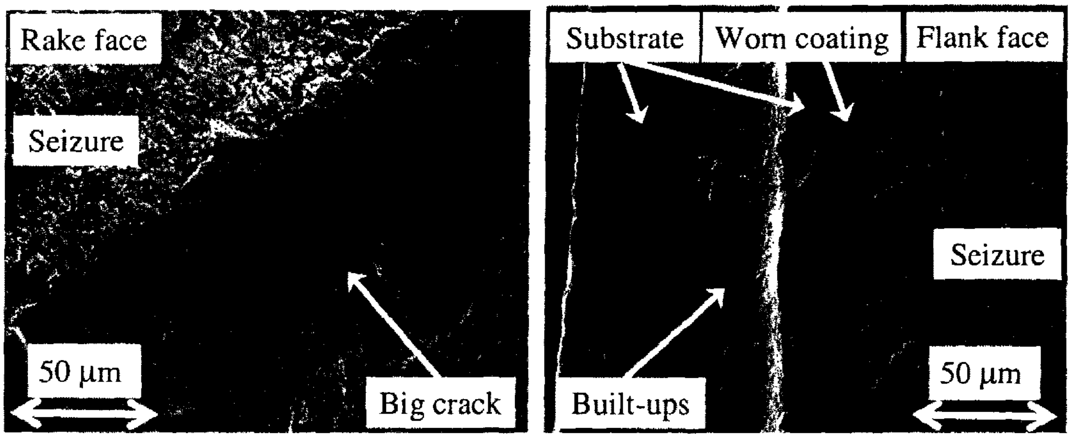

e) TiAlCrN/NbN 200 m cutting length

Figure 6.30 SEM images and EDX results of ball end mill with TiAlCrN/NbN coating during the wear progress

Each wear zone had different wear mechanisms. The dominant wear mechanism for the worn coating zones was abrasion wear. Within the catastrophic stage of wear the worn coating band on the rake face disappeared and the seizure zone became directly connected to the exposed substrate (Figures 6.28d-e). Regarding the worn substrate zones, when the substrate was first exposed, the dominant wear mechanism was abrasion. This wear mechanism dominated approximately up to a length of cut of 100 m (Figures 6.28b-c). When the exposed substrate material started to get wider, the cutting temperature became higher and hence chemical (diffusion) wear became dominant and the craters were formed on the rake face (Figure 6.30d). The zones of build-up were related to the seizure, and wear mechanisms such as adhesive, abrasion as well as diffusion. Seizure intensified after the cutting length of 150m due to temperature growth (Figures 6.28d-e). As the cutting temperature and stress increased, a parallel to the cutting edge crack of more than 50 μm appeared within the exposed substrate zone.

6.8.2 The formation of tribo-films

To understand the mechanism of adaptability and confirm the formation of tribo-films of nano-multilayered TiAlCrN/NbN coating, a photoelectron spectrum (XPS) study on the worn tool surfaces and an elemental mapping analysis by SEM/EDX were carried out.

Figure 6.31 shows the photoelectron spectra from the rake face of a TiAlCrN/NbN coated worn ball end mill. The interpretation of the spectra was made based on complex investigation of the changes in the intensity at the positions of Ti 2p, Al 2p, Cr 2p and Nb 3d lines for the coating after wear. It was found that intensive tribo-oxidation took place on the surface of the hard coating within the wear zone. All the metallic elements of the coating were oxidized during friction under high temperatures and the corresponding tribo-oxides were formed such as Ti-O, Al-O, Cr-O and Nb-O. Tribo-oxidizing intensity was different for each metallic component in the complex nitrides. As shown in Figure 6.31a, the titanium in the complex nitrides transform to TiO_2 rutile, and its quantity is 62.0% in comparison to Ti in nitride (38.0%). Figure 6.31b shows that 70.0% of Al in nitride was transformed to an Al_2O_3 sapphire-like phase. The Al 2p line binding energy for tribo-oxide has a higher binding energy than corresponding equilibrium nitride or alpha and gamma-Al_2O_3 phases (73.9 eV). The Al oxide binding energy for these tribo-films is higher (74.8 eV; Figure 6.31b), and this value is very close to what corresponds to sapphire. This data corresponds to previously published data on sapphire-like tribo-films formations during high performance cutting.

Figure 6.31c presents XPS spectra of Cr-O-based tribo-oxide films. The chromium is oxidized when forming of 28.0% Cr^{+3} and 39.0% Cr^{+4} oxides. These films have some lubricious properties and could improve wear behavior acting in synergy with protective alumina-based films. The intensity of tribo- oxidation of Nb is very high (Figure 6.31d) at high cutting temperatures. Two types of Nb-O tribo-films are formed as a result of tribo-oxidation during cutting, i.e., 45.0% of NbO and 28.0% of Nb_2O_5. In summary, the tribo-films, formed during cutting process, consist of protective sapphire-like tribo-oxides (Figure 6.31b) with some amount of non-protective rutile-like oxides (Figure 6.31a) and polyvalent lubricious tribo-oxides of Cr (Figure 6.31c) and Nb (Figures 6.29d).

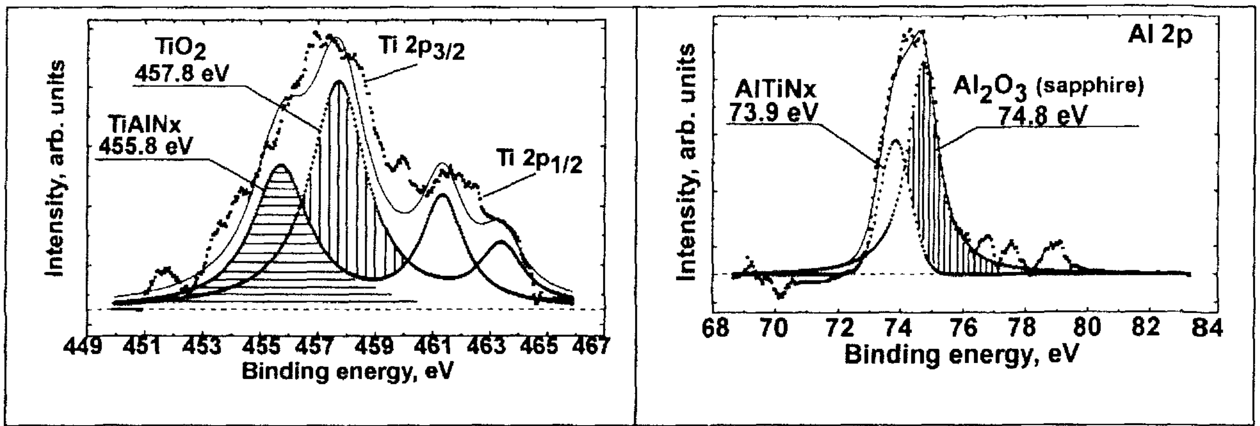

a) Ti 2p photoelectron spectra

b) Al 2p photoelectron spectra

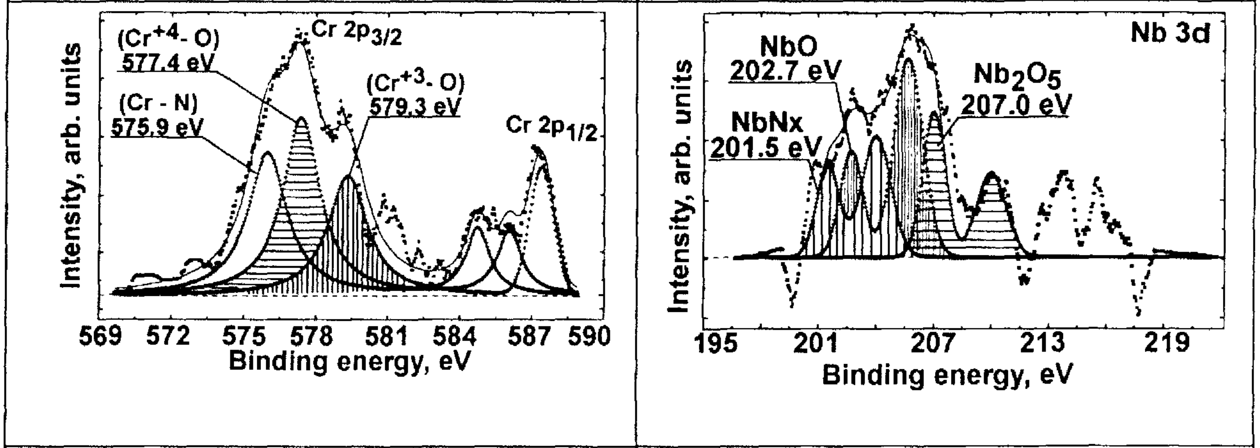

c) Cr 2p photoelectron spectra

d) Nb 3d photoelectron spectra

Figure 6.31 XPS of the worn surface of the TiAlCrN/NbN coated tool

It is noticed that for conditions of high-performance machining, the Nb-based oxide tribo-films could significantly enhance wear resistance at elevated temperatures. The formed oxides have high thermal stability due to the presence of strong inter-atomic bonds in a compound with a heavy atomic nucleus. Therefore, the TiAlCrN/NbN coating is able to perform its protective functions on the cutting tool.

One more reason for the tool life improvement of the TiAlCrN/NbN coated cutting tool is the ability of Nb-O tribo-films to dissipate energy during friction at elevated temperatures. It is known from the literature that one of the features of Nb-based oxides is their high electro conductivity at high temperatures (Table 6.11) compared to other tribo-oxides such as alumina, rutile and Cr-based tribo-oxides. This property is consistent with metallic materials which then indicates that it could work as a solid lubricant and possess an increased ability to dissipate energy during friction. This is an important property for an interrupted cutting process like ball end milling.

Table 6.11 Specific electro-resistance (SER) of different oxides vs. temperature [Crist, 2000; Samsonov (Ed.), 1976]

Oxide	Temperature, ^{o}C	Specific electro-resistance (SER), Ohm·m
Al_2O_3	800	3.5×10^{6}
	1000	5×10^{4}
	1100	10^{4}
TiO_2	800	1.2×10^{2}
	1200	8.5×10^{2}
Cr_2O_3	800	78
	1000	40
	1488	21.3
WO_3	800	2×10^{3}
Nb_2O_5	1200	8×10^{-2}
	1500	2.8×10^{-3}

To further support this hypothesis, High Resolution Electron Energy Loss Spectroscopy (HREELS) analysis of the worn surface of the cutting tools with TiAlCrN/NbN coating was performed. Figure 6.32 shows the HREELS spectra from the worn surface of the TiAlCrN/NbN coated cutting tool and it presents the high intensity of plasmon peaks. The plasmon peak intensity in the spectrum of primary electrons energy loss is related to the excitation of collective oscillations among free electrons and determined by their concentration [Kovalev and Wainstein, 2006]. High intensity peaks

(P_1-P_4 in Figure 6.32) on the spectra of the coating, which are observed at the surface of the oxide tribo-films (ionic compounds [Patscheider et al, 2001; Holleck, 1986]), indicate the existence of metallic bonds [Fox-Rabinovich, et al., 2006]. A surface with metallic bonds has a higher ability to dissipate energy during friction because the mobility of the dislocations is probably enhanced within the surface layer of the oxide tribo-films with high intensity of plasmon peaks [Fox-Rabinovich, et al., 2006]. The generation of dislocation with higher mobility could ensure stress relaxation within the friction zone and reduce the formation of an excessive amount of defects on the surface. This will prevent the surface energy from growing, reduce the intensity of surface damage and hence results in an overall lower wear rate.

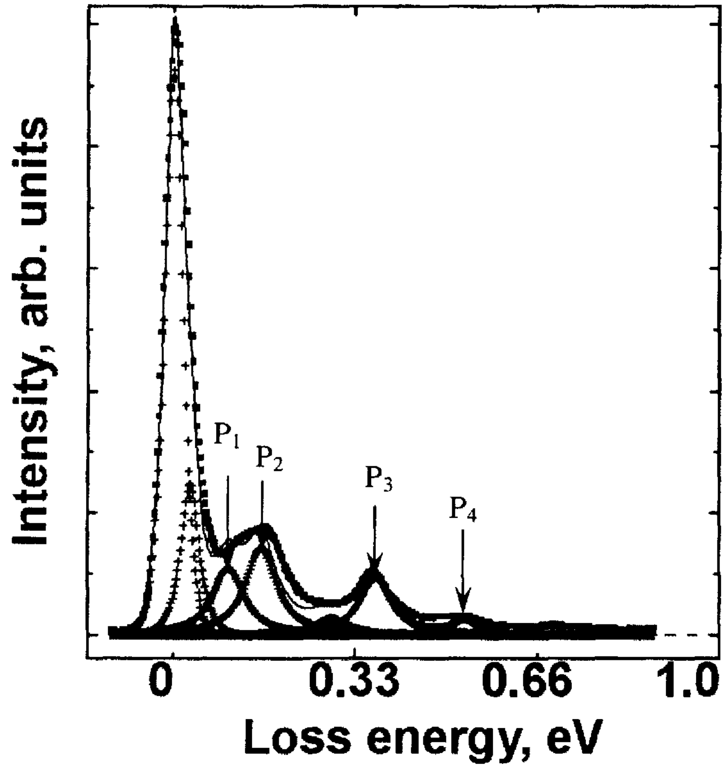

Figure 6.32 HREEL spectra of the worn surface of the TiAlCrN/NbN coated tool

An elemental mapping technique is also used to reveal the distribution of oxides on the rake and flank faces of the worn tool. Figures 6.31 and 6.32 present the elemental mapping images. The results show that intensive tribo-oxidation on both surfaces took place with the formation of two major types of oxides: the protective oxides (niobium oxide, alumina and chromium oxide) and the non-protective oxide (rutile). The protective oxide tribo-film formation is extremely beneficial to dry high speed machining conditions. It results in very low intensity seizures occurring in the flank and rake faces up to the cutting length of 150 m (Figures 6.28b-c). However, when the cutting temperature started to be higher than 1100°C, intensive oxidation occurred with the formation of non-protective oxides (rutile) (Figures 6.31-6.32). Therefore, the coating lost its protective ability and intensive seizure developed (Figure 6.30d-e).

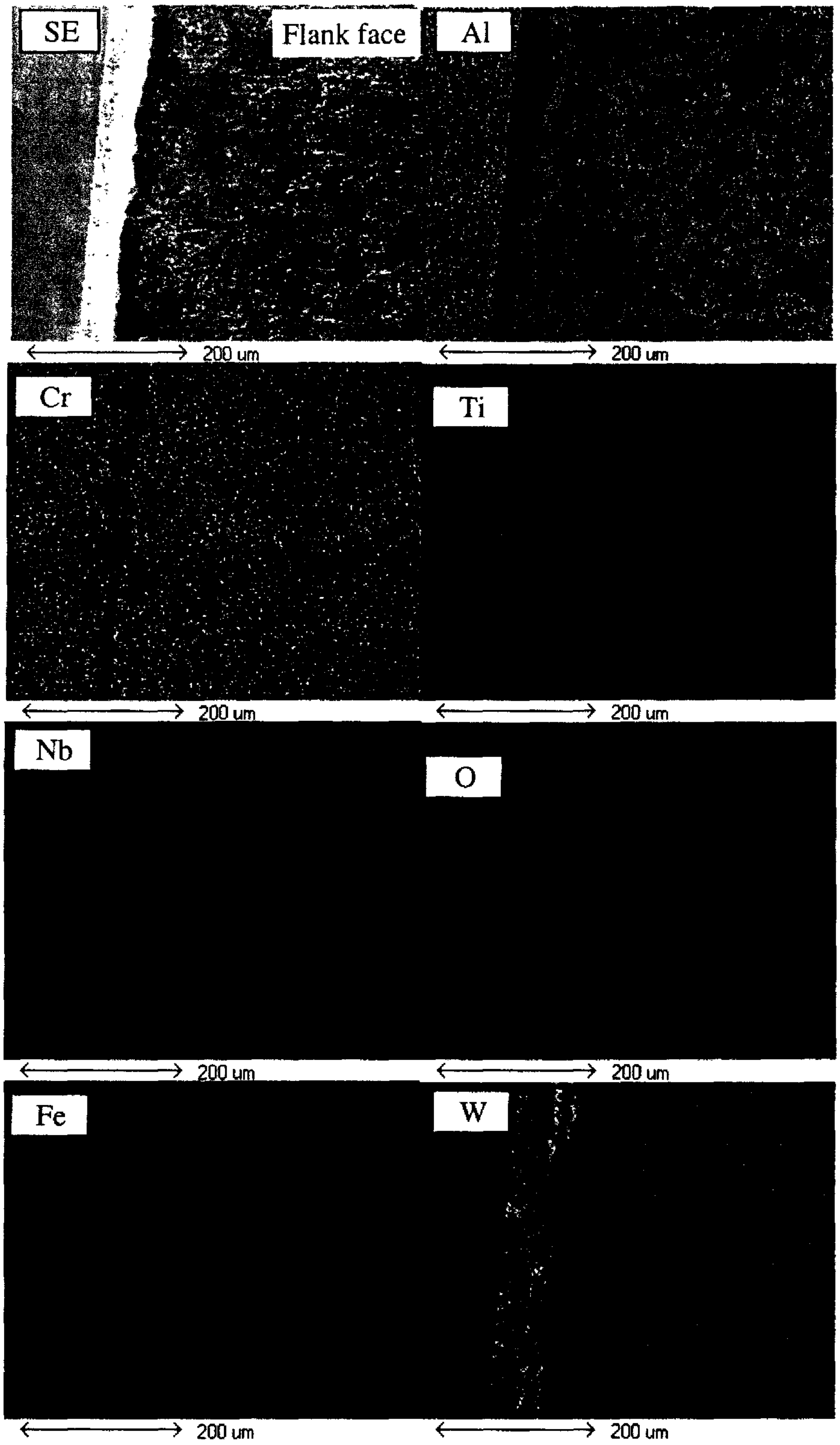

Figure 6.33 Element mapping of flank face ball end mill with TiAlCrN/NbN coating at the cutting length of 200m

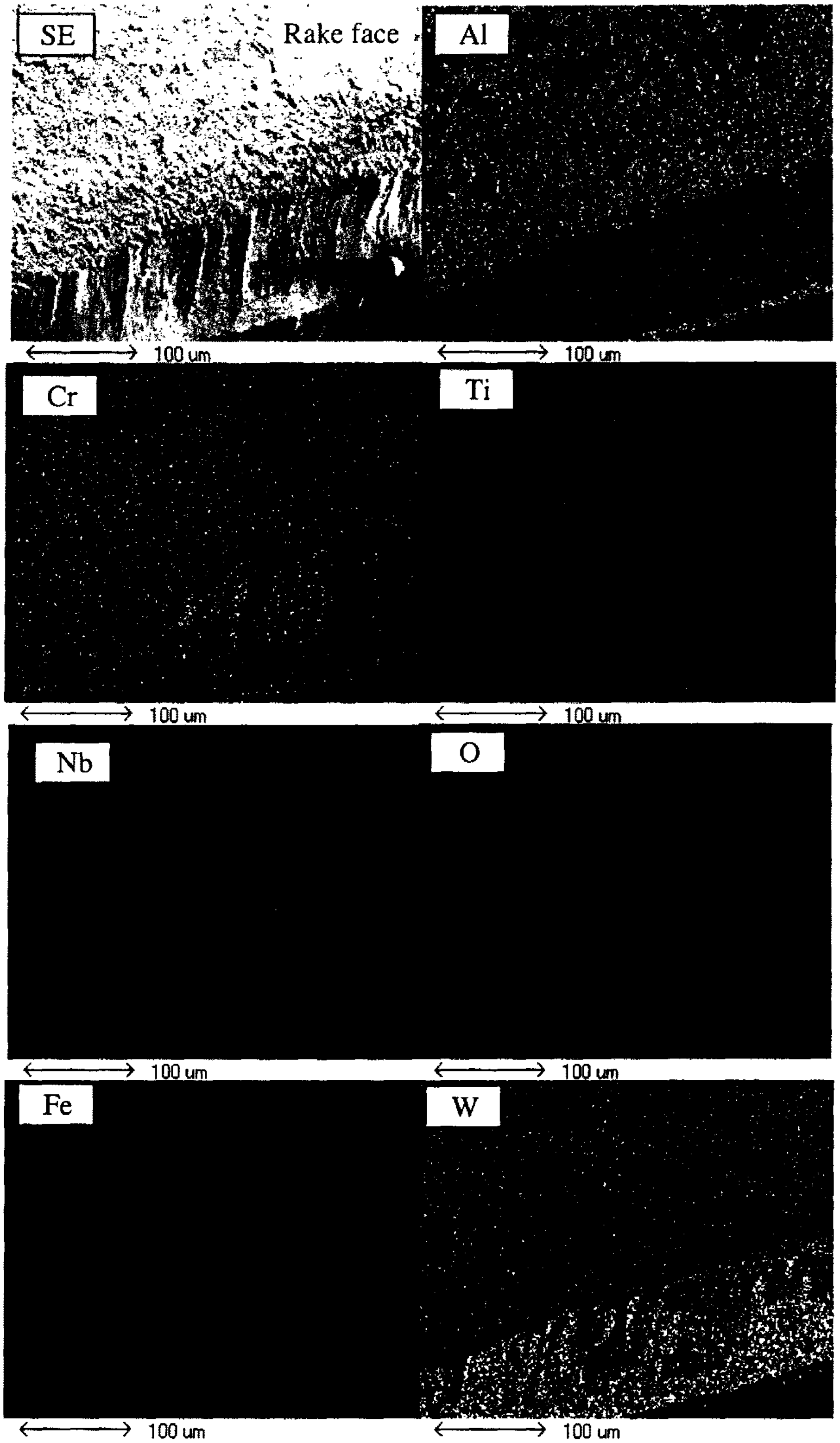

Figure 6.34 Element mapping of rake face of ball end mill with TiAlCrN/NbN coating at the cutting length of 200m

6.8.3 Chip formation

Figure 6.35 shows the progress of the chip shapes and chip undersurfaces with the length of cut. Curly chips and smooth undersurface of the chips were observed at the initial stage of wear (Figure 6.35a). In this situation, the major mode of chip flow was sliding. After the cutting of 30 meters, the shape of the chips started to become quite flat and the chip underside became wavy (Figure 6.35b) as compared to the ones generated by the new tool. In this case, the major modes of chip flow became sliding and sticking. The chips were caught by the rake face and released due to large shearing force. In addition, the un-deformed chip thickness was very small (0.06 mm). Therefore, a wavy chip surface was formed. As the cutting length grew, the shape of the chips had no significant change; however, rough "ears" on the underside of the chips were formed (Figures 6.33c-e). As the tool wear increased, the cutting edge became dull and more ploughing action instead of cutting was involved in the cutting process. This resulted in a large number and big size of "ears" (Figure 6.35e). During chip formation there were three phenomena involved. The first one was material strain hardening due to the large plastic deformation of the chip material. The second was thermal softening due to high cutting temperature. The third one was the quenching effect of the chip by the compressive air blast under the intermittent cutting operation. The quenching took place when the actual temperature at the tool/chip interface was above the temperatures of austenization for H 13 tool steel. As a result, very hard and brittle chips were formed with the structure that consisted of un-tempered martensite and retained austenite. At different wear stages, the dominant phenomenon changed. As the tool became worn, the combined effect of the strain hardening and quenching resulted in brittle chips. Therefore, a large number of cracks were formed (Figures 6.33c-e).

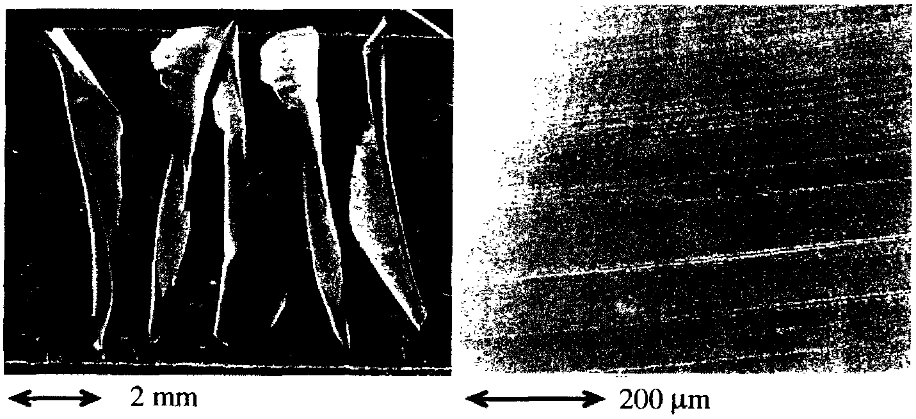

a) At the cutting length of 0.5 m

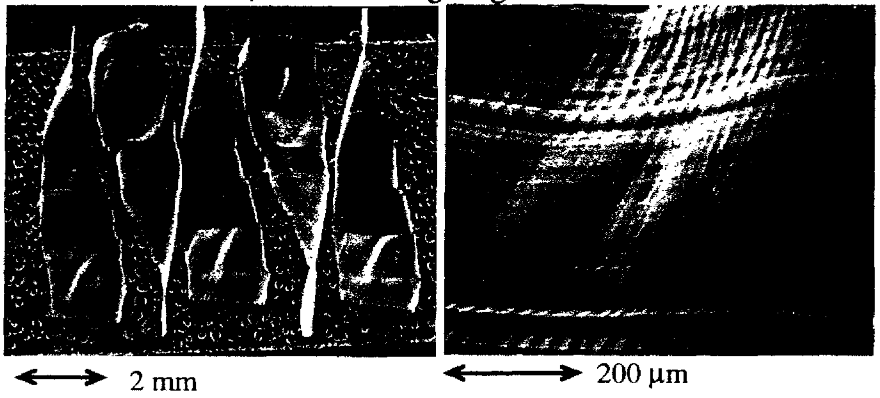

b) At the cutting length of 30 m

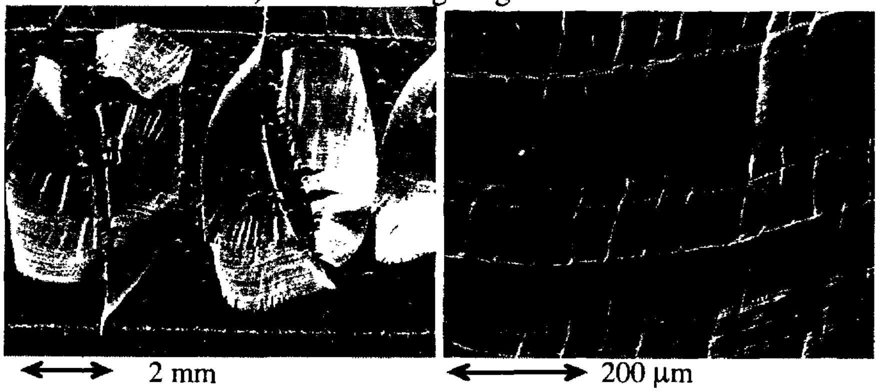

c) At the cutting length of 100 m

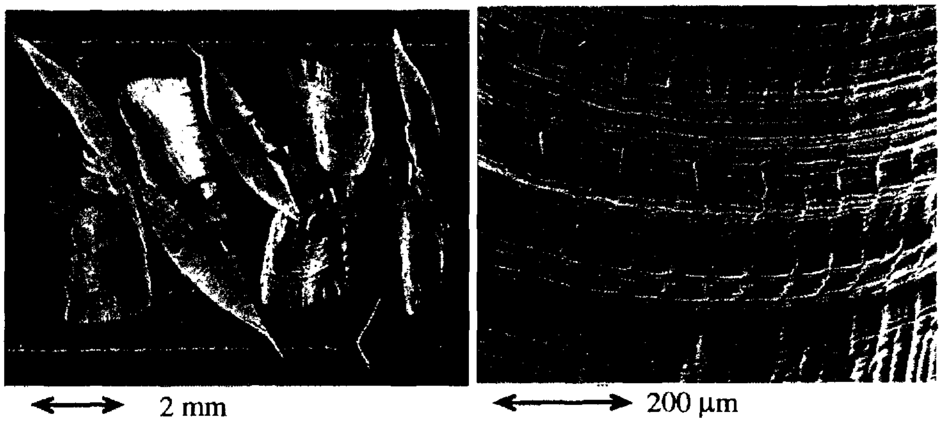

d) At the cutting length of 150 m

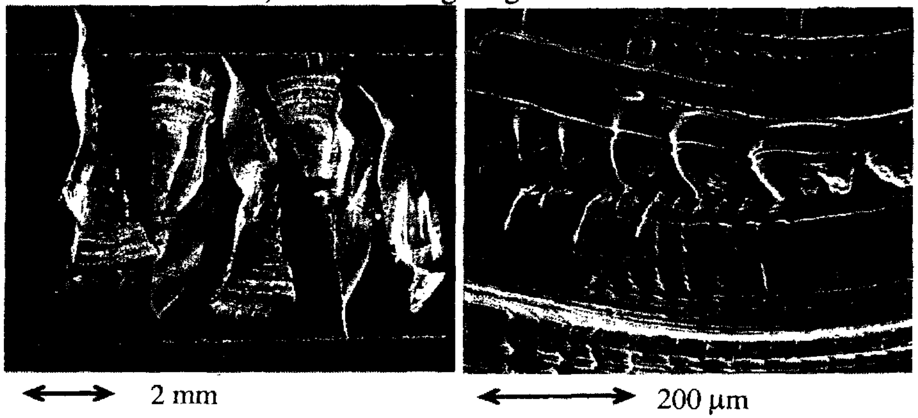

e) At the cutting length of 200 m

Figure 6.35 SEM images of chip shapes and surfaces (TiAlCrN/NbN)

The SEM images of the chip cross-sections are presented in Figure 6.36. Again, curly (Figure 6.36a), flat (Figure 6.36b) and wavy chips (Figures 6.34c-d) and brittle chips (Figure 6.36e) were observed from the low magnification images corresponding to the cutting lengths of 0.5, 30, 60, 100 and 150m. Based on the higher magnification images, continuous chip formation was observed at the cutting length of 0.5 m (Figure 6.36a). As the tool gradually got worn the regular saw-tooth chips for hard machining were formed which are shown in Figures 6.34b-e. It was also found that as the tool wear increased, the chip segmentation frequency decreased and the plastic deformations in the primary shear zone became larger and larger and the crack propagation from the free surface close to the tool tip got deeper and deeper (Figures 6.34b-e).

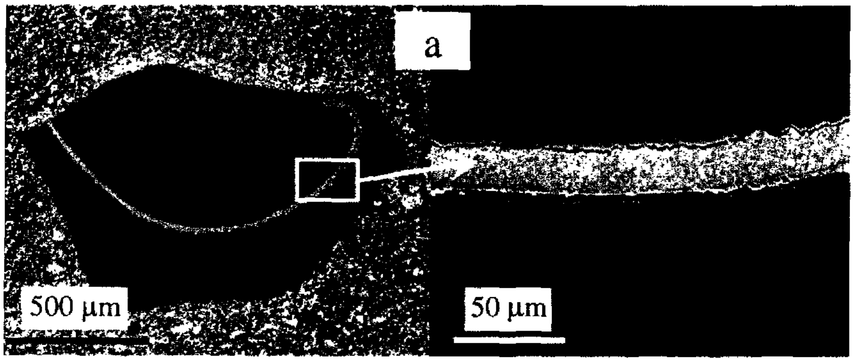

a) At cutting length of 0.5 m

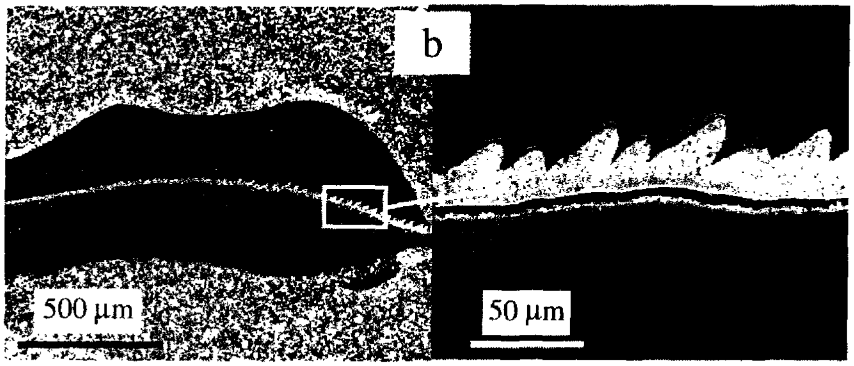

b) At cutting length of 30 m

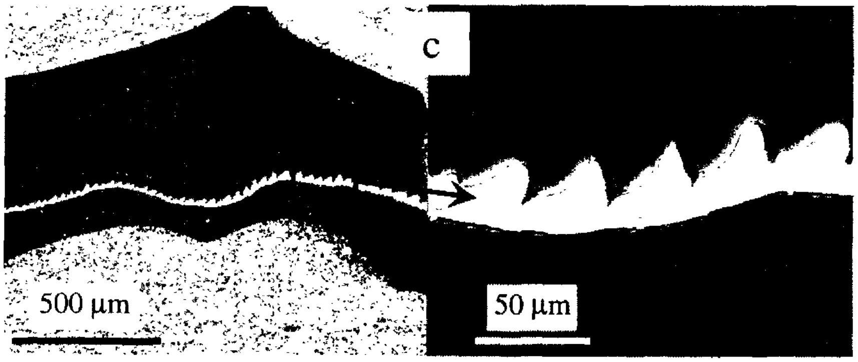

c) At cutting length of 60 m

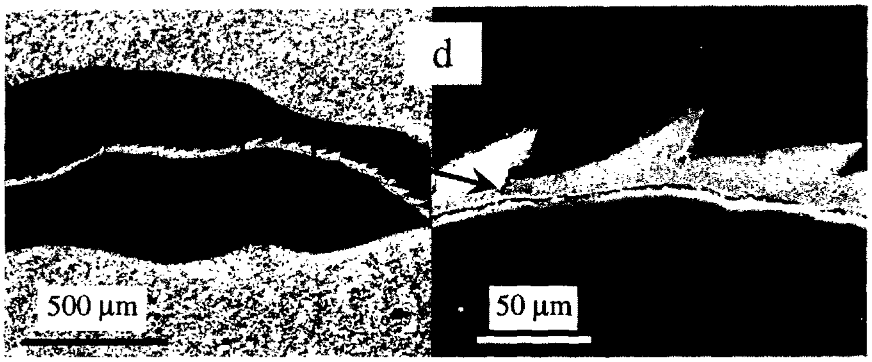

d) At cutting length of 100 m

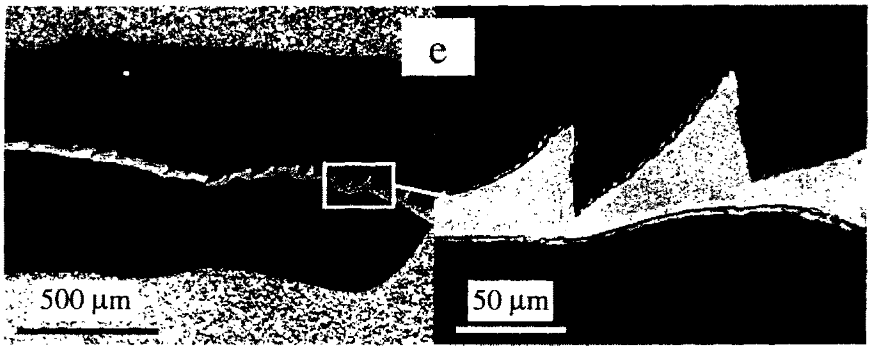

e) At cutting length of 150 m

Figure 6.36 SEM images of chip cross-section at different cutting lengths (TiAlCrN/NbN)

Figure 6.37 is the typical saw-tooth chip cross-section that was obtained from this study. Four zones were observed, i.e, 1- white layer zone due to phase transformation from the quenching phenomenon, 2- deformation zone (underside of the chip at the secondary shear zone) due to friction; 3 – shear plane/zone due to the primary shearing, 4-less deformed zone due to saw-tooth chip formation. Again, this result further confirms the combined effect of the strain hardening, thermal softening and quenching during the chip formation. From the SEM images with high magnification (Figure 6.38), it was found that the secondary shear zone became wider and wider as the cutting length increased, which indicated that the frictional force became higher and so did the cutting temperature. The chip temperatures were estimated (Table 6.12) based on the relationship between the color of the chips and chip temperature.

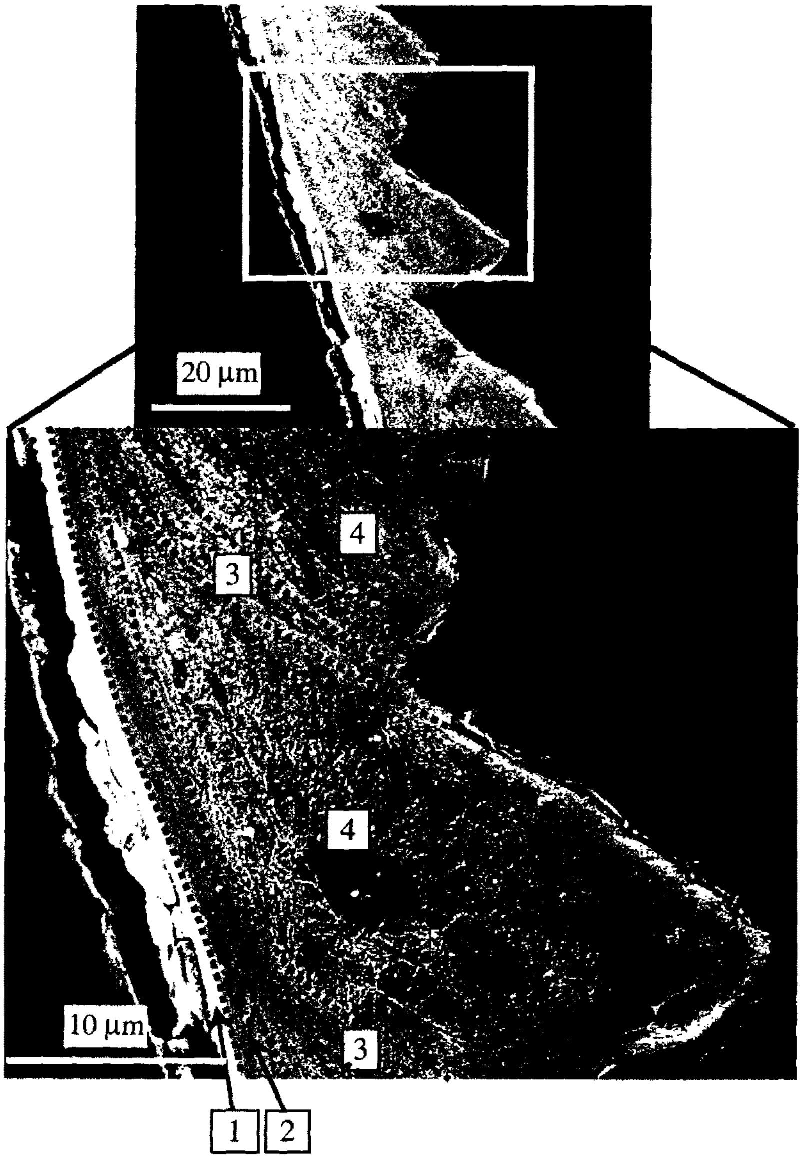

1- white layer zone due to phase transformation; 2- deformation zone underside of the chip corresponding to the secondary shear zone; 3 – shear plane corresponding to the primary shear zone 4- less less deformed zone due to saw-tooth chip formation

Figure 6.37 Four zones of saw-tooth chips (cutting length of 30 m)

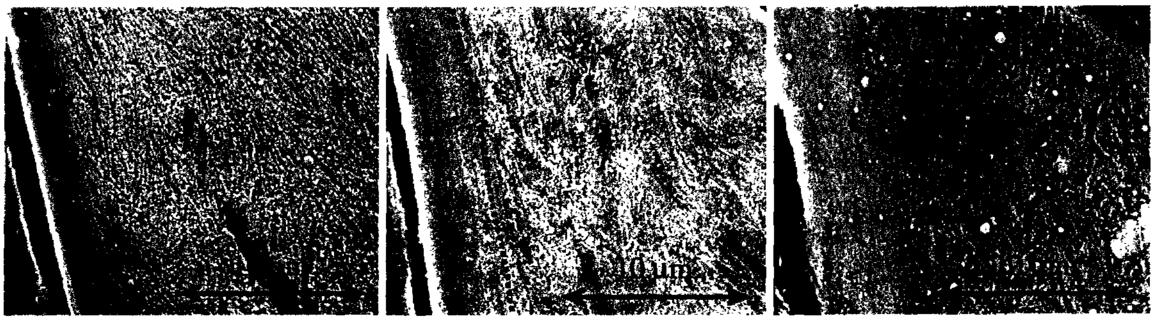

a) 4 m b) 60 m c) 150 m

Figure 6.38 SEM images of chip cross-sections (1- secondary shear zones)

Table 6.12 Chip color vs. chip temperature (TiAlCrN/NbN (4 at. %)

Cutting length (m)	Color of chips	Estimated temperature (°C)
0.5	Brownish purple	860 - 920
30	Blue + purple + brown	900-960
60	Blue + green + purple	960-1020
100	Green + blue + purple	>1000
150	Green + silver	>1100
200	Green + silver + radish brown (brittle chips)	>1100

Coating efficiently protects the rake and flank surfaces of the cutting tool and prevents interaction with the workpiece material through the formation of tribo-films. However, a relatively small area around the cutting edge (within a range of 30-50 microns) controls the wear rate of the cutting tool due to the high concentration of stress and high temperature generation within this area during friction. Thus the wear resistance of the coated tool depends on both substrate material and the coating applied. To sustain intensive heat generation at the cutting edge the coating has to be able to perform protective functions at temperatures above 1000°C.

6.9 Improvement in Productivity

The potential capability of the TiAlCrN/NbN coating for further improvement of productivity was tested at cutting speeds of 300 m/min, 350 m/min and 400 m/min, and the tool life curves are shown in Figure 6.39. Figure 6.40 shows that the cutting lengths can be completed at the cutting speed from 300 m/min to 400 m/min when the tool wear criterion is set to be 0.25 mm. It can be seen that even when the cutting speed goes up to 400 m/min, the tool life can still maintain 62.5% of the one at the cutting speed of 300 m/min.

As discussed previously, the cutting tools with the TiAlCrN/NbN coating can sustain wear resistance under extremely aggressive cutting conditions. This is attributed to the synergistic action of the oxides formed during cutting.

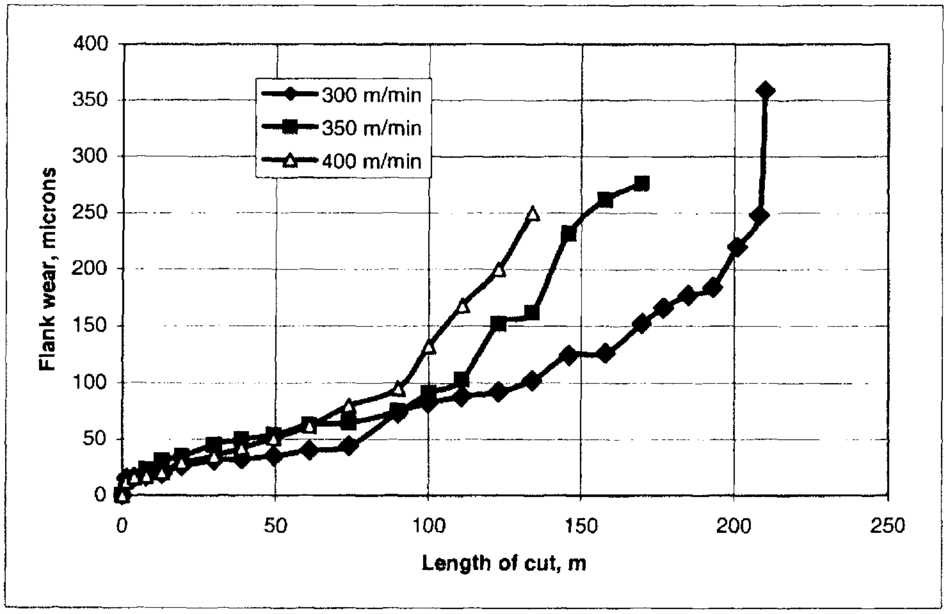

Figure 6.39 Tool life curves of the coated tools with TiAlCrN/NbN coating

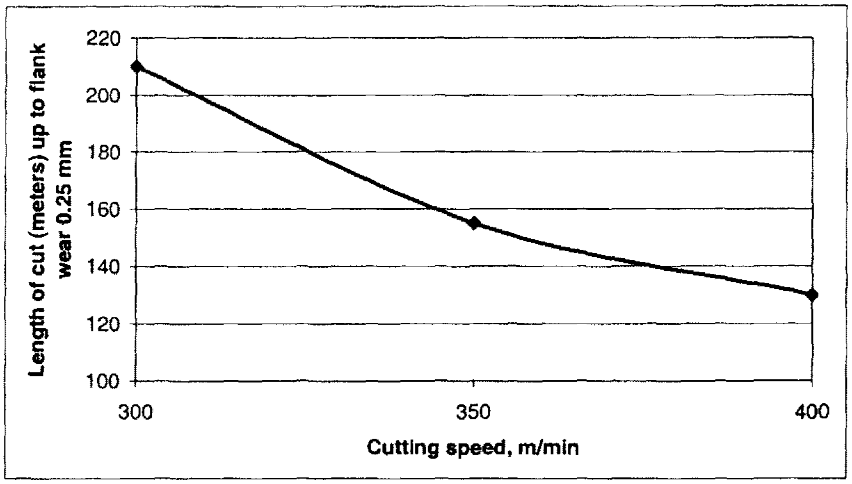

Figure 6.40 Cutting lengths vs. cutting speeds when flank wear is 0.25 mm

The material removal rate (MRR) for milling is calculated by:

$$MRR = n \cdot f_t \cdot N \cdot a_p \cdot a_e$$

where n is the number of teeth, f_t is the feed per tooth, N is the spindle speed, a_p is the axial depth of cut and a_e is the radial depth of cut.

Table 6.13 lists the calculated material removal rate corresponding to the cutting speed. It can be seen that the material removal rate is significantly increased with the application of the advanced self-adaptive coating TiAlCrN/NbN.

Table 6.13 Material removal rate vs. cutting speed

Cutting speed (m/min)	220	300	350	400
Material removal rate (mm^3/min)	2520	3439	4013	4586

Chapter 7

Conclusions and Future Work

7.1 Conclusions

Nano-multilayered self-adaptive TiAlCrN based PVD coatings have been investigated for application in dry high performance machining of a hardened material. The coatings were deposited on solid fine-grained cemented carbide Mitsubishi ball-nose end mills by using a hybrid coater with a combined plasma-enhanced cathodic arc source and an unbalanced magnetron sputtering unit. Comprehensive characterization of the coatings was performed including: hardness, elastic modulus, coefficient of friction and oxidation resistance. Cutting tests using a variety of coated tools was performed by dry ball nose milling the hardened AISI H13 (HRC 55-57) die steel under extreme cutting conditions associated with high performance machining. Using a dynamometer, optical microscopy, SEM/EDX, XPS, and TEM, cutting forces, tool wear, morphology of the cutting edge and tool surface, wear types, wear mechanisms, wear progression, tribo-oxide formation, chip shape, chip surface and chip formation mechanisms were studied in this research. Based on the results of this research the following findings can be concluded:

1. More than four times tool life improvement under severe cutting conditions was achieved by the application of the self-adaptability concept (nano-multilayered TiAlCrN/NbN coating comparing with monolayered TiAlCrN coating).
2. A significant improvement on productivity or material removal rate was achieved by increasing the cutting speed (Table 6.12).
3. The best coating among the coatings investigated was found to be a nano-multilayered TiAlCrN/NbN coating followed by the TiAlCrN/WN coating.
4. The tribo-oxides were found to form under friction and work as either liquid or solid lubricants in the cutting zone depending on their melting points (Table 6.7).
5. Solid lubricants were found to be extremely beneficial for the improvement of tool performance. In contrast, liquid lubricants do not give any significant improvement in tool life under the proposed cutting conditions.
6. The formed tribo-oxides provide a synergetic action to protect the cutting tool by lubricating the cutting zone to reduce friction (like Cr-O and W-O films), insulating the substrate from thermal attack (like Al-O films), and dissipating energy to reduce surface damage (as Nb-O films).
7. Super hard coatings with poor tribological properties were found to not provide as good a tool performance for the proposed application.
8. An optimal contact length at the coated tool/chip interface exists for a ball end milling process. Too short of a contact length results in a short tool life (Figures 6.19, 6.20). The ability to maintain the optimal contact length at the tool/chip interface is one of the keys to achieving a longer tool life.

9. By means of SEM/EDX and XPS techniques, the study of tool wear progression over the life of the tool exhibits an overall picture showing how the tool wear grows and transforms from one type to another and indicates which wear mechanisms are dominant at different wear stages (Figure 6.28).
10. Heat generation during cutting strongly depends on the development of tool wear. The estimated cutting temperature, using the color of the chips as an indicator can be in the range of 850-1100°C or above mainly depending on the tool wear, cutting speed and lubricity in the cutting zone (Tables 6.5, 6.6 and 6.11).
11. Continuous chips are generated only with a new sharp cutting edge possessing good lubricity in the cutting zone. Saw-tooth chips are generated as the tool wears. The height of the saw-tooth effect grows as the tool wear increases (Figure 6.34).
12. The mechanisms of the saw-tooth chip formation for the proposed cutting conditions are described using crack theory combined with thermal softening and strain hardening effects.
13. As the tool wear increases, the frequency of chip segmentation and the degree of chip curling decrease and the height of the saw-tooth increases, which indicates a higher pressure imposed on the cutting tool and a more dynamic effect on the manufacturing system.
14. Four zones in the chip cross-section of the saw-tooth chips are revealed. The combined effect of strain hardening, thermal softening and the quenching

phenomena of the workpiece material on the chip formation was identified (Figures 6.35 and 6.36).

15. Due to the fact that coating protects the substrate while the substrate supports the coating, a coated tool should be treated as a composite (coating/substrate) material. Both the hardness and the toughness of the substrate have a significant influence on coated tool performance, especially for the severe cutting conditions under which the substrate is gradually exposed at the cutting edge along with the wear progression.

In summary, the improvement of tool performance and manufacturing productivity mainly depends on the ability of a hard coating to adapt under severe friction conditions.

7.2 Recommendations for Future Work

Based on the present research, further research is recommended as follows:

1. Advanced cutting temperature measuring devices or more accurate methods of cutting temperature estimation for milling applications must be developed for future research as temperature plays a major role in determining the performance of a coating.
2. It is recommended that the characterization of the coating properties, especially tribological property, be extended to the temperature range of 1000 to 1200°C.

3. From the unacceptable performance of TiAlCrN/TaN coating at the cutting speed of 300 m/min due to the short contact length, this coating may achieve better performance at higher cutting speed since the resulting higher cutting temperature usually accelerates seizure and a small amount of seizure is needed to get and maintain an optimal contact length.
4. For further enhancement of oxidation resistance and thermal stability at high temperature, Y, Si and Hf may be considered as the additional elements due to the high melting points of their oxides.
5. Further research also needs to be conducted to determine the nature of the complex alloy oxides (such as AL-Ti-O, Al-Ti-Cr-Nb-O, etc.) forming to further understand the role of each metallic oxides that forms.

References

Abrao, A.M., Aspinwall, D.K., Ng, E.-G., *Temperature evaluation when machining hardened hot work die steel using PCBN tooling*, Industrial Diamond Review 56(569), pp. 40-45, 1996.

Abrao, A.M., Aspinwall, D.K., *Temperature evaluation of cutting tools during machining of hardened bearing steel using polycrystalline cubic boron nitride and ceramic cutting tools,* Material Science & Technology 13 (5), pp. 445-450, 1997.

Astakov, V.P., *Tribology in metal cutting, in Mechanical Tribology.* In *Materials, Characterization, and Application*; Liang, H.; Totten, G., Eds. ; Marcel Dekker: New York, 2004; 307-389.

Barry, J., Byrne, G., *The mechanisms of chip formation in machining hardened steels,* Transactions of the ASME Journal of Manufacturing Science and Engineering 125, pp. 528-535, 2002.

Beake, B. D., Lau, S. P., and Smith, J. F., *Evaluating the fracture properties and fatigue wear of tetrahedral amorphous carbon films on silicon by nano-impact testing,* Surface & Coatings Technology 177-178, pp. 611-615, 2004.

Beake, B. D., Smith, J. F., *Nano-impact testing – an effective tool for assessing the resistance of advanced wear-resistant coatings to fatigue failure and delamination,* Surface & Coatings Technology 188-189, pp. 594-598, 2004.

Beake, B.D., Smith, J.F., Gray, A., Fox-Rabinovich, G.S., Veldhuis, S.C., Endrino, J.L., *Investigating the correlation between nano-impact fracture resistance and hardness/modulus ratio from nanoindentation at 25-500* ^{o}C *and the fracture resistance and lifetime of cutting tools eith* $Ti_{1-x}Al_xN$ $(x = 0.5$ *and* $0.67)$ *PVD coatings in milling operations,* Surface & Coatings Technology 201, pp. 4585-4593, 2007.

Bershadskiy, L.I. *On self-organizing and concept of tribosystem self-organizing,* Friction and Wear 13(6), pp. 1077-1094, 1992.

Boehner, J., *High speed machining of sculptured surfaces in hardened tool steel,* Master Thesis, Fraunhofer Inst of Production Technology, 1998.

Boehner, J., Dumitrescu, M., Elbestawi, M.A, El-Wardany, T.I. and Chen, L., *Effect of Carbide Tool Grades and Cutting Edge Geometry on Tool Life During High Speed Machining of Hardened Tools Steel,* Proceedings of the 2nd International German and French Conference on High Speed Machining, pp. 37-46, 1999.

Boehner, J., Dumitrescu, M., Elbestawi, M.A, El-Wardany, T.I. and Chen, L., *Influence of Material Microstructure on Tool Performance in High Speed Machining,* Transactions of the North American Manufacturing Research Institution of Society of Manufacturing Engineers, XXVII North American Manufacturing Research Conference (NAMRC), pp. 129-134, 1999.

Bouzakis, K. D., Michailidis, N., Erkens, G., Thin hard coatings stress-strain curve determination through a FEM supported evaluation of nanoindentation test results, *Surface and Coatings Technology* 142-144, pp.102-109, 2001.

Bouzakis, K. D., Michailidis, N., Hadjiyiannis, S., Skordaris, G., Erkens, G., *The effect of specimen roughness and indenter tip geometry on the dtermination accuracy of thin hard coatings stress-strain laws by nanoindentation,* Material Characterization 49, pp.149-156, 2003.

Bouzakis, K. D., Skordaris, G., Mirisidis, J., Hadjiyiannis, S., Anastopoulos, J., Michailidis, N., Erkens, G., Cremer, R., *Determination of coating residual stress alterations demonstrated in the case of annealed films and based on a FEM supported continuous simulation of the nanoindentation*, Surface & Coatings Technology 174-175, pp. 487-492, 2003.

Bouzakis, K.D., Siganos, T., Leyendecker, T., Erkens, G., *Examination of superficial layer effect on nitride coatings failure mechanisms during impact testing,* Proceedings of The 3rd Inrenational Conference - The Coatings in Manufacturing Engineering, pp.373-382, 2002.

Bouzakis, K.D., Michailidis, N., Hadjiyiannis, S., Erkens, G., *Impact test performance interpretation based on coatings stress-strain curves,* Proceedings of The 3rd Inrenational Conference- The Coatings in Manufacturing Engineering, pp.417-428, 2002.

Braghini Jr,A., Coelho, R.T., *An Investigation of the Wear Mechanisms of Polycrystalline Cubic Boron Nitride (PCBN) Tools when End Milling Hardened Steels at*

Low/Medium Cutting Speeds, Int. J. of Advanced Manufacturing Technology 17, pp. 244-257, 2001.

Bruno, L., Furgiuele, F.M., Sciumé, G., *Mechanical characterization of a CVD diamond coating by nano-indentation test,* Journal of Engineering Materials and Technology 125, pp. 309-314, 2003.

Celis, J.P., Drees, D., Huq, M.Z., Wu, P.Q., De Bonte, M., *Hybrid processes - a versatile technique to match process requirements and coating needs*, Surface & Coatings Technology 113(1-2), pp. 165-181, 1999.

Childs, T.H.C. *Friction modeling in metal cutting*, Wear 260, pp.310-318, 2006.

Chou, Y.K., Evans, C.J., *White layers and thermal modeling of hard turned surfaces,* International Journal of Machine Tools and Manufacture 39(12), pp. 1863-1881, 1999.

Chou, Y.K., Evans, C.J., *Cubic boron nitride tool wear in interrupted hard cutting,* Wear, 225-229 (1), pp. 23-245, 1999.

Chu, T.H., Wallbank, J., *Determination of the temperature of a machined surface,* J. Manuf. Sci. Eng. Trans. ASME 120 (2), pp. 259-263, 1998.

Costa, A.K., Camargo Jr, S.S., *Properties of amorphous SiC coatings deposited on WC-Co substrates,* Materials Research 6(1), pp. 39-42, 2002.

Crist, B.V., *XPS handbook of the element and native oxides,* John Wiley & Sons, New York, pp. 458, 2000

Davies, M.A., Chou, Y., Evans, C.J., *On chip morphology, tool wear and cutting mechanics in finish hard turning,* Annals of the CIRP 45(1), pp.77-82, 1996.

Dewes, R.C., Aspinwall, D.K., *A review of ultra high speed milling of hardened steels*, J. Materials Processing Technology 69, pp. 1-17, 1997.

Dewes, R.C., Ng, E-G., Chua, C.K., Newton, P.G., Aspinwall, D.K., *Temperature measurement when high speed machining hardened mould/die steel,* J. Materials Processing Technology 92-93, pp. 293-301, 1999.

Dimla, D.E.S., *Sensor signals for tool wear monitoring in metal cutting operation- a review of methods*, International Journal of Machine Tools and Manufacture, 40 (8), pp. 1073-1098, 2000.

Donohue, L.A., Münz, W.-D., Lewis, D.B., Cawley, J., Hurkmans, T., Trinh, T., Petrov, I. and Greene, I.E., *Large-scale fabrication of hard superlattice thin films by combined steered arc evaporation and unbalanced magnetron sputtering*, surface & Coaings Technology 93 (1), pp. 69-87, 1997.

Dyrda K., Sayer M., *Critical loads and effective frictional force measurements in the industrial scratch testing of TiN on M2 tool steel,* Thin Solid Films, 355-356, pp. 277-283, 1999.

Eizner, B.A., Markov, G.V., and Minevich, A.A., *Deposition stages and applications of CAE multicomponent coatings,* Surface & Coating Technology 79, pp. 178-191, 1996

Elbestawi, M.A., Srivastavi, A.K., El-Wardany, T.I., *A model for chip formation during machining of hardened steel,* Annals of the CIRP 45(1), pp.71-76, 1996.

El-Wardany, T.I., Kishawy, H.A., Elbestawi, M.A., *Surface integrity of die material in high speed hard machining, Part 2: Microhardness variations and residual stresses,* J. Manuf. Sci. Eng. Trans. ASME 122(4), pp. 632-641, 2000.

El-Wardany, T.I., Mohammed, E., Elbestawi, M.A., *Cutting temperature of ceramic tools in high speed machining of difficult-to-cut materials,* International Journal of Machine Tools and Manufacture 36 (5), pp. 611-634, 1996.

Erdemir, A., *A crystal-chemical approach to lubrication by solid oxides,* Tribology Letters 8, pp. 97-102, 2000.

Erdemir, A., *A crystal chemical approach to the formulation of self-lubricating nanocomposite coatings,* Surface & Coatings Technology 200, pp. 1792-1796, 2005.

Erkens, G., Cremer, R., Hamoudi, T., Bouzakis, K.-D., Mirisidis, I., Hadjiyiannis, S., Skordaris, G., Asimakopoulos, A., Kombogiannis, S., Anastopoulos, J., and Efstathiou, K., *Properties and performance of high aluminum containing (Ti,Al)N based supernitride coatings in innovative cutting applications,* Surface and Coatings Technology 177-178 , pp.727-734, 2004

Fallböhmer, P., Altan, T., Tönshoff, H.K., Nakagawa, T., *Survay of die and mold manufacturing industry,* J. of Materials Processing Technology, 59, pp.158-168, 1996.

Fallböhmer, P., Rodríguez, C.A., Özel, T., Altan, T., *High-speed machining of cast iron and alloy steels for die and mold manufacturing*, J. of Materials Processing Technology, 98, pp. 104-115, 2000.

Fenske, G.R., et al., *Characterization of coating wear phenomena in nitride and carbide-coated tool insert,* Surface and Coatings Technology, 36, pp. 791-800, 1988.

Fox-Rabinovich, G.S., Yamomoto, K., Veldhuis, S.C., Kovalev, A.I., Dosbaeva, G.K., *Tribological adaptability of TiAlCrN PVD coatings under high performance dry machining conditions,* Surface & Coatings Technology 200, pp. 1804-1813, 2005.

Fox-Rabinovich, G.S., Totten, G.E., Eds., *Self-organization during friction- advanced surface-engineered materials and systems design*, CRC Press, a Taylor & Francis Group, 2006.

Fox-Rabinovich, G.S., Yamamoto, K., Veldhuis, S.C., Kovalev, A.I., Shuster L.S. and Ning, L., *Self-adaptive wear behavior of nano-multilayered TiAlCrN/WN coatings under severe machining conditions,* Surface and Coatings Technology 201(3-4), pp. 1852-1860, 2006.

Fox-Rabinovich, G.S., Wilkinson, D.S., Veldhuis, S.C., Dosbaeva, G.K., Weatherly, G.C., *Oxidation resistant Ti-Al-Cr alloy for protective coating applications,* Intermetallics 14, pp. 189-197, 2006.

Fox-Rabinovich, G.S., Weatherly, G.C., Wilkinson, D.S., Kovalev, A.I., Wainstein, D.L., *The role of chromium in protective alumina scale formation during the oxidation of ternary TiAlCr alloys in air,* Intermetallics 12(2), pp. 165-180, 2004.

Fox-Rabinovich, G.S., Weatherly, Dodonov, A.I., Kovalev, A.I., Shuster, L.S., Veldhuis, S.C., Dosbaeva, G.K., Wainstein, D.L., Migranov, M.S., *Nano-crystalline filtered arc deposited (FAD) TiAlN PVD coatings for high-speed machining applications,* Surface & Coatings Technology 177-178, pp. 800-811, 2004.

Gekonde, H.O., Subramanian, S.V., *Tribology of tool-chip interface and tool wear mechanisms,* Surface & Coatings Technology 149 (2), pp. 151-160, 2002.

Gilmore, R.,Baker, M.A., Gibson, P.N., Gissler, W., Stoiber, M., Losbichler, P., Mitterer, C., *Low-friction TiN-*MoS_2 *coatings produced by dc magnetron co-deposition,* Surface & Coatings Technology 108-109(1-3), pp.345-351, 1998.

Gorokhovsky, V., Bowman, C., Gannon, P., VanVorous, D., Voevodin, A.A., Rutkowski, A., Muratore, C., Smith, R.J., Kayani, A., Gelles, D., Shutthanandan, V., Trusov, B.G., *Tribological performance of hybrid filtered arc-magnetron coatings. Part I: Coating deposition process and basic coating properties characterization,* Surface and Coatings Technology 201(6), pp. 3732-3747, 2006,

Grzesik, W., Nieslony, P., *Thermophysical-property-based selection of tool protective coatings for dry machining of steels,* Journal of Manufacturing Science and Engineering, Transactions of the ASME 125(4), pp. 689-695, 2003.

Han, J.G., Yoon, J.S., Kim, H.J. and Song, K., *High temperature wear resistance of (TiAl)N films synthesized by cathodic arc plasma deposition,* Surface & Coating Technology 86-87 (1-2), pp. 82-87, 1996.

Harry, E., Rouzaud, A., Juliet, P., Pauleau, Y., *Adhesion and failure mechanisms of tungsten-carbon containing multilayered and graded coatings subjected to scratch tests,* Thin Solid Films 342, pp.207-213, 1999.

Hirao, M., Terashima, A., Joo, H.Y., Shirase, K., Yasui, T., *Behavior of cutting heat in high speed cutting,* J. Jpn, Soc. Precision Eng., 64(7), pp. 1067-1071, 1998.

Holleck, H., *Material selection for hard coatings,* The Journal of Vacuum Science and Technology A 4 (6), pp. 2661-2669, 1986.

Holleck, H., Schier, V., *Multilayer PVD coatings for wear protection,* Surface and Coatings Technology 76-77, pp. 328-336, 1995.

Jehn, H.A., *Multicomponent and multiphase hard coatings for tribological applications,* Surface and Coatings Technology 131, pp.433-440, 2000.

ISO 8688-1, *Tool Life Testing in Milling – Part 1: Face Milling,* International Standard, 1989.

Ikeda, T., Sato, H., *Phase formation and characterization of hard coatings in the Ti---Al---N system prepared by the cathodic arc ion plating method,* Thin Solid Films 195, pp. 99-110, 1991.

Ivkovic, B., *Some results of thin coatings test obtained by the scratch tester,* Proceedings of The 3rd Inrenational Conference- The Coatings in Manufacturing Engineering, pp.349-354, 2002.

Jaspers, S.P.F.C., Dautzenberg, J.H., *Material behavior in metal cutting: strains, strain rates and temperatures in chip formation,* Journal of Materials Processing Technology 121, pp. 123-135, 2002.

Jeon, J.-H., Choi, S.R., Chung, W.S. and Kim, K.H., *Synthesis and characterization of quaternary Ti–Si–C–N coatings prepared by a hybrid deposition technique,* Surface and Coatings Technology 188-189, pp. 415-419, 2004.

Kalss, W., *Latest developments and applications in coating technologies*, Balzers Ltd., http://hssforum.com/Aachen/08_Kalss.pdf

Kishawy, H.A.,.Elbestawi, M.A, *Effect of Process Parameters on Chip Morphology when Machining Hardened Steel,* Proc. 1997 ASME International Mechanical Engineering Congress and Exposition, Dallas, Texas, 1997.

Kishawy, H.A., Wilcox, J., *Tool wear and chip formation during hard turning with self-propelled rotary tools,* Int. J. of Machine Tools & Manufacture 43, pp. 433-439, 2003.

Kishawy, H.A., *Chip Formation and Surface Integrity in High Speed Machining of Hardened Steel,* Ph.D Thesis, McMaster University, 1998.

Knotek, O., Leyendecker, T., Jungblut, F., *On the properties of physically vapour-deposited Ti-Al-V-N coatings,* Thin Solid Films 153, pp.83-90, 1987.

Knotek, O., Munz, W.D., LEyendecker, T., *Industrial deposition of binary, ternary, and quaternary nitrides of titanium, zirconium, and aluminum,* Journal of Vacuum Science & Technology A (Vacuum, Surfaces, and Films) 5(4), p 2173-2179, 1987.

Komanduri, R., Schroeder, T., Hazra, J., von Turkovich, B.F., Flom, D.G., *On the catastrophic shear instability in high-speed machining of an AISI 4340 steel,* ASME J. Eng. Ind. 104, pp. 121-131, 1982.

Konig, W, Berktold, A., Koch, K.F., *Turning versus grinding – A comparison of surface integrity aspects and attainable accuracy*, Annals of the CIRP 42(1), pp. 39-43, 1993.

Konig, W., Klinger, M., Link, R., *Machining hard materials with geometrically defined cutting edges – field of applications and limitations,* Annals of the CIRP, 39(1), pp.61-64, 1990.

Konig, W., Kommanduri, R., Toenshoff, H.K., Ackerschott, G., *Machining of Hard Materials,* Annals of the CIRP 33(2), pp.417-427, 1984.

Kopac, J., Sokovic, M., Dolinsek, S., *Tribology of coated tools in conventional and HSC machining,* Journal of Materials Processing Technology 118(1-3), pp. 377-384, 2001.

Kostetsky, B.I., *An evolution of the materials' structure and phase composition and the mechanisms of the self-organizing phenomenon at external friction,* Friction and Wear 14(4), pp. 773-783, 1993.

Kukla, R., *Magnetron sputtering on large scale substrates: an overview on the state of the art*, Surface & Coatings Technology 93 (1), pp. 1-6, 1997.

Lahres, M., Doerfel, O., Neumüller, R., *Applicability of different hard coatings in dry machining an austenitic steel*, Surface & Coatings Technology 120-121, pp. 687-691, 1999.

Leshock, C.E., Shin, Y.C., *Investigation on cutting temperature in turning by a tool-work thermocouple technique,* J. Manuf. Sci. Eng. Trans. ASME 199 (4), pp. 502-508, 1997.

Lewis, D.B., Donohue, L.A.; Lembke, M.; Munz, W.-D.; Kuzel, R.; Valvoda, V.; Blomfield, C.J., *The influence of the yttrium content on the structure and* *properties of* $Ti_{1-x-y-z}Al_xCr_yY_zN$ *PVD hard coatings*, Surface & Coatings Technology 114(2-3), pp. 187-199, 1999.

Lezanski, P., Shaw, M.C., *Tool face temperatures in high speed milling,* J. Eng. Ind. Trans. ASME 112 (2), pp. 132-135, 1990.

Limido, J., Espinosa, C., Salaun, M., Lacome, J.L., *A new approach of high speed cutting modeling: SPH method,* J. Phys. IV France 13, pp. 1195-1200, 2006.

Liu, Y.-R., Liu, J.-J., Zhu, B.-L., Luo, Z.-B., Miao, H.-Z., Computer simulation of the temperature distribution on the surface of ceramic cutting tools, Wear 210(1-2), pp. 39-44, 1997.

Loeffler, F. H.W., *Systematic approach to improve the performance of PVD coatings for tool applications,* Surface & Coatings Technology 68-69, pp. 729-740, 1994.

Lugscheider, E., Knotek, O., Barimani, C., Leyendecker, T., Lemmer, O., and Wenke, R., *PVD hard coated reamers in lubricant-free cutting,* Surface & Coating Technology 112, pp.146-1512, 1999.

Luo, Q., Rainforth, W.M., Münz, W.-D., *TEM observations of wear mechanisms of TiAlCrN and TiAlN/CrN coatings grown by combined steered-arc/unbalanced magnetron,* Wear, 225-229, pp. 74-82, 1999.

Matsumoto, Y., Barash, M.M., Liu, C.R., *Effect of hardness on the surface integrity of AISI 4340 steel,* J. Eng. Ind. Trans. ASME, 108 (3), pp. 169-175, 1986.

Matsumoto, Y., and Hsu, D-C, *Workpiece temperature rise during the cutting of AISI 4340 steel,* Wear 116(3), pp. 309-317, 1987.

McGee, F.J., *High speed machining – study: methods for aluminium workpieces,* Am. Machinist, pp. 121-126, 1979.

Larsson, M., Hollman, P., Hedenqvist, P., Hogmark, S., Wahlström, U., and Hultman, L., *Deposition and microstructure of PVD TiN---NbN multilayered coatings by combined reactive electron beam evaporation and DC sputtering,* Surface and Coatings Technology 86-87, Part 1, pp.351-356, 1996,

Ning, L., Stephen, S.C., Yamamoto, K., *Investigation of nano-structured PVD coatings for dry high speed machining,* Machining Science & Technology 11 (1), pp. 45-59, 2007.

Nakayama, K., Arai, M., Kanda, T., *Machining characteristics of hard materials,* Annals of the CIRP 37(1), pp.89-92, 1988.

Ng, E.G., Aspinwall, D.K., *The effect of workpiece hardness and cutting speed on the machinability of AISI H13 hot work die steel when using PCBN tooling,* Journal of Manufacturing Science and Engineering, Transactions of the ASME 124(3), pp. 588-594, 2002.

Ning, Y., Rahman, M., Wong, Y.S., *Investigation of chip formation in high speed end milling,* Journal of Material Processing Technology113, pp.360-367, 2001.

PalDey, S., Deevi, S.C., *Properties of single layer and gradient (Ti,Al)N coatings,* Materials Science and Engineering A 361(1-2), pp. 1-8, 2003.

PalDey, S., Deevi, S.C., *Single layer and multilayer wear resistant coatings of (Ti, Al)N: a review,* Materials Science & Engineering A 342, pp. 58-79, 2003.

Palmai, Z., *Chaotic phenomena in fast plastic deformation (in the case of cutting),* Materials Science Forum 473-474, pp. 369-374, 2005.

Pflüger, E., Schröer, A., Voumard, P., Donohue, L., Wünz, W.-D., *Influence of incorporation of Cr and Y on the wear performance of TiAlN coatings at elevated temperatures,* Surface & Coatings Technology 115(1), pp. 17-23, 1999.

Poulachon, G. and Moisan, A., *A contribution to the study of the cutting mechanisms during high speed machining of hardened steel,* Annals of CIRP 47 (1), pp. 73-76, 1998.

Prengel, H.G., Santhanam, A.T., Penich, R.M., Jindal, P.C. and Wendt, K.H., *Advanced PVD-TiAlN coatings on carbide and cermet cutting tools,* Surface & Coating Technology 94-95, pp. 597-602, 1997.

Prengel, H.G., Pfouts, W.R., Santhanam, A.T., *State of the art in hard coatings for carbide cutting tools,* Surface & Coatings Technology 102, pp. 183-190, 1998.

Rebholz, C., Ziegele, H., Leyland, A., Matthews, A., *Structure, mechanical and tribological properties of Ti-B-N and Ti-Al-B-N multiphase thin films produced by electron-beam evaporation,* Journal of Vacuum Science & Technology A (Vacuum, Surfaces, and Films) 16(5), p 2851-2857, 1998.

Restello, S., Boscarino, D. and Rigato, V., *A study of Ti–C–N(H) and Ti:CN*$_x$*(H) coatings grown with a magnetron sputtering/PECVD hybrid deposition process,* Surface and Coatings Technology 200(22-23), pp. 6230-6234, 2006, Rodriguez, Ciro A., *Ball-Nose End Milling – Development of Criteria for Automatic Selection of Spindle Speed and Feed Rate*, Ph.D. Dissertation, The Ohio State University, 1997.

Samsonov, G.V. (Ed.), *Physico-chemical properties of oxides, Handbook*, Metallurgy, Moscow, 1976.

Savan, A., Pfluger, E., Goller, R., Gissler, W., *Use of nanoscaled multilayer and compound films to realize a soft lubrication phase within a hard, wear-resistant matrix,* Surface and Coatings Technology 126, pp. 159-165, 2000.

Schäffer, E. and Kleer, G., *Mechanical behavior of (Ti,Al)N coatings exposed to elevated temperatures and an oxidative environment*, Surface & Coating Technology 133-134, pp. 215-219, 2000.

Schneider, D., Schwarz, T., Schultrich, B., *Determination of elastic modulus and thickness of surface layers by ultrasonic surface waves,* Thin Solid Films 219(1-2), pp. 92-102, 1992.

Schönjahn, C., Bamford, M., Donohue, L.A., Lewis, D.B., Forder, S. and Münz, W.-D., *The interface between TiAlN hard coatings and steel substrates generated by high energetic* Cr^+ *bombardment*, surface & Coaings Technology 125 (1-3), pp. 66-70, 2000.

Schulz, H., Moriwaki, T., *High-speed machining*, Annals of the CIRP, 41(2), pp.637-643, 1992.

Shaw, M.C., Vyas, A., *Chip formation in the machining of hardened steel,* Annals of CIRP 42(1), pp.29-33, 1993.

Smith, I.J., Gillibrand, D., Brooks, J.S., Münz, W.-D., Harvey, S. and Goodwin, R.,*Dry cutting performance of HSS twist drills coated with improved TiAlN* , surface & Coaings Technology 90(1-2), pp.164-171,1997.

Stephenson, D.A., Ali, A., *Tool temperatures in interrupted metal cutting,* J. Eng. Ind. Trans. ASME 114 (2), pp. 127-136, 1992.

Stoiber, M., Perlot, S., Mitterer, C., Beschliesser, M., Lugmair, C., Kullmer, R., *PACVD TiN/Ti–B–N multilayers: from micro- to nano-scal,*. Surface & Coatings Technolology 177–178, pp. 348–354, 2004.

Suzuki, T., Huang, D. and Ikuhara, Y., *Microstructures and grain boundaries of (Ti,Al)N films,* Surface & Coating Technology 107, pp. 41-47, 1998.

Takago, S., Gotoh, M., Sasaki, T., Hirose, Y., *The residual stress measurement of TiCN PVD films,* JCPDS-International Centre for Diffraction Data, Advances in X-ray Analysis 45, pp. 365, 2002.

Tlusty, J., *High-speed machining*, Annals of the CIRP, 42 (2), pp. 733-738, 1993.

Tönshoff, H.K., Denkena, B., Friemuth, T., Spengler, Chr., *Influence of different grinding processes on coating adhesion on cutting tools,* Proceedings of the 3rd International Conference - The Coatings in Manufacturing Engineering and EUREKA Partnering Event, pp. 3-16, Nov., 2002.

Tönshoff, H.K., Seegers, H., *X-Ray diffraction characterization of pre-treated cemented carbides for optimizing adhesion strength of sputtered hard coatings,* Surface and Coatings Technology 142, pp.1100-1104, 2001.

Tönshoff, H.K., Mohlfeld, A., *Surface treatment of cutting tool substrates,* International Journal of Machine Tools & Manufacture 38, pp.469-476, 1998.

Trent, E.M., Wright, P.K., *Metal cutting* (Fourth Edition), Butterworth-Heinemann, 2000.

Vyas, A., Shaw, M.C., *Mechanics of saw-tooth chip formation in metal cutting,* ASME J. Manuf. Sci. eng. 121, pp. 163-172, 1999.

Veprek, S., *Conventional and new approaches towards the design of novel superhard materials,* Surface and Coatings Technology 97, pp. 15-22, 1997.

Veprek, S., Männling, H.–D., Jilek, M., Holubar, P., *Avoiding the high-temperature decomposition and softening of* $(Al_{1-x}Ti_x)$ *coatings by the formation of stable superhard* nc-$(Al_{1-x}Ti_x)N$/a-Si_3N_4 *nanocomposite,* Materials Science and Engineering A366, pp. 202-205, 2004.

Veprek, S., Mukherjee, S., Karvankova, P., Männling, H.–D., He, J.L., Moto, K., *Limits to the strength of super- and ultrahard nanocomposite coatings,* J. Vac. Sci. Technol. A 21(3), pp. 532-544, 2003.

Veprek, S., Nesládek, P., Niederhofer, A., Glatz, F., Jílek, M., Šíma, M., *Recent progress in the superhard nanocrystalline composites: towards their industrialization and understanding of the origin of the superhardness,* Surface & Coatings Technology 108-109, pp. 138-147, 1998.

Wang, J.Y., Liu, C.R., *New concept for decoupling the cutting forces due to tool flank wear and chip formation in hard turning,* Machining Science and Technology 2(1), pp. 77-90, 1998.

Wang, J.Y., Liu, C.R., *Effect of tool flank wear on the heat transfer, thermal damage and cutting mechanics in finish hard tuning,* CIRP Annals - Manufacturing Technology 48(1), pp. 53-58, 1999.

Wang, L., Saito, K., Jawahir, I. S., *Infrared temperature measurement of curled chip formation in metal machining,* Proceedings of the Transactions of the North American Manufacturing Research Institution of SME, NAMRC XXIV, Ann Arbor, MI, USA, pp. 87-92, 1996.

Wang, Y., *A study of PVD coatings and die materials for extended die-casting die life*, Surface & Coating Technology 94-95, pp. 60-63, 1997.

Xie, Y., Hawthone, H.M., *Effect of contact geometry on the failure modes of thin coatings in the scratch adhesion test,* Surface & Coatings Technology 155, pp.121-129, 2002.

Yamamoto, K., Sato, T., Takahara, K. and Hanaguri, K., *Properties of (Ti, Cr, Al)N coatings with high Al content deposited by new plasma enhanced arc-cathode,* Surface & Coatings Technology 174-175, pp. 620-626, 2003.

Yamamoto, K., Kujime, S. and Takahara, K., *Properties of nano-multilayered hard coatings deposited by a new hybrid coating process: Combined cathodic arc and unbalanced magnetron sputtering,* Surface & Coatings Technology 200(1-4), pp. 435-439, 2005.

Yao, S.H. and Su, Y.L., *The tribological potential of CrN and Cr(C,N) deposited by multi-arc PVD process,* Wear 212(1), 1997, pp. 85-94

Yen, Y.-C., Sartkulvanich, P., Al-Zkeri, I., Sohner, J., and Altan, T., *Prediction of Cutting Forces, Tool Stresses, Temperatures and Tool Wear in High Speed Machining*,http://nsmwww.eng.ohiostate.edu/prediction_of_cutting_forces_tool_stresses.pdf, 2002.

Young, H.T., Chou, T.L., *Investigation of edge effect from the chip-back temperature using IR thermographic techniques,* J. Mater. Process. Technol. 52 (2-4), pp. 213-224, 1995.

Zhang, S., Sun, D., Fu, Y., Du, H., *Recent advances of superhard nanocomposite coatings: a review,* Surface & Coatings Technology 167, pp. 113-119, 2003.

Zhen-Bin, H., Komanduri, R., *Modeling of thermomechanical instability in machining,* International Journal of Mechanical Sciences 39 (11), pp. 1273-131, 1997.

Appendix A

Progress of Wear, Chip Formation and Cutting Forces

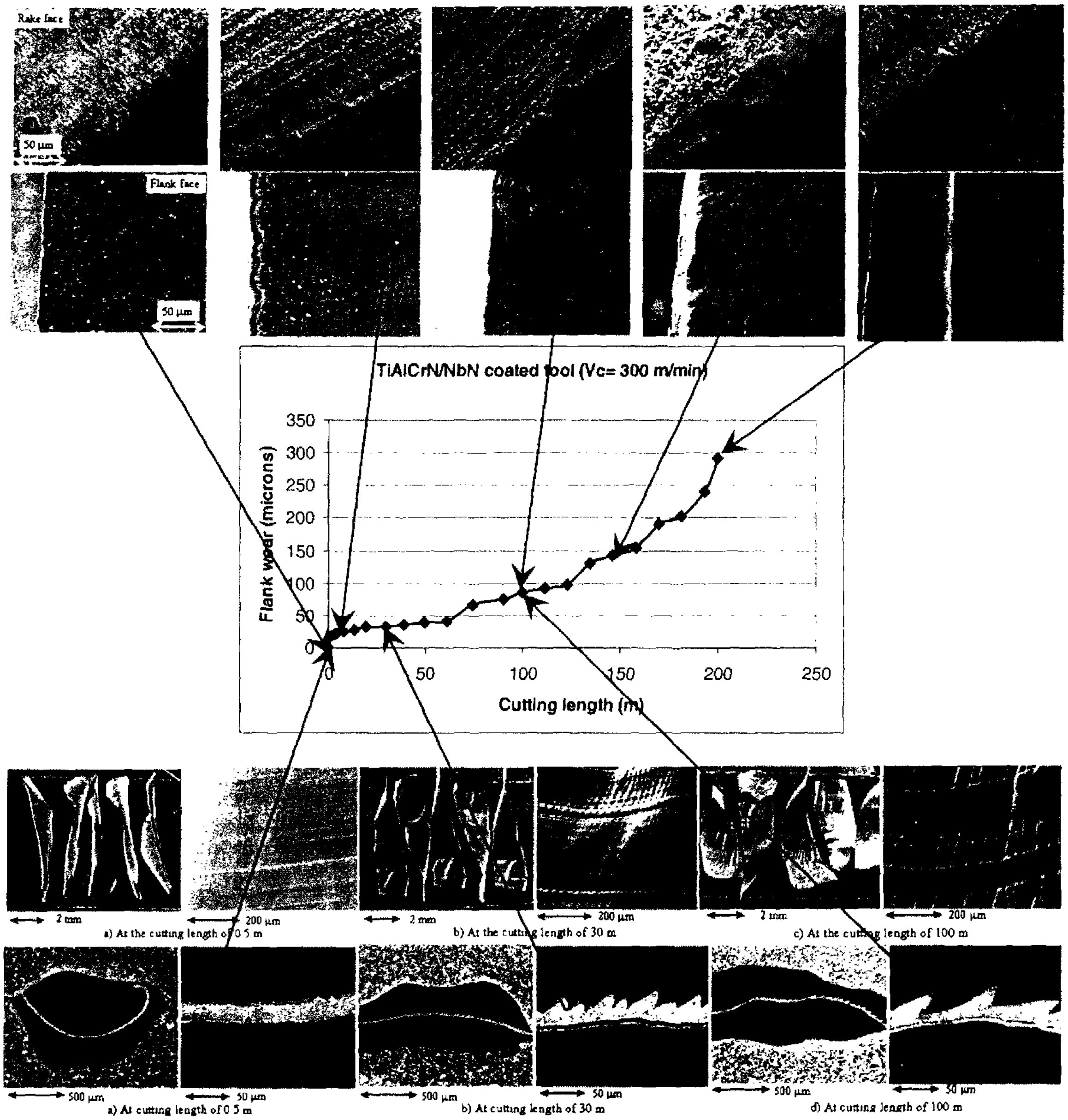

Figure A.1 The effect of tool wear on tool surface, chip shape and chip type

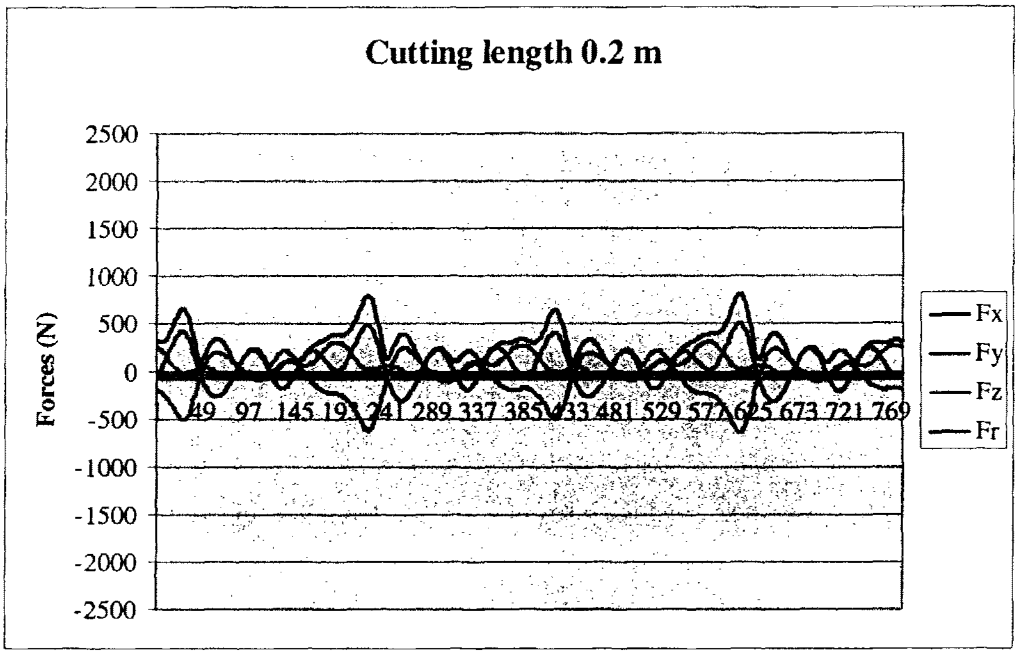

Figure A.2 Cutting forces at cutting length of 0.2 m (TiAlCrN/NbN coating, cutting speed of 300m/min)

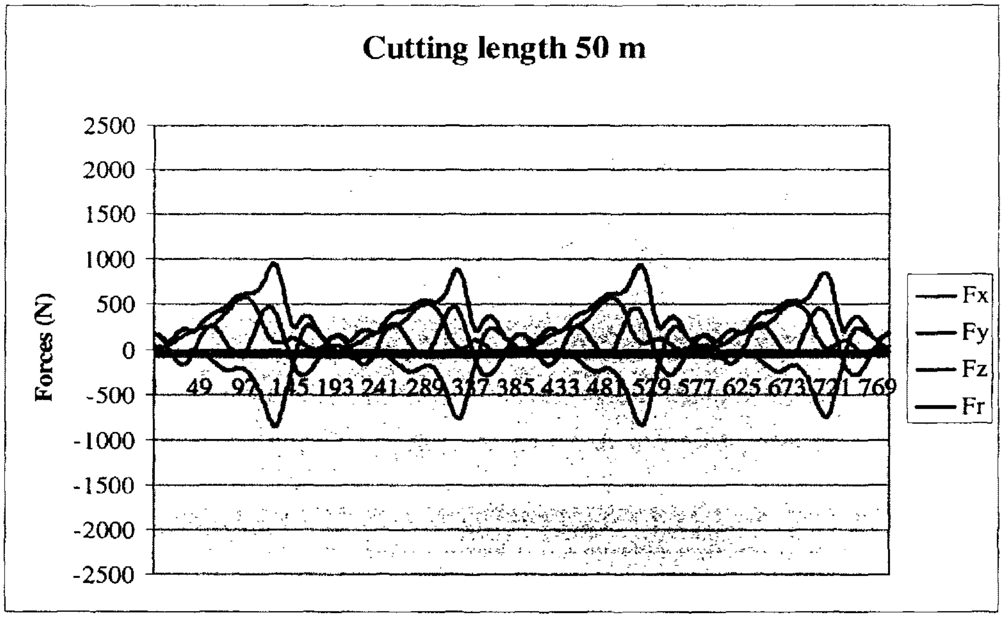

Figure A.3 Cutting forces at cutting length of 50 m (TiAlCrN/NbN coating, cutting speed of 300m/min)

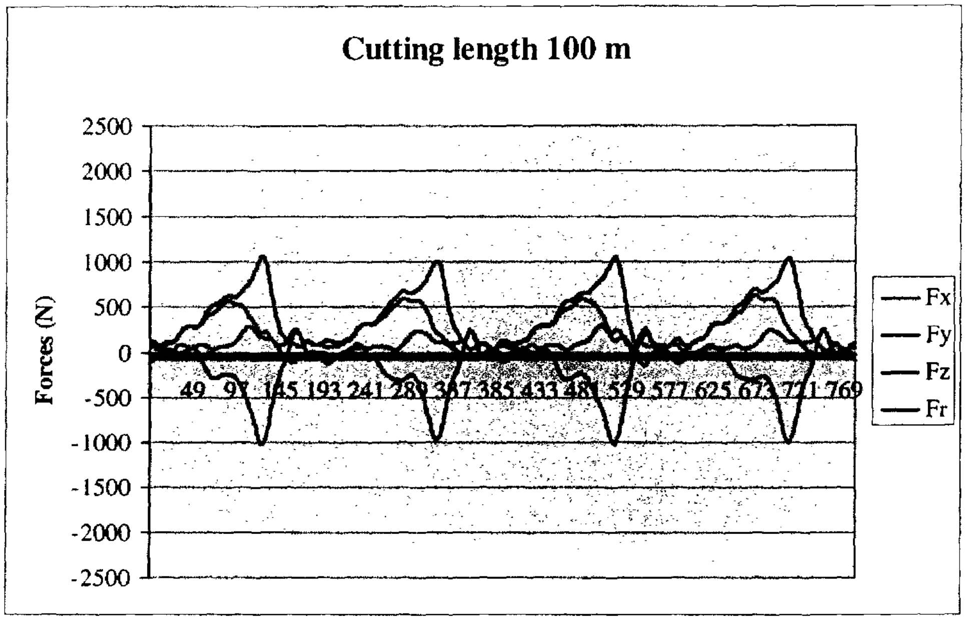

Figure A.4 Cutting forces at cutting length of 100 m (TiAlCrN/NbN coating, cutting speed of 300m/min)

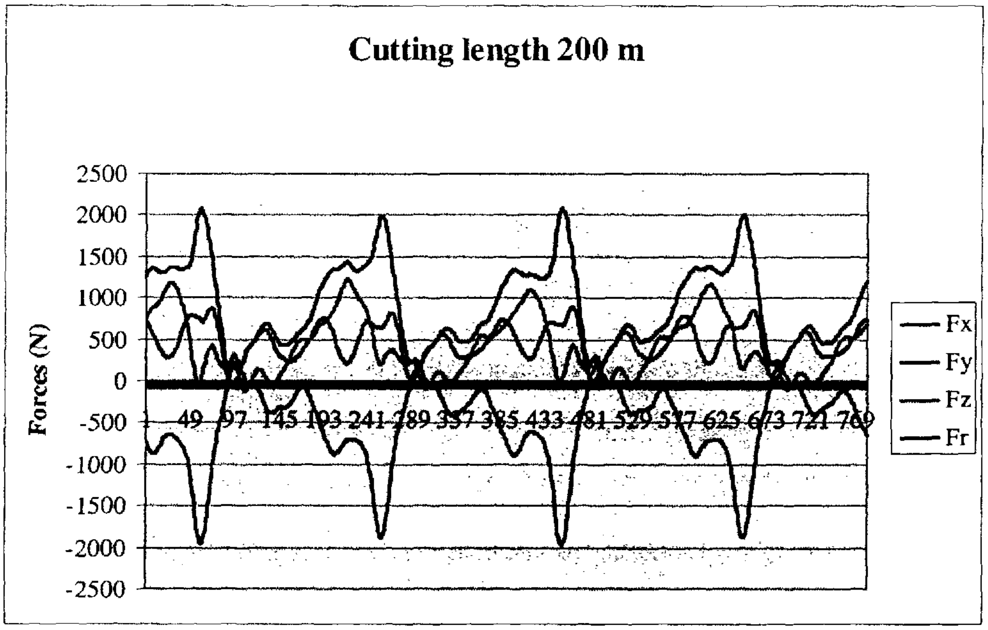

Figure A.5 Cutting forces at cutting length of 200 m (TiAlCrN/NbN coating, cutting speed of 300m/min)

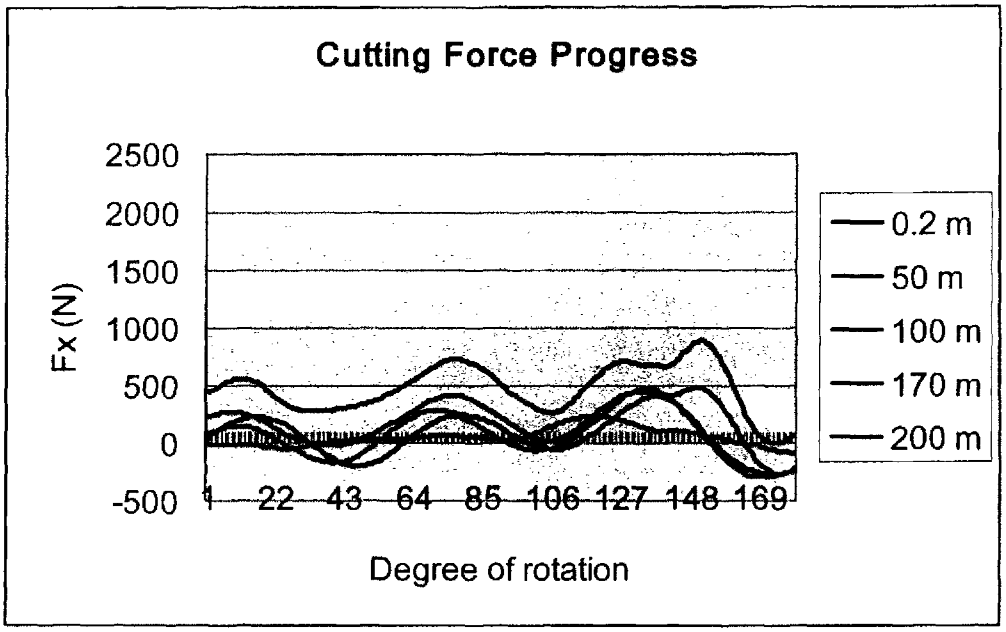

Figure A.6 Cutting force progress along X axis
(TiAlCrN/NbN coating, cutting speed of 300m/min)

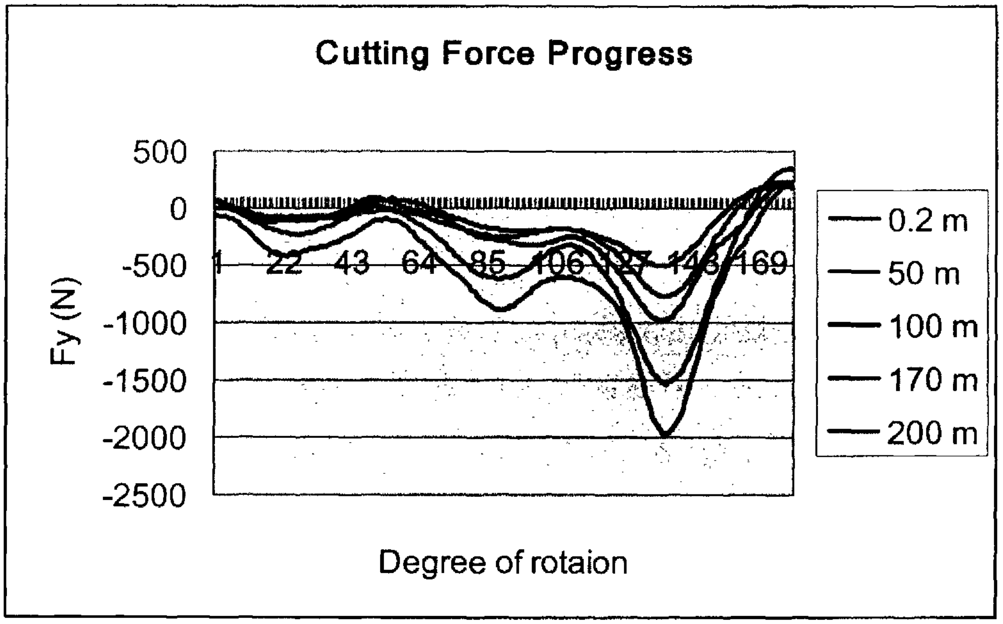

Figure A.7 Cutting force progress along Y axis
(TiAlCrN/NbN coating, cutting speed of 300m/min)

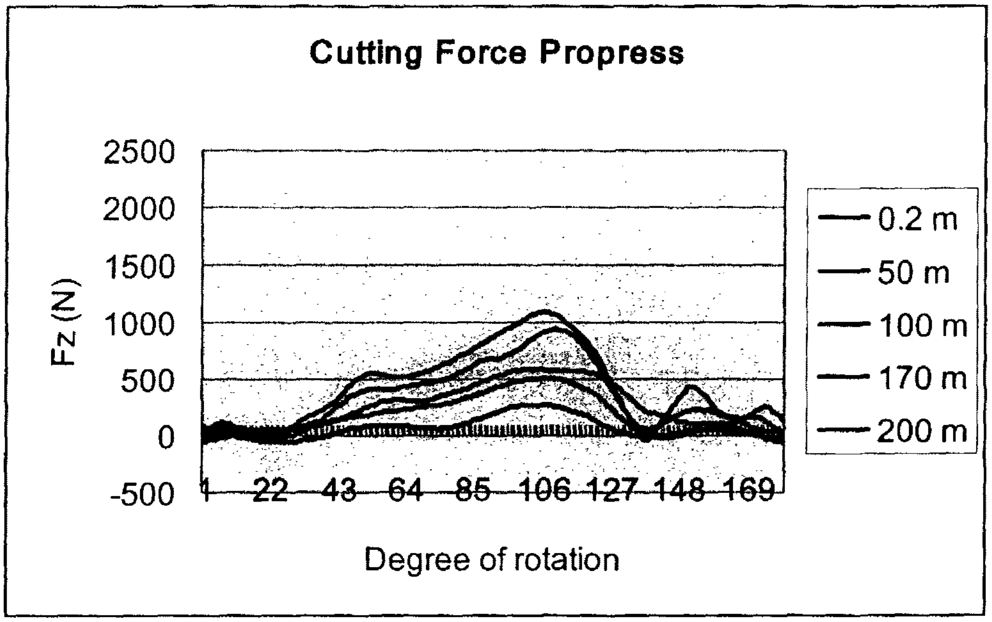

Figure A.8 Cutting force progress along Z axis
(TiAlCrN/NbN coating, cutting speed of 300m/min)

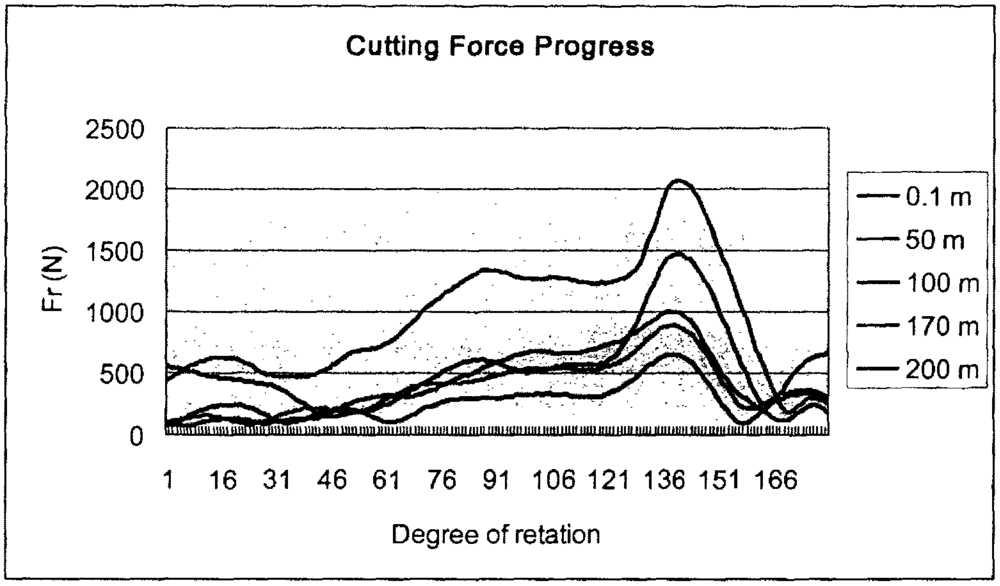

Figure A.9 Progress of resultant cutting force
(TiAlCrN/NbN coating, cutting speed of 300m/min)

Appendix B

Typical Variation in Tool Life

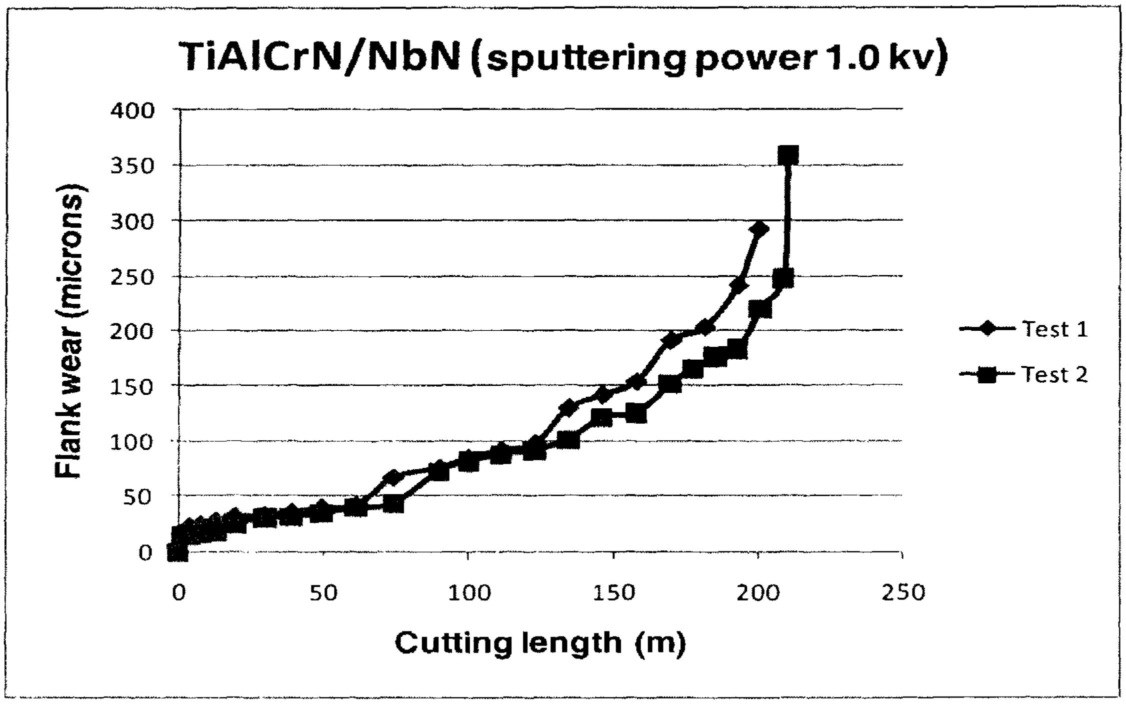

Figure B.1 Tool life of C-2SB ball end mills with TiAlCrN/NbN coatings deposited by sputtering power of 1.0 kv (cutting speed: 300 m/min)

Appendix C

Tool Life of C-2MB Ball End Mills

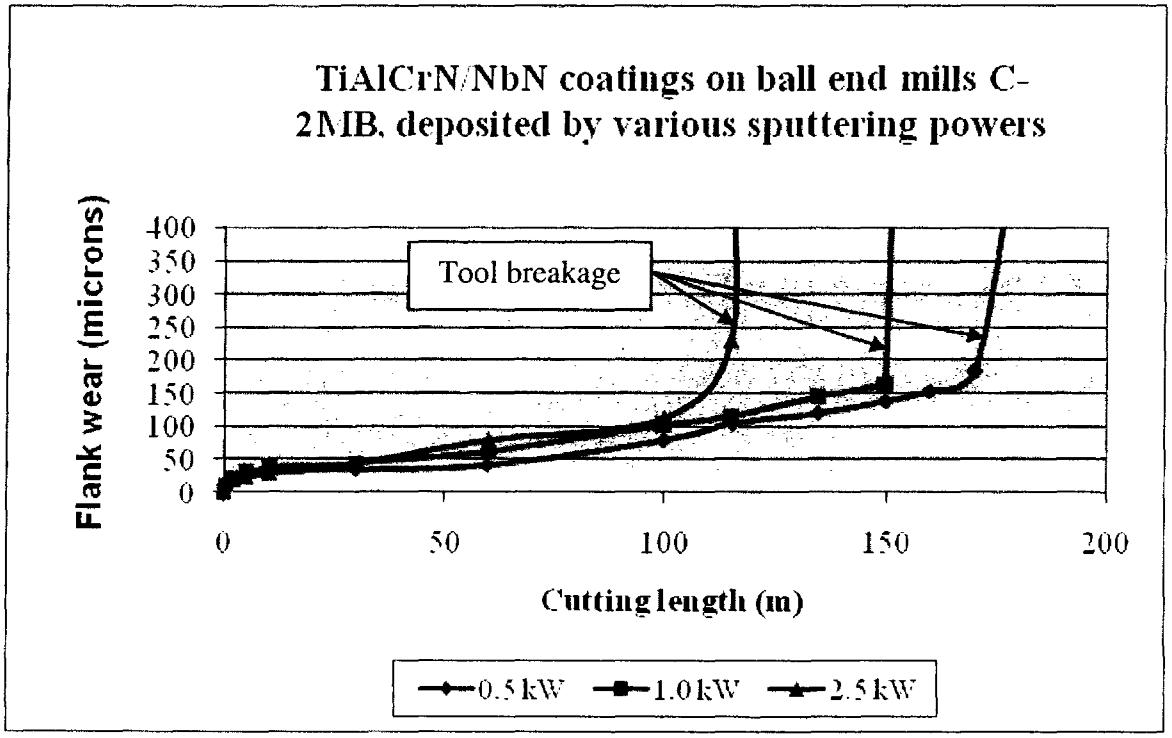

Figure C.1 Tool life of C-2MB ball end mills with TiAlCrN/NbN coatings deposited by various sputtering powers (cutting speed: 300 m/min)